The University Of Sheffield.

Carbon Capture and Utilisation processes: a techno-economic assessment of synthetic fuel production from CO_2

Thesis submitted to the Department of Chemical and Biological Engineering, University of Sheffield, for the Degree of Doctor of Philosophy (PhD)

By

Pelayo García-Gutiérrez

Department of Chemical and Biological Engineering

University of Sheffield

September 2016

Abstract

Carbon Capture and Utilisation (CCU) is seen globally as one of the available technologies that can contribute to avoiding the effects of global warming while securing energy supply by utilising CO_2 as a carbon source for chemical and fuel production. This thesis has measured the technical and economic performance of seven Carbon Capture and Utilisation (CCU) process designs (Base Case Models) based on best available technology. This was the first attempt to compare different routes of similar Technology Readiness Level to manufacture a liquid fuel from CO_2. In addition, this thesis also examines the techno-economic feasibility of selective CO_2 capture processes from biogas streams using ionic liquids as physical absorbents to assess the potential improvements that this developing technology could have on process performance.

The selected Base Case Models were modelled using the process simulation software Aspen Plus to determine mass and energy balances. In addition, an economic assessment was developed using Aspen Plus Economic Analyzer (APEA) and MS Excel to determine capital, operating and production costs.

The results revealed that the synthetic route based on CO_2 capture and steam methane reforming was the most promising CO_2-to-fuels route since it was able to achieve the highest overall plant energy efficiency (17.9%) and the lowest fuel production costs (£95.46 per GJ [LHV]); however this process cannot currently compete commercially with conventional fossil fuels. Further research in the specific areas suggested in this work is encouraged in order to bring fuel production costs down.

It was also demonstrated that the evaluated ionic liquids cannot compete with MEA in terms of bio-methane production costs; however, the simulation methodology developed in this study can be used as a basis for further work in the area since it allows consideration of ionic liquids made of any combination of cation and anion as well as different gas streams.

Acknowledgements

Firstly I would like to thank my supervisors Prof Ray W. K. Allen and Dr Rachael H. Elder for their encouragement, advice and support during my PhD.

I would like to extend my gratitude to members of the 4CU Project for being such excellent work colleagues. Specially, I would like to acknowledge Dr Ioanna Dimitriou, whose expertise in chemical process simulation helped organise my ideas and take the work forward. I would also like to thank Dr Johan Jacquemin and Corina McCrellis at QUB for their essential support during the ionic liquid simulations. This modelling work would have not been completed without their invaluable contribution.

This thesis, as well as the 4CU Project, is funded by the Engineering and Physical Sciences Research Council (EPSRC). Therefore I am deeply grateful for making this research possible.

Finally, endless thanks to my family and friends, in the UK and Spain, who have always provided emotional support throughout my life. My dearest thanks go to my parents Isabel and José Ginés. I owe them both too much to express in words.

Table of Contents

List of Tables

List of Figures

Abbreviations

GHG	Greenhouse Gas
CCS	Carbon Capture and Storage
CCU	Carbon Capture and Utilisation
CDU	Carbon Dioxide and Utilisation
IPHE	International Partnership for Hydrogen and Fuel Cells in the Economy
EU	European Union
TRL	Technology Readiness Level
IUPAC	International Union of Pure and Applied Chemistry
STP	Standard Temperature and Pressure
GWP	Global Warning Potential
EOR	Enhanced Oil Recovery
SOEC	Solid Oxide Electrolysis Cell
TPB	Triple Phase Boundary
IGCC	Integrated Gasification Combined Cycle
MEA	Monoethanolamine
SILM	Supported Ionic Liquid Membrane
VLE	Vapour-Liquid Equilibrium

COSMO-SAC	COnductor-like Screening Model with Segment Activity Coefficient
COSMO-RS	COnductor like Screening MOdel for Real Solvents
LCA	Life Cycle assessment
KOGAS	Korea Gas Corporation
DME	Dimethyl ether
JOGMEC	Japan Oil, Gas and Metals National Corporation
GTL	Gas To Liquids
NETL	National Energy Technology Laboratory
RWGS	Reverse Water Gas Shift
PSA	Pressure Swing Adsorption
CHP	Combined Heat and Power
REA	Renewable Energy Association
WWTP	Waste Water Treatment Plant
NIST	National Institute of Standards and Technology
DECC	Department of Energy and Climate Change
ENRTL-RK	Electrolyte Non-Random Two-Liquid-Redlich–Kwong
NRTL	Non-Random Two-Liquid
HETP	Height Equivalent to a Theoretical Plate
VOC	Volatile Organic Compound
ASU	Air Separation Unit
PR-BM	Peng-Robinson with Boston-Mathias
KIER	Korean Institute of Energy and Research
FT	Fischer-Tropsch
LTFT	Low Temperature Fischer-Tropsch
HTFT	High Temperature Fischer-Tropsch

WGS	Water Gas Shift
BTL	Biomass To Liquids
TIGAS	Topsoe Integrated GASoline
MTG	Methanol To Gasoline
ASF	Anderson–Schulz–Flory
UNIFAC	UNIQUAC Functional-group Activity Coefficients
UNIQUAC	UNIversal QUAsiChemical
ASME	American Society of Mechanical Engineers
APEA	Aspen Process Economic Analyzer
ARD	Average Relative Deviation
DFT	Density Functional Theory
LHV	Lower Heating Value
TCI	Total Capital Investment
TDC	Total Direct Cost
DEC	Delivered Equipment Cost
SMDS	Shell Middle Distillate Synthesis
UKPIA	United Kingdom Petroleum Industry Association

1. INTRODUCTION

This thesis is grounded in the EPSRC-funded *4CU Project* (officially called “A Coordinated, Comprehensive approach to Carbon Capture and Utilization (4CU Project, 2012; EPSRC, 2012). Specifically, this thesis is based on the work carried out in the Subproject 1 (SP1) of the aforementioned project which focuses on process analysis and optimization.

The aim of this thesis is to compare the feasibility of different CO_2 capture and utilisation processes in order to identify the most promising routes for the conversion of Carbon Dioxide into a synthetic fuel. Due to the lack of published work on techno-economic assessments of carbon dioxide utilisation processes, this thesis also aims at directing further research and development on the topic. The identification of the “best” synthetic routes is carried out through “whole system” mass and energy balances, which are calculated by using the commercial package Aspen Plus® as the process simulation software. In order to allow a fair and robust comparison among the different process concepts, initially the methodology considers only the best available and proven technology. Then, developing technologies such as CO_2 capture using ionic liquids are included in the different conceptual designs in order to examine the potential improvements in process performance (technical and economic) that these developing technologies might have.

Interpretation of the most promising process concepts can be carried out in a number of ways, such as: mass and energy efficiencies, lowest capital costs, lowest production costs, most environmentally benign or most socially acceptable. From the point of view of a chemical company investing in a project, the most promising process will be that which can generate the greatest profit. However, other factors must be taken into account at this stage of development such as the potential impacts that the process might have on the environment and the local community. Since the environmental and social impacts on the local community are

covered by other researchers from a different Subproject (SP2) of the 4CU project, this research will focus on efficiencies and costs to judge the different process designs and then identify the most promising technologies.

Since the process concepts considered in this study (CO_2 to fuels processes) are at an early stage of development, many assumptions will have to be made in order to be able to model such systems. Assuming parameters based on common practice (rules of thumb) involves a certain degree of uncertainty introduced into the system; therefore, a sensitivity analysis will be carried out in order to quantify the uncertainty in the different model parameters and examine how they can affect production costs.

Stabilization of greenhouse gas (GHG) emissions, increasingly high energy prices and securing the energy supply within an increased energy demand context have become major challenges in the UK as well as whole continental Europe. Carbon Capture and Storage (CCS) is seen as one of the available technologies that can contribute to reduce CO_2 emissions (Figueroa *et al.*, 2008; European Academies Science Advisory Council, 2013); however it does not solve the issues related to dependence on fossil fuels, when most of them are imported to Europe *(*Styring *et al.*, 2011). In addition, not every country has enough storage capacity and the distance between the emission points and the storage locations make the cost of transport and storage excessive (Styring *et al.*, 2011). Other reasons for searching alternative solutions to CCS may include risks related to leakage of stored CO_2 (Styring *et al.*, 2011) or environmental impacts due to capture, transport and sequestration of the CO_2 (Zapp *et al.*, 2012). As an alternative, Carbon Dioxide Utilisation (CDU) has attracted increasing interest in recent years as a way to mitigate GHG while reducing dependence on fossil fuels. The aim of CDU is to utilise CO_2 as a carbon source for

chemical and fuel production and thus generate value from CO_2 instead of disposing it underground.

Vast quantities of anthropogenic CO_2 are released globally every year with 31 Gt in 2011 and expected to almost double this amount by 2050 with 57 Gt (International Energy Agency, 2008). Consequently, CO_2 is (and will be) an abundant feedstock that could play a key role in securing energy supply by reducing dependence on imported fossil fuels while reducing GHG emissions to the atmosphere. Furthermore, CO_2 could be used as a chemical feedstock in the production of a wide range of chemicals (Mikkelsen *et al.*, 2010; Quadrelli *et al.*, 2011), which will further increase revenue from CDU.

Whereas CO_2 is already been used in the food industry or as a feedstock in the production of some chemicals, these markets are much smaller than that of fuels (Centi & Perathoner, 2009). Therefore, if CDU wants to make a significant contribution towards the reduction of CO_2 emissions, research should also focus on the conversion to fuels. The fact that the transportation sector is responsible for 22% of global CO_2 emissions encourages intense CDU research towards the production of fuels.

CO_2 hydrogenation is used to produce oxygenate-based fuels such as methanol and dimethyl ether. In fact, CO_2 hydrogenation towards the production of methanol has been subject of very intense research which has led to the commission of several plants, both bench and pilot scale, in Asia and Europe (Quadrelli *et al.*, 2011). However, the production of hydrocarbon fuels from CO_2 (either through direct hydrogenation or through intermediate production of syngas via the reverse water gas shift reaction) has yet to be demonstrated. This is mainly due to the fact that the production of hydrocarbons via hydrogenation of CO_2 requires higher amounts of hydrogen and energy than oxygenates (Centi & Perathoner, 2009). However, there is a remarkable lack of published work on techno-economic feasibility studies in this area that supports

this argument. It is worth noting that hydrocarbons produced via the reverse water gas shift reaction coupled with Fischer-Tropsch synthesis (an industrial process that converts syngas to liquid fuels) are particularly attractive due to their ability to produce fully substitutable diesel and gasoline and thus, unlike alcohols and ethers, can be readily incorporated and integrated with conventional markets and supply chains.

The high hydrogen and energy requirements of CO_2-to-fuels processes are one of the main issues for the commercialization of these technologies. In order to make CDU processes as environmentally benign as possible, hydrogen should be made from renewable sources (wind, solar, *etc.*) or produced within the process. This endogenous production of hydrogen is especially interesting from the economic point of view since fossil-derived hydrogen is considerably cheaper than that produced from renewable sources (IPHE, 2011).

This thesis considers biogas produced from the anaerobic digestion of sewage sludge as the source of carbon in all process concepts. The biogas is formed mainly of CO_2 and CH_4, which is currently the main chemical feedstock for hydrogen production (via steam reforming of natural gas). One of the reasons why anaerobic digestion of sewage sludge was chosen is that this is a waste produced in vast amounts; in the EU, approximately 10 million tonnes (dry basis) of sewage sludge are generated per year (Appels *et al*., 2011). In this way, large amounts of waste can be converted into energy (fuels) via CO_2 utilisation. Furthermore, the anaerobic digestion of sewage sludge, despite its relatively small scale, has the highest biogas production capacity worldwide with about 0.59 m^3 of methane per kg of organic dry solids (Owens & Chynoweth, 1993).

It is widely known that large-scale production of fuels is necessary if a significant proportion of conventional fuels are to be replaced by fuels produced from alternative sources, e.g. CO_2 (AMEC, 2007; Dimitriou &

Bridgwater, 2010). In light with this, the relatively small scale of anaerobic digestion of sewage sludge could affect the commercial implementation of synthetic fuels derived from this carbon source. At the current early stage of development, anaerobic digestion of sewage sludge is seen as a suitable target application for synthetic fuel production, as explained earlier in this section; however, all process concepts developed in this thesis are sufficiently flexible to allow consideration of other carbon sources with industrial relevance if need be. These carbon sources could span from flue gases produced at fossil fuel-based power plants to exhaust gases form steel or cement plants, among others. In addition, the effect on production costs of the plant size will be assessed later in a sensitivity analysis.

Another reason for considering biogas produced form the anaerobic digestion of sewage sludge is that it is an important energy source due to its CH_4 content. This methane could be used either for providing the necessary amount of hydrogen for a CO_2 hydrogenation-to-fuels process via steam reforming of methane or for providing the necessary heat and electricity by means of Combined Heat and Power (CHP).

In the United Kingdom (UK) and overseas, the application of anaerobic digestion for several types of wet waste is a subject of intense research and industrial interest. It is estimated that wet food waste, which forms 15-20% of all municipal waste, will yield between 3 and 3.5 times more methane per tonne than sewage sludge (Gray *et al.*, 2008). Recent social changes in the collection of domestic waste have produced large quantities of well segregated wet waste; therefore the technology is widely seen as having the potential to deliver a substantial impact on energy supply.

In addition to the advantages mentioned above, anaerobic digestion is a suitable target process for CO_2 utilisation technologies since it can act as a real world application requiring moderate capital investment. Furthermore, biogas production in the water industry is a process of a

smaller scale than, for instance, electricity generation facilities. This permits technology development from lab scale to pilot and demo scale more easily than if a larger flowrate of flue gas was to be processed (*e.g.* flue gases from coal-based or natural gas-based power plants).

With regard to contribution to knowledge, this research demonstrates the useful application of process analysis and modelling techniques to CDU processes, in particular CO_2-to-fuels technologies. The results are essential to inform industry about which synthetic routes show the greater potential regarding process efficiency and production costs. In addition, outcomes from this work will help policy makers to identify the most suitable developing technologies for synthetic fuel production from CO_2 and then to prevent research resources being spent in the wrong direction.

1.1 The 4CU project

The work from this thesis is part of the EPSRC-funded “4CU project”. The existence of this project signifies the level of interest in this topic and this interest will only increase as concern grows over the remaining fossil resources, climate change and energy security.

Carbon Dioxide Utilisation (CDU) is seen globally as one of the available technologies that can contribute to avoiding the effects of global warming. However, there are few options for economically isolating a pure stream of CO_2 from a practical process gas mixture and even fewer viable reaction routes which allow CO_2 to be converted into, for example, a synthetic fuel. Moreover, research found in literature tends to consider narrow-based research results devoid of the context required if serious effort is to be made to consider commercial implementation.

The 4CU project takes a comprehensive approach to solve those problems by developing novel separation techniques allied with advanced reactor studies to yield useful reaction routes from CO_2 to

fuel. This fuel will be carbon-neutral in the sense that the carbon would otherwise have been emitted to the atmosphere, for instance by breakdown in landfill. The project involves over 30 researchers (Academics, Post-doctoral Research Associates and PhD students) from four different universities (The University of Sheffield, Queens University Belfast, University College London and The University of Manchester) as well as a number of industrial and international collaborators. The work is of general application and it is intended to ensure coordination and thermodynamic discipline throughout the project by applying the findings to a model process system; biogas sweetening within the water industry.

The structure of the 4CU project and the interconnection between the different Sub-projects can be seen in Fig. 1.1.

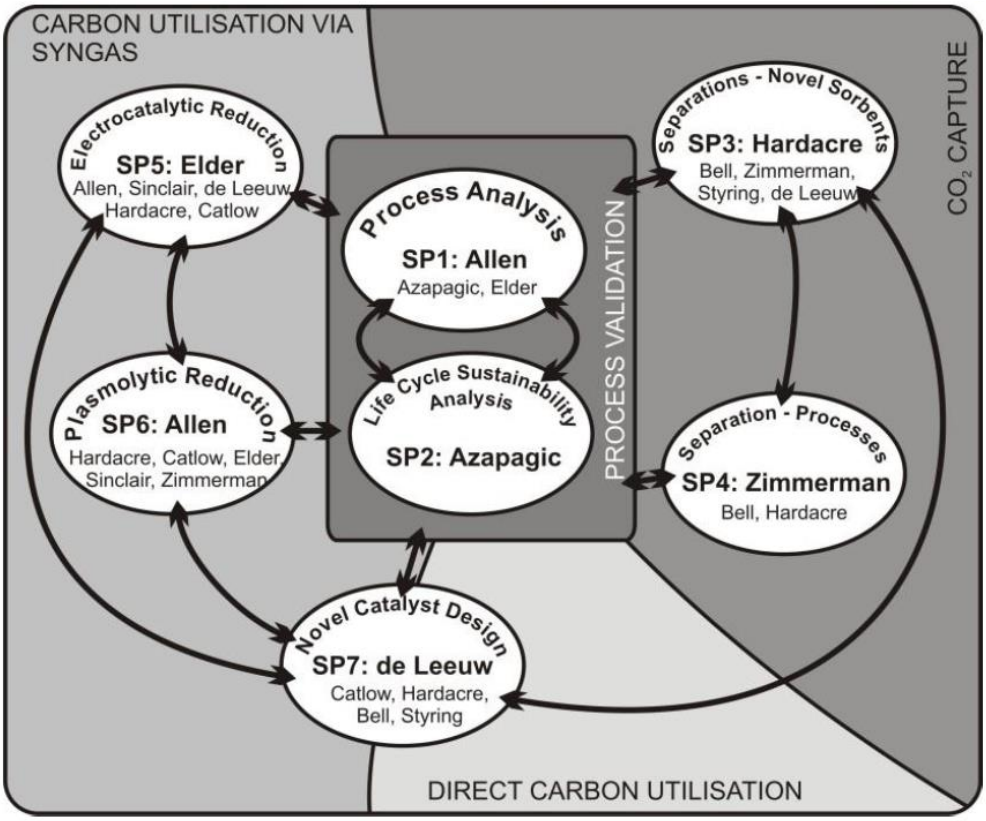

Fig. 1.1 Structure and interconnection between SPs

Sub-projects 3 to 7 provide an ambitious research activity covering a range of advances in Chemistry, Chemical Engineering and Materials Science that are likely to take Carbon Dioxide Utilisation (CCU) forward. Sub-projects 1 and 2, by contrast, provide further research demonstrating how these advances will integrate within whole processes aimed at successful delivery of CDU. It must be noted that while this thesis forms a prominent part of the Sub-project 1 *(SP1: Process Analysis)*, it is also involved in Sub-project 2 activities in terms of Sustainability Assessments.

The Industrial and Overseas Academic Steering Committee is formed by 13 members from across Europe and the USA and across different market sectors. The full list of institutions present in the Steering Committee and their country of origin can be found in Table 1.1.

Table 1.1 Industrial and Overseas Academic Steering Committee

Institution	Country of origin
DLR	Germany
Tata Steel	UK
University of Bari	Italy
University of Messina	Italy
CNRS Clermont Ferrand	France
AECOM	UK
SINTEF	Norway
EDF Energy	France
Johnson Matthey	UK
CEFIC	Belgium
RWTH Aachen University	Germany
Technical University of Denmark	Denmark
Idaho National Laboratory	USA

It is the 4CU project's ambition to put the UK at the forefront of international work in this field by creating a step change in the capability of the UK industrial and research communities to understand and analyse schemes for converting CO_2 into fuels. This is done by providing a model example and a 'tool box' of relevant unit operations, catalysts, materials and sustainability assessment techniques. This is the first attempt of its kind in the UK and it is emphasised that it is very different from previous work on CCS since the focus will be on Utilisation rather than Storage.

1.2 Thesis objectives and structure

1.2.1 Objectives

The main objectives of this thesis are as follows:

- Measure the technical performance in terms of mass yield, energy yield and overall energy efficiency of the selected process concepts by using the process simulation software AspenPlus to determine mass & energy balances.
- Build an economic model for each process design in order to estimate capital investment, Operating and Maintenance (O&M) and fuel production costs.
- Compare the technical and economic feasibility of different CO_2 capture and utilisation processes in order to identify the most promising routes for the conversion of carbon dioxide into a synthetic fuel.
- Develop a novel methodology based on the COSMO-SAC model to simulate CO_2 capture plants using ionic liquids.
- Conduct a sensitivity analysis on production costs for each process concept with respect to key performance and economic parameters.

The modelling task of this techno-economic study is the development of a steady-state representation of different CO_2 capture and utilisation process concepts. This will enable calculation of mass and energy balances and thus overall process efficiencies for each process concept. In addition, the mass and energy balances will be used to estimate the costs associated with selected process designs from which conclusions will be drawn in terms of recommendations for investors and policy makers.

1.2.2 Thesis structure

Chapter 2 describes the current status of CO_2 capture and utilisation technologies at different Technology Readiness Level (TRL). Some examples of successful implementation at industrial level of CO_2 transformations are also reviewed.

Chapter 3 includes a description of the processes developed to convert biogas into a synthetic fuel. Initially, the synthetic routes consider only the best available and proven technology. Then, these base case models are adapted to consider a developing technology: CO_2 capture using ionic liquids.

Chapter 4 describes the simulation methodology followed to model the different process designs in Aspen Plus. Performance indicators such as electricity produced by the CHP plant or thermal energy required by the CO_2 capture plant are included.

Chapter 5 presents the process simulation results from the evaluated process designs. A performance comparison in terms of mass yield, energy yield and overall energy efficiency of the selected process designs is also included.

Chapter 6 discusses the methodology used to economically assess the selected process concepts which are compared in terms of capital,

operating and production costs. Sensitivity analyses are carried out in order to evaluate the effect of different process parameters on fuel production costs.

Chapter 7 summarises the main results of this work and draws conclusions from them. Recommendations for future work in the field are also included in this chapter.

2. CO_2 CAPTURE AND UTILISATION

2.1 Background

It is widely accepted among the scientific community that the recent increase in man-made emissions of greenhouse gases, such as carbon dioxide (CO_2) is the main reason behind the observed rise in average global temperatures (Stocker *et al.*, 2013; Skeptical Science, 2014). In fact, it is believed that CO_2 represents three quarters of the global man-made GHG emissions (Aydin *et al.*, 2010). As discussed in the previous chapter, Carbon Capture and Storage (CCS) has emerged in the recent years as one of the options in the mitigation technology portfolio that can contribute significantly towards the stabilisation of GHG emissions; however it does not solve the issues related to dependence on fossil fuels, storage capacity, cost of transport and storage and risks related to leakage of stored CO_2.

Aiming at partially solving these issues, Carbon Dioxide Utilisation has emerged as an alternative to complement CCS by converting the CO_2 into valuable products and then generating revenue from them instead of simply disposing of the CO_2 underground. This is of paramount importance as CDU considers the CO_2 as a resource and not as a waste, bearing in mind that the CO_2 molecule contains a carbon atom and our society relies on carbon to obtain fuels, materials such as polymers and commodity chemicals.

This chapter covers the main physical-chemical aspects of the CO_2 molecule and its transformations to value-added products, with a focus on transformations to fuels, given the main objectives of this thesis. A review of the emerging industrial applications of CO_2 conversion to fuels is also included.

2.2 The CO_2 molecule

Carbon dioxide (CO_2) is a naturally occurring molecule formed by two atoms of oxygen each covalently double bonded to a single carbon atom. It has a molecular weight of 44 Da and it is a gas at Standard Temperature and Pressure (IUPAC's STP: 0 °C and 1 bar; (IUPAC, 2014)). It occurs naturally in the Earth's atmosphere as a result of volcanic eruptions, plant and animal respiration as well as from forest fires. It is essential to the growth of photosynthetic plants (also known as green plants), which use solar radiation to convert carbon dioxide and water into sugars with oxygen being produced as a waste product. These are key elements of the so called natural carbon cycle by means of which the level of CO_2 in the Earth's atmosphere is controlled and, as a consequence, the temperature of the planet.

The CO_2 molecule is infrared active due to two of its three vibrational modes: an anti-symmetric stretch and a bend. This infrared vibration activity is responsible of the role of CO_2 as a greenhouse gas. The Earth's atmosphere is transparent to visible light coming directly from the Sun, which hits the surface of the Earth and is reemitted as infrared radiation. Although the main constituents of the atmosphere (nitrogen and oxygen) are also transparent to infrared radiation, other trace components such as carbon dioxide, water vapour, methane and nitrous oxide absorb a fraction of the radiation resulting in global warming (North, 2015).

Carbon dioxide is neither the only greenhouse gas nor the most potent. Methane has a Global Warming Potential (GWP) of about 86 times higher than CO_2 (over a lifetime of 20 years) while nitrous oxide's GWP is 268 times higher that carbon dioxide's GWP over a lifetime of 20 years (Forster *et al.*, 2007); however, CO_2 is present in the Earth's atmosphere at a much higher concentration than other GHGs. In 2013, the concentration of CO_2 in the atmosphere reached at 400 ppm by volume, an increase of nearly 50% since the start of the industrial

revolution (North, 2015). Burning fossil fuels to produce energy is believed to be responsible for the increase in CO_2 concentration in the atmosphere, a problem that will be aggravated in the near future as energy consumption is expected to grow steadily over the coming decades (British Petroleum, 2014).

Due to both double bonds present in the molecule of CO_2, it is a thermodynamically very stable compound with a standard enthalpy of formation (ΔH) of -394 $kJ \cdot mol^{-1}$. As a result, it has been traditionally assumed that chemical transformations of carbon dioxide are going to be thermodynamically unfavourable. However this is not entirely true since the enthalpy of reaction is determined by the difference between the enthalpy of formation of the products and that of the reactants; therefore it is even possible for chemical transformations of CO_2 to be exothermic, as depicted in Scheme 2.1, for industrial production of ethylene carbonate from ethylene oxide and carbon dioxide (North, 2015).

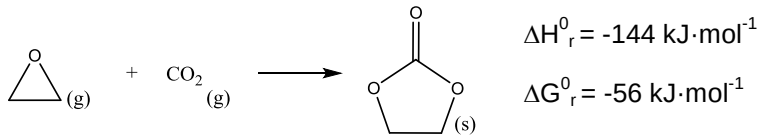

Scheme 2.1 Synthesis of ethylene carbonate from carbon dioxide and ethylene oxide

A more rigorous approach to analyse whether chemical reactions are thermodynamically favourable or not relies on the free energy of reaction (ΔG_r) where $\Delta G_r = \Delta H_r - T\Delta S_r$. It should be taken into account that any chemical reactions are driven by differences in the Gibbs free energy between the reactants and the products of the reaction. Ultimately, in order to consider CO_2 as a 'chemical feedstock' the relative stability of the products as compared to the reactants must be noted. Fig. 2.1 shows the Gibbs free energy of formation of CO_2 and

related carbonaceous and other common substances (Jiang *et al.*, 2010).

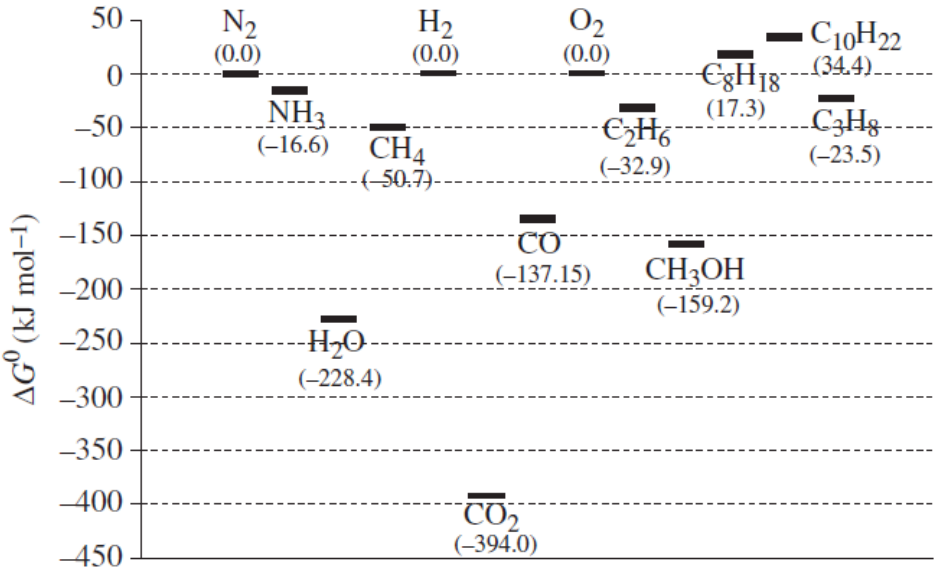

Fig. 2.1 Gibbs free energy of formation for selected chemicals

It is a common situation for CO_2 chemistry that not only is ΔG_r positive but also the reaction has high activation energy, so development of a suitable catalyst is required to achieve equilibrium more rapidly and at milder temperatures.

Carbon dioxide is currently being used in a number of industrial processes, as it shown in Table 2.1.

Table 2.1 Chemical produced commercially from CO_2 and their scale of production (North, 2015)

Chemical	Scale of production (tonne·year^{-1})
Urea	157,000,000
Aromatic polycarbonates	605,000
Salicylic acid	90,000
Cyclic carbonates	80,000
Aliphatic polycarbonates	76,000
Methanol	4000

As one can see, urea has by far the largest scale of production. It must also be noted that 14 million tonnes of CO_2 are used per annum as an additive in the hydrogenation of carbon monoxide to methanol (Mikkelsen *et al.*, 2010). The industry uses approximately 120 million tonnes of CO_2 per annum, excluding the CO_2 used in Enhanced Oil Recovery (EOR), where CO_2 is not chemically converted (Mikkelsen *et al.*, 2010). In addition, EOR allows the continuous use of a fossil resource such as oil which has been suggested to have very little or no impact on the life cycle CO_2 emissions compared to conventional extraction and use of oil (Jaramillo *et al.*, 2009).

2.3 Transformations of CO_2

In this section, a review of the main transformations of CO_2 with the potential to make a significant difference in the process industry will be presented. CDU is a vast area of research and as a consequence it is not intended to show in this section every possible transformation of CO_2 but only the ones with the greatest potential in the short to medium term.

2.3.1 Chemical transformations

One group of possible products that can be synthesised from CO_2 is the organic carbonates. Since organic carbonates are currently being produced from toxic substances such as phosgene, alternative reaction routes are being researched. Organic carbonates can be produced from the dehydration reaction of alcohols with carbon dioxide by using an appropriate catalyst, as shown in Scheme 2.2.

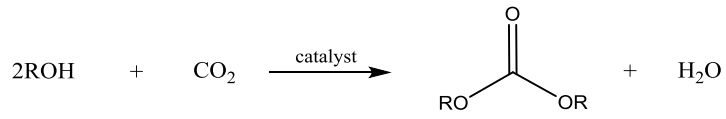

Scheme 2.2 Formation of carbonates from alcohols by a dehydrative condensation with CO_2

The main drawback of these reactions is that they do not proceed in high yields mainly due to the deactivation of the catalyst caused by the by-product water. Furthermore the syntheses of carbonates are often highly endothermic which requires energy being imported into the system or the utilisation of reactants with high free energy content so that the ΔG_r can be lowered (Mikkelsen *et al.*, 2010).

Another group of compounds that can be produced from CO_2 are organic carbamates. Carbamates are stable substances derived from the unstable carbamic acid when two molecules of primary or secondary amines react with CO_2, as depicted in Scheme 2.3. It is the mechanism on which the CO_2 capture using amines is based (Styring, 2015).

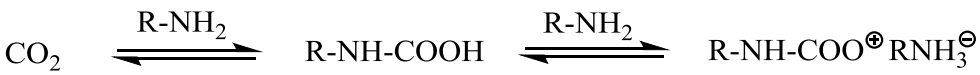

Scheme 2.3 Formation of alkylammonium alkylcarbamate from two molecules of amine (R-NH_2) and CO_2

Also using amines, substituted ureas such as N-N'-dialkylurea can be produced using ionic liquids as a reaction media and a dehydrating agent as shown in Scheme 2.4 (Mikkelsen *et al.*, 2010).

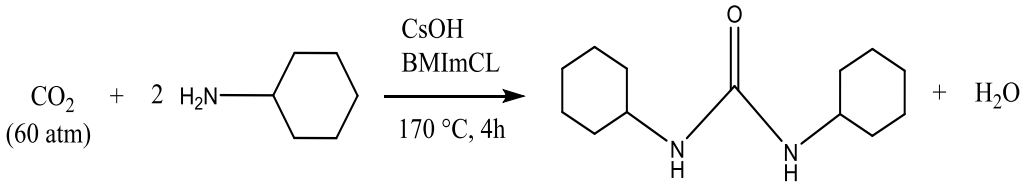

Scheme 2.4 Synthesis of substituted ureas from CO_2, primary amines and an ionic liquid (BMImCl)

Similarly, isocyanates can also be synthesised from CO_2 using amines over organometallic Ti^{IV} and U^{V} catalysts (Quadrelli *et al.*, 2011), as shown in Scheme 2.5.

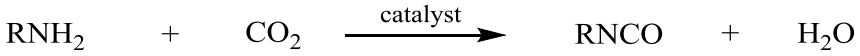

Scheme 2.5 Synthesis of isocyanates (RNCO) from an amine and CO_2

Another class of organic compounds that can be formed from CO_2 is carboxylic acids. Carboxylation of carbon nucleophiles with CO_2 as an electrophile is a basic method to obtain carboxylic acids. Grignard reagents can be used as nucleophiles which react with CO_2 at atmospheric pressure as shown in Scheme 2.6 (Mikkelsen *et al.*, 2010).

Scheme 2.6 Synthesis of carboxylic acids from CO_2 and a Grignard reagent

Esters and lactones can also be formed by combining some unsaturated compounds and carbon dioxide with metal complexes acting as catalysts as depicted in Scheme 2.7. Among the unsaturated compounds, olefins, dienes and acetylenes are good candidates for these reactions (Mikkelsen *et al.*, 2010).

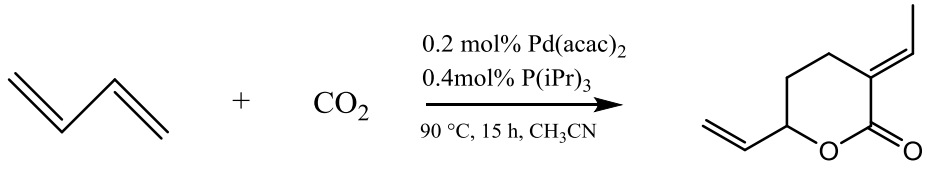

Scheme 2.7 Synthesis of a lactone from 1,3-butadiene and CO_2 over a palladium catalyst

Another way of chemically transform the molecule of CO_2 into value-added products is via its hydrogenation. CO can be manufactured in this from CO_2 via the reverse water gas shift reaction shown in Scheme 2.8.

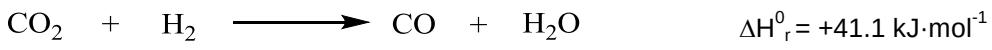

Scheme 2.8 The Reverse Water Gas Shift (RWGS) reaction

The water-gas-shift reaction has been extensively employed for the last several decades in order to adjust H_2/CO ratio in the syngas for Fischer-Tropsch applications (see section 4.1.3.5) and also to oxidise CO to CO_2 during production of H_2 by steam reforming of methane (Muradov, 2009). The reverse-water-gas-shift reaction, while not being historically attractive due to low demand, has attracted significant attention recently as a way to mitigate CO_2 emissions through CO_2 utilisation. The main issues regarding this reaction are its high enthalpy of reaction (requiring over 650 °C to significantly displace the equilibrium to CO and H_2) and the stability of the $ZnAl_2O_4$-based catalyst at such high temperature (Oh-Shim *et al.*, 2003).

Another class of processes that has been extensively investigated is the hydrogenation of CO_2 using both homogeneous and heterogeneous catalysts. Among this group, one of the most important reactions is the catalytic conversion of CO_2 to methanol as shown in Scheme 2.9. The hydrogenation carbon dioxide to produce methanol has attracted significant attention recently as a way to store off-peak electricity from renewable sources; methanol can be either used directly as a chemical feedstock or converted further to valuable products such as dimethyl ether or gasoline, among others.

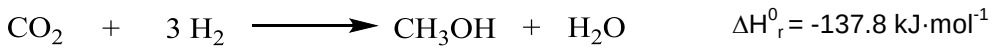

Scheme 2.9 Catalytic hydrogenative conversion of CO_2 to methanol

As one can see from Scheme 2.9, water is produced as a by-product from the above reaction; a third of the hydrogen is converted to water which can be considered wasteful. Furthermore, the process from CO_2 is less thermodynamically favourable than that from CO (Hu *et al.*, 2013). It becomes clear then that for successful implementation of this CO_2 utilization process to methanol at a commercial scale, further development of the catalysts being used (mainly copper, zinc and their oxides) is needed.

Another key factor in the industrial application of this technology is the availability of CO_2 and H_2. The first should not be an issue as long as a concentrated stream of CO_2 is available from processing plants (via CO_2 capture) such as steel making facilities, cement factories, among others, and also from power plants.

The availability of H_2 is more controversial since it is currently being manufactured from fossil fuels (mainly natural gas and naphtha) which in turn produces vast amounts of GHGs; therefore neither the reliance on fossil fuels is not solved nor the environmental performance of the

process over the life cycle. On the other hand, H_2 can be produced from water in a more environmentally sustainable way via electrochemical, thermal or photo-catalytic means as long as energy (in the form of heat, electricity or both) is brought to the process from renewable sources (Mikkelsen *et al.*, 2010).

There is an alternative way to produce methanol: the ‘‘Carnol-process’’. This is a synthetic method developed at the Brookhaven National Laboratory (USA), whereby hydrogen is produced by thermal decomposition of methane with solid carbon formed as a by-product. The produced hydrogen is reacted with CO_2 to produce methanol and water as a by-product (Mikkelsen *et al.*, 2010). The Carnol process is shown in Scheme 2.10.

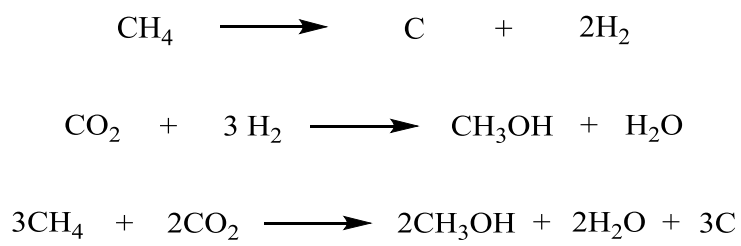

Scheme 2.10 Two-step Carnol process for methanol production

The hydrogenation of CO_2 can also be used to produce higher alcohols. These processes are thermodynamically favourable in terms of the Gibbs free energy, since water, a stable molecule with a highly positive free energy, is always produced as a by-product. An example of hydrogenation of CO_2 to ethanol using heterogeneous catalysis is shown in Scheme 2.11 (ΔH^0_r = -221.6 kJ·mol^{-1}).

Scheme 2.11 Hydrogenation of CO_2 to produce ethanol

A similar reaction to the one depicted above, is the hydrogenation of CO_2 to form hydrocarbons such as methane over nickel, ruthenium and rhodium catalysts known as the “Sabatier reaction” (Mikkelsen *et al.*, 2010), as shown in Scheme 2.12 (ΔH^0_r = -259.9 kJ·mol^{-1}).

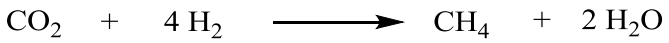

Scheme 2.12 Hydrogenation of CO_2 to produce methane (“Sabatier reaction”)

Each mole of CO_2 converted needs 4 moles of H_2 and again the availability of H_2 becomes crucial given the fact that these reactions are suitable for CO_2 mitigation only if renewable energy sources are utilised to manufacture hydrogen and to supply the heat required in those reactions.

Formic acid can also be manufactured from CO_2 hydrogenation over a Rhodium catalyst with bulky ligands at moderate to high pressures (up to 40 bar) (Mikkelsen *et al.*, 2010) as shown in Scheme 2.13.

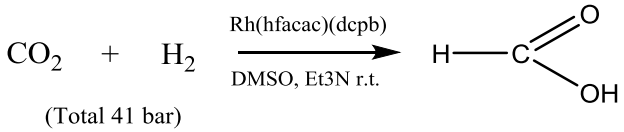

Scheme 2.13 Formation of formic acid by hydrogenation of CO_2 over a rhodium catalyst

2.3.2 Photo-electrocatalytic reduction of CO_2

Reducing CO_2 to value-added products by means of light energy is an area that has been intensively investigated. In an attempt to mimic the ability of green plants to reduce CO_2 to sugars, research in the area has concentrated on the development of materials that can be used as catalysts and energy converters for the photochemical process. Transitional metals are perhaps the most employed compounds to do

so since they absorb a wide portion of the solar light spectrum, have excited states that are maintain over time, are able to activate small molecules and cope well with degradation issues (Mikkelsen *et al.*, 2010).

Different systems have been researched for photochemical CO_2 reduction. The systems differ from each other depending on what is used as a photosensitizer and what is used as a catalyst. Typical systems consist of $Ru(bpy)_3^{2+}$ as both a photosensitizer and as a catalyst or $Ru(bpy)_3^{2+}$ as a photosensitizer and another metal complex as a catalyst (*Mikkelsen et al.*, 2010). There are dozens of systems that have been studied in the literature but a detailed review of these systems is beyond the scope of this thesis.

The photochemical process is usually carried out at room temperature and pressures, being the typical products formate ($HCOO^-$) and CO (Yan *et al.*, 2015). Formate is produced in these systems in a total quantum yield of 15% and CO as a minor product. It has been reported that, for the most optimised systems, the reduced products can be formed in a 40% yield (Mikkelsen *et al.*, 2010).

Although significant advances on photochemical reduction of CO_2 have been achieved in the recent times, challenges have been identified in order to make these systems more efficient and then being able to implement them commercially. The challenges are reproduced from Yan *et al.* (2015) as follows:

1. Photo-catalytic systems rely on the use of expensive and scarce noble metal in order to perform the photosynthetic process efficiently.
2. The current state of the art systems cannot reduce CO_2 efficiently enough with respect to the energy applied to the process.

3. A photosensitizer that can absorb a wide portion of the solar light spectrum and is highly catalytic for CO_2 reduction has not been identified to date.
4. A mechanism of electrocatalysis at the semiconductor interfaces is yet to be suggested.

2.3.3 Chemical and electrochemical reduction of CO_2

As discussed earlier in this chapter, during the hydrogenation of CO_2 to methanol one third of the hydrogen employed in the process (on a molar basis) is consumed to produce water. One way to avoid this is by reducing the CO_2 to CO by using another reducing agent different from H_2. This is the case of the (reverse) Boudouard reaction shown in Scheme 2.14.

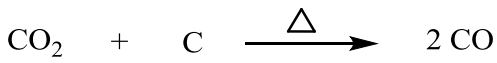

Scheme 2.14 Thermal reduction of CO_2 with carbon to produce carbon monxide

The thermal reaction between CO_2 and carbon (or a carbon rich source, e.g. coal, biomass, *etc.*) is highly endothermic and only progresses at temperatures of 800 °C or above (Mikkelsen *et al.*, 2010). Once CO has been produced, methanol can be synthesised by adding the right amount of H_2 to CO and then make syngas which can be converted into methanol over a heterogeneous catalyst (LeBlanc *et al.,* 1994).

CO_2 can also be reduced to CO in an electrolysis cell. In an electrolysis process, electricity is passed through a substance that undergoes chemical change. A typical example of this technology is water electrolysis to produce gaseous H_2 and O_2. Despite the different configurations of electrolysers, they all consist of an anode (positive electrode), a cathode (negative electrode) and an electrolyte that serves as the medium for charge movement between electrodes.

With respect to its operating temperature, electrolysers can be generally classified into:

a) Low Temperature Electrolysers (LTE): T<200 °C
b) High Temperature Electrolysers (THE); T>700 °C

Low temperature electrolysers such as alkaline and proton exchange membrane (PEM) have been available for many years with energy efficiencies of up to 75% (Laguna-Bercero, 2012). On the contrary, high temperature systems have only attracted significant attention in the last years. In spite of this, it is recognised that High Temperature Electrolysis has an important role to play in the future energy portfolio (Elder *et al*., 2015).

Recent investigations have shown that Solid Oxide Electrolysis Cells (SOEC) can be used to co-reduce simultaneously H_2O and CO_2 at high temperature (over 700 °C) to produce syngas (CO + H_2) (Zhan *et al.*, 2009; Stoots *et al.*, 2010; Ebbesen *et al.*, 2011; Graves *et al.*, 2011; Ebbesen *et al.*, 2012). The co-electrolysis of CO_2 and H_2O allows the formation of syngas (as opposed to “dry” CO_2 electrolysis that produces just CO) which is a precursor to synthetic fuels such as methanol, dimethyl ether or long chains hydrocarbons via Fischer-Tropsch synthesis (Elder *et al.*, 2015). Fig. 2.2, shows the operation of a SOEC.

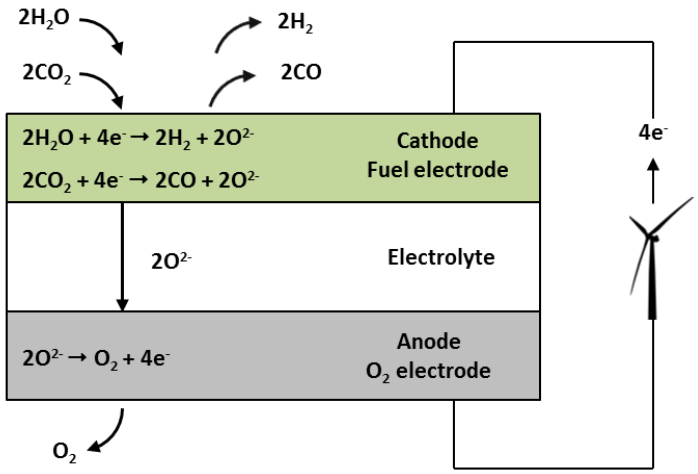

Fig. 2.2 A Solid Oxide Cell operating in electrolysis mode (adapted from Elder *et al.* (2015))

As depicted in Fig. 2.2, electricity is used to chemically reduce the feed (CO_2 and H_2O) to produce H_2 and CO plus oxide ions (O^{2-}), which travel through the electrolyte from cathode to anode.

Operating at higher temperatures can be justified after taking into consideration the thermodynamics of the process. Scheme 2.15 shows that the electrolytic reductions of carbon dioxide and water are both endothermic.

$$H_2O \longrightarrow H_2 + 1/2\ O_2 \quad \Delta H^0_r = 268\ kJ{\cdot}mol^{-1}$$

$$CO_2 \longrightarrow CO + 1/2\ O_2 \quad \Delta H^0_r = 283\ kJ{\cdot}mol^{-1}$$

Scheme 2.15 Electrochemical reduction of water and carbon dioxide

As one can see, the total energy required to electrolyse CO_2 and H_2 at constant temperature and pressure corresponds to the enthalpy of reaction. According to the definition of the Gibbs free energy, the following is true: $\Delta G_r = \Delta H_r - T\Delta S_r$. In other words and for the co-

electrolysis of CO_2 and H_2O, the total energy required for the co-electrolysis process to take place (ΔH_r) is composed of a free energy term (ΔG_r) and a entropy term ($T\Delta S_r$), where ΔG_r must be provided as electrical energy, while the term $T\Delta S_r$ must be provided as thermal energy. Therefore, as the temperature increases, the electrical energy required decreases, making the process more efficient. In addition, reaction kinetics increase at high temperature according to Arrhenius equation, which leads to a decreased internal resistance in the cell and then, following the Ohm's law, a greater current for the same voltage (Elder *et al.*, 2015).

As for the materials employed to manufacture the SOEC, different systems have been suggested depending on whether they are to be used as the electrolyte, the fuel electrode or the oxygen electrode. An electrolyte material must have good oxide ion conductivity but very low electronic conductivity, while being chemically stable at different operating conditions and having a thermal expansion coefficient similar to that of the electrodes. Four systems have been suggested in the literature as having high oxide ion conductivity: electrolytes based on zirconia (ZrO_2), ceria (CeO_2), lanthanum gallate ($LaGaO_3$) and bismuth oxide containing materials (Elder *et al.*, 2015). The addition of other materials, known as dopants, increases the ion conductivity while minimising the electronic conductivity. The most commonly used system of this kind is known as yttria stabilised zirconia (YSZ).

The selection of materials to act as electrodes is also challenging. Besides the issues that apply to the electrolyte, such as chemical and thermal stability, other specific constraints affect the material selection and design of electrodes. The performance of the electrode is determined by how efficient the interaction between ionic, electronic and gas phases is. The region where these three phases co-exist forming a reaction site is called the triple phase boundary (TPB) and the larger this point is, the higher the electrode efficiency (Elder *et al.*,

2015); therefore, understanding the TPB is of paramount importance when designing efficient electrodes.

2.3.4 Biological transformations of CO_2

Photosynthesis is the process by which green plants use light energy from the Sun to convert CO_2 and water into carbohydrate molecules, such as sugars. Therefore, replicating natural photosynthesis for large scale CO_2 transformations is an area of research that has attracted significant attention in the last years.

In general, photosynthesis is an inefficient process, especially in larger plants which use a vast amount of energy to build their structure. On the contrary, smaller plants experience a considerably higher photosynthetic efficiency since they do not need to use as much energy to build their structure. An extreme example of these small plants is the case of micro-algae (also called single-cell algae) which are the simplest and smallest form of vegetal life. Unlike larger plants, microalgae rely only on water as their supporting structure, allowing the cells to use a much larger amount of energy for reproduction (Mikkelsen *et al.*, 2010). It can be then expected that microalgae are capable of using solar light to convert CO_2 with an efficiency ten times greater than that of terrestrial plants (Mikkelsen *et al.*, 2010).

Due to the potential of microalgae cultivation for CO_2 fixation, research has focussed on finding suitable algal strains. Much of the research in the field has concentrated on the development of bioreactors. Due to the fact that the fixation rate of CO_2 by the algae is very slow, photobioreactors systems are very important since they allow the deployment of a vast area of algae cultivation which enhances the fixation of CO_2. The most widely used type of photobioreactor currently being exploited on a commercial scale is an open pond called a raceway pond (Mikkelsen *et al.*, 2010). However, open pond photo-bioreactors often suffer from contamination by other organisms and

current research is going towards the optimization of closed systems. It is claimed that closed systems give an increased algae concentration which translates into an easier harvesting process (Mikkelsen *et al.*, 2010).

A different type of biological transformation of CO_2 is that carried out through non-photosynthetic pathways by anaerobic microorganisms (bacteria methanogens). This type of microorganism grows optimally between 20 and 95 °C and only uses carbon monoxide and hydrogen or carbon dioxide and hydrogen as the source of carbon and energy (Mikkelsen *et al.*, 2010). Scheme 2.12 shows the biocatalytic conversion of CO_2 into CH_4 by methanogen organisms.

This biological conversion of CO_2 to methane is able to operate at moderate temperatures (around 35 °C) and is not affected by the presence of other gases in the systems besides CO_2 and H_2O. By contrast, the catalytic hydrogenation of CO_2 into methane (also known as the Sabatier reaction), require temperatures of up to 700 °C and pressures of up to 20 atm (Mikkelsen *et al.,* 2010). In addition the catalyst used in the reaction suffers from poisoning by sulphur present in the flue gas. Therefore the synthesis of methane from CO_2 and H_2 via biological pathways offers an alternative to the conventional thermal process. It must be noted that large scale production of methane by methanogens is only suitable for CO_2 mitigation provided that renewable energy sources are utilised to manufacture hydrogen.

2.3.5 Reforming

Synthesis gas (a mixture consisting mainly of CO and H_2) is industrially manufactured by reacting methane and steam; a process called “steam methane reforming” (Scheme 2.16).

$$CH_4 + H_2O \longrightarrow CO + 3H_2 \qquad \Delta H^0_r = +206.3\ kJ{\cdot}mol^{-1}$$

Scheme 2.16 Steam methane reforming

As opposed to steam reforming, “dry” methane reforming can be employed to manufacture synthesis gas by reacting CO_2 and methane over a nickel-based catalyst. The reaction (Scheme 2.17) is strongly endothermic and only progresses at elevated temperatures of up to 1000 °C (Mikkelsen *et al.*, 2010).

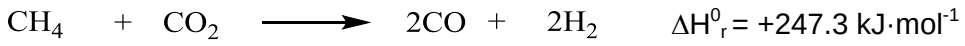

Scheme 2.17 “Dry” methane reforming

A similar process to form syngas is known as “bi-reforming”, where steam reforming and dry reforming are combined at temperatures in the range 800-1000 °C (Scheme 2.18).

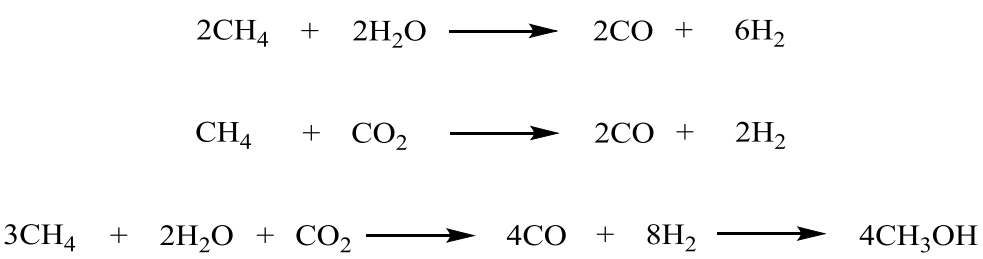

Scheme 2.18 Bireforming process involving a 3:2:1 ratio of $CH_4/H_2O/CO_2$

Regarding industrial application, catalyst deactivation is the main problem with reforming reactions, especially with dry reforming, mainly due to coke formation, which is thermodynamically favoured at temperatures below 900 °C. The formation of coke has been attributed to the Boudouard reaction and the cracking of methane shown in Scheme 2.19 (Mikkelsen *et al.*, 2010).

Scheme 2.19 Formation of carbon from the Boudouard reaction and by cracking of methane

Since the equilibrium of the Boudouard reaction can be shifted to the left by increasing the temperature, one way of minimising coke formation would be to perform the dry reforming reaction at temperatures higher than 900 °C; however, catalyst stability becomes an issue in this range of temperatures (Mikkelsen *et al.*, 2010). Therefore, research is currently focussing on the development of catalyst (mainly nickel-based) that can operate at high temperatures and for a long period of time.

2.3.6 Synthesis of higher hydrocarbons

Despite the fact that different alternatives have been proposed to replace fossil fuels for the transport sector, such as hydrogen fuel cells and Li-ion batteries, it is recognised that petrol and diesel vehicles will continue to dominate our transport requirements for, at least, the next two decades (British Petroleum, 2014). The concept of carbon-neutral hydrocarbon fuels from CO_2 has attracted significant attention recently as they can help stabilize GHG emissions throughout the life cycle, while securing the energy supply. The idea underlying this approach is to take the CO_2 back into a hydrocarbon molecule, provided that all energy sources used in the processes and in the manufacturing of any raw materials, *e.g.* hydrogen, are also carbon neutral.

The conversion of CO_2 into higher liquid hydrocarbons can be achieved via *direct* or *indirect* routes, as depicted in Fig. 2.3.

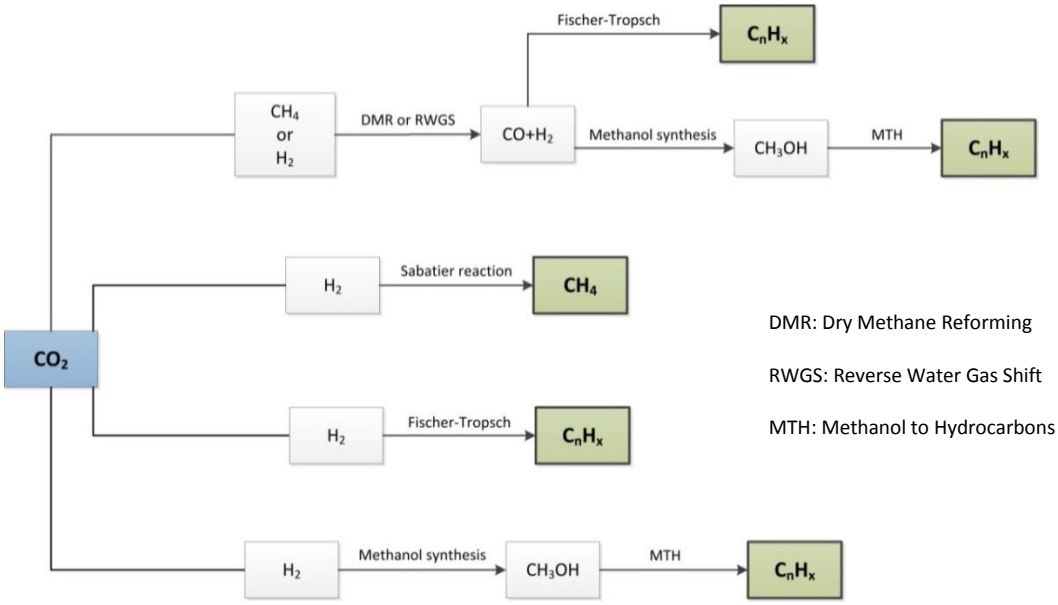

Fig. 2.3 Direct and indirect routes to hydrocarbon fuels (adapted from France *et al.* (2015))

In Fig. 2.3, the *indirect routes* (top level in Fig. 2.3) are those which employ synthesis gas as an intermediate from which hydrocarbons or oxygenates (such as methanol) are produced through Fischer-Tropsch synthesis or methanol synthesis respectively.

Direct routes for the conversion of CO_2 into a synthetic hydrocarbon fuel employ the reaction between CO_2 and H_2 over a modified Fischer-Tropsch catalyst (Ni-based or Fe-based). In this process, an initial reverse water gas shift reaction takes place generating syngas followed by a Fischer-Tropsch synthesis whereby higher hydrocarbons are produced (France *et al.*, 2015).

The hydrocarbon fuel production from CO_2 allows for the use of a carbon neutral fuel that is entirely compatible with current transport infrastructure and vehicles. Furthermore, this fuel contains no sulphur, nitrogen and metal-containing compounds and it has a very low content of aromatics. It seems then that if renewable resources are used in the

manufacture of such fuels, they might have a significant contribution in the future transport fuels portfolio while reducing CO_2 emissions.

2.3.7 Inorganic transformations

The conversion of CO_2 into solid carbonates – a process known as carbon mineralisation, is being actively researched since it may allow permanently storage of CO_2 into solid materials. The process combines CO_2 with minerals that contain calcium and/or magnesium to produce stable solid magnesium and calcium carbonates. Although the process is thermodynamically favoured, it is kinetically challenging; therefore, most of the research in the area is focussed on accelerating the processes involved.

It has been suggested by researchers that instead of injecting CO_2 into geological formations to permanently store it – a process known as *in situ carbon mineralization*, the minerals can be mined and reacted with CO_2 to produce value-added products such as carbonates – a process known as *ex situ carbon mineralization* (Gadikota & Park, 2015). This process may solve the issues associated with the long-term stability of the geologically stored CO_2.

There are two schemes for carbon mineralization: the *engineered weathering of silicate minerals* and *carbonation of alkaline industrial wastes*. The first approach considers the reaction between CO_2 and earth abundant minerals such as olivine [$(Mg,Fe)_2SiO_4$] and serpentine [$(Mg,Fe)_3(OH)_4(Si_3O_5)$]. The minerals need to be mined and ground for ex situ carbon mineralization. The second scheme uses alkaline industrial wastes such as fly ash, bottom ash, cement kiln dust or steel slag, among others, and combines them with CO_2 to produce solid carbonates. The characteristics of each of these two approaches are summarised in Table 2.2.

Table 2.2 Characteristics of silicate minerals and industrial wastes routes (adapted from Gadikota & Park (2015))

Silicate minerals	Industrial wastes
CO_2 storage capacity is in the order of 10^{12} tonnes of carbon.	Limited to about 300 Mt of wastes produced annually
Crystalline structure may be an obstacle to reactivity	Lack of crystalline structure and disordered surfaces improve reactivity
Requires pre-processing such as mining, crushing, dissolution, *etc.*	Pre-processing is not necessary.
CO_2 needs to be sent to the mining site.	In many cases, CO_2 and industrial wastes are produced at the same facility.
Depending on the type of mineral, extreme reaction conditions may be needed to ensure high conversions.	Due to their high reactivity, high conversions are achieved even at room temperature.

Carbon mineralization can also be used for CO_2 capture from the atmosphere by using basic absorbents such as calcium hydroxide $Ca(OH)_2$ or potassium hydroxide KOH and combining them with CO_2. In these processes calcium carbonate $CaCO_3$ and potassium carbonate K_2CO_3 are formed respectively. The CO_2 absorption is an exothermic reaction while the desorption is an endothermic reaction, which is an obstacle to commercial implementation of this technology due to energy costs associated with the release of CO_2; however, there is an ongoing effort towards the development of carbon mineralization to capture CO_2 from the atmosphere. One promising process consists of the reaction between KOH and CO_2 to form K_2CO_3, which is then electrolysed in water. This allows not only the release of CO_2 but also the production of gaseous H_2, with a limited input of energy (Mikkelsen *et al.*, 2010).

2.3.8 Integrated capture and conversion

Integrated CO_2 utilisation consists of processes in which the capture of CO_2 from a practical industrial stream is not necessary. Instead, the gaseous stream containing CO_2 is used, which avoids the costs associated with CO_2 capture. There are two main processes that have been suggested suitable for integrated CO_2 utilisation using flue gas directly: mineralisation and tri-reforming.

Mineralisation using flue gas is a similar process to the mineralisation of CO_2 explained in section 2.3.7, being the main difference that CO_2 capture is not required in this case. It is beyond the scope of this document to go deeper on this kind of processes, given their similarities with ex situ mineralisation processes. It is worth highlighting though that flue gas mineralisation processes differ from each other in the type of feedstock used, the operating conditions (pressure and temperature) and the additives being used.

The tri-reforming process directly uses flue gas and methane for the production of syngas. This process, that has been actively investigated, combines the endothermic CO_2 reforming of methane (also known as “dry” reforming) and steam reforming of methane with the exothermic partial oxidation of methane and catalytic combustion of methane in a single reactor (Pekdemir, 2015). Table 2.3 show the reactions involved and their standard enthalpy of reaction ($\Delta H°_{298}$).

Table 2.3 Main reactions of the tri-reforming process

Reaction name	Chemical reaction	$\Delta H°_{298}$ (kJ·mol^{-1})
DRM: Dry Reforming of Methane	$CH_4 + CO_2 \rightarrow 2CO(g) + 2H_2(g)$	+247.3
SRM: Steam Reforming of Methane	$CH_4 + H_2O \rightarrow CO_2(g) + 3H_2(g)$	+206.3
POM: Partial Oxidation of Methane	$CH_4 + 1/2O_2 \rightarrow CO(g) + 3H_2(g)$	-35.6
CCM: Catalytic Combustion of Methane	$CH_4 + 2O_2 \rightarrow CO_2(g) + 2H_2O(g)$	-880.0

This process makes use of the CO_2 as well as the H_2O and O_2 in the fluegas. The incorporation of the last two reactions produces heat that is used in the first two reactions. The demand of O_2 can be satisfied by injecting air in the reactor, since it has been suggested that the presence of N_2 in the reactor should not pose a problem for the process (Halmann & Steinfeld, 2006). The CH_4 can be supplied from natural gas, but in order to make the process as environmentally benign as possible it can also be supplied from biogas (a methane-rich gaseous mixture consisting mainly of CH_4, CO_2 and trace impurities). Conversions of up to 97% of CH_4 and 80% of CO_2 have been reported over a suitable catalysts at equilibrium temperature of 850 °C and atmospheric pressure (Song & Pan, 2004).

2.3.9 Prospective in CO_2 conversions

Many of the processes described in this section have the potential of mitigating CO_2 emissions with large scale use of CO_2 (Mikkelsen *et al.*, 2010). It is believed though that the development of suitable catalysts will play a key role in the conversion of CO_2 on an industrial scale. There are therefore ongoing efforts to develop catalytic systems that can achieve simultaneously high energy efficiency, high reaction rates and high value products (Hu *et al.*, 2013). However, the fact that many

of the reaction mechanisms involved in CO_2 conversions are not well known has been identified as an hindrance to commercial deployment (Hu *et al.*, 2013).

Another important aspect in CO_2 utilisation is that, if a significant contribution to reducing the accumulation of CO_2 in the atmosphere is to be made, the raw materials, *e.g.* hydrogen and energy inputs, *e.g.* electricity to the processes must come from renewable, low-carbon sources. This will ensure that the environmental impacts (global warming potential, acidification, *etc.*) associated with the processes are low over the life cycle of the system considered.

The cost of developing the aforementioned technologies could also prevent them from becoming a reality, since conventional, fossil resources are usually cheaper. It is crucial then that public and private organizations work closely in order to develop the processes at the right pace so that eventually costs would be brought down (Hu *et al.*, 2013).

2.4 Previous studies of CCU systems

As in any other chemical system, process simulations are very valuable if serious effort is to be made to consider commercial implementation of syngas production from CO_2/H_2O co-electrolysis. Ideally a cradle-to-grave life cycle assessment is needed in order to evaluate overall process efficiency, cost and environmental impacts over the whole life cycle. A study by O'Brien *et al.* (2009) using UniSim process simulator showed that a high temperature electrolyser operating at 800 °C coupled with a high temperature gas cooled nuclear reactor achieved up to 50% overall efficiency. The main product from the co-electrolysis plant was syngas. The integral co-electrolysis model assumes local chemical equilibrium among the four process-gas species (CO_2, H_2O, H_2 and CO) via the water-gas shift reaction. Results from the UniSim electrolysis model were validated by comparison with results obtained from a fully three-dimensional computational fluid dynamics model

developed using FLUENT, and by comparison with experimental data. The authors did not consider in their model the methane production from syngas (methanation reaction). The main drawback from this study is that it is assumed that a stream of pure CO_2 is readily available in the plant, which is fed into the co-electrolyser. This is an oversimplification especially when the source of electricity to drive the co-electrolysis process is assumed to be a nuclear plant, where a source of CO_2 is not available. In a real world application, CO_2 would have to be captured from an industrial source, *e.g.* a coal-fired power plant, and transported to the co-electrolysis plant site. The CO_2 capture and transport processes will lower considerably the overall efficiency of the process. In addition, results on syngas production costs were not provided by this study.

A techno-economic analysis study by Fu *et al.* (2010) also considered high temperature steam/CO_2 electrolysis, in this case, for the production of Fischer-Tropsch liquid fuels. As in the study by O'Brien *et al.* (2009), the calculation of the composition of the cathode outlet gas, a local chemical equilibrium model was used, where a chemical equilibrium of the RWGS reaction at the cathode outlet temperature was assumed. The methanation reaction was not considered in the model. The electrolyser operated at 800 ^{o}C and was fed with CO_2 and steam. Conversely to the study by O'Brien *et al.* (2009), Fu *et al.* (2010) assumed that the electrolyser was operated in thermoneutral mode, *i.e.* the enthalpy increment of the reaction system is exactly balanced by the electrical energy input to the system and therefore, an external heat input to the electrolyser is not needed. Nevertheless, the steam/CO_2 feedstock needs to be heated up to 800 °C prior to be fed to the electrolyser (68 kW heat load). The authors do not specify the source of this high-temperature heat. The results showed that FT diesel could be produced at a price of 1.6 €·litre^{-1} (baseline scenario: CO_2 price 160 €·t^{-1}, electricity price 56 €·MWh^{-1}, no O_2 sale credit).

Another techno-economic analysis study by Becker *et al.* (2012) was carried out to assess the feasibility of synthetic fuel production via high temperature co-electrolysis of steam and CO_2. In this case, the methanation reaction (methane production from syngas) was considered. The authors modelled a system in which CO_2 captured from the flue-gases of a coal-fired power plant was fed along with steam into a high temperature electrolyser (800 °C) to produce syngas. The syngas was converted in a slurry bubble column FT synthesis reactor and the synthetic fuel upgrading island was also included in the study. The authors demonstrate that methane formation is negligible at atmospheric pressure, which validates the assumption of water-gas-shift equilibrium. This study is the only one of the three assessed in this section that considered the conversion of CO_2 to fuels from the source (power plant flue gas) to the final market product (gasoline and diesel). Furthermore, the authors developed a comprehensive energy integration methodology so that the combustion of the FT offgas stream can be used to pre-heat the steam/CO_2 feedstock up to 800 °C. This is particularly interesting since the authors claim that the only plant inputs needed to produce gasoline and diesel are water, CO_2 and electricity.

2.5 CO_2 capture from power plants

The purpose of CO_2 capture is to generate a concentrated stream of pure CO_2 so that it can be reacted with other chemicals to produce value added products (fuels, chemicals, *etc.*) given sufficient input of energy and a suitable catalyst. Depending on the process and/or source of CO_2 in question, there are three main approaches to capturing the CO_2 generated from the fossil fuel feed: Post-combustion capture, pre-combustion capture and oxy-combustion (oxyfuel) technology. Fig. 2.4 gives an overview of CO_2 capture systems.

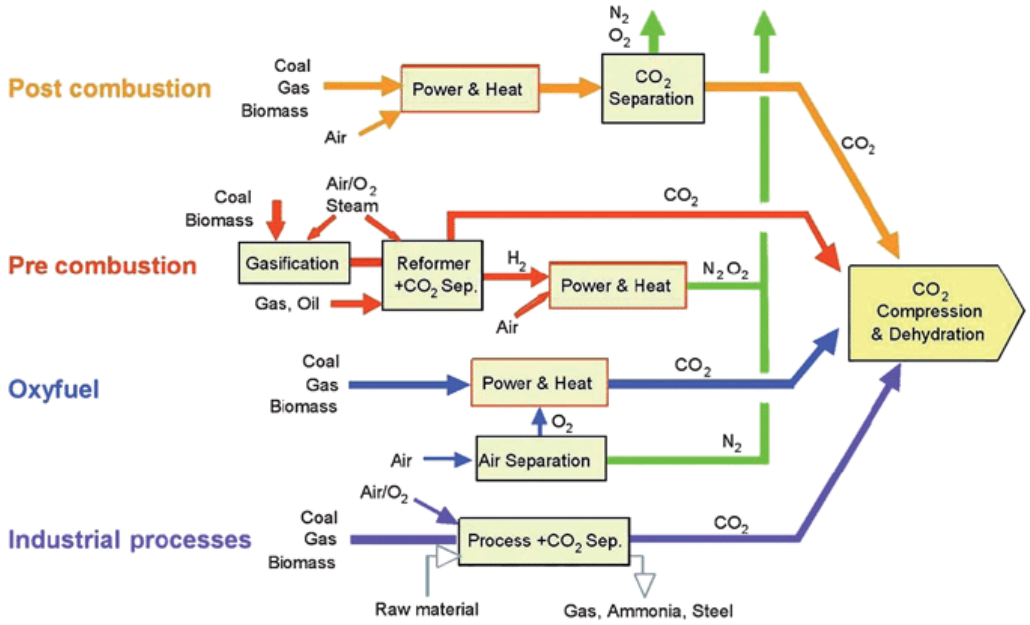

Fig. 2.4 Overview of CO_2 capture technologies (Working Group III of the Intergovernmental Panel on Climate Change, 2005)

2.5.1 Post-combustion capture

Post-combustion systems separate CO_2 from the flue gases produced by the combustion of the fuel in air. It is widely believed that post combustion technologies present the greatest near term potential for reduction of CO_2 emissions because they can be retrofitted to existing fossil fuel-based power plants and may be applied to other industrial emitters of CO_2 such as cement and steel production plants. Fig. 2.5 depicts a simplified post-combustion capture block diagram.

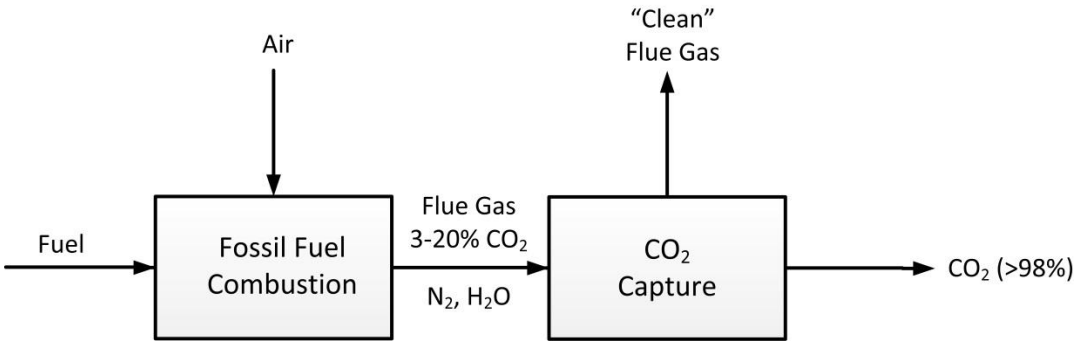

Fig. 2.5 A simplified block diagram of post-combustion CO_2 capture

Current operational challenges in post-combustion capture have been addressed through the use of different methods such as chemical absorption, adsorption, gas separation membranes, and cryogenic distillation. The basic operation as well as advantages and disadvantages of these technologies are highlighted in Table 2.4.

Table 2.4 Basic operation of post-combustion capture technologies (Spigarelli & Kawatra, 2013)

	Operations	Advantages	Disadvantages
Absorption	A gaseous component (CO_2) is separated from a gas stream by the use of an absorbent.	End of the pipe solution. Allows flexibility of operation in plants.	Costly technology due to energy penalties. Corrosion and Environmental concerns.
Adsorption	A gaseous component (CO_2) is separated from a gas stream by the use of an adsorbent.	Allows CO_2 capture from either post or pre-combustion gas streams.	Technology still under research. Adsorbent recovery issues.
Membrane separation	Membrane acts as a filter to remove one or more gas components from a mixture and generate a component rich (CO_2) permeate.	Currently used commercially for CO_2 removal from natural gas. High capture efficiency.	Very sensitive to impurities in use gas. High operating costs.
Cryogenic distillation	CO_2 is physically separated from other gas stream constituents on the basis of dew and sublimation points.	It has been utilised for years to separate atmospheric air into its primary components. No chemical reagents are needed.	Limited to high CO_2 concentrations (>70% vol.). High capital cost of equipment as well as high operating cost

Despite the fact that carbon dioxide capture using solid adsorbents is considered one of the most promising technologies for CCS (Figueroa *et al.*, 2008), of all the approaches that can be taken for post combustion capture of CO_2, amine absorption is currently the most mature technology on the market.

2.5.2 Pre-combustion capture

In pre-combustion technologies the primary fuel (coal, natural gas, *etc.*) is processed in a gasifier using air or (preferably) oxygen and steam to produce syngas (a mixture comprising mainly CO and H_2). CO is then converted to CO_2 to produce a gas stream consisting of CO_2 and the H_2 from which the CO_2 is separated. Since the CO_2 is captured and stored, H_2 gas stream is then used as a carbon-free fuel source for energy production. Pre-combustion can be used in natural gas or coal based plants that employ Integrated Gasification Combined Cycle (IGCC) technology (Working Group III of the Intergovernmental Panel on Climate Change, 2005). Fig. 2.6 depicts a simplified pre-combustion capture block diagram.

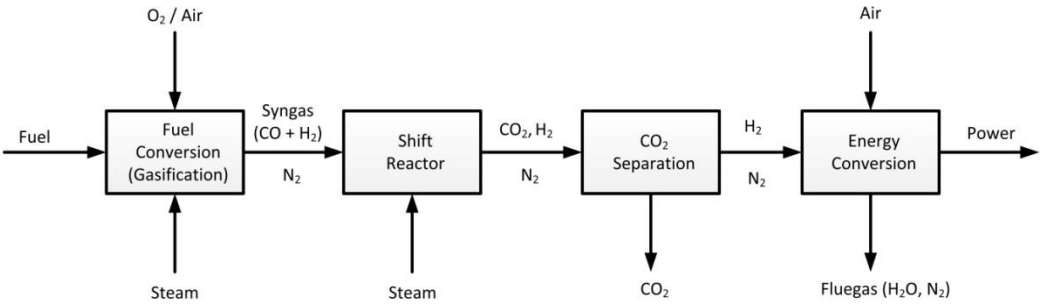

Fig. 2.6 Block diagram for pre-combustion capture of CO_2

Currently, four pre-combustion capture technologies exist, namely: Selexol, Rectisol, Fluor, and Purisol. Going into too much depth here is beyond the scope of this research. However, it must be noted that these pre-combustion technologies are proven industrial scale processes (Gale *et al.*, 2009). The fact that increased CO_2 partial pressure allows

for efficient separation techniques or solvent regeneration by pressure reduction is much more energy efficient than heating the solvent (as in post-combustion technologies). On the contrary, a disadvantage that must be noted is the fact that for non-gaseous feed stocks (*i.e.* coal or crude oil) the syngas stream must be cleaned due to impurities present in the material being gasified (Gale *et al.*, 2009). Furthermore, IGCC systems have high investment and operating costs (Kanniche *et al.*, 2010).

2.5.3 Oxy-combustion (Oxy-fuel)

In oxy-combustion technologies the fuel is combusted in an O_2/CO_2 atmosphere as opposed to air. This produces a gas stream containing CO_2, H_2O, and other trace impurities. Cooling and compressing the gas stream removes the water vapour. Fig. 2.7 depicts a simplified oxy-combustion block diagram.

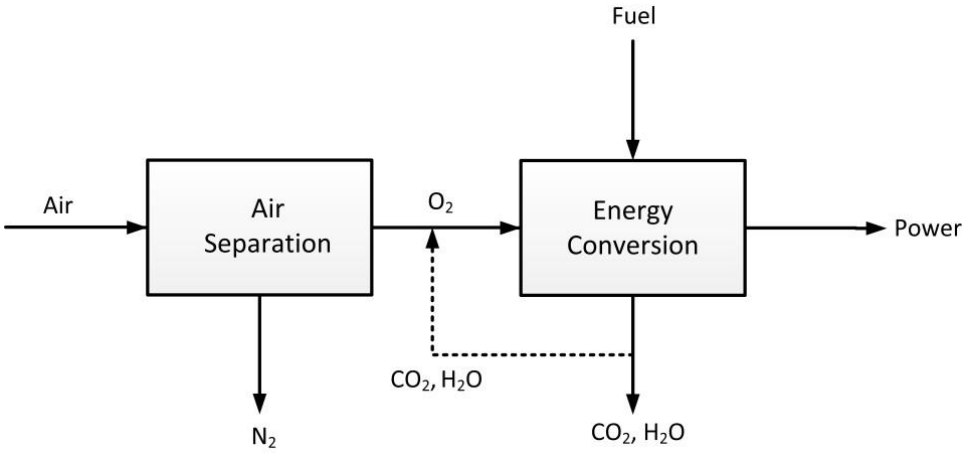

Fig. 2.7 Simplified block diagram of oxy-fuel processes

A fraction of the flue gas stream (CO_2 and H_2O) may be recycled and added to the oxygen stream to control the flame temperature in the

furnace since pure oxygen has a combustion temperature of about 3500 °C (Spigarelli & Kawatra, 2013).

This technology may have potential as a capture option since the concentration of N_2 in the flue gas is (ideally) zero, as opposed to when air is used for combustion, which lowers the processing needed (Working Group III of the Intergovernmental Panel on Climate Change, 2005).

Although oxy-fuel systems are able to capture nearly all of the CO_2, there are drawbacks. Firstly, large volume of O_2 is required which increases the capital and operating costs. Secondly, oxy-combustion equipment increases plant footprint (Spigarelli & Kawatra, 2013).

2.5.4 CO_2 capture using ionic liquids

As previously discussed in this chapter, addressing climate change concerns during the coming decades will likely require significant contributions from CCS (Zhang *et al*., 2012) and CDU (Styring *et al.*, 2011). Currently, the most developed large scale CO_2 capture technologies that can produce an enriched stream of CO_2 are based on amine solvents such as monoethanolamine (MEA) (Notz *et al*., 2011; Rubin *et al*., 2012; Zhu *et al*., 2013). The advantages of using such solvent rely on the fact that they offer a high CO_2 absorption capacity and relatively low cost. On the contrary, they are generally prone to evaporate, liable to be corrosive at elevated temperatures and expensive to regenerate due to the energy penalty (Zhu *et al.*, 2013; Kittel *et al.*, 2009; Abu-zahra *et al.*, 2007). In recent years, alternative materials have been suggested for CO_2 capture, including: KS-1 solvent, Econamine FG+SM, ionic liquids, amidoxim, metal–organic frameworks, microporous organic polymers, zeolitic imidazolate frameworks and membranes, among others (Zhang *et al.*, 2012).

Ionic liquids are among the class of novel solvents that have high CO_2 affinity and therefore have attracted significant attention in recent years (Brennecke & Gurkan, 2010; Zhang *et al.*, 2012). They offer a number of advantages against amine-based solvents such as their extremely low vapour pressure, which prevents the solvent from being released to the atmosphere and causes lower energy penalty in the CO_2 stripping/solvent regeneration, and their low corrosivity (Reddy, 2009; Zhang *et al.*, 2012). In fact, a CO_2 capture simulation study performed by Shiflett *et al*. (2010) showed a 16% reduction in the energy penalty of the process when using [bmim][Ac] ionic liquid compared to a commercial monoethanolamine (MEA) process. Other aspects such as the cost of running such a plant remain unclear due to the high selling price of the ionic liquid, although it is expected to decrease as the demand for the solvent increases. Another key feature of ionic liquids for CO_2 capture is the vast number of possible combinations of cation and anion, which allows the solvent to be custom made for specific applications (Lee & Lin, 2015).

Currently, research efforts focus on reducing the issues concerned with industrial applications of ionic liquids. These efforts can be summarised as follows (Zhang *et al*., 2012):

1. The synthesis of novel ionic liquids with enhanced absorption capacity by functionalization with an amine or other groups.
2. Designing supported ionic liquids membrane materials (SILMs) that allow the tunability of the system´s physical/chemical properties for specific applications. In most cases, the tunability of the properties consists of reducing the viscosity of the sorbent in order to increase the gas mass transfer rate into the liquid.
3. The measurement and model-based estimation of the physical/chemical properties of the multi-component systems containing the gaseous species present in the flue gas (CO_2, N_2, O_2, *etc.*) and the ionic liquids.

4. The study of the transport properties, kinetics and the design of CO_2 capture processes with ionic liquids considering real industrial gases. Furthermore, the assessment and comparison of energy consumption and economic performance of CO_2 capture processes using ionic liquids is of paramount importance.

5. The life cycle environmental impacts, toxicity and risk assessment of ionic liquids have been subjected to intense research; however, life cycle assessment (LCA) studies on specific ionic liquids used in CO_2 capture systems are scarce.

Point 3 in the above list is especially important since experimental data are often needed to determine the physical properties of the ionic liquid as well as its interaction with the gaseous species. Properties such as heat capacity, liquid viscosity, liquid density or vapour-liquid-equilibrium (VLE) data are often needed if robust models are to be built. The need for developing costly and time consuming experimental set-ups to measure physical/chemical properties of the pure ionic liquids and the ionic liquid-gas mixture is seen as one of the hindrances to developing process simulation studies (Basha *et al.*, 2014; Basha *et al.*, 2013; Shiflett *et al.*, 2010). In this study, a novel methodology is developed to determine the suitability of ionic liquids for use in CO_2 capture processes as well as the costs associated with such processes. The methodology is based on the predictive COSMO-SAC activity coefficient model, where the interaction between the gas and the IL is determined through the screening charges on the molecular surfaces obtained from quantum mechanical solvation calculations (Lee & Lin, 2015); therefore, no experimental data are needed to quantify the interaction between the gases and the liquid. The methodology can also be used to obtain the mass and energy flows required to perform the LCA studies highlighted in point 5 of the above list.

2.6 Emerging industrial applications of CO_2 transformations

In the previous section, developing technologies for CO_2 utilisation have been summarised. The range of products is broad with complex processes involved, which make them difficult to scale-up. Demo and pilot plants have been built in the recent years focussing mainly on lower alcohols, polymers, reduction reactions and mineral carbonates. The following sections will provide a summary of these emerging applications for carbon dioxide conversion.

2.6.1 Methanol plants

Methanol is mainly used as a chemical feedstock and to a lesser extent for use as fuel blends. It is one of the top commodity chemicals with a global demand of 61 Mt in 2012 (Armstrong, 2015). Due to this fact and that it is the simplest of the alcohols (which eases the synthesis process), methanol is an ideal candidate for CO_2 utilisation. In addition, methanol is currently produced via catalytic hydrogenation of CO, where CO and hydrogen are produced from steam reforming of methane (or natural gas). This gives the process a high carbon footprint, which brings another reason to consider the manufacture of methanol from CO_2.

The process to manufacture methanol from CO_2 is described in Scheme 2.9. It is not a complex process as it only needs CO_2, H_2 and energy. However, hydrogen needs to be produced and in order to make the process as environmentally benign as possible, the preferable way of manufacturing H_2 is via water electrolysis, which is costly. Furthermore, a concentrated stream of CO_2 is required too.

The Iceland-based company Carbon Recycling International Ltd has been producing renewable methanol at its pilot plant since 2007. The process benefits from being located at a volcanic area, from where it takes the CO_2. The electricity required to electrolyse water and manufacture H_2 is also generated at a nearby geothermal power plant.

The current production rate is 5 million litres per annum that are sold as a fuel blend (CRI Ltd, 2012).The company has signed an agreement with Methanex Inc., the world's largest producer of methanol, to build large-scale projects (50 million litres per annum), which can be replicated worldwide (Methanex Corporation, 2013).

The Japanese chemical company Mitsui Chemicals utilises CO_2 to produce 100 tonnes of methanol per annum at their pilot plant in Osaka. This process uses the flue gas that also contains NO_x and SO_x from their ethylene production plant and water photolysis to synthesize hydrogen (Armstrong, 2015). The reaction is carried out over a copper- and zinc-based catalyst and the final product is used as a precursor for plastic production (Armstrong, 2015).

2.6.2 CO_2 reduction pilot plants

Mantra Venture Group is using electrochemical reduction to produce formic acid and formate salts from CO_2. The company has finished the design stage of their pilot plant at the Lafarge cement plant in Richmond, Canada, with a design capacity of 100 kg of CO_2 transformed per day (Mantra Energy, 2014). The aim of Mantra Venture Group is to use the flue gas from the cement plant and renewable electricity to produce chemicals that do not need further processing and that are exportable directly from the plant (Armstrong, 2015).

2.6.3 Reforming processes

The Korea Gas Corporation (KOGAS) is using its proprietary adiabatic auto-thermal technology to synthesise DME directly from CO_2, CH_4, O_2 and H_2O. The tri-reforming process detailed in Table 2.3 produces syngas in the first step and DME is produced from syngas in a second step. The process uses a proprietary catalyst at 200-300 °C achieving conversions of up to 68% of CO (Armstrong, 2015).

In Japan the Gas to Liquids (GTL) process developed by JOGMEC and Nippon GTL Research Technology Association converts natural gas into clean liquid fuels with up to 40 mol% CO_2 in the feedstock (Armstrong, 2015). The process uses the tri-reforming technology to produce syngas from CH_4, CO_2 and O_2 and H_2O over a noble metal-based catalyst. The syngas is then transferred to a Fischer-Tropsch reactor where waxes and light oil are produced, obtaining zero emission of CO_2 (within the plant boundaries) with recycling of unreacted syngas, according to a simulation study by Ha *et al.* (2010). Finally, the heavy products are fed to the hydrocracking upgrading unit where kerosene, naphtha and gas oil are produced at a rate of 500 barrels per day (Quadrelli *et al.*, 2011).

2.6.4 Polymer plants

Ongoing research has focused on the conversion of CO_2 into plastics since these are capable of sequestering CO_2 over long periods of time. There are several companies that are very close to the commercialization of CO_2-derived plastics, which can incorporate up to 50% CO_2 by weight (Armstrong, 2015).

The German company Bayer Material Science, in partnership with RWE, RWTH Aachen University and the CAT Catalytic Centre, is currently producing through the so called “dream reaction” the precursor to make polyurethane foam from CO_2. The CO_2 is captured using a monoethanolamine scrubber from the Niederaussem coal-fired power plant operated by RWE (Bayer MaterialScience, 2012). Cradle-to-grave Life Cycle Assessments (LCA) have been carried on the process with results indicating that the Bayer process has a life cycle reduction in CO_2 emissions of 9% compared to polyurethane foam produce from fossil fuels (Armstrong, 2015). Due to the successful research and development at Bayer’s pilot plant, the company has announced its plans to scale-up the technology to produce flexible foams from CO_2 at a rate of several thousands of tonnes per annum.

Novomer Inc., a company based in the United States, converts waste CO_2 from ethanol production into poly propylene carbonate and poly ethylene carbonate containing up to 50% CO_2 by weight (Armstrong, 2015). The company has developed a low cost, cobalt-based catalyst to synthesise the polymers at low temperature and pressure. In partnership with the US Department of Energy National Energy Technology Laboratory (NETL), Albemarle Corp. and the Eastma Kodak Company, Novomer built a demonstration plant to test commercial and environmental feasibility of the production process. After successful results, the company announced the construction of the first-full scale CO_2-to-polimers plant which started production in January 2015 with a capacity of 7 tonnes of poly propylene carbonate poliol per day (Chemical Engineering, 2015).

The Chinesse company Jiangsu Jinglon-CAS Chemical Co. Ltd is also recovering CO_2 from an ethanol production waste stream to convert it into propylene carbonate poliol. Currently the company produces 22,000 tonnes of propylene carbonate poliol with plans of building a full-scale plant by 2016 with a capacity of 100,000 tonnes per annum (Sizhen, 2011).

The Japanese company Asahi Kasei Chemicals Corporation manufactures polycarbonate by means of an award winning phosgene-free process that uses CO_2, ethylene oxide and bisphenol A as feedstocks. This novel process is relevant not only for incorporating CO_2 into the polymer but also for eliminating the highly toxic phosgene. In 2002, the company started the commercial production of polycarbonate with the first plant built in Taiwan producing at a rate of 65,000 tonnes per annum. The process has been licensed worldwide since then with plants in South Korea, Russia and Saudi Arabia (Armstrong, 2015).

2.6.5 Mineralization plants

Mineralization is another key target in CDU since it normally integrates capture, storage and utilisation into a single process, what reduces the costs and environmental impacts related CO_2 utilisation. In addition, mineralization processes are often exothermic, which further reduces the cost and emissions.

Carbon8 Systems Ltd is a UK-based company founded as a result of ongoing research at different universities in the country. The company produces carbonate-based construction aggregate from CO_2 and industrial solid waste, contaminated soils and air pollution control residues (*e.g.* fly ash from municipal waste incinerators). In 2012, the company commissioned a full-scale production plant in Suffolk (UK) capable of producing 36,000 tonnes of aggregate per annum (Armstrong, 2015).

Calera Corporation and Skyonic are producing calcium carbonate and sodium carbonate by means of Carbon Mineralization at their plants in California and San Antonio respectively. Skyonic estimates that in 2015 commercial production will begin sequestering up to 225,000 tonnes of CO_2 (Armstrong, 2015).

3. DESCRIPTION OF PROCESS CONCEPTS

3.1 Base Case Models

3.1.1 Overview

As discussed in the Introduction, this work will compare the feasibility of different CO_2 capture and utilisation processes in order to identify the most promising routes for the conversion of carbon dioxide into a liquid hydrocarbon. The source of CO_2 will be the biogas produced from the anaerobic digestion of sewage sludge in a wastewater treatment plant. Initially the methodology considers only the best available and proven technology (Base Case Models); then, a developing technology, CO_2 capture using ionic liquids, is included in the different conceptual designs in order to examine the potential improvements, if any, that this developing technology could have in process performance.

The CO_2 utilisation system considered in this study is shown in Fig. 3.1.

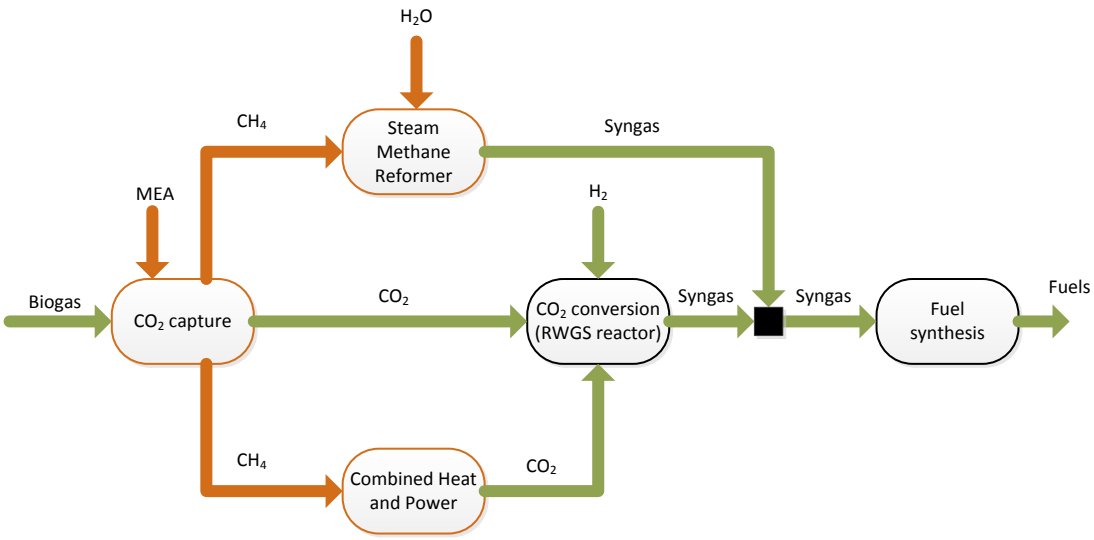

Fig. 3.1 Process system for the production of fuels from biogas via CO_2 utilisation (orange lines represent process units that are not present in all process concepts. In some cases, the CO_2 capture plant is placed after the CHP for post-combustion CO_2 capture).

It consists of five sections or process steps: CO_2 capture from biogas, heat and power generation, syngas production, conversion of CO_2 to

CO and fuel synthesis. This CO_2 utilisation system is fulfilled in seven different process design configurations (Base Case Models) which are grounded on typical biogas valorisation technologies. Table 3.1 shows the different technologies involved in the different process designs along with the main process steps.

Table 3.1 Summary of the technologies involved in the different process designs

Process sections	PD-MEA1	PD-MEA2	PD-CHP1	PD-CHP1-OXY	PD-CHP2	PD-CHP2-OXY	PD-CHP1-POST
CO_2 capture[a]	✔	✔			✔	✔	✔
CHP[b]							
Air-combustion			✔		✔		✔
Oxy-combustion				✔		✔	
H_2 recovery[c]	✔	✔	✔	✔	✔	✔	✔
Syngas production[d]	✔		✔	✔	✔	✔	✔
CO_2 conversion[e]	✔	✔	✔	✔	✔	✔	✔
Fuel synthesis[f]	✔	✔	✔	✔	✔	✔	✔

[a]MEA-based CO_2 capture. [b]Combined Heat and Power. [c]Pressure Swing Adsoprtion (PSA). [d]Steam reforming of methane. [e]Reverse Water-Gas-Shift (RWGS). [f]Fischer-Tropsch synthesis.

The choice the CO_2 utilisation process system depicted in Fig. 3.1 is justified by the following facts:

1. The thesis focuses on liquid fuel production.

2. Only the best available technology in each process step is considered.
3. It allowed fully implementation in Aspen Plus using existing or modified Aspen models.

The different process designs are depicted in more detail as block diagrams in Fig. 3.2 - Fig. 3.8. The first process design (PD-MEA1 in Table 3.1 and Fig. 3.2) incorporates a monoethanolamine (MEA) gas treatment unit, which is often used to upgrade biogas to the same standards as natural gas by removing CO_2 and other trace constituents (Tippayawong *et al.*, 2010) as well as a methane steam reformer for syngas manufacturing.

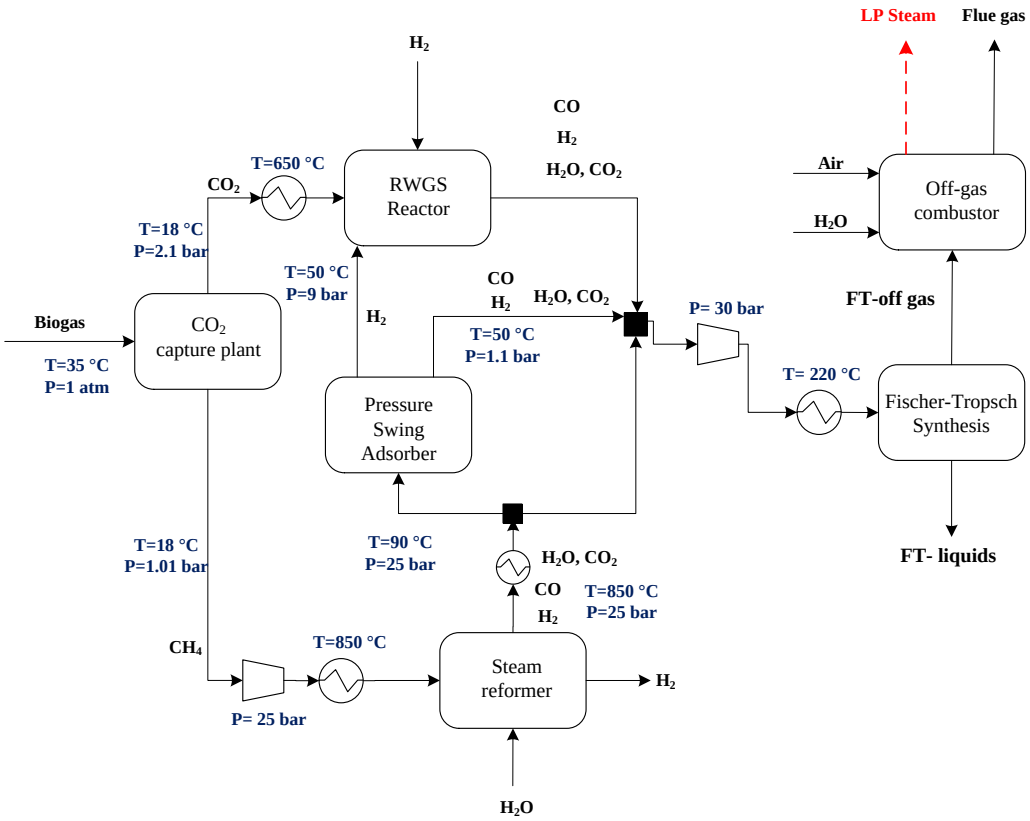

Fig. 3.2 Process flow diagram of PD-MEA1

It was already highlighted in the Introduction that the high hydrogen and energy requirements of CO_2-to-fuels processes are one of the main issues for the commercialization of these technologies. In light with this, the selection of PD-MEA1 as one of the base case models is of particular interest because it permits the generation of H_2 *in situ* via steam reforming of methane. This endogenous production of hydrogen via steam methane reforming is especially interesting from the economic point of view since fossil-derived hydrogen is considerably cheaper than that produced from renewable sources (IPHE, 2011).

Similarly to PD-MEA1, PD-MEA2 (shown in Fig. 3.3) also incorporates a monoethanolamine (MEA) gas treatment unit; however PD-MEA2 does not include steam methane reforming since the upgraded bio-methane is assumed to be injected into the natural gas grid.

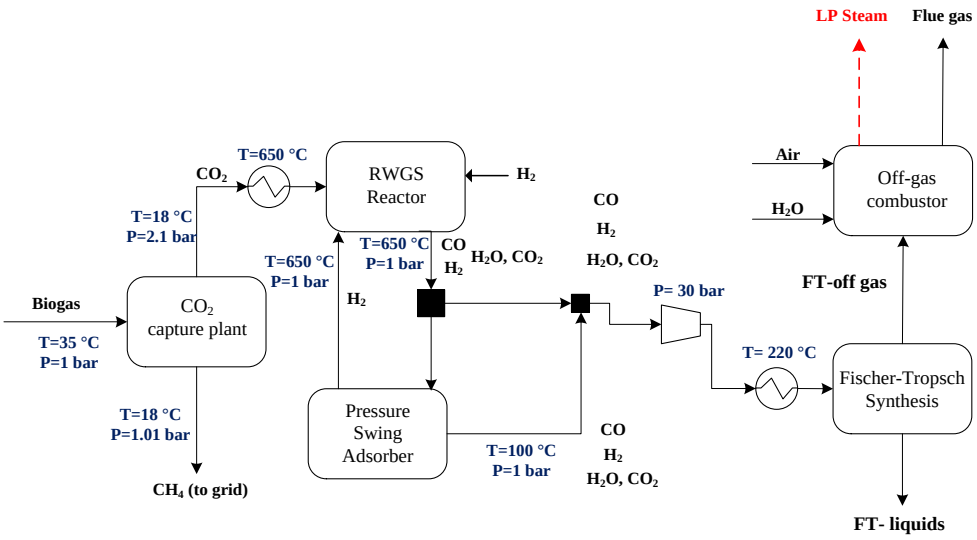

Fig. 3.3 Process flow diagram of PD-MEA2

PD-MEA2 was chosen to assess the importance of generating H_2 *in situ* (as in PD-MEA1) in terms of process efficiency and costs. The aim is to evaluate whether is more convenient to export the upgraded bio-methane at the expense of having to obtain the hydrogen externally or,

by contrast, to produce H_2 within the plant via steam methane reforming.

The third case (PD-CHP1, Table 3.1 and Fig. 3.4) is based on another biogas application: combustion of untreated biogas in a combined heat and power (CHP) unit to produce electricity and heat.

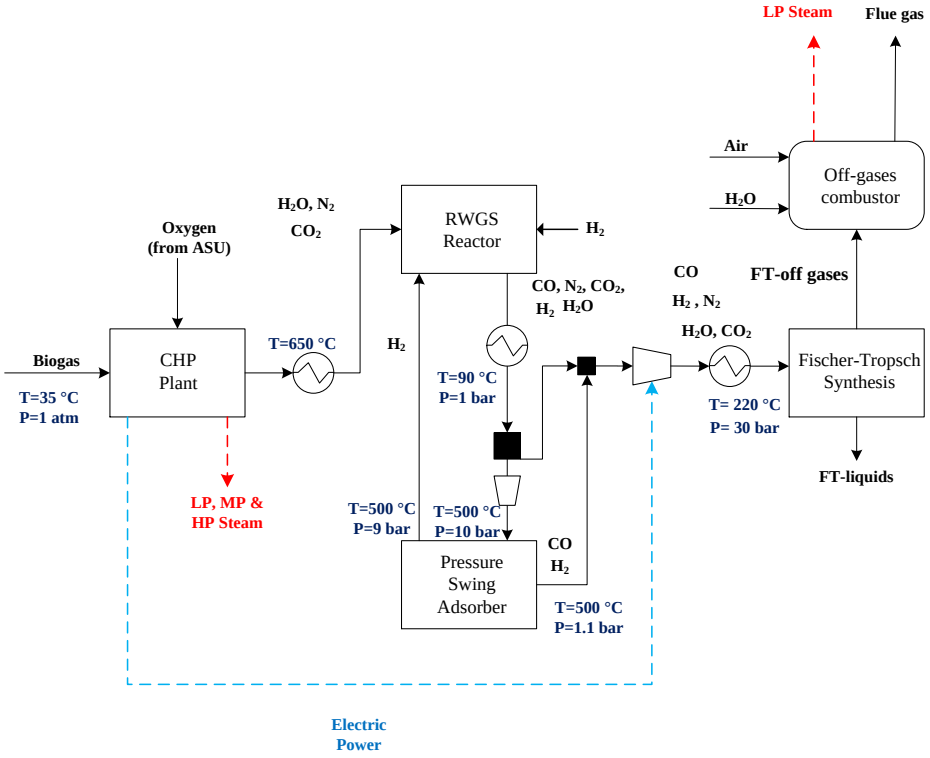

Fig. 3.4 Process flow diagram of PD-CHP1

The selection of PD-CHP1 as one of the base case models was made in order to investigate the effect of a combined heat and power (CHP) plant on process performance and costs. Combustion of “raw” biogas in a CHP plant is a common application in the water industry. Usually, the heat produced by the plant is used to raise the temperature in the anaerobic digesters while the electricity is usually consumed within the plant or exported to the grid (ADE, 2015). In PD-CHP1, the heat generated by the CHP plant is still used to warm up the digesters while

the electricity is used to power electric equipment such as pumps and compressors employed in the CDU plant.

The fourth design (PD-CHP1-OXY, Table 3.1 and Fig. 3.5) is equivalent to PD-CHP1, although PD-CHP1-OXY employs oxygen for oxy-combustion of the untreated biogas in the CHP unit.

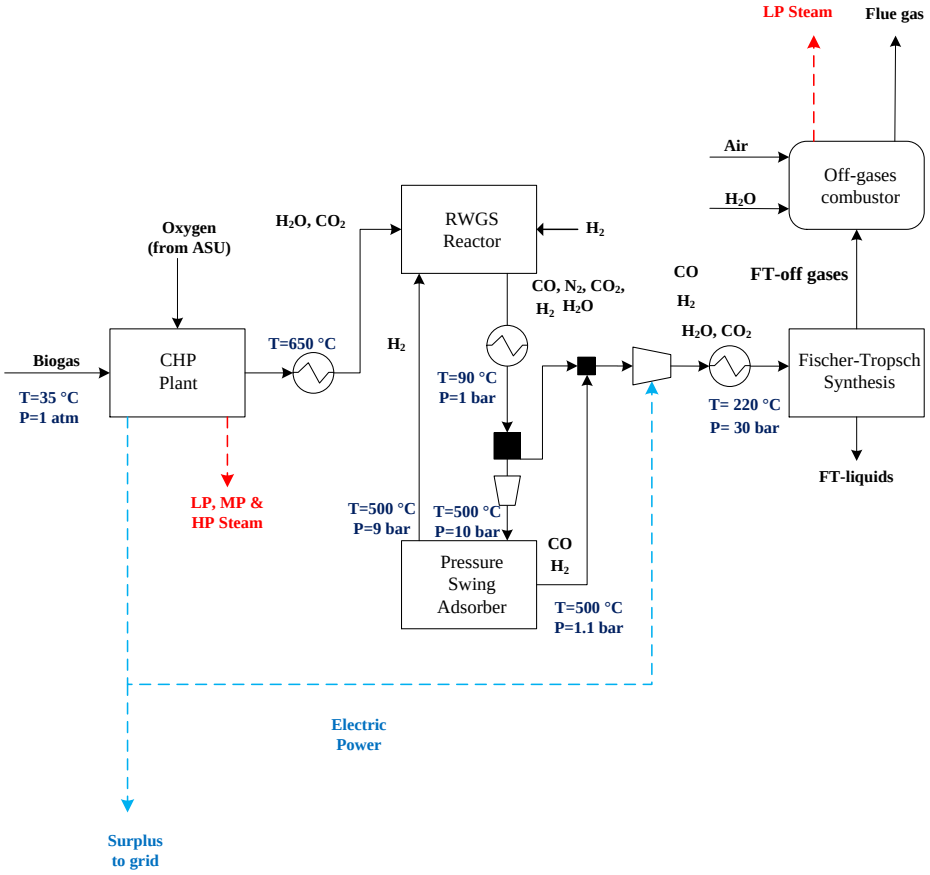

Fig. 3.5 Process flow diagram of PD-CHP1-OXY

Oxy-combustion was chosen in PD-CHP1-OXY since it was anticipated that a large volume of flue gas produced by the CHP unit would have to be processed downstream, which eventually would result in a large energy consumption (heating, cooling and electricity) as well as high capital costs related to the large scale of the equipment involved. In order to assess the effect that reducing the volume of the CHP exhaust stream could have on process performance and thus on overall costs,

additional process concepts are considered in this study, which use oxy-combustion of the biogas instead of combustion with air. This, on one hand, will reduce the volume of exhaust gas to be processed downstream (since there are no inert gases like N_2 in the oxygen stream). On the other hand, producing a large amount of pure oxygen from air will incur in additional costs; therefore, the trade-off between the lower volume of exhaust stream and the additional cost of oxygen production will be assessed and quantified.

The fifth design (PD-CHP2, Table 3.1 and Fig. 3.6) comprises an MEA CO_2 capture system placed before the CHP plant which in this case is fed with the upgraded bio-methane (*i.e*. more concentrated in CH_4) rather than untreated biogas as in the second case; thus, this is a pre-combustion CO_2 capture system.

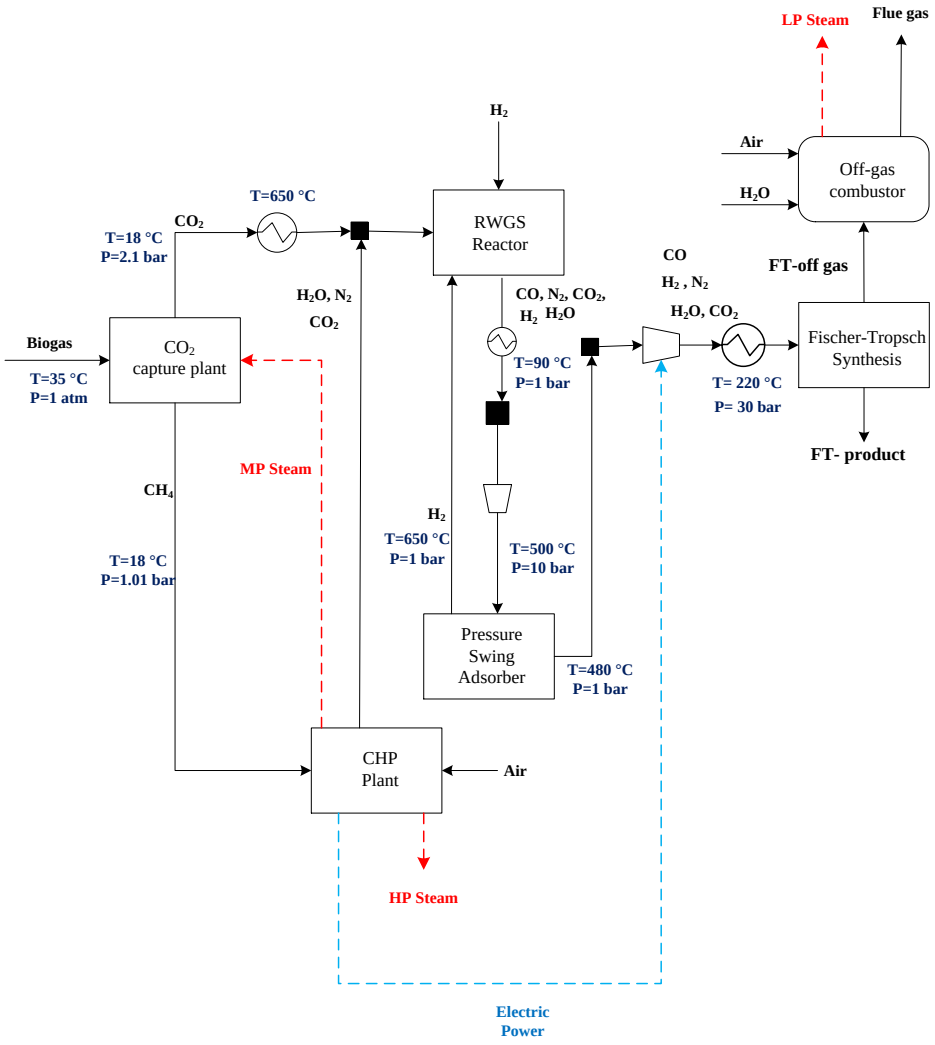

Fig. 3.6 Process flow diagram of PD-CHP2

The main difference between PD-CHP1 and PD-CHP2 is the CO_2 capture plant, which is present in the latter. By capturing the CO_2 in the biogas, upgraded bio-methane can be combusted in the CHP plant instead of raw biogas. This is of particular interest since, by doing this, the CHP plant efficiency can be increased by increasing the energy density of the fuel to be burnt. However, there is an energy penalty in the CO_2 capture plant as a result of the MEA re-generation. Thus, the trade-off between increased CHP plant efficiency and CO_2 capture energy penalty can be investigated by comparing PD-CHP1 and PD-CHP2 in terms of process efficiency and costs.

The sixth configuration (PD-CHP2-OXY, Table 3.1 and Fig. 3.7) is similar to PD-CHP2 but PD-CHP2-OXY employs oxygen for oxy-combustion of the upgraded bio-methane in the CHP unit.

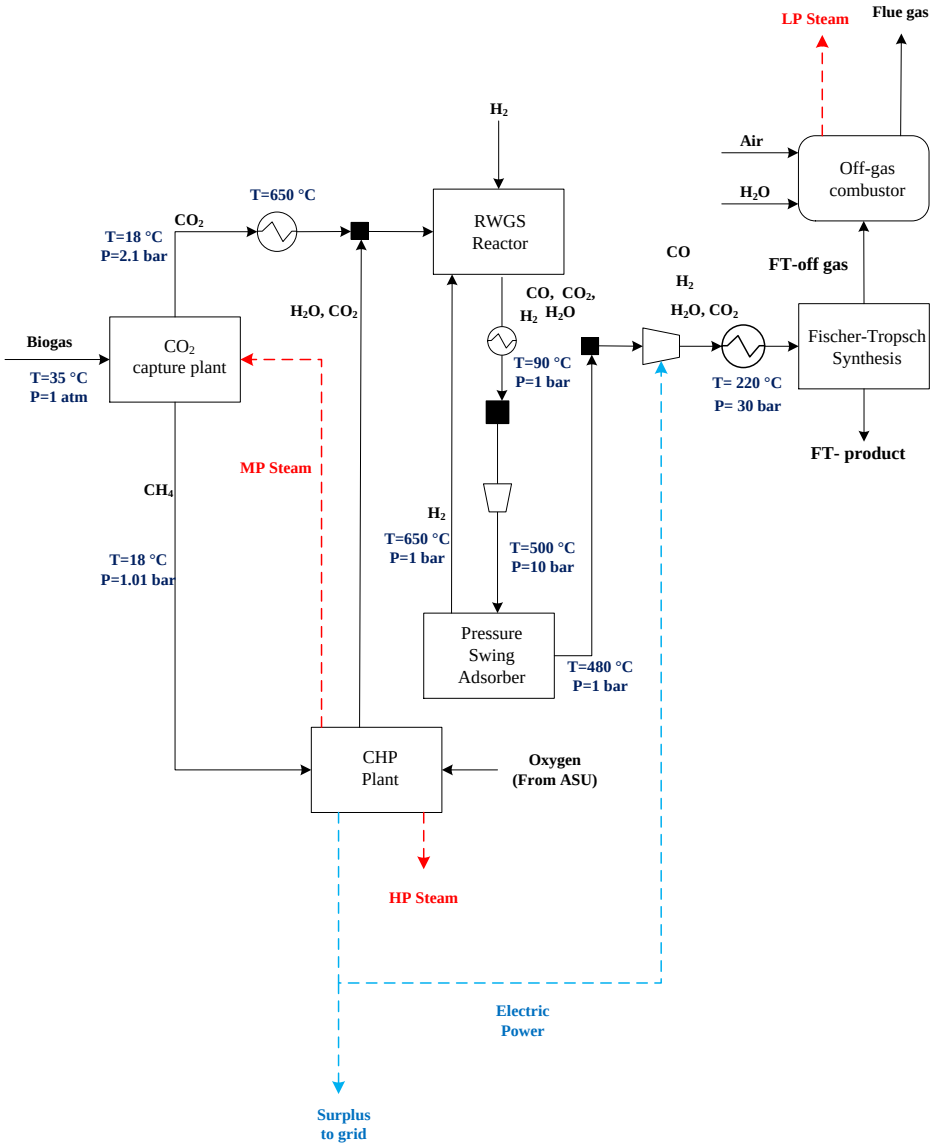

Fig. 3.7 Process flow diagram of PD-CHP2-OXY

As with PD-CHP1-OXY, PD-CHP2-OXY was chosen in order to assess the effect that reducing the volume of the CHP exhaust stream could have on process performance and thus on overall costs. An additional process concept is considered (PD-CHP2-OXY), which use oxy-combustion of the biogas instead of combustion with air.

The seventh design (PD-CHP1-POST in Table 3.1 and Fig. 3.8) is similar to PD-CHP1 but an MEA unit is incorporated after the CHP plant so that this process design is based on post-combustion CO_2 capture (Hunt *et al.*, 2010).

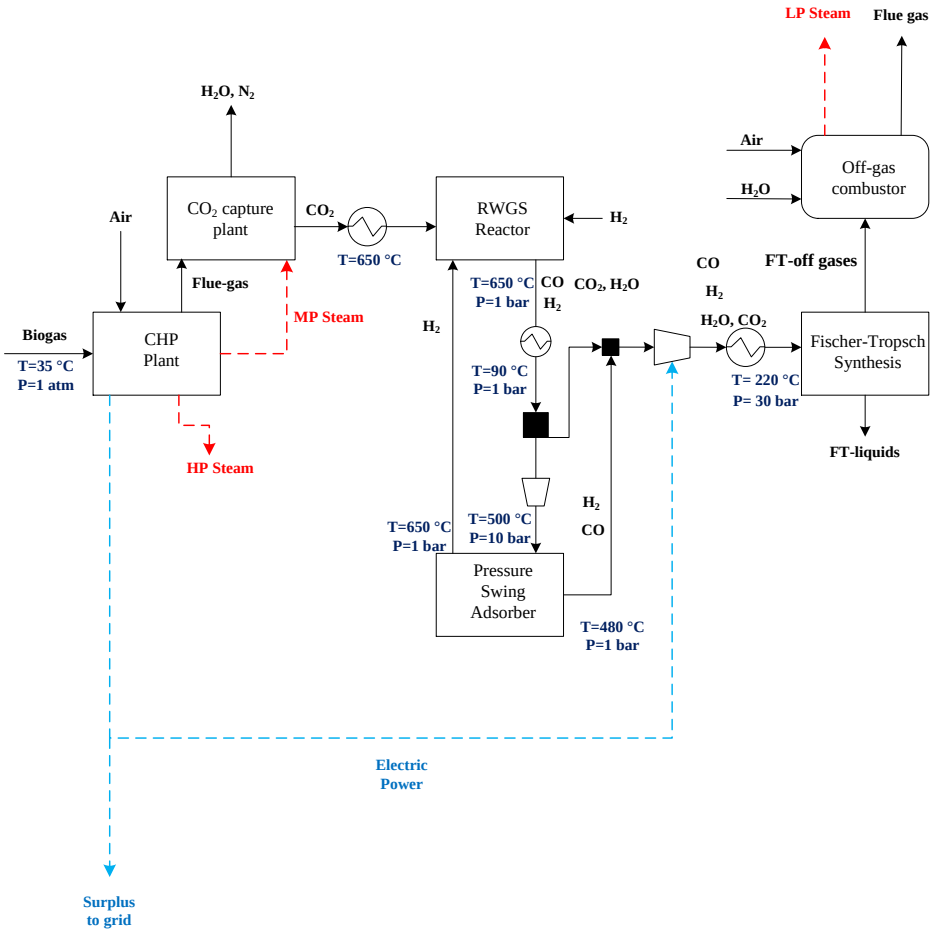

Fig. 3.8 Process flow diagram of PD-CHP1-POST

As discussed before in this section, a large volume of flue gas produced by the CHP unit has to be processed downstream in the CDU plant, which eventually results in a large energy consumption as well as high capital costs related to the large scale of the equipment involved. The process design PD-CHP1-POST includes CO_2 capture plant so that it allows the removal of the excess air used in the CHP plant, which acts as an inert diluent, decreasing the efficiency of the downstream processes and necessitating higher power consumption for the subsequent syngas compression.

3.1.2 Plant size and feedstock

Biogas produced from the anaerobic digestion of organic matter is the feedstock in the proposed CO_2 utilisation process system because of its high CO_2 concentration (which eases separation), its high energy content (due to its CH_4 content) and the fact that it is an established industry with a high degree of implementation worldwide (Appels *et al.* 2011; Owens & Chynoweth 1993). This last consideration is important since the Base Case Models considered in this thesis use only the best available and proven technology. It should be emphasised that the conclusions from this research are not limited exclusively to biogas feedstocks as the processes considered allow the use of any other gas stream containing $CO_{2,}$ such as flue gas from industrial sources; however, the consideration of alternative feedstock would be a subject of further study in the area and thus is not included in this work.

This work considers as feedstock biogas produced at a rate of 3,775 $kg \cdot h^{-1}$ via anaerobic digestion of primary and secondary sludge, at an industrially relevant figure typified by the Minworth Waste Water Treatment Plant (WWTP) operated by Severn Trent in Birmingham, UK (REA, 2013). The effect on production costs of several process parameters, such as plant size, will be assessed later in this work.

3.2 CO_2 capture using ionic liquids

As discussed in section 2.5.1, the most developed large scale CO_2 capture technologies that can produce an enriched stream of CO_2 are based on amine solvents such as monoethanolamine (MEA) (Notz *et al.*, 2011; Rubin *et al.*, 2012; Zhu *et al.*, 2013). The advantages of using such solvents that they offer a high CO_2 absorption capacity and a relatively low cost. On the other hand, they are generally prone to evaporate, liable to be corrosive at elevated temperatures and expensive to regenerate due to the energy penalty (Zhu *et al.*, 2013; Kittel *et al.*, 2009; Abu-zahra *et al.*, 2007). In the recent years,

alternative materials have been suggested for CO_2 capture, including: KS-1 solvent, Econamine FG^{+SM}, ionic liquids, amidoxim, metal–organic frameworks, microporous organic polymers, zeolitic imidazolate frameworks and membranes among others (Zhang *et al.*, 2012).

Ionic liquids are among the class of novel solvents that have high CO_2 affinity and therefore have attracted significant attention in recent years (Brennecke & Gurkan, 2010; Zhang *et al.*, 2012). They offer a number of advantages against amine-based solvents such as their extremely low vapour pressure, which prevents the solvent from being released to the atmosphere, and their low corrosivity (Reddy, 2009; Zhang *et al.*, 2012). Furthermore, the vast number of possible combination of cations and anions allows the solvent to be custom made for specific applications (Lee & Lin, 2015).

It is known that a potential candidate ionic liquid for CO_2 capture processes must possess a high CO_2 affinity, significant pressure/temperature dependence of CO_2 solubility and high selectivity towards CO_2 solubility over other components present in the gas mixture, such as CH_4, N_2, H_2, H_2S, *etc.* (Lee & Lin, 2015). Consequently, many studies have focussed on these desirable properties of the candidate ionic liquid, either experimentally or through mathematical modelling; however, just a few studies (Basha *et al.*, 2014; Basha *et al.*, 2013; Eisinger & Keller 2014; Shiflett *et al.*, 2010) have focussed on whole-scale process analysis, which is essential if serious effort is to be made to consider commercial implementation of this technology.

Besides considering MEA-based CO_2 capture, this thesis also examines the techno-economic feasibility of selective CO_2 capture processes from biogas streams using ionic liquids as physical absorbents. The aim of this study is to identify the most promising ionic liquid for biogas upgrading in terms of process efficiency and costs. In order to do so, a new simulation methodology has been developed, which enables the

estimation of physical properties of the ionic liquids as well as the solubility of the gaseous species (CO_2 and CH_4) in them. This simulation methodology can be used as a basis for further work in the area since it allows consideration of ionic liquids made of any combination of cation and anion as well as different gas streams.

3.2.1 Process description

The target application considered in this study is biogas upgrading (up to 95 vol. % CH_4) using ionic liquids which selectively absorb CO_2 physically. Three different processes have been studied, each of them employing a different ionic liquid. The design of the three processes is identical, differing only in the type of ionic liquid used; this will allow a fair comparability between the processes in terms of energy requirements, solvent capacity, solvent loss and cost.

The flow diagram of the biogas upgrading plant is shown in Fig. 3.9. It is a pressure-swing regenerative process based on the one suggested by Shiflett *et al*. (2010). It consists of a multistage compressor, a packed absorption column for CO_2 absorption, a flash evaporator for solvent regeneration, a centrifugal pump for solvent recirculation, a pre-absorber solvent cooler and a gas turbine for electricity recovery.

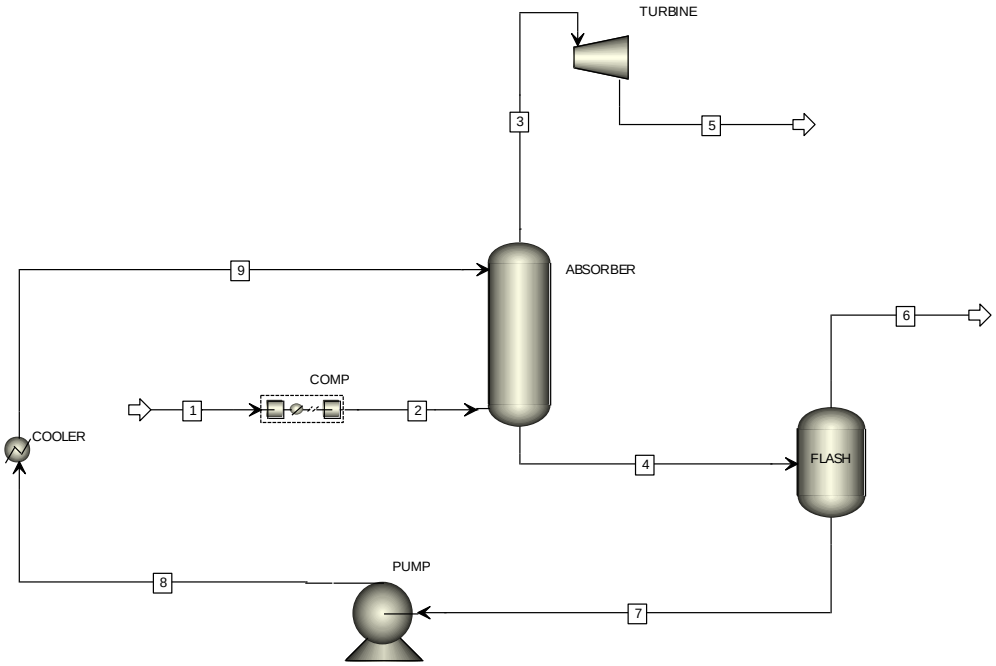

Fig. 3.9 Process flow diagram of the biogas upgrading plant

The biogas (*1*) generated from anaerobic digestion of sewage sludge in a Waste Water Treatment Plant (WWTP) is compressed from atmospheric pressure and temperature (1 atm and 15 °C) to the column's operating pressure of 30 bar in a multistage gas compressor with intercooling. The compressed biogas at 15 °C and 30 bar is fed counter-currently into the packed absorption column with the ionic liquid (*9*) at 15 °C and 30 bar, which selectively absorbs CO_2 in the biogas to form a CO_2-rich ionic liquid solution. The upgraded bio-methane stream (*3*) lean in CO_2 (95 vol. % CH_4) is released from the top of the absorber while the ionic liquid solution rich in CO_2 (*4*) is fed into a flash drum. The ionic liquid is regenerated in the flash drum by pressure swing, *i.e.* by realising its pressure to 0.01 bar. It is then recycled back by the centrifugal pump to the absorption column for re-use, while the concentrated CO_2 stream (*6*) is released from the top of the flash drum. It should be noted that since this is a pressure-swing capture process, external supply of heating is not involved in any of the unit operations.

The three ionic liquids selected to act as physical absorbents for CO_2 capture are: 1-*Ethyl-3-methylimidazolium bis[(trifluoromethyl)sulfonyl]imide*, *1-Hexyl-3-methylimidazolium bis[(trifluoromethyl)sulfonyl]imide and trihexyl(tetradecyl)phosphonium bis[(trifluoromethyl)sulfonyl]imide*. Their molecular structures are depicted in Figs. 3.10-3.12.

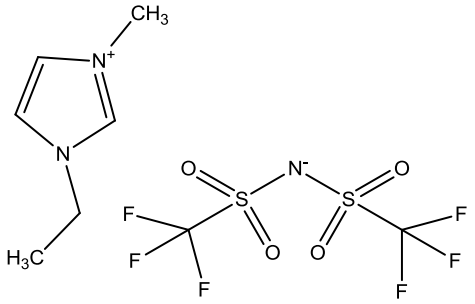

Fig. 3.10 1-ethyl-3-methylimidazolium bis[(trifluoromethyl)sulfonyl]imide, $[C_2MIm][Tf_2N]$

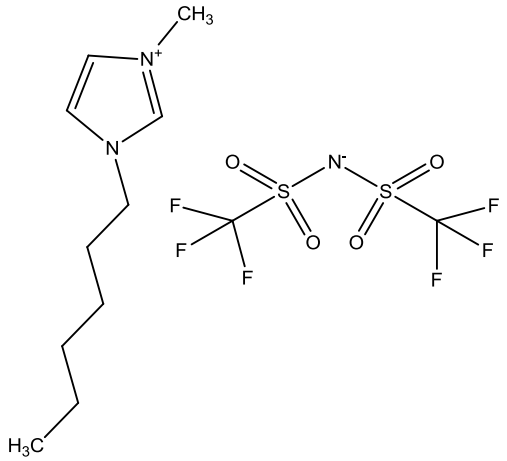

Fig. 3.11 1-hexyl-3-methylimidazolium bis[(trifluoromethyl)sulfonyl]imide,$[C_6MIm][Tf_2N]$

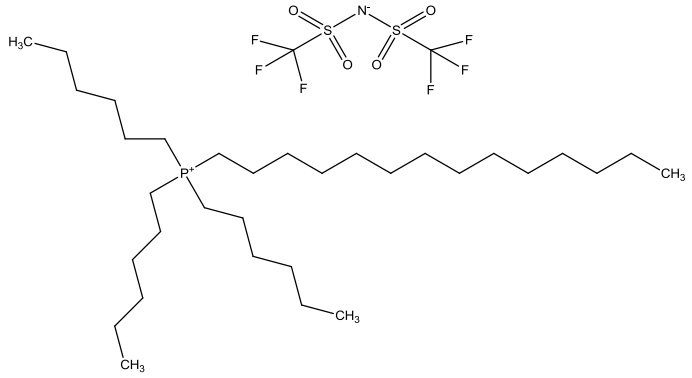

Fig. 3.12 Trihexyl(tetradecyl)phosphonium bis[(trifluoromethyl)sulfonyl]imide, $[P_{66614}][Tf_2N]$

The three ionic liquids have the same anion, namely bis[(trifluoromethyl)sulfonyl]imide, ($[Tf_2N]^-$) and are based on three different cations: *e.g.* two 1-alkyl-3-methylimidazolium ($[C_nMIm]^+$ whit *n* = 2 or 6) and the trihexyl(tetradecyl)phosphonium ($[P_{66614}]^+$). The bis{(trifluoromethyl)sulfonyl}imide anion has been selected as ILs based on this anion have a high affinity for CO_2 capture (Cadena *et al.*, 2004) in comparison with those base on, for instance, the hexafluorophosphate ($[PF_6]^-$) anion (Anthony *et al.*, 2005). Imidazolium cations have been selected as they are very well reported in the literature and they have a particular structure presenting an unsaturated ring (*i.e.* the positive charge is mainly delocalised on the cation structure) *a contrario* of the phosphonium cation which presents a charge mainly localised on the Phosphorus atom. Furthermore, the selected phosphonium cation has an acyclic structure containing very large alkyl chain lengths that increase the cohesive energy of this cation in comparison with selected imidazolium cations. In fact, Van der Waals forces are higher in the phosphonium than selected imidazolium cations, in contrast to the Coulombic forces. In other words, this cation's selection allows investigation of impacts of cation structure, cation-anion interaction on the CO_2 uptake and process modelling and costing. Finally, the reasons why these ionic liquids have been chosen as

solvents for selective CO_2 capture in this study are their high CO_2 affinity and CO_2/CH_4 selectivity (Lee & Lin 2015; Sumon & Henni 2011; Lei *et al.,* 2014; Zhang *et al.*, 2012) as well as the availability of data regarding pure component physical properties (NIST, 2013).

4. SIMULATION METHODOLOGY

4.1 Background

Model-based representations of chemical, physical, biological, and other technical processes as unit operations are essential to fully understand the behaviour of whole systems. In these cases, the use of computer programs becomes beneficial as they allow the solution of thousands of algebraic equations in seconds (Peters *et al.*, 2004). Furthermore, process simulation software can be used in all the three stages of a chemical process: research & development, design and production (Aspen Technology, 2013c).

Process simulation software can be divided into two groups: dynamic and steady-state (Dimitriou, 2012). In dynamic simulation, time is a variable that is taken into account in the model so that variations of process variables with time are analysed allowing the prediction and control of chemical processes in real time. On the other hand, steady-state simulation can be used for applications where time is not considered in the model and thus the variation of process variables with time is not taken into account. They are particularly useful for process development and optimization as a result of the mass and energy balances estimations. If these tools are used by an experienced engineer, they can provide an accurate estimate for process equipment and raw materials needs as well as process heating, cooling and electricity requirements (Dimitriou, 2012).

Steady-state simulation software generally models a chemical process as a group of unit operations interconnected by material streams. Unit operations can be also interconnected by heat and/or work streams (Aspen Technology, 2013d). The unit operations may include distillation columns, absorbers, heat exchangers, reactors, compressors, pumps, *etc.*, which are represented by material/energy balances and thermodynamic principles (Dimitriou, 2012).

There are two types of steady-state simulation software: sequential-modular and simultaneous or equation oriented simulation programs. In sequential-modular simulation programs, such as Aspen Plus, the entire flow sheet is solved by solving the process units in the same order as they appear in the process; therefore, the results streams of a given unit operation become the input data for the next one, up to the last unit (Aspen Technology, 2013d). By contrast, simultaneous or equation oriented simulation programs, *e.g.* IPSEpro, represent the flow sheet as an equation system containing the total number of equations and variables; thus, the system is solved in one step avoiding the need of having to calculate the output of a given unit operation to be able to solve the one that precedes it (Dimitriou, 2012).

4.1.1 Process simulation with Aspen Plus

The material and energy balances as well as the utility requirements necessary for the techno-economic assessments carried out in this thesis have been calculated using the commercial software Aspen Plus. AspenPlus® is a sequential-modular simulator developed by Aspen Tech that is commonly used by the world's leading chemical and speciality chemical organizations to design and optimize their process plants (Aspen Technology, 2013c). The different types of process simulation software highlighted in section 4.1 offer a number of advantages as well as disadvantages; however, Aspen Plus has been chosen over other options because it holds the following advantages:

- It provides a vast database of components and physical properties for both pure components and mixtures. If a component is not present in the database, Aspen Plus enables the user to develop a new database for the new component.
- Although its modelling approach usually involves longer calculation times, this is off-set by the fact that the calculation path can be followed, which helps troubleshoot convergence issues.

- It possesses a user-friendly interface that clearly exposes all the program´s features. Furthermore, already built process simulation examples as well as equipment technical data are accessible from the user interface.
- Simulation of a vast range of unit operations is possible from the user-interface.
- The process flowsheet with the mass and energy balances calculations can be integrated with in other software developed by Aspen Tech such as Aspen Process Economic Analyzer, Aspen Energy Analyzer, *etc*.

4.1.2 General conditions

Ambient conditions and the characteristics of the feedstock (biogas) are given in the following sections. In order to make the results from the different process concepts comparable, both ambient conditions and biogas characteristics were kept constant in all cases.

4.1.2.1 Ambient conditions

Ambient conditions of all processes and unit operations considered in this study were set by default in Aspen Plus to 15°C and 1 atm (Aspen Technology, 2013d).

4.1.2.2 Characteristics of the feedstock

The biogas is generated from anaerobic digestion of sewage sludge under mesophilic conditions in a Waste Water Treatment Plant (WWTP) at atmospheric pressure and 35 °C. The WWTP considered in this study is based on the Minworth Sewage Treatment Works in West Midlands (UK) (Source). This facility was chosen because it is a large WWTP, which allows economies of scale. In addition, the WWTP has been recently retrofitted with a water scrubber to produce upgraded bio-methane (95 vol. % CH_4), which allows comparability with some of the

CDU process concepts included in this thesis (biogas upgrading using ionic liquids). The composition of the "raw" biogas is 35 mol. % CO_2 and 65 mol. % CH_4 (Appels *et al.*, 2011). It is assumed that neither NH_3 nor H_2S are present in the biogas since ammonia is not produced when sewage sludge is employed as the feedstock and hydrogen sulphide is produced only in trace amounts (Dimitriou *et al.*, 2015). Although biogas produced at WWTPs is usually saturated with water, it is assumed that a drying pre-treatment has been carried out prior to feeding it to CO_2 utilisation plant. The biogas is produced by the WWTP´s anaerobic digester at a rate of 3,775 $kg \cdot h^{-1}$ (Severn Trent Water, 2015).

4.1.3 Base Case Models

As discussed in the previous chapter, the CO_2 utilisation system considered in this thesis is fulfilled in seven different process design configurations (Base Case Models) which are grounded on typical biogas valorisation technologies, *i.e.* combined heat and power (CHP) and biogas upgrading to bio-methane). They consist of five sections: CO_2 capture from biogas, heat and power generation, syngas production, conversion of CO_2 to CO and fuel synthesis. It must be emphasised that only the best available technology (high technology readiness level (TRL)) is considered in each section within the different base case models studied. The anaerobic digester that produces the biogas from sewage sludge is not included in the process designs since it is not a specific unit operation of the CO_2 utilisation plant, but it is already a part of the Waste Water Treatment Plant (WWTP). The WWTP uses anaerobic digestion to reduce the volume of secondary sludge by converting it into biogas and solid digestate. The following sections will describe in detail the technology involved in the different process steps as well as the modelling methodology followed to represent each of them. It should be noted that this section of the work (Base Case Models) consists of a novel implementation of Aspen Plus

standard features to get data which had not been published before. A full summary of the stream results and unit operations (for PD-CHP2 chosen as an example) can be found in the Supporting information (enclosed CD). The results (technical and economic) from the Base Case Models using the methodology described in the following sections were published in *Energy and Environmental Science* (Dimitriou *et al.,* 2015). When data were obtained as a result of collaboration, it is appropriately stated.

4.1.3.1 CO_2 capture using monoethanolamine (MEA)

The flow diagram of the CO_2 capture unit is shown in Fig. 4.1. To convert CO_2 into a liquid fuel, a concentrated stream of CO_2 needs to be generated by isolating it from biogas. As discussed previously in this thesis, among the available technologies to capture CO_2 from a gas stream, amine-based regenerative systems have been identified as the most suitable technology that has achieved commercial success. This technology has been used by the natural gas industry for over 60 years to remove CO_2 from natural gas to produce food and beverage grade CO_2; the most common amine used is MEA due to its low cost (Spigarelli & Kawatra, 2013). Furthermore, as it was highlighted in section 2.5, post-combustion technologies present the greatest near term potential for reduction of CO_2 emissions because they can be retrofitted to existing industrial emitters. Among the post-combustion capture alternatives, amine-based reactive absorption is currently the most mature technology on the market (Notz *et al.*, 2012; Zhu *et al.*, 2013).

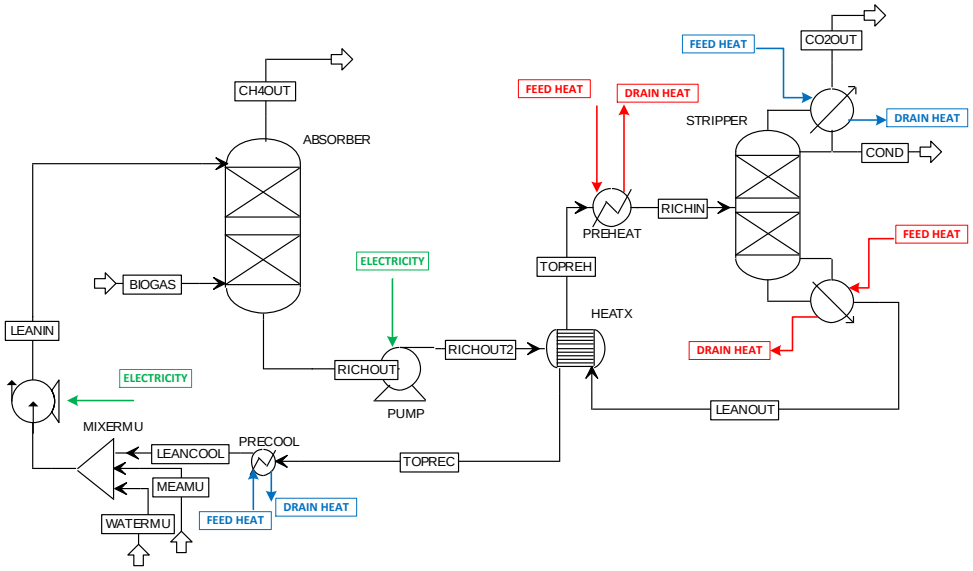

Fig. 4.1 Process flow diagram of the CO_2 capture plant as implemented in Aspen Plus

In the packed absorption column, the biogas (PD-MEA1, PD-MEA2, PD-CHP2, PD-CHP2-OXY) or the CHP exhaust stream (PD-CHP1-POST) is fed counter-currently with an MEA aqueous solution which reacts with and absorbs CO_2 to form an MEA carbamate soluble salt. The reaction mechanism related to the process can be seen in Fig. 4.2 (Xie *et al.*, 2010).

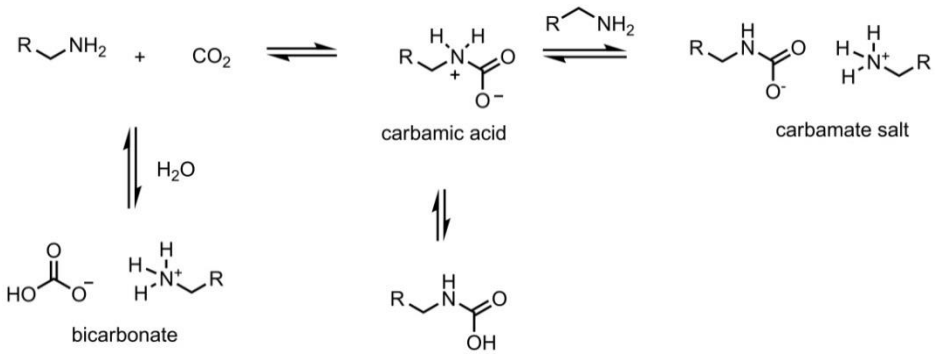

Fig. 4.2 Reaction mechanism of monoethanolamine with CO_2 in aqueous solution

As one can see, 2 moles of MEA will be needed to absorb (to react with) 1 mole of CO_2. The absorption (forward) reaction will be

exothermic while the regeneration (backward) reaction will be endothermic.

The gas stream lean in CO_2 is released from the top of the absorber while the MEA solution rich in CO_2 is pumped to a heat exchanger in which the solution is heated to its bubble point (about 120 °C) and then fed into the stripping column. MEA is regenerated in the stripper and recycled to the absorber for re-use ("LEANOUT" stream, Fig. 4.1). The regeneration conditions are maintained by the reboiler which uses medium-pressure steam as the heat source. Steam which acts as stripping gas in the column, is recovered in the condenser and fed back to the stripper, while the concentrated CO_2 stream is released from the top of the stripper for downstream processing.

The Aspen Plus features called "Design specifications" are used to obtain the desired molar split fractions in both the absorber and the stripper. In the absorber, a design specification measured the CH_4 concentration in the stack stream and adjusted the lean MEA flow rate to ensure that a target CH_4 concentration of 95 mol.% in the bio-methane is achieved. The 95 mol. % value is a common set point in biogas upgrading plants (DECC, 2014b; Rajendran *et al.*, 2014). In the case of the post-combustion CO_2 capture (PD-CHP1-POST), design specification measured the CO_2 flow rate in the stack stream and adjusted the lean MEA flow rate to ensure that a target of 90% absorption efficiency (mole basis) is met. In the stripper, a design specification measured the CO_2 molar concentration in the CO_2 product stream and adjusted the reflux ratio to achieve a 98 % vol. purity target (Sonderby *et al.*, 2013).

A parametric study on the technical and economic performance of a CO_2 capture plant that uses MEA carried out by Abu-zahra *et al.* (2007) found that the optimum concentration of MEA in the amine solution was 30 wt. % at a temperature of 30 °C, which also avoided equipment corrosion problems associated with higher concentrations of MEA. The

optimum operating pressure of both the absorber and stripper was found to be 1.013 bar and 2.1 bar respectively (Abu-zahra *et al.*, 2007). As for the CO_2 lean solvent loading (which is a measure of the degree of regeneration of the solvent in the stripper) an optimum value of 0.32 mol CO_2/mol MEA was taken from the same reference as above.

In the CO_2 capture plant, the absorber and stripper columns are modelled using the *RadFrac* subroutine which is suitable for modelling all types of multistage vapour-liquid fractionation operations (Aspen Technology, 2013d). The rigorous “rate-based” calculation option was used in the *RadFrac* model so that mass transfer rates can be calculated at each stage. The other calculation option available, equilibrium calculation, assumes that equilibrium is achieved at each stage, which was not appropriate in the systems studied in this thesis. The thermodynamic and physical properties are estimated using the ENRTL-RK (Electrolyte Non-Random Two-Liquid-Redlich–Kwong) method which is suitable for mixed electrolyte systems containing water up to medium pressures. This method is based on the Unsymmetric Electrolyte NRTL property model. It uses the Redlich–Kwong equation of state for estimating the vapour phase properties, the unsymmetric reference state (infinite dilution in aqueous solution) for ionic species, the Henry's law for solubility of supercritical gases and the unsymmetric Electrolyte NRTL method of handling zwitterions. The ENRTL-RK uses a single thermodynamics framework to calculate the activity coefficients, Gibbs free energy and enthalpy, instead of using separate models as in the ELECNRTL method, which reduces calculation times while increasing simulation flexibility. This method is coupled with an electrolyte calculation option which models the electrolyte solution chemistry as well as the reactions that take place in both the absorber and the stripper. The electrolyte solution chemistry has been modelled with a “CHEMISTRY” option in Aspen Plus, which is used as the global electrolyte calculation option in the simulation model. The five equilibrium reactions implemented in the “CHEMISTRY” option in

Aspen Plus are highlighted in Fig. 4.3, according to the Aspen MEA rate-based model (AspenTech, 2012c).

Reaction 1 $MEAH^+ + H_2O \rightleftharpoons MEA + H_3O^+$

Reaction 2 $MEACOO^- + H_2O \rightleftharpoons MEA + HCO_3^-$

Reaction 3 $2H_2O \rightleftharpoons H_3O^+ + OH^-$

Reaction 4 $CO_2 + 2H_2O \rightleftharpoons HCO_3^- + H_3O^+$

Reaction 5 $HCO_3^- + H_2O \rightleftharpoons CO_3^{2-} + H_3O^+$

Fig. 4.3 Equilibrium reactions implemented in the "CHEMISTRY" option in Aspen Plus

The equilibrium constants are computed by Aspen Physical Property System from the Gibbs free energies of the reaction.

In addition to the electrolyte solution chemistry, two reaction models, called ABSORBER and STRIPPER respectively, have been created. In both the absorber and stripper, all reactions are assumed to be in chemical equilibrium except those of CO_2 with OH^- and CO_2 with MEA, according to the Aspen MEA rate-based model (AspenTech, 2012c). The reactions implemented in the ABSORBER and STRIPPER reactions models in Aspen Plus are highlighted in Fig. 4.4.

Reaction 1 (equilibrium) $MEAH^+ + H_2O \rightleftharpoons MEA + H_3O^+$

Reaction 2 (equilibrium) $2H_2O \rightleftharpoons H_3O^+ + OH^-$

Reaction 3 (equilibrium) $HCO_3^- + H_2O \rightleftharpoons CO_3^{2-} + H_3O^+$

Reaction 4 (kinetic) $CO_2 + OH^- \rightarrow HCO_3^-$

Reaction 5 (kinetic) $HCO_3^- \rightarrow CO_2 + OH^-$

Reaction 6 (kinetic) $MEA + CO_2 + H_2O \rightarrow MEACOO^- + H_3O^+$

Reaction 7 (kinetic) $MEACOO^- + H_3O^+ \rightarrow MEA + CO_2 + H_2O$

Fig. 4.4 Reactions implemented in the ABSORBER and STRIPPER reactions models in Aspen Plus

Power law expressions are used for the rate-controlled reactions (reactions 4-7 in Absorber/Stripper). The general power law expression is given by Eq. 4.1.

$$r = k(T/T_0)^n \, exp\left[\left(\frac{-E}{R}\right)\left(\frac{1}{T} - \frac{1}{T_0}\right)\right] \prod_{i=1}^{N} (x_i \gamma_i)^{a_i} \quad \text{Eq. 4.1}$$

where r is the rate of reaction, k the pre-exponential factor, T the absolute temperature, T_0 the reference temperature, n the temperature exponent, E the activation energy, R the universal gas constant, N the number of components in the reaction, x_i the mole fraction of component *i*, γ_i the activity coefficient of component *i,* and a_i the stoichiometric coefficient of component *i* in the reaction equation.

In Aspen Plus T_0 is not specified; therefore the reduced power law expression is used, as defined by Eq. 4.2.

$$r = kT^n \, exp\left(\frac{-E}{RT}\right) \prod_{i=1}^{N} (x_i \gamma_i)^{a_i} \quad \text{Eq. 4.2}$$

In Eq. 4.2, the temperature exponent n is zero whereas k and E are given in Table 4.1 (AspenTech, 2012).

Table 4.1 Parameters *k* and *E* in Eq. 4.2

Reaction number	$\boldsymbol{k}$	$\boldsymbol{E}$ $(\boldsymbol{cal \cdot mol^{-1}})$
6	$1.33 \cdot 10^{17}$	13249
7	$6.63 \cdot 10^{16}$	25656
8	$3.02 \cdot 10^{14}$	9856
9 (Absorber)	$5.52 \cdot 10^{23}$	16518
9 (Stripper)	$6.50 \cdot 10^{27}$	22782

The packed absorber and stripper characteristic used in the process designs PD-MEA1, PD-MEA2, PD-CHP2 and PD-CHP2-OXY as implemented in Aspen Plus are summarised in Table 4.2. It should be noted that in these process designs the CO_2 is separated from the biogas stream.

Table 4.2 Specification of the packed absorption and stripping columns (PD-MEA1, PD-MEA2, PD-CHP2 and PD-CHP2-OXY)

Specification	**Absorber**	**Stripper**
Number of theoretical stages	5	10
Calculation type	Rate-based	Rate-based
Condenser	None	Kettle
Reboiler	None	Partial-vapour-liquid
Reflux ratio (molar)	N/A	0.47002
Boilup ratio (molar)	N/A	0.05575
Convergence algorithm	Standard	Standard
Packing type	Pall rings (25 mm)	Pall rings (25 mm)
Column diameter (m)	0.7	0.3
Packing height (m)	10	5

The packed absorber and stripper characteristic used in the process design PD-CHP1-POST as implemented in Aspen Plus are summarised in Table 4.3. It should be noted that in this process design the CO_2 is separated from CHP exhaust stream.

Table 4.3 Specification of the packed absorption and stripping columns (PD-CHP1-POST)

Specification	Absorber	Stripper
Number of theoretical stages	5	10
Calculation type	Rate-based	Rate-based
Condenser	None	Kettle
Reboiler	None	Partial-vapour-liquid
Reflux ratio (molar)	N/A	0.50001
Boilup ratio (molar)	N/A	0.06525
Convergence algorithm	Standard	Standard
Packing type	Pall rings (25 mm)	Pall rings (25 mm)
Column diameter (m)	3	1.8
Packing height (m)	20	5

The number of theoretical stages was chosen as the minimum that made the model converge. Any further increase in the number of theoretical stages did not result in any improvements in performance. The rate-based calculation method was chosen since it is a fundamental, rigorous approach which avoids the approximations of efficiency and Height Equivalent to a Theoretical Plate (HETP). Rate-based distillation calculations directly account for the mass and heat transfer rate processes in the system of equations representing the separation unit (Aspen Technology, 2013d).

The height of the absorption column was specified as the one to achieve the desired CH_4 purity in the upgraded bio-methane (95 mol. % CH_4) or the desired 90% absorption efficiency (PD-CHP1-POST) with a minimum lean MEA solution flow-rate. As for the stripping column, its height was specified as the one to achieve the desired regeneration of the MEA solution (0.32 mol CO_2/mol MEA).

The diameter of both the absorber and the stripper were chosen as the minimum that complied with the Aspen Plus default column flooding condition (a vapour velocity value 80% of that which would cause flooding).

Although random packings are characterised by lower mass transfer rates than structured packing they offer lower costs and achieve better liquid distribution (Sonderby *et al.*, 2013); therefore, pall rings were used in the absorber and stripper as the type of packing. The liquid and vapour phase binary mass transfer coefficients as well as the total interfacial area for mass transfer were estimated using the Billet & Schulte's correlation, which provides good estimates of mass transfer-related parameters over a wide range of packing types, sizes and operating conditions (Billet & Schultes, 1993).

The liquid and vapour phase binary mass transfer coefficients $k_{i,k}^{L}$ and $k_{i,k}^{V}$ are defined respectively by Billet & Schulte as:

$$k_{i,k}^{L} = C_L \left(\frac{g\rho_t^L}{\mu^L}\right)^{0.167} \sqrt{\frac{D_{i,k}^L}{d_h}} \left(\frac{u_s^L}{a_p}\right)^{0.333} \qquad \text{Eq. 4.3}$$

$$k_{i,k}^{V} = C_V \left(\frac{1}{\sqrt{\varepsilon - h_t}}\right) \sqrt{\frac{a_p}{d_h}} D_{i,k}^{V} Re_V^{0.75} Sc_{V\,i,k}^{0.333} \qquad \text{Eq. 4.4}$$

where C_L and C_V are the mass transfer coefficient parameters for liquid and vapour respectively, characteristic of the shape and structure of the packing, g the gravitational gravity, ρ_t^L the density of the liquid, μ^L the viscosity of the liquid, $D_{i,k}^L$ and $D_{i,k}^V$ the diffusivity of the liquid and vapour respectively, d_h the hydraulic diameter, u_s^L the superficial velocity of the liquid, a_p the specific area of the packing, ε the void fraction of the packing, h_t the fractional holdup and Re_V and $Sc_{V,i,k}$ the Reynolds and Schmidt number for the vapour, respectively.

The total interfacial area for mass transfer a^I is defined as:

$$a^I = a_e A_t h_p \qquad \text{Eq. 4.5}$$

where A_t is the cross-sectional area of the column, h_p the height of the packed section and a_e the effective surface area per unit volume of the column, which is calculated using:

$$a_e = a_p \frac{1.5}{\sqrt{a_p d_h}} \left(\frac{u_s^L d_h \rho_t^L}{\mu^L}\right)^{-0.2} \left(\frac{\left(u_s^L\right)^2 \rho_t^L d_h}{\sigma}\right)^{0.75} \left(\frac{\left(u_s^L\right)^2}{g d_h}\right)^{-0.45} \qquad \text{Eq. 4.6}$$

where σ is the liquid surface tension.

As depicted in Fig. 4.1, a centrifugal pump is used in order to pressurize the rich MEA solution to the stripper´s operating pressure (2.1 bar). The centrifugal pump is modelled using the Aspen *Pump* subroutine. The pump efficiency is set to 0.7, which is assumed to be a reasonable value for centrifugal pumps (Coulson *et al.*, 1995).

A heat exchanger is also used to preheat the rich MEA solution to its bubble point thanks to the heat provided by the lean MEA solution, which is heated in the stripper by means of medium-pressure steam. The heat exchanger is modelled using the Aspen *HeatX* subroutine assuming a constant value of the overall heat transfer coefficient, U=0.85 $kW \cdot K^{-1} \cdot m^{-2}$ (default value in aspen Plus) and a short-cut calculation method, which is able to provide accurate results at this stage of development (Aspen Technology, 2013d).

Table 4.4 shows the specifications of all other equipment not included in Tables 3.3-3.4 for the process designs PD-MEA1, PD-MEA2, PD-CHP2 and PD-CHP2-OXY and PD-CHP1-POST as implemented in Aspen Plus.

Table 4.4 Specifications of the CO_2 capture plant equipment of the process designs PD-MEA1, PD-MEA2, PD-CHP2, PD-CHP2-OXY, PD-CHP1-POST

Unit operation	Aspen Plus block	Specification
Pump	*Pump*	Discharge pressure: 3.1 bar
Heat Exchanger	*HeatX*	Hot stream outlet temp.: 51 °C
Stripper pre-heater	*Heater*	Vapour fraction [a]: 0
Absorber pre-cooler	*Heater*	Hot stream outlet temp.: 30 °C

[a]The vapour fraction value of zero corresponds in Aspen Plus to the mixture bubble point

The CO_2 capture model accounts for any solvent evaporative losses from both the absorber and striper, which are a consequence of the relatively high vapour pressure of the MEA. In addition to the evaporative losses, degradation of the solvent occurs during the stripping/regeneration of the MEA, mainly through thermal and oxidation pathways (Strazisar *et al.*, 2003; Zoannou *at al.*, 2013); however, due to the complexity inherent to the MEA degradation mechanism, the solvent losses due to degradation are not calculated by the model. Instead, a MEA top-up rate of 175 mmol of MEA per mol of CO_2 captured is specified in order to account for the degradation and evaporation losses (Zhu *et al*., 2013), which was taken into account in the economic assessment presented in Chapter 6. This is a key issue regarding operation of amine-based CO_2 capture plants since the cost of the solvent may represent up to 75% of the operating costs of the plant *(*Strazisar *et al.*, 2003).

The thermal energy required by the reboiler to regenerate the solvent (per tonne of CO_2 captured) and the amount of MEA solution needed (also per tonne of CO_2 captured) were the parameters chosen to assess the performance of the CO_2 capture plant. The results from the capture

plant used in the process designs PD-MEA1, PD-MEA2, PD-CHP2 and PD-CHP2-OXY are summarised in Table 4.5. It should be noted that in these process designs the CO_2 is separated from the biogas stream.

Table 4.5 Performance indicators of the CO_2 capture plant (PD-MEA1, PD-MEA2, PD-CHP2 and PD-CHP2-OXY)

Reboiler thermal energy ($GJ \cdot h^{-1}$)	CO_2 captured ($tCO_2 \cdot h^{-1}$)	**GJ/tCO_2**
8.9360 Solvent circulation ($m^3 \cdot h^{-1}$) 75.1315	2.1906	**4.0792** **m^3/tCO_2** **34.2968**

The results from the capture plant used in the process design PD-CHP1-POST are summarised in Table 4.6. It should be noted that in this process design the CO_2 is separated from CHP exhaust stream.

Table 4.6 Performance indicators of the CO_2 capture plant (PD-CHP1-POST)

Reboiler thermal energy ($GJ \cdot h^{-1}$)	CO_2 captured ($tCO_2 \cdot h^{-1}$)	**GJ/tCO_2**
23.0506 Solvent circulation ($m^3 \cdot h^{-1}$) 164.9478	5.7985	**3.9753** **m^3/tCO_2** **28.4468**

In order to put the above results in context, they will be compared against the results given in the parametric study by Abu-zahra *et al.* (2007). The authors obtained a value of 3.29 GJ/tCO_2 for the thermal energy required by the reboiler and 27.8 m^3/tCO_2 for the amount of solvent circulated to achieve 90% absorption efficiency. As one can see, the results shown in Tables 3.6 and 3.7 above compare well with the benchmark values. As for the capture plants that absorb the CO_2

from the biogas streams, the deviations can be explained by the higher amount of CO_2 removed in the cases studied in this thesis (97% CO_2 removed from the biogas streams against 90% in the study by Abu-zhara *et al*. The 97% CO_2 removal efficiency corresponds to the desired CH_4 concentration in the upgraded bio-methane (95 mol. %).

4.1.3.2 Combined heat and power generation

Biogas produced from the anaerobic digestion of waste is, in most cases, utilised in a Combined Heat and Power unit (CHP unit) for the combined generation of heat and electricity, in one single, highly efficient process. These installations typically offer an electrical efficiency of 33% and a thermal efficiency of 45% while the emissions of Volatile Organic Compounds (VOCs) are very limited (Smet *at al.*, 1999). CHP systems are often divided into different categories, depending on the energy output of the unit. The largest units are found in industrial complexes and are able to produce up to several thousand kW of electric power. On the other extreme, micro-CHP units are used in individual households and small businesses and can produce up to about 2 kW of electric power (ADE 2015). In a typically sized waste water treatment plant (40,000 m^3 waste water per day), CHP systems can produce over 200 kW of electric power (EPA, 2011).

In addition to the combined generation of heat and electricity, the CHP combustion process considered in this work will also provide a flue gas containing CO_2, which is processed downstream and eventually converted into a liquid fuel. This provides the opportunity to consider not only a biogas stream but also flue gases, which broadens the relevance of the work to a much wider range of circumstances.

A representation of the CHP plant considered in this study is shown in Figs. 4.5 and 4.6. The CHP model is based on a previous model developed by Aspen Plus (Aspen Technology, 2012a) that was adapted to the specific requirements of this work (flowrates, temperatures, split

ratios, *etc.*). Firstly, the biogas or the upgraded bio-methane (depending on the process configuration) is compressed from 1 bar to 8 bar. It is then mixed with steam (8 bar) and compressed air and then burned in the combustor to produce hot gas at 750 °C. Steam is used to lower the combustion temperature (below 750 °C) to minimise NO_X formation (Aspen Technology, 2012a). The combustor is modelled using a Gibbs reactor block (*RGibbs*) which models single-phase chemical equilibrium by minimizing Gibbs free energy, subject to atom balance constraints. The amount of air/oxygen fed into the combustor is maintained by a calculator block that varies its flowrate depending on the amount of CH_4 coming into the combustor. The hot gas is first passed through a gas turbine for electricity generation and then to the steam generation area to recover heat. In the steam generation area, the gas passes through five heat exchangers (modelled using the *HeatX* subroutine) and is cooled down by water or steam. As a result, electricity is produced in the steam turbine as well as three different grade steams: low-pressure (LP) steam at 1.013 bar, medium-pressure (MP) steam at 5 bar and high-pressure (HP) steam at 24 bar. All the compressors and turbines used in the CHP plant were modelled using the *Compr* model in Aspen Plus. For the compressors, an isentropic efficiency of 72% was assumed while for the turbines a value of 60% was used (Hanlon, 2001).

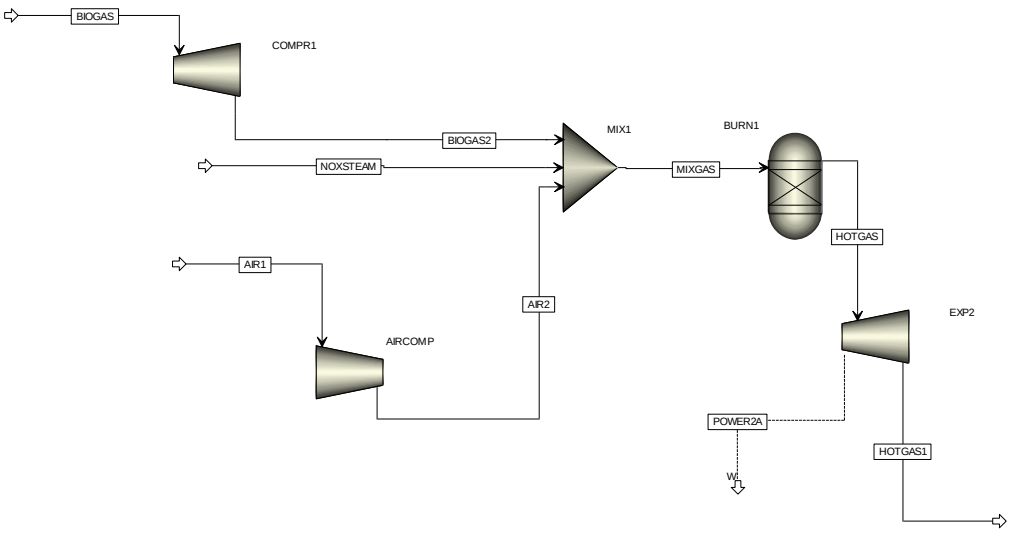

Fig. 4.5 Schematic representation of the gas turbine section in the CHP plant (Aspen Technology, 2012a)

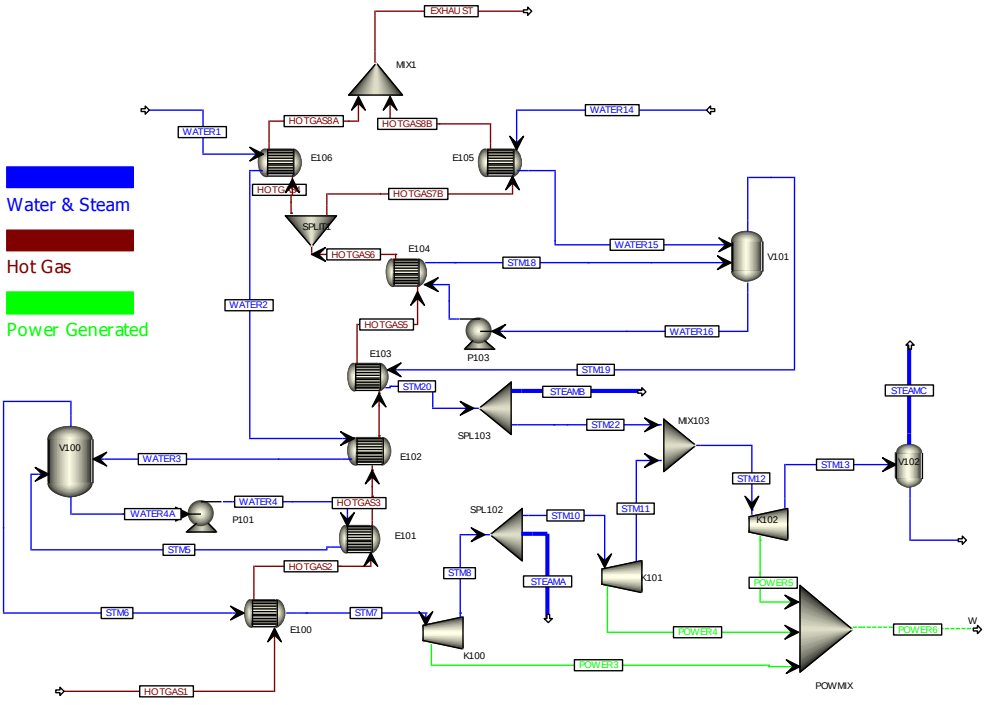

Fig. 4.6 Schematic representation of the steam turbine section in the CHP plant (Aspen Technology, 2012a)

Fig. 4.5 and 4.6 depict in fact a combined cycle gas turbine (CCGT). The CHP plant was chosen to be modelled as a CCGT due to the availability of model units in the Aspen library to model such system. According to a report by Aspen Tech (Aspen Technology, 2012a), the result from the model depicted in Figs. 4.5 and 4.6 are comparable to those obtained from a gas engine-based CHP plant. At the scale considered in this work for the CHP plant (5-10 MWe) a number of issues could arise regarding the operation of a small scale CCGT; however, it is considered that an analysis of such issues would be outside the scope of this study.

The process concepts evaluated in this study that consider a CHP unit to utilise the biogas (or upgraded bio-methane), namely PD-CHP1, PD-CHP1-OXY, PD-CHP1-POST, PD-CHP2, PD-CHP2-OXY, produce a flue gas (exhaust stream) that is fed into the RWGS reactor for CO_2 hydrogenation to syngas. As discussed in section 3.1.1, additional process concepts are considered in this study, which use oxy-combustion of the biogas instead of combustion with air, in order to assess the effect that reducing the volume of the CHP exhaust stream could have on process performance and thus on overall costs.

A cryogenic air separation unit (ASU), which is a mature technology, was considered to supply the oxygen to the oxy-combustor. Cryogenic distillation has been the predominant air separation technology for large-scale operations for over 75 years (NETL, 2012). Its use is recommended when volumes of oxygen higher than 100 tons per day are required (which is the case of the processes considered in this thesis) (Rao & Muller, 2007). The cryogenic ASU delivers oxygen (99.9 mol. %) at 8 bar since this is the pressure that we need in the burner. The ASU plant was not modelled in this study. Alternatively, since ASU is a well-established and mature technology, the production costs of O_2 at 99.9 mol. % and 8 bar were retrieved from the literature with a value of $\$35_{1994}$/tonne of oxygen, considering that the ASU is located next to

the CO_2 utilisation plant and therefore no transport costs are involved (Rao & Muller, 2007).

Since high temperatures and pressures are involved in the CHP plant, the property method called Peng-Robinson with Boston-Mathias (PR-BM) modification has been used to estimate the thermodynamic and physical properties of the all pure and binary systems involved. The PR-BM property method uses the Peng Robinson cubic equation of state with the Boston-Mathias alpha function for all thermodynamic properties (Aspen Technology, 2013). The Peng-Robinson equation-of-state is the basis for the PR-BM property method. The model has been implemented with choices of different alpha functions and has been extended to include advanced asymmetric mixing rules, if needed (Aspen Technology, 2013b). The default PR-BM property method uses the Boston-Mathias alpha function and standard mixing rules. These default property methods are recommended for gas processing applications such as the CHP plant.

Table 4.7 shows the electrical power and steam produced by the CHP plant in each process concept.

Table 4.7 Electrical power and steam generated by the CHP plant

	Total Power (kW)	**Steam C @ 1.01 bar ($kg \cdot h^{-1}$)**	**Steam B @ 5 bar ($kg \cdot h^{-1}$)**	**Steam A @ 24 bar ($kg \cdot h^{-1}$)**
PD-CHP1	7096	11346	458	1589
PD-CHP1-OXY	8364	9420	380	1319
PD-CHP2	7179	11152	450	1561
PD-CHP2-OXY	8443	9228	373	1292
PD-CHP1-POST	7096	11346	458	1589

In terms of electricity generation, the CHP plants employing oxy-combustion are able to produce more electrical power than the ones using combustion with air. This increased electricity generation is a consequence of the lower volume of oxidant (oxygen) being compressed in the oxy-combustion cases, what translates in a lower electricity consumption by the compressor and then a higher net electricity output in the plant. As for the CHP plants of the process concepts PD-CHP2 and PD-CHP2-OXY (CHP plants employing upgraded bio-methane as the feedstock), they produce electricity at a higher rate than their equivalent process using raw biogas as the feedstock, PD-CHP1 and PD-CHP1-OXY. Once again, this is explained by the lower volume to be compressed in the CHP plants using upgraded bio-methane, since in these cases most of the CO_2 in the biogas had been removed.

As for the steam, its production rate is directly proportional to the amount of hot flue gases coming into the steam generation area as well as to the temperature of the hot flue gases. Since the combustion temperature is controlled by injecting low pressure steam so that the hot flue gases are below 750 °C (in all cases considered), the difference between the steam production rates of the process designs are solely a consequence of the different flowrate of hot flue gases coming into the steam generation area.

4.1.3.3 Syngas production

The main process for producing syngas currently used in Fischer-Tropsch synthesis is steam reforming of methane which is a well-understood and proven technology (Wang *et al.*, 1996). The steam methane reforming is by far the most widely used technology for the industrial synthesis of hydrogen, amounting to nearly 40% of the global hydrogen production (Muradov, 2009). It is a mature technology that

has been in use for decades and that allows flexibility in terms of scale, from small units producing less than $1t \cdot h^{-1}$ to large manufacturing units producing several hundred of tones per hour (Muradov, 2009). The steam methane reformer employed in this study is depicted in Fig. 4.7.

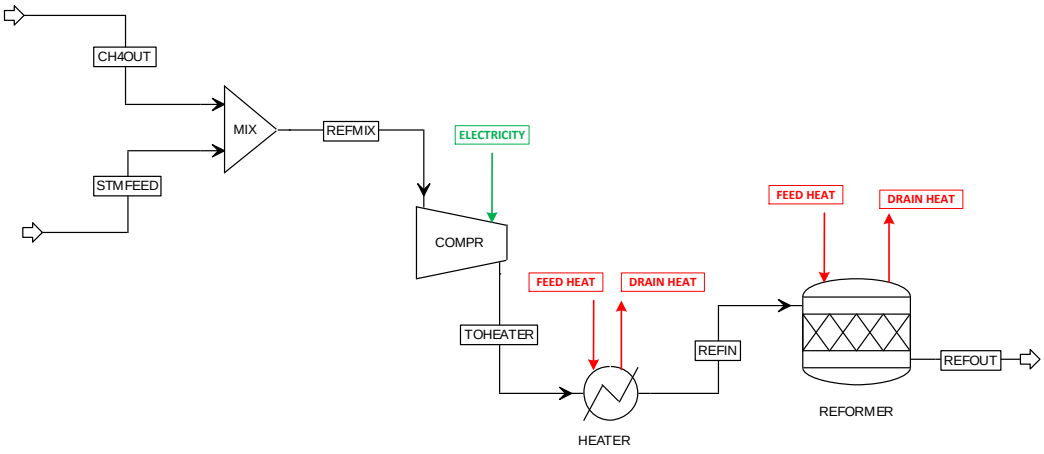

Fig. 4.7 Process flow diagram of the steam methane reformer as implemented in Aspen Plus

As one can see from Fig. 4.7, the upgraded bio-methane from the CO_2 removal section is utilised either in a methane steam reformer (PD-MEA1 concept, Fig. 3.2) or in the CHP plant (PD-CHP2 and PD-CHP2-OXY concepts, Figs. 3.6 and 3.7). In the process concept using a methane steam reformer (PD-MEA1), the CH_4-rich gas stream leaving the MEA absorption column is mixed with steam (2.6 MPa) and the resulting mixture is compressed to 25 bar, modelled using the *Compr* subroutine in Aspen Plus with an isentropic efficiency of 72% (Hanlon 2001), and then preheated to 850 °C before it is fed to the catalytic reforming reactor (Muradov, 2009). The steam/methane mixture is passed through a set of externally heated reformer tubes filled with nickel catalyst. Even though nickel shows less catalytic activity than some noble metals and it is more prone to deactivation (*e.g.* by coking), its use is justified by its relatively low cost (Muradov, 2009). The

steam/methane mixture is converted to CO and H_2 at 850 °C and 25 bar according to the following reaction:

$$CH_4 + H_2O \rightarrow CO + 3H_2 \qquad \Delta H^0 = 206\ kJ \cdot mol^{-1}$$

As one can see, the reaction is highly endothermic and it is favoured by low pressures since there is a net increase in the moles of gas produce during the reaction (from 2 mol of gas to 4 mol of gas). However, in most industrial application areas, hydrogen is required at high pressures; therefore, the reformers are operated at pressures between 20 a 26 bar (Muradov, 2009). In addition, elevated pressures allow for more compact reactor designs, which increases the reformer´s efficiency and decreases capital costs related to the reactor materials.

Although the theoretical molar ratio of steam to methane is 1:1, an excess of steam (H_2O:CH_4 = 1.2:1) is used to prevent deactivation of the catalyst owing to carbon deposition on its surface (Muradov, 2009). The amount of steam that is fed into the reformer is varied by a calculator block so that the H_2O:CH_4 molar ratio remains fixed at H_2O:CH_4 = 1.2:1. A pressure swing adsorption (PSA) system is used after the reformer to recover the excess of H_2 which is recycled back to the RWGS reactor. The steam reformer is modelled using a stoichiometric reactor block, known as *RStoic* in Aspen Plus, with a fractional conversion of CH_4 set to 80 % (Muradov, 2009). The unconverted CH_4 remains in the syngas stream.

As in the CHP plant, the Peng-Robinson with Boston-Mathias (PR-BM) modification property method has been used to estimate the thermodynamic and physical properties of all pure and binary systems involved.

4.1.3.4 CO_2 conversion

Reverse water gas shift (RWGS) process

The water-gas-shift reaction has attracted significant attention for the last several decades in order to adjust H_2/CO ratio in the syngas for

Fischer-Tropsch applications and also to oxidise CO to CO_2 during production of H_2 by steam reforming of methane (Muradov, 2009). By contrast, the reverse-water-gas-shift reaction has not attracted much attention due to low demand.

$$CO_2 + H_2 \rightarrow CO + H_2O \qquad \Delta H^0 = 41.2\ kJ \cdot mol^{-1}$$

The CO_2 conversion technology evaluated in this study is a RWGS reaction process based on the CAMERE pilot plant operated by the Korean Institute of Energy and Research (KIER) and Korea Gas Corporation (KOGAS) (Park *et al.*, 2004). The CAMERE process produces methanol from CO_2 in two steps: (1) conversion of CO_2 to CO and water in a RWGS reactor and (2) methanol synthesis after an intermediate water removal. Similar to the CAMERE process, the shift reactor in this study is operated over a $ZnAl_2O_4$ catalyst at 650 °C and atmospheric pressure with a feed gas mixture of CO_2 and H_2 preheated before the reactor. The CO_2 conversion process (RWGS reactor) evaluated in this thesis is shown in Fig. 4.8.

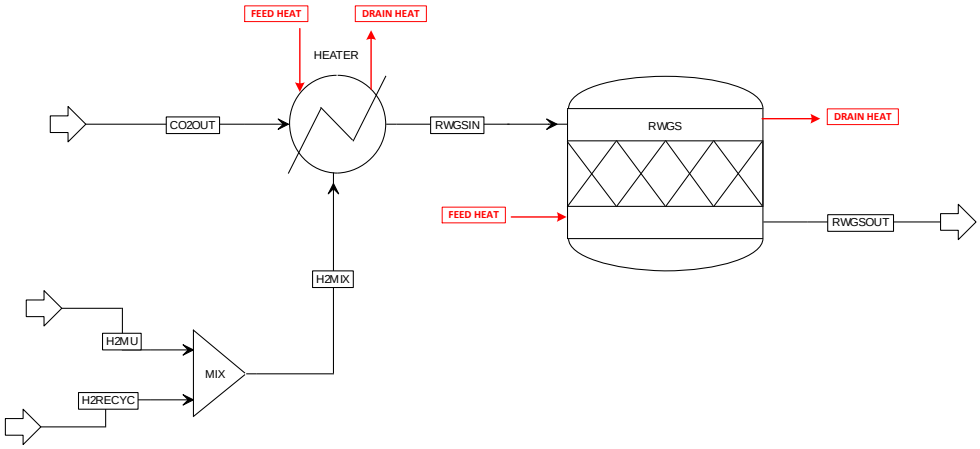

Fig. 4.8 Process flow diagram of the RWGS reactor as implemented in Aspen Plus

An excess of hydrogen (H_2:CO_2 = 3:1) is used to prevent carbon (coke) deposition on the catalyst surface. Similarly to the SMR, the amount of hydrogen that is fed into the RWGS reactor is varied by a calculator block so that the H_2:CO_2 molar ratio remains fixed at H_2:CO_2 = 3:1. The

feed CO_2-rich gas is produced by the MEA plant in the process concepts PD-MEA1, PD-MEA2, PD-CHP2 and PD-CHP2-OXY while in PD-CHP1 and PD-CHP1-OXY the CO_2 is generated in the CHP plant. In PD-CHP1-POST, the RWGS reactor is fed with the CO_2-rich produced by the post-combustion CO_2 capture plant

Although the CAMERE process described above is not a technology that has been implemented commercially at a global scale (as SMR has), it is used in this study because it fulfils the requirement for best available technology regarding CO_2 hydrogenation to syngas.

As with the steam methane reformer, the RWGS reactor is modelled using a stoichiometric reactor block, known as *RStoic* in Aspen Plus, with a fractional conversion of CO_2 set to 65% (Park *et al.*, 2004). The Peng-Robinson with Boston-Mathias (PR-BM) modification property method has been used to estimate the thermodynamic and physical properties of the all pure and binary systems involved in this process.

Hydrogen recovery

A pressure swing adsorption (PSA) system is used after the reformer (PD-MEA1) or the RWGS reactor (PDMEA-2, PD-CHP1, PD-CHP2, PD-CHP1-OXY, PD-CHP2-OXY and PD-CHP1-POST) to recover the excess H_2, which is recycled to the RWGS reactor for re-use. In the PSA process, highly volatile components with low polarity, such as hydrogen, are practically non-adsorbable as opposed to other molecules like N_2, CO, CO_2, hydrocarbons and water vapour. PSA is an established industrial process used extensively for gas or liquid separation and therefore its use is justified in this study as “best available technology”. Fig. 4.9 shows a representation of the Pressure Swing Adsorption (PSA) process.

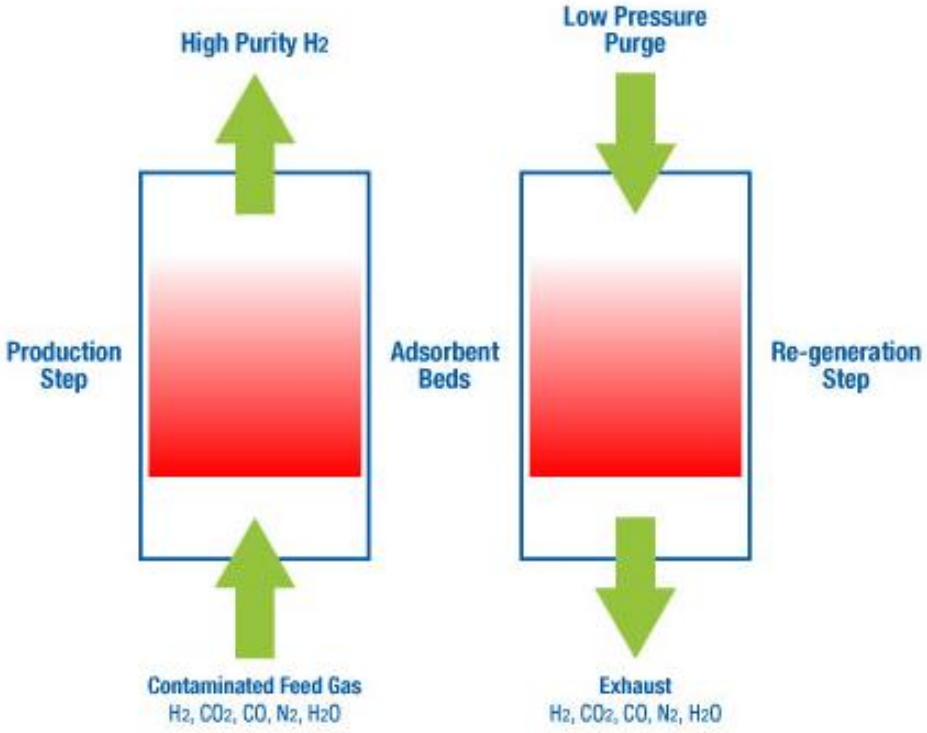

Fig. 4.9 Schematic representation of the PSA processes

In this study, the adsorption step is operated at moderate pressure (10 bar) until the equilibrium loading is reached, similarly to the Linde PSA technology (Linde, 2014). The adsorbent is regenerated by lowering the pressure to slightly above atmospheric.

As explained in section 4.1.3.5, the FT synthesis process should be operated at H_2:CO molar ratios of around 2 in order to achieve a high FT liquid production. The H_2/CO ratio in the syngas stream before the Fischer-Tropsch synthesis is well above 2 in all process concepts considered; therefore a pressure swing adsorption (PSA) process is employed to isolate the excess hydrogen. Since only a fraction of hydrogen needs to be separated from the syngas stream, a certain percentage of the syngas is directed to the PSA unit. This percentage is varied by a design specification, which measures the H_2/CO molar ratio in the syngas coming from the SMR and the RWGS reactor and

modifies the split fraction to the PSA process so that the H_2/CO molar ratio in the stream fed to Fischer-Tropsch reactor remains at 2. After the PSA, the syngas re-joins the main gas line and enters the FT reactor. The PSA unit was modelled using the *Sep* subroutine in Aspen Plus where an 85% hydrogen recovery was set according to Lau *et al.* (2002). The hydrogen leaves the PSA unit with a purity of 99.999 mol. % in H_2 (Linde, 2014).

The Peng-Robinson with Boston-Mathias (PR-BM) modification property method has been used to estimate the thermodynamic and physical properties of all pure and binary systems involved in this process.

4.1.3.5 Fuel synthesis

Discovered by Franz Fischer and Hans Tropsch in 1923, the Fischer–Tropsch (FT) process converts a mixture of CO and H_2 (syngas) into a variety of organic compounds, mainly hydrocarbon products of variable chain length, in the presence of a catalyst. The FT reactions are highly exothermic and can be represented by the following general reaction:

$$CO + 2H_2 \rightleftharpoons -CH_2 - + H_2O \;\; \Delta H^0 = -165\ kJ \cdot mol^{-1}$$

The general reaction describes the formation of linear alkanes ($-CH_2-$) which are the main products of FT synthesis. Alkenes, aromatic compounds and oxygenates, such as alcohols and ethers, can be also produced although in much lower quantities than alkanes (Dimitriou *et al.*, 2015).

Depending on the operating temperature of the process, two types of FT synthesis can be distinguished: low-temperature Fischer–Tropsch (LTFT) and high-temperature Fischer–Tropsch synthesis (HTFT). LTFT operates at temperatures between 200-250 °C which favour the production of liquid fuels up until middle distillates (Dry, 2002; Spath and Dayton, 2003). On the other hand, high-temperature Fischer–

Tropsch synthesis (HTFT) is operated at 300–350 °C, which results in higher gas and lower distillate yields (Dry, 2002). The FT process is generally operated at pressures ranging from 20–40 bar (Tijmensen *et al.*, 2002). In general, optimal operation of the FT synthesis process consists of low temperatures, high operating pressures and H_2:CO molar ratios of around 2 in order to achieve a high proportion of liquid fuels (De Klerk *et al.*, 2013).

Two types of catalysts are commercially used for FT fuel synthesis: Iron/based and cobalt-based catalysts. Cobalt-based catalysts have a higher selectivity for the production of alkanes and do not promote the water-gas-shift (WGS) reaction (Dimitriou, 2012). By contrast, the use of iron-based catalysts results in a higher WGS activity and lower liquid selectivity than cobalt catalysts (Jager & Espinoza, 1995). For this reason, the use of a cobalt-based catalyst is assumed in this thesis.

There are three main types of FT reactors: fluidised bed, fixed bed and slurry phase reactor (Bergman *et al.*, 2005; van der Drift & Boerrigter, 2006). In this study, the FT reactor is assumed to be equivalent to the Sasol Slurry phase reactor, the latest development of FT reactor technology by Sasol (Fleisch *et al.*, 2002), which represents the best available technology needed in this study.

The Fischer-Tropsch synthesis is a well-developed technology. The first and most widely known company that produces Fischer-Tropsch-derived fuels is the South African organisation, Sasol. The company developed the first FT reactors, the Arge reactors, back in the 1950s and has developed and commissioned improved reactor designs since then. The company´s last development, the Sasol Slurry Phase Distillate (SSPD) reactor, was commercialised in the early 1990s and is able to produce 2,500 barrels of synthetic fuels per day (Dimitriou, 2012). Other major petrochemical companies like Shell have demonstrated commercial operation of FT plants in Qatar and Malaysia (Dimitriou, 2012).

Fischer-Tropsch synthesis is not the only commercial technology that allows the conversion of syngas to a hydrocarbon mixture. The petrochemical company Mobil (today ExxonMobil) developed in the 1970s the methanol-to-gasoline (MTG) technology. This technology consists of two process steps. The first step is the methanol synthesis from syngas which takes place at temperatures of 300–400 ^{o}C and pressures of 30 - 40 bar, over a zinc chromite (ZnO/Cr_2O_3) catalyst (LeBlanc *et al.*, 1994). The second step is the MTG process itself whereby crude methanol is first dehydrated to form a mixture of DME, methanol and water and then the mixture is directly converted to C_5-C_{10} hydrocarbons by synthetic zeolite catalysts (ZSM-5) (Allum & Williams, 1988; Maiden 1988).

In addition to the MTG technology developed by Mobil, there is at least one more synthetic fuel technology that has achieved commercial success. This process is called Topsoe Integrated Gasoline Synthesis (TIGAS) and was developed by Topsoe in the 1980s (Dimitriou, 2012). It mainly differs from the MTG technology in the incorporation of the methanol synthesis and the DME synthesis into a combined methanol and DME synthesis process, thus eliminating the intermediate methanol production step.

Although the other fuel synthesis technologies could have been considered in this study, it was decided that the Fischer-Tropsch synthesis will be the fuel synthesis technology of choice in every process concept evaluated. The main reason for this is that the Fischer-Tropsch synthesis is more developed and proven technology than the other two. Furthermore, it was anticipated that both the MTG and TIGAS technologies would result in higher production costs of the fuel manufactured since they are more complex in nature due to the increased number of reaction steps involved (as opposed to the direct syngas to hydrocarbons conversion carried out by the Fischer-Tropsch reaction). This anticipation is supported by a recent techno-economic

study on Biomass-to-liquids (BTL) processes by Dimitriou (2012), which concludes that the conversion of biomass into liquid fuels through both the MTG and TIGAS technologies results in higher fuel production costs in all the cases considered.

The Fischer-Tropsch synthesis is not a selective process since it produces a wide range of products. Nevertheless, this high variability of products can be seen as a positive aspect since FT products cover the entire range of petrochemical products, such as gasoline, jet fuel and diesel provided that adequate process control exists in the process (Dimitriou *et al.*, 2015). FT fuels are high quality, free of sulphur and aromatic compounds and, unlike other fuels such as oxygenates, they can be easily assimilated in the existing transport infrastructure.

Because the FT synthesis is not a selective process, *i.e.* it produces a wide range of products, mainly paraffins, an upgrading plant is often placed after the FT reactor so that the FT liquid products (FT "syncrude") meets market requirements. Seven major unit operations are involved in the FT product upgrading: distillation, hydrogen production, wax (C_{20+}) hydrocracking, naphtha (C_{5-10}) hydrotreating, middle distillate (C_{11-19}) hydrotreating, C_5/C_6 isomerization, and catalytic reforming (C_{7-10}) (Becker *et al.*, 2012). As one can see from a report by Bechtel (1998), the modelling effort to accurately represent the upgrading unit is considerable. Given the main objectives of this thesis it was decided that an upgrading unit will not be considered and therefore the main product of all process concepts will be FT syncrude. This decision does not compromise the achievement of the thesis objectives since this work will help identify the most promising routes for the conversion of carbon dioxide into a synthetic fuel. It is assumed that the upgrading unit would be nearly identical in each process concept and thus its consideration would not affect, in terms of comparability, the overall process efficiencies and production costs.

The FT synthesis employed in this study is depicted in Fig. 4.10.

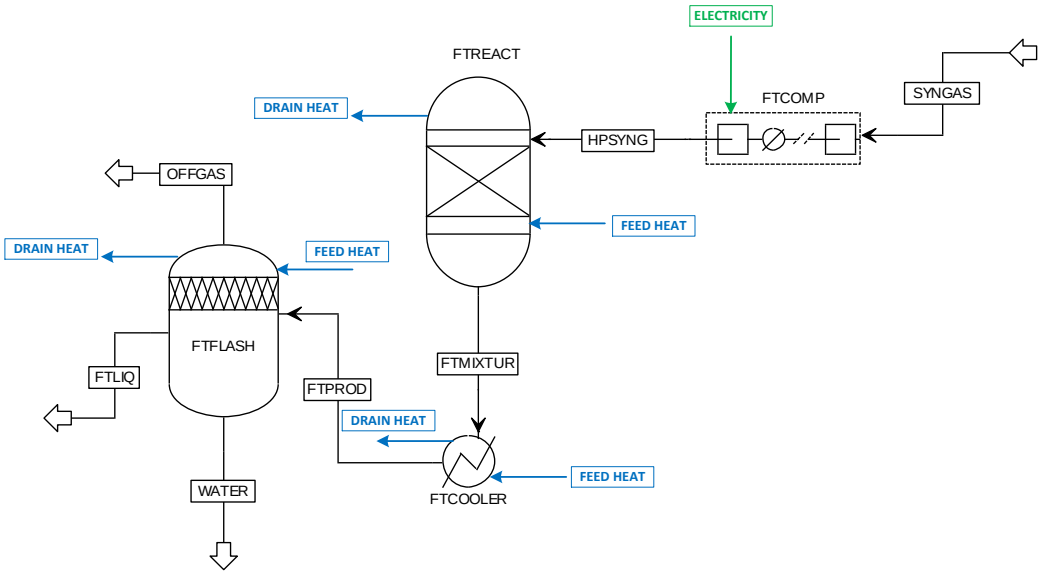

Fig. 4.10 Process flow diagram of the Fischer-Tropsch synthesis as implemented in Aspen Plus

The syngas with H_2:CO molar ratio of 2:1 is fed to a multistage compressor (*MCompr* subroutine in Aspen Plus with an isentropic compression efficiency of 72% (Hanlon, 2001) where it is compressed to 30 bar. The FT reactor is modelled using a yield reactor block (*RYield* subroutine in Aspen Plus). In order to use the *RYield* block in Aspen Plus, the mass yields (mass fractions) of all products (hydrocarbons, water, unreacted CO and unreacted hydrogen) need to be determined first. These mass yields were calculated in a separate spreadsheet as a result of a collaboration with Dr Ioanna Dimitriou at The University of Sheffield and subsequently implemented in Aspen Plus. The ASF distribution model was employed to calculate the FT product stream mass yields.

As mentioned earlier in the section, the FT synthesis is not a selective process and thus a wide range of products are obtained. As a consequence, a quantitative approximation of product distribution is necessary. The most widely used approach to quantitatively

approximate the FT product distribution is the Anderson–Schulz–Flory (ASF) method. According to this method, the produced carbon chain can either undergo further addition of a $–CH_2–$ group or the chain can terminate. The ASF-product distribution model is represented by Eq. 4.7:

$$C_n = \alpha^{n-1}(1-\alpha) \quad \text{Eq. 4.7}$$

where C_n is the molar fraction of a hydrocarbon product consisting of n carbon atoms and α the chain growth probability which determines the hydrocarbon product distribution. The chain growth probability α is influenced by a number of factors, such as the type and age of catalyst, the H_2:CO molar ratio in the feed gas, reactor type and operating condition (Dimitriou *et al.*, 2015). In this study, the ASF hydrocarbon distribution was taken up to a carbon number of 30 due to the negligible amount of parafins of longer chain (Dimitriou *et al.*, 2015). The production of aromatic compounds, oxygenates and olefins is assumed to be negligible since the presence of these compounds is typically small for low-temperature Fischer-Tropsch (Kaneko *et al.*, 2000).

A chain growth probability of 0.85, which favours the production of middle distillates, was chosen for the estimation of the product composition based on reported literature values (Swanson *et al.*, 2010a). The single-pass CO conversion was set to 80% (Dimitriou *et al.*, 2015).

As for the property method, the Peng-Robinson with Boston-Mathias (PR-BM) modification property method has been used to estimate the thermodynamic and physical properties of the all pure and binary systems involved in the FT process.

The mass yields needed by the FT reactor block in Aspen (*RYield*) for all the process concepts considered are shown in Table 4.8. It must be noted that N_2 and CO_2 are considered as inert components in the FT synthesis; therefore these components are not included in the mass

yield basis shown in Table 4.8. In all cases the FT reactor operates at a temperature of 220 °C and 30 bar of pressure.

Table 4.8 Component mass yield implemented in the FT reactor

	PD-MEA1	PD-MEA2	PD-CHP1	PD-CHP1-OXY	PD-CHP2	PD-CHP2-OXY	PD-CHP1-POST
Aspen Component	Mass Yield	Mass Yield	Mass Yield	Mass Yield	Mass Yield	Mass Yield	Mass Yield
CO	0.1309	0.1106	0.1076	0.1115	0.1086	0.1111	0.1108
H_2	0.0130	0.0110	0.0107	0.0111	0.0108	0.0111	0.0110
H_2O	0.5225	0.6503	0.6618	0.6497	0.6580	0.6500	0.6517
CH_4	0.0731	0.0079	0.0056	0.0058	0.0063	0.0065	0.0057
ETHANE	0.0108	0.0091	0.0089	0.0092	0.0090	0.0092	0.0092
PROPANE	0.0135	0.0114	0.0111	0.0115	0.0112	0.0114	0.0114
BUTANE	0.0151	0.0128	0.0124	0.0129	0.0125	0.0128	0.0128
PENTANE	0.0159	0.0135	0.0131	0.0136	0.0132	0.0135	0.0135
HEXANE	0.0162	0.0137	0.0133	0.0138	0.0134	0.0137	0.0137
HEPTANE	0.0160	0.0135	0.0131	0.0136	0.0133	0.0136	0.0135
OCTANE	0.0155	0.0131	0.0127	0.0132	0.0129	0.0132	0.0131
NONANE	0.0148	0.0125	0.0122	0.0126	0.0123	0.0126	0.0125
DECANE	0.0139	0.0118	0.0115	0.0119	0.0116	0.0118	0.0118
UNDECANE	0.0130	0.0110	0.0107	0.0111	0.0108	0.0111	0.0110
N-DOD-01 (C_{12})	0.0121	0.0102	0.0099	0.0103	0.0100	0.0102	0.0102
N-TRI-01 (C_{13})	0.0111	0.0094	0.0091	0.0094	0.0092	0.0094	0.0094
N-TET-01 (C_{14})	0.0101	0.0086	0.0083	0.0086	0.0084	0.0086	0.0086
N-PEN-01 (C_{15})	0.0092	0.0078	0.0076	0.0079	0.0077	0.0078	0.0078
N-HEX-01 (C_{16})	0.0084	0.0071	0.0069	0.0071	0.0069	0.0071	0.0071
N-HEP-01 (C_{17})	0.0076	0.0064	0.0062	0.0064	0.0063	0.0064	0.0064

N-OCT-01 (C_{18})	0.0068	0.0057	0.0056	0.0058	0.0056	0.0058	0.0058
N-NON-01 (C_{19})	0.0061	0.0051	0.0050	0.0052	0.0051	0.0052	0.0052
N-EIC-01 (C_{20})	0.0055	0.0046	0.0045	0.0046	0.0045	0.0046	0.0046
N-HEN-01 (C_{21})	0.0049	0.0041	0.0040	0.0041	0.0040	0.0041	0.0041
N-DOC-01 (C_{22})	0.0043	0.0037	0.0036	0.0037	0.0036	0.0037	0.0037
N-TRI-02 (C_{23})	0.0038	0.0032	0.0032	0.0033	0.0032	0.0033	0.0033
N-TET-02 (C_{24})	0.0034	0.0029	0.0028	0.0029	0.0028	0.0029	0.0029
N-PEN-02 (C_{25})	0.0030	0.0026	0.0025	0.0026	0.0025	0.0026	0.0026
N-HEX-02 (C_{26})	0.0027	0.0023	0.0022	0.0023	0.0022	0.0023	0.0023
N-HEP-02 (C_{27})	0.0024	0.0020	0.0019	0.0020	0.0020	0.0020	0.0020
N-OCT-02 (C_{28})	0.0021	0.0018	0.0017	0.0018	0.0017	0.0018	0.0018
N-NON-02 (C_{29})	0.0018	0.0015	0.0015	0.0016	0.0015	0.0016	0.0015
N-TRI-03 (C_{30})	0.0107	0.0090	0.0088	0.0091	0.0089	0.0091	0.0091

Table 4.8 shows that a fairly large amount of water is produced in all process concepts. This was expected mainly due to: a) water present in the syngas; b) one mole of water is produced per mole of CO fed into the reactor (assuming full conversion of CO), given the Fischer-Tropsch synthesis general reaction: $CO + 2H_2 \rightleftharpoons -CH_2 - +H_2O$.

The FT reactor's gas effluent is fed into a three phase separator (modelled with the *Flash3* subroutine in Aspen Plus) to remove water and heavy hydrocarbons from the residual vapour. The FT off-gas which mainly consists of light hydrocarbons (C_1–C_4) and unconverted syngas is combusted to generate low pressure steam which is utilised by the anaerobic digesters, whereas the liquid products are sent to a central refinery plant for further upgrading. The FT off-gas combustor is depicted in Fig. 4.11.

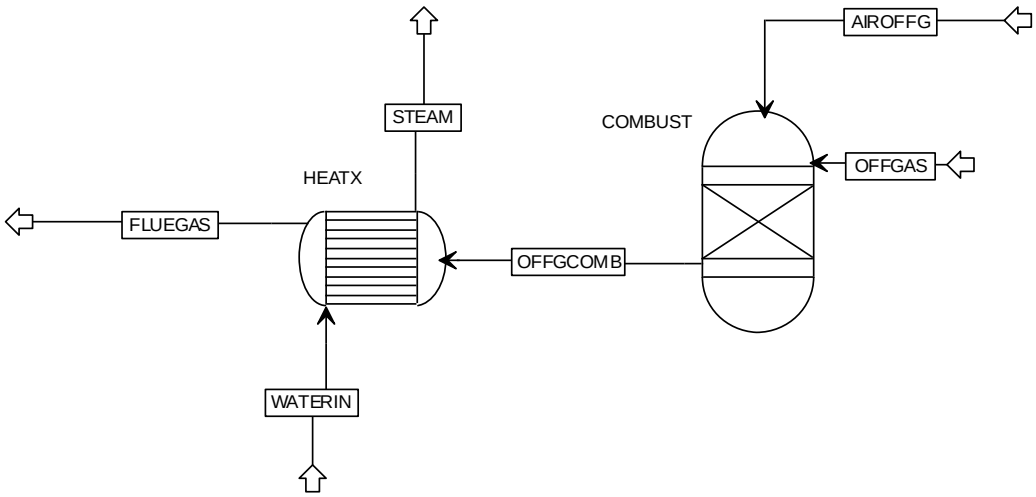

Fig. 4.11 Process flow diagram of the FT off-gas combustor

The FT off-gas combustor is modelled using the *RGibbs* subroutine in Aspen Plus which models single-phase chemical equilibrium by minimizing the Gibbs free energy, subject to atom balance constraints. The hot flue gas produced by the combustion is passed through a heat exchanger (*HeatX* block in Aspen), which is fed with water on the cold side to produce low pressure steam.

4.1.4 Processes using ionic liquids for CO_2 capture

This section reviews the simulation methodology developed in order to model the ionic liquid-based CO_2 capture processes described in

section 3.2.1. It consists of a novel modelling approach, which produces data hitherto not calculable, *e.g.* plant efficiencies, capital costs, operating and maintenance costs, *etc.* When data were obtained as a result of a collaboration, it is appropriately stated.

The process flowsheets of the three studied biogas upgrading plants have been developed using Aspen Plus as the process simulation software, which enabled the estimation of mass and energy balances as well as utility requirements. These calculations were then used as the inputs for the techno-economic assessments.

The COSMO-SAC property method has been used in Aspen Plus to model the different unit operations present in this study. This model is regarded as a robust preliminary tool for fast screening and design of ILs for CO_2 capture as it readily provides relevant information on gas-liquid interaction without having to rely on either binary interaction parameters or experimental data (Lee & Lin, 2015; Palomar *et al.*, 2011; Sumon & Henni, 2011; Zhang *et al.*, 2008), which often consume time and resources. COSMO-SAC is a solvation model (COnductor-like Screening Model with Segment Activity Coefficient) that describes the electrical interactions in the molecular surface of polarizable species (Aspen Technology, 2013b). Although it requires complex quantum mechanics calculations, they only have to be done once for a particular molecule, after which the results can be stored. Unlike other activity coefficient models such as UNIFAC or UNIQUAC, individual atoms are used for phase equilibria as the building blocks instead of functional groups. This enables the COSMO-SAC model to be more flexible as it can be applied to a wider range of systems, for instance complex molecules such as the ionic liquids considered in this study which are not present in the Aspen Plus database.

The solubility of a gas in a solvent is determined assuming identical fugacity of the gas in both the vapour and liquid phases (Lee & Lin, 2015),

$$y_i P \bar{\phi}_i = P_i = x_i \gamma_i(T, P, x) f_i(T, P) \quad \text{Eq. 4.8}$$

where x_i and y_i are the mole fraction of the gas in the vapour and liquid phases respectively, P the total pressure of the system, P_i the partial pressure of the gas, $\bar{\phi}_i$ the fugacity coefficient in the vapour phase, γ_i the activity coefficient in the liquid phase and f_i the fugacity of the gas molecule (CO_2 and CH_4 in this study) in a hypothetical liquid state at pressure P and temperature, T. Given the extremely low vapour pressure of the liquids considered in this study (Brennecke & Gurkan, 2010; Zhang *et al.*, 2012) and the nature of the gaseous species (CO_2 and CH_4), it can be assumed that the vapour phase has an ideal behaviour (*i.e.* $\bar{\phi}_i = 1$) and thus the solubility of the gas in the liquid phase (x_i) can be calculated at a given pressure P and temperature T and partial pressure of the gas P_i using:

$$P_i = x_i \gamma_i(T, P, x) f_i(T, P) \quad \text{Eq. 4.9}$$

The COSMO-SAC model calculates the liquid activity coefficient γ_i following Eq. 4.10:

$$\ln \gamma_i = \frac{A_i}{a_{eff}} \sum_{\sigma_m} p_i(\sigma_m)[\ln \Gamma_S(\sigma_m) - \ln \Gamma_i(\sigma_m)] + \ln \gamma_i^{SG} \quad \text{Eq. 4.10}$$

where A_i is the molecular surface area of component *i*, a_{eff} the standard segment surface area, $p_i(\sigma_m)$ the sigma profile of component *i*, $\Gamma_S(\sigma_m)$ the segment activity coefficient of segment σ_m in the solvent mixture, $\Gamma_i(\sigma_m)$ the segment activity coefficient of segment σ_m in component *i* and γ_i^{SG} the Staverman-Guggenheim model for combinatorial contribution to γ_i.

In the COSMO-SAC model, the probability distribution of surface charge density, called the sigma profile $p_i(\sigma_m)$, describes the electronic nature of the molecule of study as:

$$p_i(\sigma_m) = \frac{A_i(\sigma_m)}{A_i} \qquad \text{Eq. 4.11}$$

It must be noted that in Aspen Plus, the COSMO-SAC model does not require binary parameters in order to account for the interaction between components but it requires six input parameters that are genuine of the COSMO-SAC model for each component. The first parameter called *CSACVL* is the component volume parameter which is always defined in cubic angstroms. The remaining parameters *SGPRF1* to *SGPRF5* are five molecular component sigma profile parameters. All six input parameters are obtained using the COSMO-RS (COnductor-like Screening Model for Real Solvents) methodology. In this study the COSMO*thermX*® program (COSMO*logic*, 2015) is used to perform the COSMO-RS calculations and thus obtain the parameters needed by the COSMO-SAC property method in Aspen Plus. A detailed explanation on how the COSMO*thermX*® program was used can be found in section 4.1.4.8 In addition to these genuine six parameters, the COSMO-SAC property method in Aspen needed a set of pure component physical properties as detailed in section 4.1.4.7.

The following sections describe in detail the Aspen Plus implementation of the different unit operations that are included in the biogas upgrading plant.

4.1.4.1 Biogas compressor

Biogas is produced by the anaerobic digester plant at atmospheric pressure. Since the packed absorber operates at 30 bar in order to enhance the absorption process, biogas needs to be compressed to the absorber´s operating pressure. A multistage centrifugal compressor with intercooling was used for the compression of the biogas, which was modelled using the Aspen *Compr* subroutine. The specifications of the compressor are shown in Table 4.9.

Table 4.9 Biogas compressor specifications

Specification	Value
Number of stages	3
Compression type	Isentropic using ASME method
Discharge pressure (bar)	30
Isentropic efficiency (default)	0.72
Intercooling outlet temperature (°C)	120
Outlet temperature from last stage (°C)	15

The compression type was chosen to be isentropic with an isentropic efficiency of 0.72, which is the default value in Aspen Plus. The rigorous ASME calculation method was used since it provides the most accurate results (Aspen Technology, 2000). Once the isentropic calculations were carried out, the process flowsheet was implemented in Aspen Process Economic Analyzer (APEA), which calculated the compressor driver efficiency, given the compression conditions and compressor type. APEA calculates then the electrical power of the compressor driver using both the isentropic efficiency and the driver efficiency. This actual compressor electrical consumption was the value used for the estimation of the total electrical power consumption in the plant. Intercooling was required to decrease the temperature of the gas being compressed to the absorber operating temperature (15 °C).

4.1.4.2 Absorption column

The actual absorption process takes place in the absorption column. This packed absorber is fed with biogas from the bottom and the ionic liquid from the top, which flow in a counter-current pattern. At the given operating conditions, the ionic liquid solution absorbs the most soluble gas, in this case CO_2, leaving the bottom of the column as a CO_2-

enriched solution. The gas stream lean in CO_2 leaves the absorber from the top. The absorption column was modelled in Aspen Plus with the *RadFrac* subroutine, which is suitable for modelling a wide range of vapour-liquid fractionation processes (Aspen Technology, 2000). The packed absorber characteristic as implemented in Aspen Plus are summarised in Table 4.10.

Table 4.10 Specification of the packed absorption column

Specification	**Value**
Number of theoretical stages	5
Calculation type	Rate-based
Condenser	None
Reboiler	None
Convergence algorithm	Sum-rates
Packing type	Pall rings
Column diameter (m)	1.2
Packing height (m)	20

Once more, the number of theoretical stages was chosen as the minimum that made the model converge. Any further increase in the number of theoretical stages did not result in any improvements in performance. A design specification is used to obtain the desired CH_4 concentration of 95 vol. % in the upgraded bio-methane stream by adjusting the flowrate of ionic liquid fed into the column.

As in the capture plant used in the Base Case Models (MEA-based CO_2 capture plant detailed in section 4.1.3.1), the rate-based calculation method was chosen to model the absorption column since it is a fundamental, rigorous approach which avoids the approximations of efficiency and Height Equivalent to a Theoretical Plate (HETP). Rate-based distillation calculations directly account for the mass and heat

transfer rate processes in the system of equations representing the separation unit (Aspen Technology 2013d).

The height of the absorption column was specified as the one to achieve the desired CH_4 purity in the upgraded bio-methane (95 mol. % CH_4) with a minimum solvent (ionic liquid) flow-rate.

The diameter of both the absorber and the stripper were chosen as the minimum that complied with the Aspen Plus default column flooding condition (a vapour velocity value 80% of that which would cause flooding).

As in the MEA-based capture process, pall rings were used in the absorber as the type of packing, which has been considered by other authors in similar CO_2 capture processes using ionic liquids as physical absorbents (Basha *et al.*, 2013; Basha *et al.*, 2014). Random packing was chosen due to its lower costs and better liquid distribution (Sonderby *et al.*, 2013), especially when using high viscosity liquids such as the ionic liquids studied in this work. The liquid and vapour phase binary mass transfer coefficients as well as the total interfacial area for mass transfer were estimated using the Billet & Schulte's correlation, as in the MEA process, which provides good estimates of mass transfer-related parameters over a wide range of packing types, sizes and operating conditions (Billet & Schultes, 1993).

4.1.4.3 Upgraded bio-methane turbine

The upgraded bio-methane stream lean in CO_2 that leaves the top of the packed absorber at high pressure (29.5 bar, assuming 0.5 bar pressure drop across the column) is fed into a turbine, which extracts energy from the stream at high pressure and converts it into useful work. The turbine was modelled in Aspen Plus using the *Compr* model with the turbine calculation type. As with the biogas compressor, the compression type was chosen to be isentropic with an isentropic efficiency of 0.72, which is the default value in Aspen Plus. Similarly,

the electrical output of the generator coupled to the turbine was calculated by Aspen Process Economic Analyzer (APEA), given the process conditions and turbine type.

4.1.4.4 Regeneration flash evaporator

The process concepts considered in this work employ pressure swing solvent regeneration option whereby physical absorption is carried out at high pressure, while the regeneration of the solvent (desorption of the gases) takes place at pressures below the atmospheric pressure. The IL-rich solution leaves the bottom of the packed absorber at high pressure and is fed into the adiabatic flash evaporator (flash drum) where the solution undergoes a reduction in pressure (from 29.5 bar to 0.01 bar). In the vessel, the liquid settles to the bottom of the vessel due to gravity while the vapour escapes through the top of the vessel.

4.1.4.5 Solvent recirculation pump

As explained in the previous sections, the regenerated IL-lean solution leaves the bottom of the flash evaporator at low pressure (0.01 bar) and needs to be brought back to the column operating pressure of 30 bar. A centrifugal pump is therefore used in order to pressurize the IL-lean solution back to the absorption column, which was modelled using the Aspen *Pump* subroutine. The pump efficiency was set to 0.7, which is assumed to be a reasonable value for centrifugal pumps (Coulson *et al.*, 1995). Then, the process flowsheet was implemented in Aspen Process Economic Analyzer (APEA), which calculated the driver efficiency, given the liquid conditions and pump type. APEA calculates then the electrical power of the pump motor using both the pump efficiency and the driver efficiency. This actual motor electrical power was the value used for the estimation of the total electrical power consumption in the plant.

4.1.4.6 Pre-absorber solvent cooler

A pre-absorber solvent cooler is included in the biogas upgrading plant to cool down the IL-lean solution back to 15 °C. This cooler needs to be used because the IL solution undergoes an increase in temperature due to the enthalpy of solution when the gases (mostly CO_2) are absorbed into the liquid in the packed absorber. Moreover, following the adiabatic flash evaporation stage, the IL-lean solution is pressurized back to 30 bar from 0.01 bar what further increases the temperature of the IL-lean solution. The cooler is modelled in Aspen Plus using the *Heater* block.

4.1.4.7 Pure component physical properties

Since the ionic liquids studied in this work are not included in the Aspen Plus component database, pure ionic liquid physical properties were retrieved from the literature and implemented in Aspen Plus. Data regression was used in order to represent accurately important properties in the desired range of pressure and temperature. It is based on maximum likelihood estimation and processes raw data to determine parameters for physical property models. The estimated parameters and their corresponding models and physical properties are shown in Table 4.11.

Table 4.11 Model parameters and corresponding physical properties

Parameter	**Property model**	**Physical property**
CPIG	Ideal gas heat capacity polynomial	Ideal gas heat capacity
DNLDIP	DIPPR equation	Liquid molar volume (liquid density)
MULAND	Andrade equation	Liquid viscosity

In all cases, the Britt-Luecke algorithm was used with the Deming initialization method (Britt & Luecke, 1973). It must be noted that the PLXANT parameter needed by the extended Antoine equation for the

estimation of the liquid vapour pressure was set to the minimum allowable value in Aspen Plus of 1×10^{-18} due to the negligible vapour pressure inherent to ionic liquids (Brennecke & Gurkan, 2010; Zhang *et al.*, 2012). The data sources of the ionic liquid´s ideal gas heat capacity, liquid density and liquid viscosity are given in Table 4.12.

Table 4.12 Data sources of the ionic liquids physical properties

	$[C_2MIm][Tf_2N]$	**$[C_6MIm][Tf_2N]$**	**$[P_{66614}][Tf_2N]$**
Ideal gas heat capacity	(Paulechka *et al.*, 2007)	(Blokhin *et al.*, 2006)	(Ferreira *et al.*, 2013)
Liquid density	(Jacquemin *et al.*, 2007)	(Widegren & Magee, 2007)	(Neves *et al.*, 2011)
Liquid viscosity	(Schreiner *et al.*, 2010)	(Widegren & Magee, 2007)	(Neves *et al.*, 2011)

The results from the data regressions of the ionic liquids' physical properties are discussed. The experimental values included in Figs. 4.12-4.14 were retrieved from the literature as described in Table 4.12.

Fig. 4.12 shows the experimental values of the ideal gas heat capacity, C_P at different temperatures as well as the results from the data regression in Aspen Plus. As one can see, the results predicted by Aspen Plus compare well with experimental temperature.

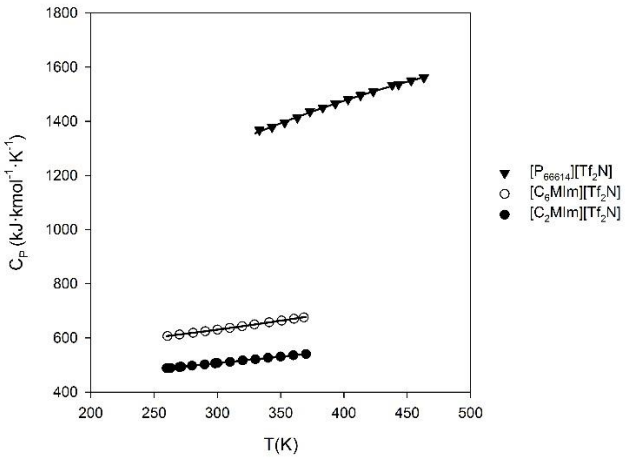

Fig. 4.12 Heat capacity of the selected ionic liquids as a function of temperature. Solid lines represent Aspen predictions

Similarly, the viscosity of the three ionic liquids reported in the literature at different temperatures, μ along with the predicted values from Aspen Plus are included in Fig. 4.13.

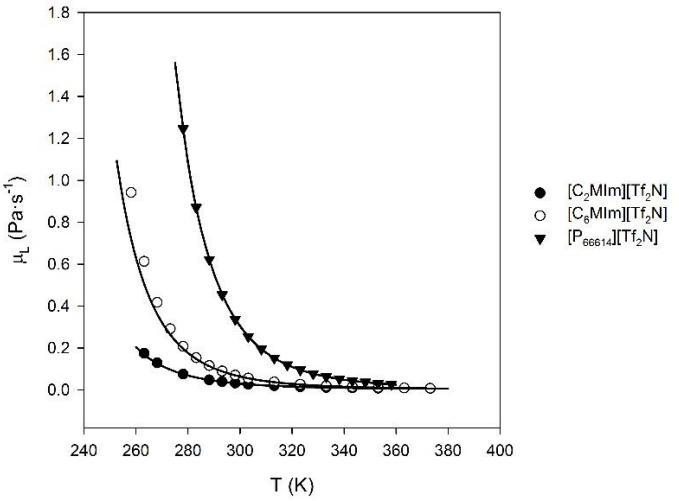

Fig. 4.13 Viscosity of the selected ionic liquids as a function of temperature. Solid lines represent Aspen predictions

The predicted viscosity of the ionic liquid correlates well with the experimental data reported in the literature. Finally, the density of the

ionic liquids within a range of temperatures is shown in Fig. 4.14 along with the predicted values.

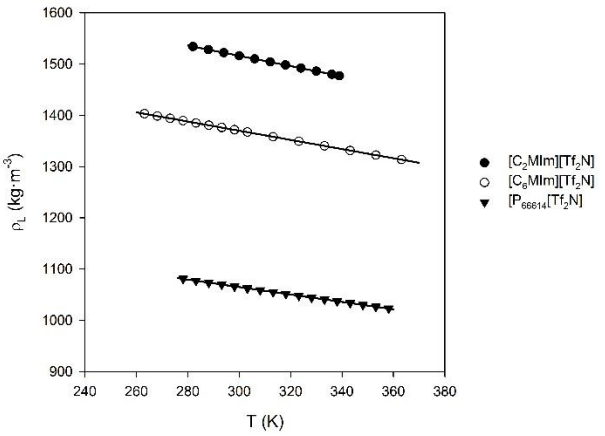

Fig. 4.14 Density of the selected ionic liquids as a function of temperature. Solid lines represent Aspen predictions

In addition to the properties shown in Table 4.12, a range of scalar physical properties, *i.e.* non-temperature or pressure dependent, are shown in Tables 4.13-4.15. The molecular weights of the ionic liquids were retrieved from the Sigma-Aldrich catalogue (SIGMA-ALDRICH, 2015). The boiling point, critical temperature, critical pressure, critical volume and acentric factor of the ionic liquids were estimated using the modified Lydersen-Joback-Reid group contribution method proposed by Valderrama & Rojas (2009), which is considered the most robust and common technique for ionic liquid´s critical properties estimation. Finally, the volume parameter of the COSMO-SAC model was calculated using the COSMO*thermX*® software (COSMO*logic*, 2015).

Table 4.13 Scalar properties of [C_2MIm][Tf_2N] ionic liquid

Property	**Value**
Molecular weight, $g \cdot mol^{-1}$	391.310
Boiling point, K	805.930
Critical temperature, K	1244.700
Critical pressure, bar	32.610
Critical volume, $cm^3 \cdot mol^{-1}$	892.890
Acentric factor	0.182
COSMO-SAC volume parameter, $Å^3$	376.700

Table 4.14 Scalar properties of [C_6MIm][Tf_2N] ionic liquid

Property	**Value**
Molecular weight, $g \cdot mol^{-1}$	447.420
Boiling point, K	897.450
Critical temperature, K	1287.000
Critical pressure, bar	23.860
Critical volume, $cm^3 \cdot mol^{-1}$	1121.330
Acentric factor	0.354
COSMO-SAC volume parameter, $Å^3$	464.670

Table 4.15 Scalar properties of $[P_{66614}][Tf_2N]$ ionic liquid

Property	**Value**
Molecular weight, $g \cdot mol^{-1}$	764.023
Boiling point, K	1310.560
Critical temperature, K	1586.735
Critical pressure, bar	8.513
Critical volume, $cm^3 \cdot mol^{-1}$	2423.540
Acentric factor	0.892
COSMO-SAC volume parameter, $Å^3$	973.494

4.1.4.8 Sigma profiles

As part of a collaboration with Dr Johan Jacquemin at Queen's University Belfast (QUB), the 3D molecular structure optimisation of each investigated ion and gas and the generation of their COSMO file were performed using TURBOMOLE quantum chemistry package (Ahlrichs *et al.*, 1989) and were then visualised using COSMOthermX® program (version C30_1501, COSMO*logic* 2015). The structures were optimized at QUB with a convergence criterion of 10−8 Hartree in the gas phase. The TURBOMOLE 6.0 program package was used for all the density functional theory (DFT) calculations using the Resolution of Identity approximation (Weigend & Häser, 1997). The B3LYP functional (Talaty *et al.*, 2004) was chosen for geometry optimization and all calculations were finished with the def-TZVP basis set (Talaty *et al.*, 2004), combining the RI technique calculations as recommended by COSMO*logic* (COSMO*logic,* 2015). The σ-profile for each ion or gas was generated at QUB from its COSMO file using COSMOthermX® (COSMO*logic* 2015), and the σ -profile for each ionic liquid was determined as the sum of the cation and anion σ -profiles. These sigma profiles were then implemented in Aspen Plus within the COSMO-SAC property method.

To test the functionality of the modified Aspen databank, the CH_4 and CO_2 solubility data in selected ionic liquids were firstly modelled. This choice was made for a number of reasons: firstly, the single gas solubility in solvent can be relatively easily calculated in Aspen Plus by simulating a flash simulator. Secondly, CO_2 and CH_4 solubility data are already reported in the literature for the three selected ionic liquids at elevated pressures (Carvalho *et al.*, 2009; Liu *et al.,* 2013; Zubeir *et al.,* 2015; Kumełan *et al.,* 2007; Carvalho *et al.,* 2010). Thirdly, the COSMO-RS model has previously been used at QUB for predicting data of the gas solubility in ionic liquids (Manan *et al.*, 2009). Figs. 4.15-4.19 show how the solubility data predictions from Aspen Plus correlates with experimental data (when available) for both CO_2 and CH_4 in the three ionic liquids. In general, the Aspen predictions compare reasonably well, in terms of Average Relative Deviation (ARD), with experimental data (10.35%-27.23% ARD for CO_2 and 26.72%-36.14% ARD for CH_4). These ARD values are in the range of those reported by other authors using COSMO calculations for gas solubility predictions in ionic liquids (Lee & Lin, 2015). Only at elevated pressure (above the ionic liquid's critical pressure) the COSMO-SAC model predictions start to deviate considerably from the experimental values.

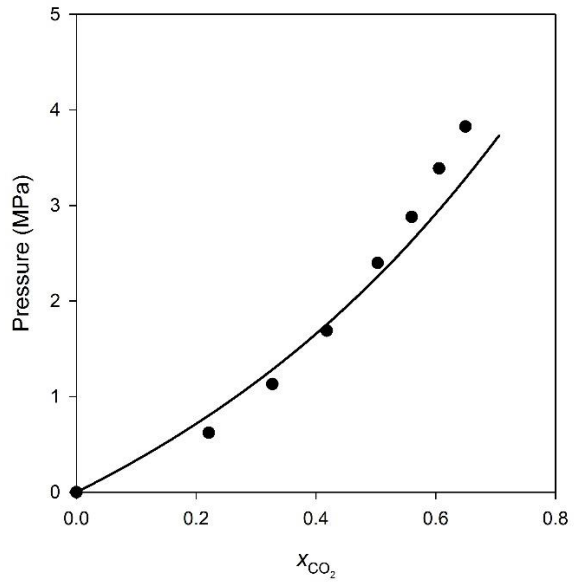

Fig. 4.15 P-x solubility data for CO_2 in $[C_2MIm][Tf_2N]$. Experimental data from Carvalho *et al.* (2009). Solid line represents Aspen predictions

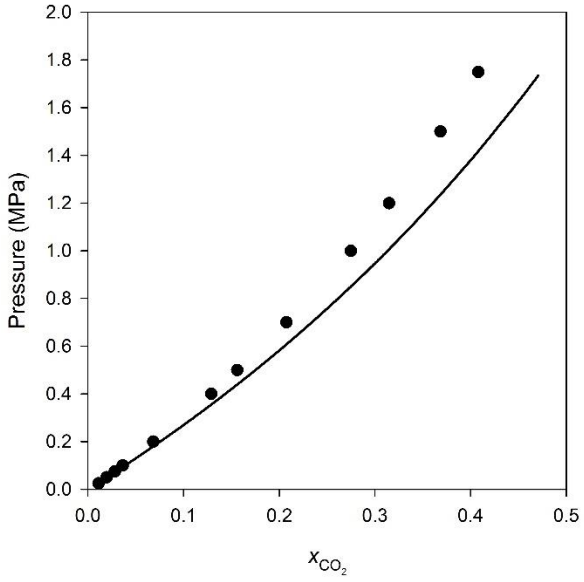

Fig. 4.16 P-x solubility data for CO_2 in $[C_6MIm][Tf_2N]$. Experimental data from Liu *et al.* (2013). Solid line represents Aspen predictions

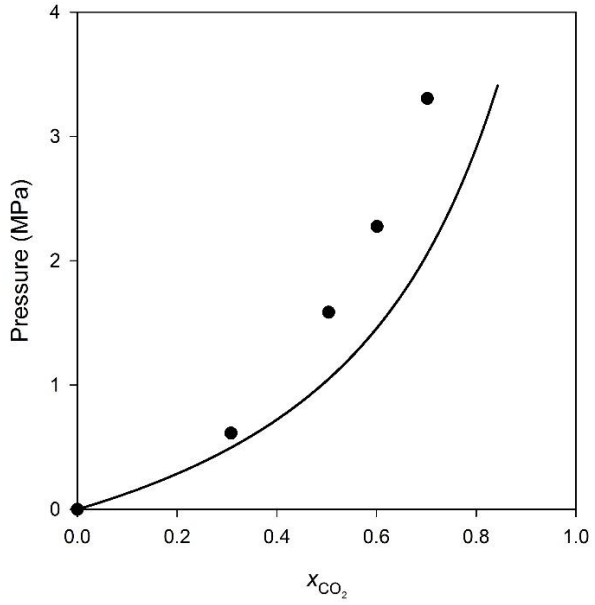

Fig. 4.17 P-x solubility data for CO_2 in $[P_{66614}][Tf_2N]$. Experimental data from Zubeir *et al.* (2015). Solid line represents Aspen predictions

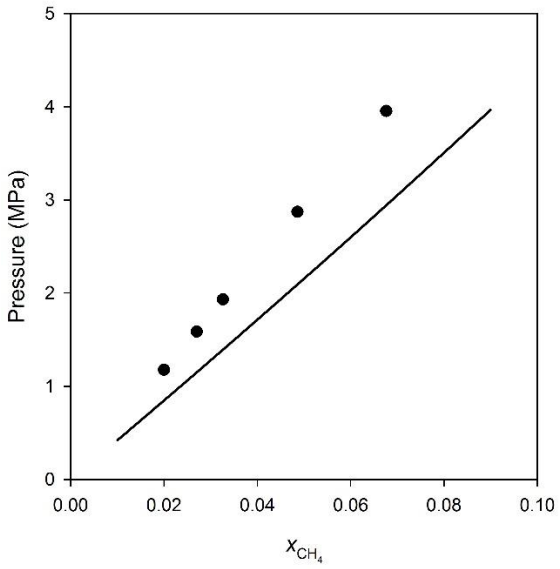

Fig. 4.18 P-x solubility data for CH_4 in $[C_2MIm][Tf_2N]$. Experimental data from Kumelan *et al.* (2007). Solid line represents Aspen predictions

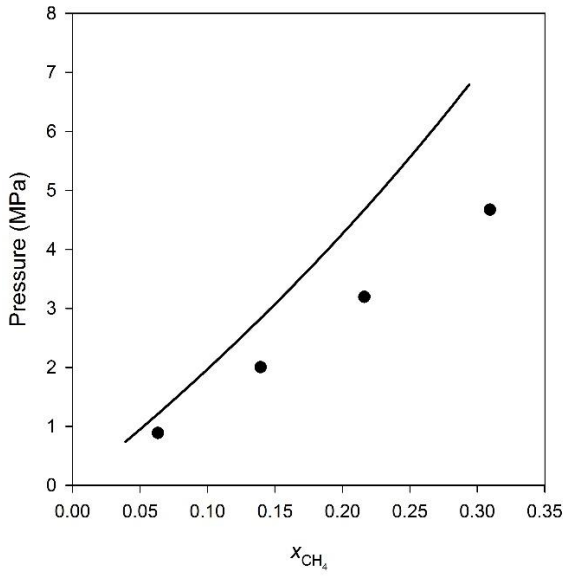

Fig. 4.19 P-x solubility data for CH_4 in $[C_6MIm][Tf_2N]$. Experimental data from Carvalho *et al.* (2010). Solid line represents Aspen predictions

Tables E.11-E.15 in Appendix E show the sigma profiles (SGPRF1, SGPRF2, SGPRF3, SGPRF4 and SGPRF5) obtained from the COSMO calculations in COSMO*therm*®.

5. SIMULATION RESULTS

5.1 Introduction

In this section, the results of the process performance of each process concept are presented. The process performance will be assessed in terms of biogas-to-liquids mass yield, energy yield and overall energy efficiency. In addition, the flow sheets of the different process concepts are presented along with a comparison of the process performance between concepts. The results presented in this chapter as well as in Chapter 6 provided the basic input data for the sustainability assessments carried out by collaborators of the 4CU Project based at The University of Manchester. These results were measured on environmental, economic and social impacts using a whole life cycle, whole-system approach that assessed the different options from 'cradle to grave' and identify opportunities for improvements. As a result of this collaboration, the team was able to identify sustainability "hotspots" and to provide recommendations for improvement in terms of environmental impacts. The results were published in *Computer Aided Chemical Engineering* (Cuéllar-Franca *et al.*, 2015) along with other publications in the progress of being published.

5.2 Definition of process performance

The feedstock-to-product mass yield, energy yield and overall energy efficiency are widely used indicators to measure the technical performance and the economic feasibility of chemical plants. The mass yield of a plant, Y_M is a measure of the mass of the feedstock (biogas in this study) that remains in the product (FT syncrude). Similarly, the energy yield of a plant, Y_E is a measure as to what extent the feedstock energy, on a Lower Heating Value (LHV) basis, remains in the products (FT-syncrude in this thesis). The LHV (also known as net calorific value) of a fuel is defined as the amount of heat released by combusting a specified quantity (initially at 25°C) and returning the temperature of the combustion products to 150°C, which assumes the latent heat of

vaporization of water in the reaction products is not recovered. LHV is used as the basis in all energy yields and overall energy efficiencies presented in this thesis. It should be noted that the Lower Heating Value (LHV) of FT-syncrude is calculated using the built-in *Aspen HYSYS Refining Correlation Manager (Corman)* in Aspen Plus. Perhaps more importantly, the overall plant energy efficiency, η_{plant} takes into account the total energy input (biogas, hydrogen, natural gas and electricity) and total energy output (FT syncrude, hydrogen and electricity). In order to allow comparability between process concepts, all hot utilities (steam and natural gas) have been normalised to total natural gas consumption, *i.e.* steam consumption is regarded as natural gas necessary to produce the required steam. In this thesis, the mass yield, energy yield and overall plant energy efficiency are defined by Eqs. 5.1-5.3, respectively.

$$Y_M = \frac{\dot{M}_{FT\ Syncrude}}{\dot{M}_{biogas}} \quad \text{Eq. 5.1}$$

where $\dot{M}_{FT\ Syncrude}$ is the mass flowrate of FT syncrude produced by the plant and $\dot{M}_{biogas}$ is the mass flowrate of biogas fed to the plant (3,775 kg·h^{-1} in all cases).

$$Y_E = \frac{\dot{M}_{FT\ Syncrude} \cdot LHV_{FT\ Syncrude}}{\dot{M}_{biogas} \cdot LHV_{biogas}} \quad \text{Eq. 5.2}$$

where $LHV_{FT\ Syncrude}$ is the is the lower heating value of FT syncrude and LHV_{biogas} is the lower heating value of biogas.

$$\eta_{plant} = \frac{\dot{M}_{FT\ syncrude} \cdot LHV_{FT\ syncrude} + \dot{M}_{H_2} \cdot LHV_{H_2} + Electricity\ produced}{\dot{M}_{biogas} \cdot LHV_{biogas} + \dot{M}_{H_2} \cdot LHV_{H_2} + \dot{M}_{NG} \cdot LHV_{NG} + \frac{Electricity\ consumed}{0.39}}$$

Eq. 5.3

where $\dot{M}_i$ is the mass flow and LHV_i is the lower heating value of the product (FT syncrude, hydrogen) or raw material (biogas, hydrogen, natural gas). The electricity consumed by the plant (taken from the grid) is divided by the overall efficiency of the power cycle assumed to be 39% (Haro *et al.*, 2013). It should be noted that the steam production by the Fischer-Tropsch off-gas combustor and/or the CHP plant (in those process designs that incorporate one) is not considered in the overall plant energy efficiency since this considers high value streams such as hydrogen, fuels or electricity unlike the low grade steam produced in the different process designs. Given said that, some of the process designs are able to produce surplus steam (after considering the heating requirements of the digesters); therefore, this surplus steam production should also be taken into account when drawing conclusions on process efficiency.

5.3 Base Case Models

As described in Section 1.2.1, the aim of this thesis is to compare the feasibility of different CO_2 capture and utilisation processes in order to identify the most promising routes for the conversion of Carbon Dioxide into a synthetic fuel. Initially the methodology will consider only the best available and proven technology (Base Case Models), which will then be adapted to consider a developing technology such as CO_2 capture using ionic liquids.

In the following sections, the results from the Base Case Models regarding process performance are presented. In all cases, the main plant input, in terms of energy (LHV), is the biogas produced the anaerobic digestion of sewage sludge. Other plant inputs include hydrogen for the CO_2 hydrogenation to syngas, natural gas for heating and electricity. The main plant output is, in all cases, FT syncrude. In some base case models, surplus heat is produced in the form of steam. The surplus steam is calculated as the remaining steam available after

deducting the heating requirements of the anaerobic digester, which were 11,338 kW in all cases, as reported by Dimitriou *et al.* (2015).

5.3.1 PD-MEA1 concept

As described in section 3.1.1, the PD-MEA1 process concept incorporates a monoethanolamine (MEA) gas treatment unit, which is often used to upgrade biogas to the same standards as natural gas by removing CO_2 and other trace constituents. The upgraded bio-methane is fed into a methane steam reformer for the production of syngas, which will be converted into FT syncrude via the Fischer-Tropsch synthesis. Fig 5.1 shows PD-MEA1 process concept implemented in Aspen Plus. Table 5.1 shows the results of the Aspen Plus simulation of the PD-MEA1 concept.

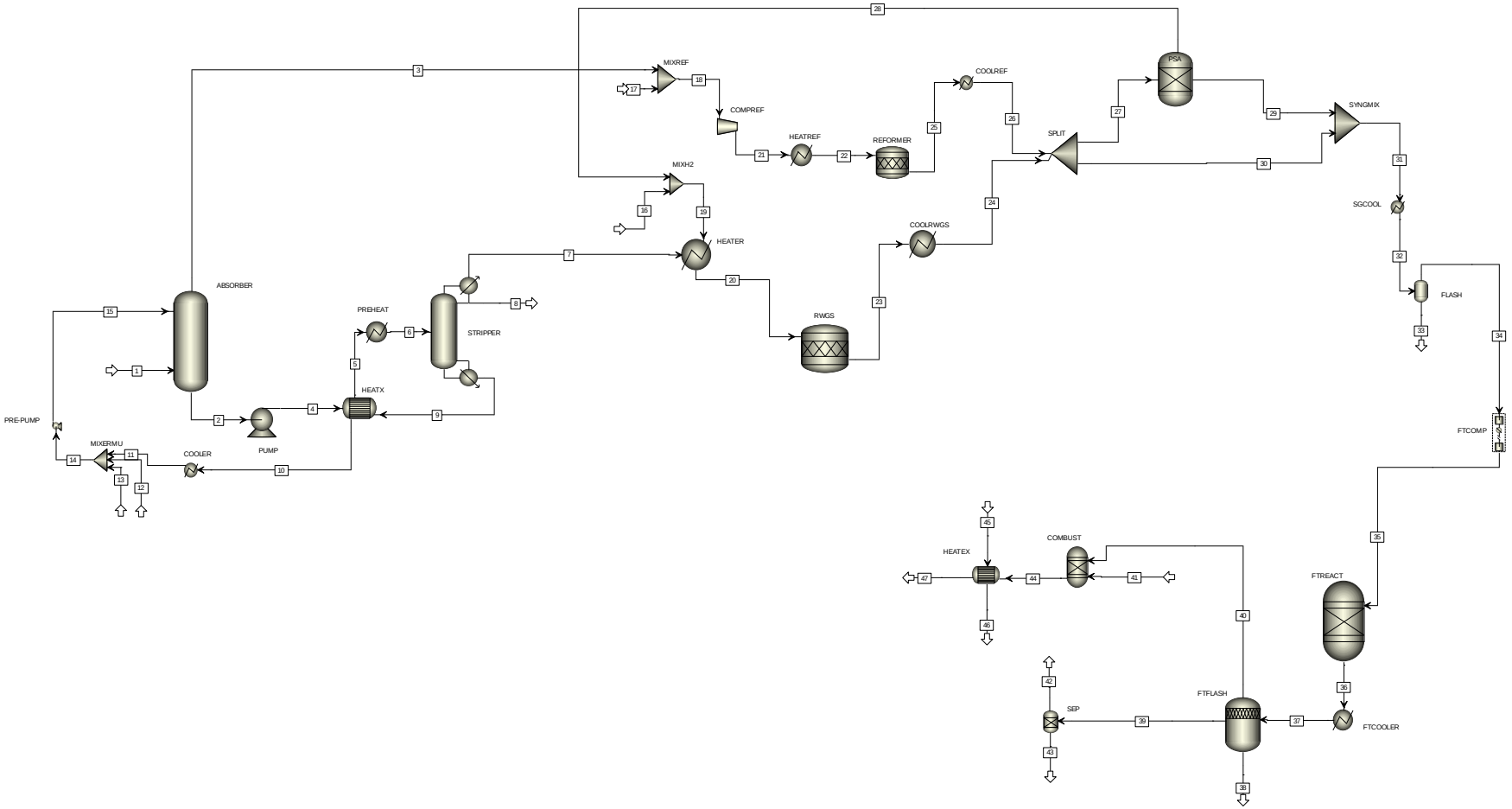

Fig. 5.1 Flow sheet of the PD-MEA1 process concept

Table 5.1 Summary of inputs, outputs and results of the PD-MEA1 concept

PLANT INPUTS		
Biogas		
LHV biogas	$MJ \cdot kg^{-1}$	20.20
Mass flow	$kg \cdot h^{-1}$	3,774.46
LHV biogas	kW	21,181.94
Hydrogen		
LHV hydrogen	$MJ \cdot kg^{-1}$	119.90
Mass flow	$kg \cdot h^{-1}$	42.85
LHV hydrogen	kW	1,427.23
Natural gas		
LHV natural gas	$MJ \cdot kg^{-1}$	48.85
Mass flow	$kg \cdot h^{-1}$	900.57
LHV natural gas	kW	12,219.09
Electricity		
Total electricity consumption	kW	3,192.00
PLANT OUTPUTS		
FT-syncrude		
LHV FT-syncrude	$MJ \cdot kg^{-1}$	32.25
Mass flow	$kg \cdot h^{-1}$	831.68
LHV FT-syncrude	kW	7,450.47
FUEL MASS YIELD	%	22.0
FUEL ENERGY YIELD	%	35.2
OVERALL PLANT EFFICIENCY	%	17.9

5.3.2 PD-MEA2 concept

Similarly to the PD-MEA1 process concept, the PD-MEA2 concept incorporates a monoethanolamine (MEA) gas treatment unit to capture the CO_2 in the biogas; however, PD-MEA2 does not incorporate a steam methane reformer for syngas production since it is assumed that

the upgraded bio-methane is sold for natural gas grid injection. The CO_2-rich stream produced by the MEA plant is fed to the RWGS reactor and converted into syngas, which will be further converted into liquid syncrude via the Fischer-Tropsch synthesis. The PD-MEA2 process concept implemented in Aspen Plus is shown in Fig. 5.2. Table 5.2 shows the results of the Aspen Plus simulation of the PD-MEA2 concept.

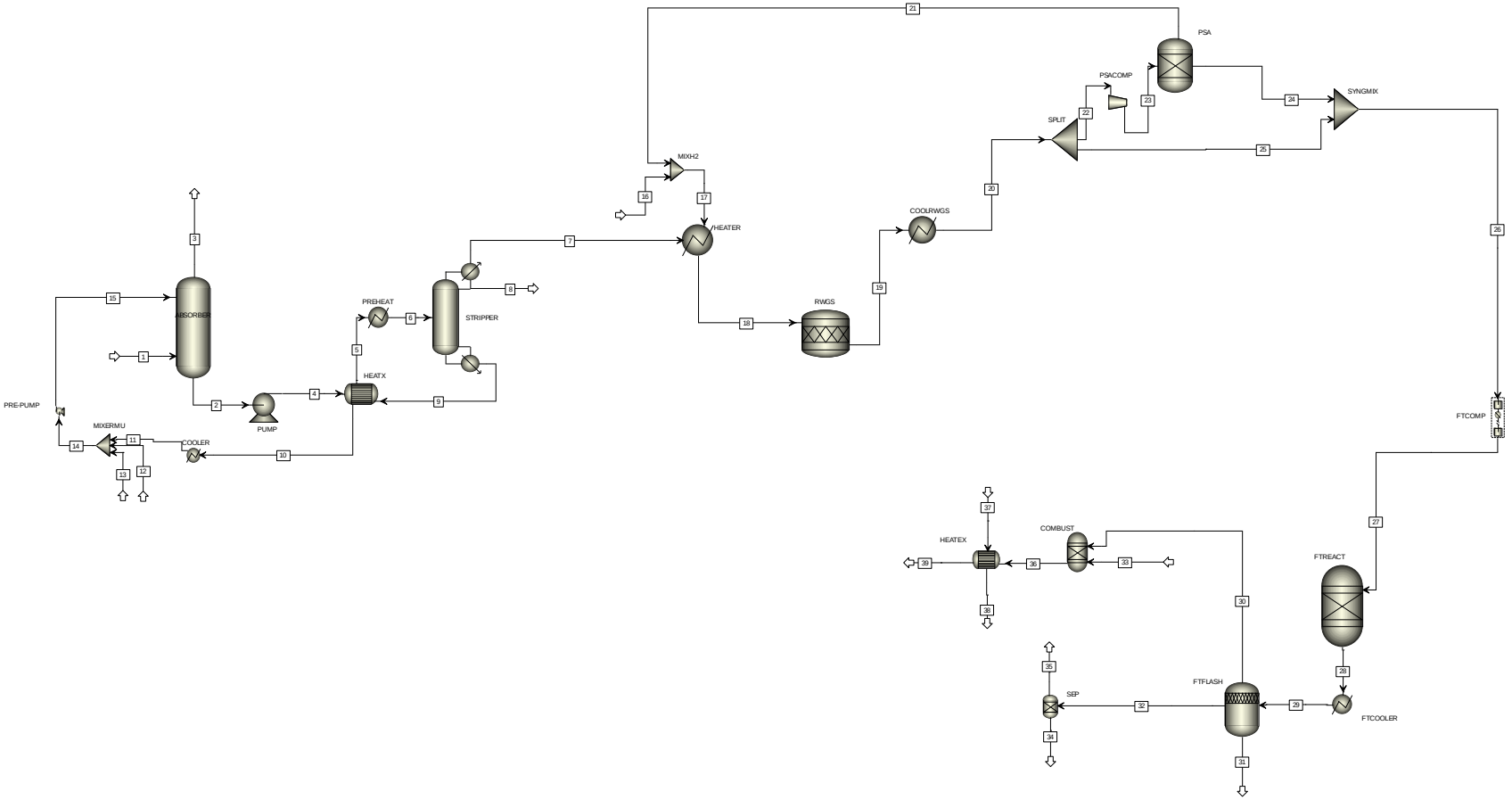

Fig. 5.2 Flow sheet of the PD-MEA2 process concept

Table 5.2 Summary of inputs, outputs and results of the PD-MEA2 concept

PLANT INPUTS		
Biogas		
LHV biogas	$MJ \cdot kg^{-1}$	20.20
Mass flow	$kg \cdot h^{-1}$	3,774.45
LHV biogas	kW	21,181.94
Hydrogen		
LHV hydrogen	$MJ \cdot kg^{-1}$	119.90
Mass flow	$kg \cdot h^{-1}$	195.67
LHV hydrogen	kW	6,516.81
Natural gas		
LHV natural gas	$MJ \cdot kg^{-1}$	48.85
Mass flow	$kg \cdot h^{-1}$	450.27
LHV natural gas	kW	6,109.41
Electricity		
Total electricity consumption	kW	1,164.00
PLANT OUTPUTS		
FT-syncrude		
LHV FT-syncrude	$MJ \cdot kg^{-1}$	32.10
Mass flow	$kg \cdot h^{-1}$	244.76
LHV FT-syncrude	kW	2,192.67
Bio-methane (95 vol. % CH_4)		
LHV FT-syncrude	$MJ \cdot kg^{-1}$	43.70
Mass flow	$kg \cdot h^{-1}$	1,645.30
LHV FT-syncrude	kW	19,959.73
FUEL MASS YIELD	%	6.5
FUEL ENERGY YIELD	%	10.4
OVERALL PLANT EFFICIENCY	%	6.0

5.3.3 PD-CHP1 concept

The PD-CHP1 process concept is based on another biogas application: combustion of untreated biogas in a combined heat and power (CHP) unit to produce electricity and heat. In this process, raw biogas is fed directly to a CHP plant, which produces heat, electricity and an exhaust stream reach in CO_2. This exhaust stream is fed to the RWGS reactor, along with a hydrogen stream, where syngas is produced via the reverse water-gas shift reaction. Finally, the syngas is converted into FT syncrude in the Fischer-Tropsch reactor. The PD-CHP1 process concept implemented in Aspen Plus is shown in Fig. 5.3. Table 5.3 shows the results of the Aspen Plus simulation of the PD-CHP1 concept.

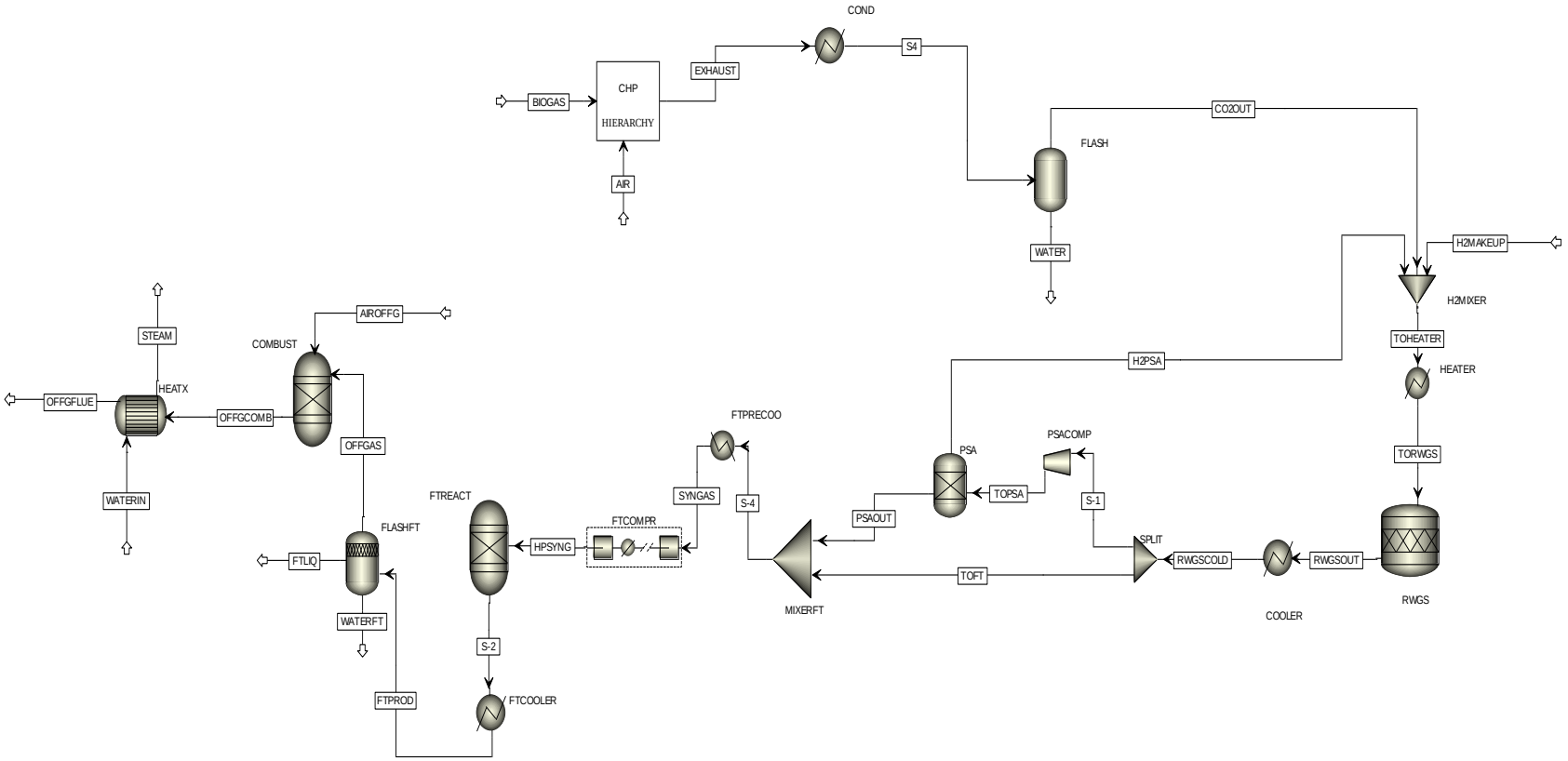

Fig. 5.3 Flow sheet of the PD-CHP1 process concept (see section 4.1.3.2 for full details of “CHP”)

Table 5.3 Summary of inputs, outputs and results of the PD-CHP1 concept

PLANT INPUTS		
Biogas		
LHV biogas	$MJ \cdot kg^{-1}$	20.20
Mass flow	$kg \cdot h^{-1}$	3,774.46
LHV biogas	kW	21,181.94
Hydrogen		
LHV hydrogen	$MJ \cdot kg^{-1}$	119.90
Mass flow	$kg \cdot h^{-1}$	575.63
LHV hydrogen	kW	19,171.59
Natural gas		
LHV natural gas	$MJ \cdot kg^{-1}$	48.85
Mass flow	$kg \cdot h^{-1}$	598.79
LHV natural gas	kW	8,124.52
Electricity		
Total electricity consumption	kW	9,664.39
PLANT OUTPUTS		
Electricity		
Total electricity production	kW	7,096.37
Steam		
Surplus steam production[a]	kW	5,411.00
FT-syncrude		
LHV FT-syncrude	$MJ \cdot kg^{-1}$	29.30
Mass flow	$kg \cdot h^{-1}$	587.07
LHV FT-syncrude	kW	5,259.14
FUEL MASS YIELD	%	15.6
FUEL ENERGY YIELD	%	24.8
OVERALL PLANT EFFICIENCY	%	16.9

[a]Saturated steam at 1.01 bar allowed to condense

5.3.4 PD-CHP1-OXY concept

The PD-CHP1-OXY process design is equivalent to PD-CHP1, although PD-CHP1-OXY employs oxygen for oxy-combustion of the untreated biogas in the CHP unit instead of air. The PD-CHP1-OXY process concept implemented in Aspen Plus is shown in Fig. 5.4. Table 5.4 shows the results of the Aspen Plus simulation of the PD-CHP1-OXY concept. It should be noted that the electricity consumed by the cryogenic oxygen plant (Air Separation Unit, ASU) has been taken into account for the calculation of the overall plant energy efficiency. A value for the electricity consumed by the ASU of 0.32 kWh per kg of O_2 produced was assumed (Aneke & Wang, 2015).

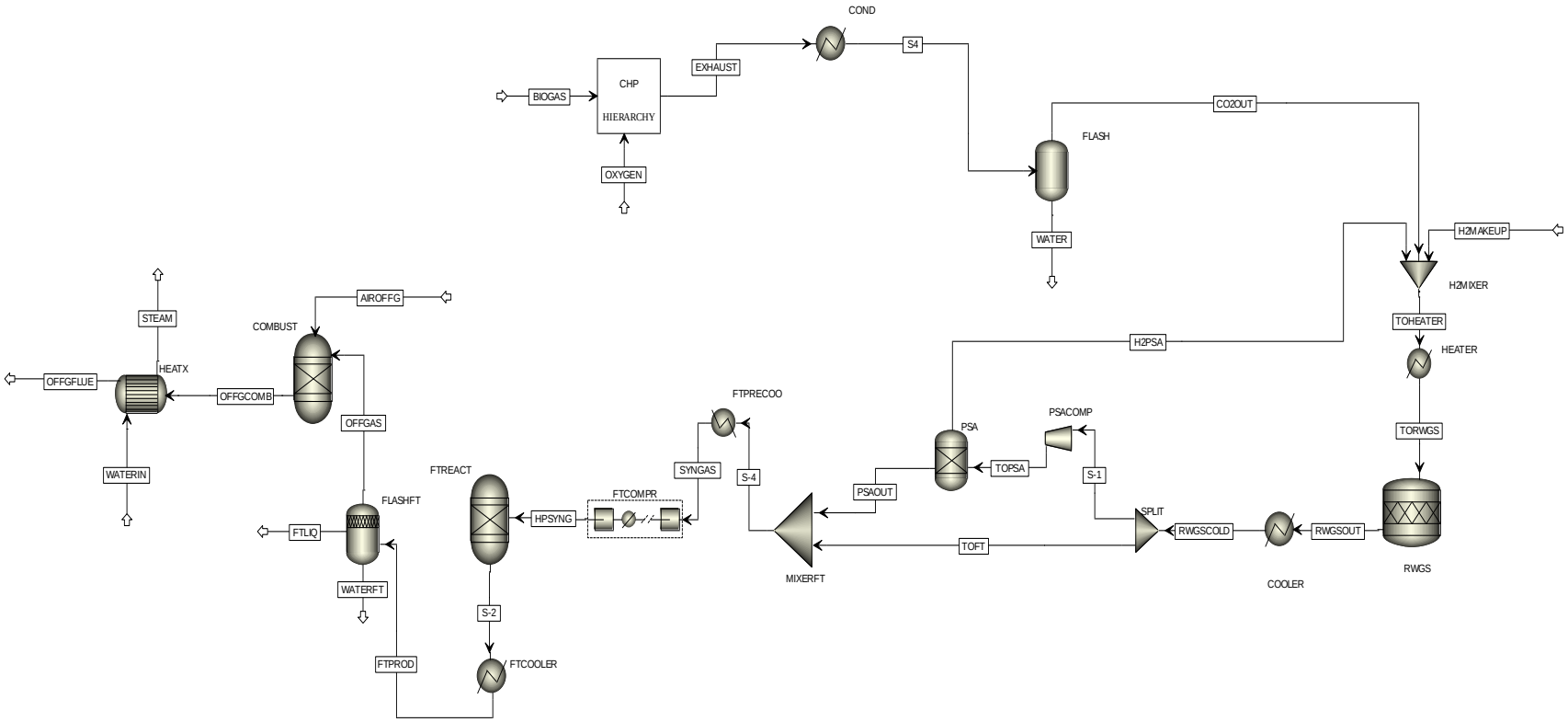

Fig. 5.4 Flow sheet of the PD-CHP1-OXY process concept (see section 4.1.3.2 for full details of “CHP”)

Table 5.4 Summary of inputs, outputs and results of the PD-CHP1-OXY concept

PLANT INPUTS		
Biogas		
LHV biogas	$MJ \cdot kg^{-1}$	20.20
Mass flow	$kg \cdot h^{-1}$	3,774.46
LHV biogas	kW	21,181.94
Hydrogen		
LHV hydrogen	$MJ \cdot kg^{-1}$	119.90
Mass flow	$kg \cdot h^{-1}$	574.05
LHV hydrogen	kW	19,118.97
Natural gas		
LHV natural gas	$MJ \cdot kg^{-1}$	48.85
Mass flow	$kg \cdot h^{-1}$	274.47
LHV natural gas	kW	3,724.03
Electricity		
Total electricity consumption	kW	5,748.27
PLANT OUTPUTS		
Electricity		
Total electricity production	kW	8,363.78
Steam		
Surplus steam production[a]	kW	3,061.00
FT-syncrude		
LHV FT-syncrude	$MJ \cdot kg^{-1}$	31.20
Mass flow	$kg \cdot h^{-1}$	705.91
LHV FT-syncrude	kW	6,323.72
FUEL MASS YIELD	%	18.7
FUEL ENERGY YIELD	%	29.9
OVERALL PLANT EFFICIENCY	%	25.0

[a]Saturated steam at 1.01 bar allowed to condense

5.3.5 PD-CHP2 concept

The PD-CHP2 process design incorporates, as the PD-CHP1 design, a CHP plant to produce heat and electricity; however in this case an MEA CO_2 capture system is placed before the CHP plant which is fed with the upgraded bio-methane (*i.e.* more concentrated in CH_4) rather than untreated biogas as in PD-CHP1; thus, this is a pre-combustion CO_2 capture system. The PD-CHP2 process concept implemented in Aspen Plus is shown in Fig. 5.5. Table 5.5 shows the results of the Aspen Plus simulation of the PD-CHP2 concept.

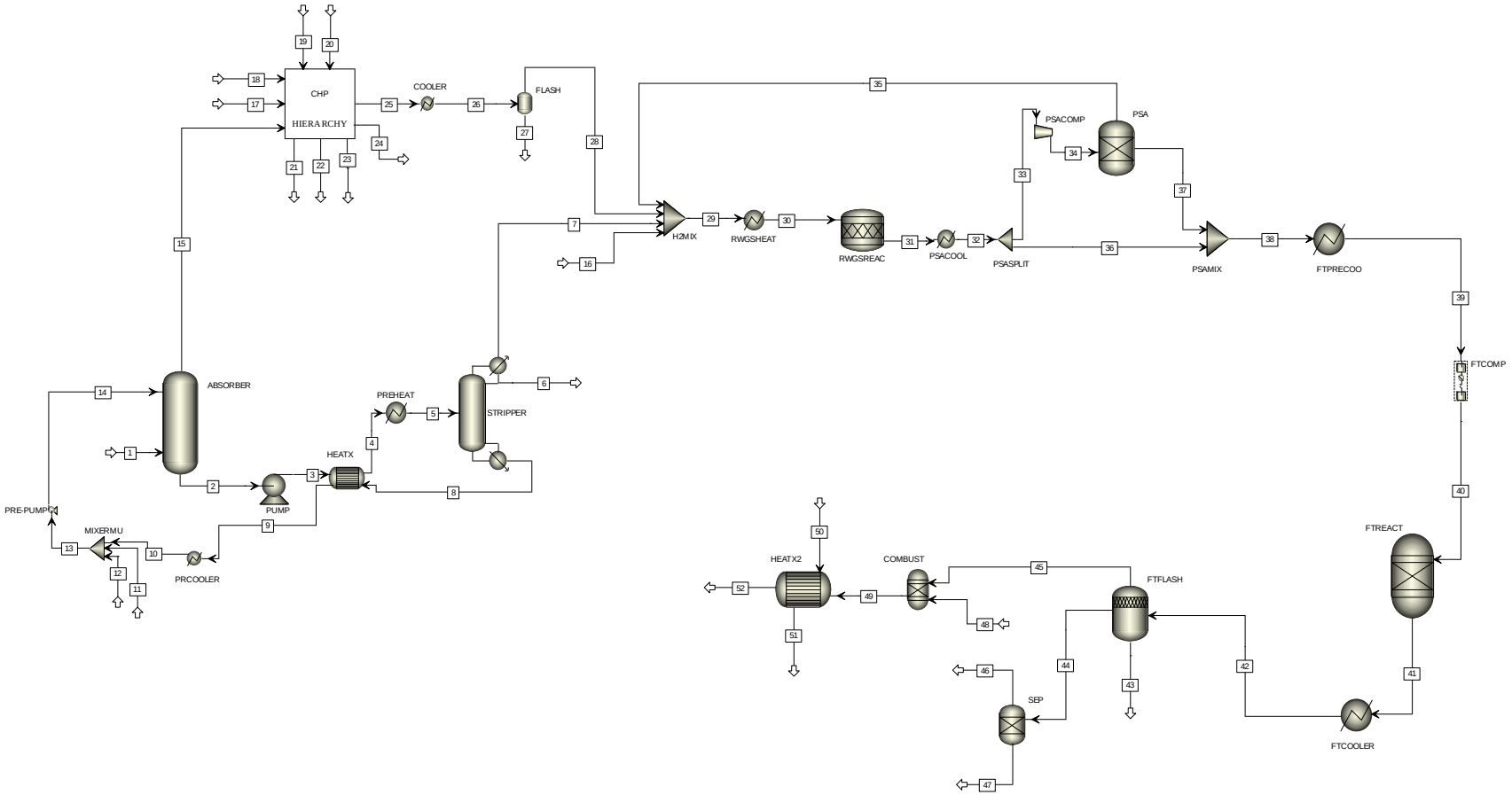

Fig. 5.5 Flow sheet of the PD-CHP2 process concept (see section 4.1.3.2 for full details of “CHP”)

Table 5.5 Summary of inputs, outputs and results of the PD-CHP2 concept

PLANT INPUTS		
Biogas		
LHV biogas	$MJ \cdot kg^{-1}$	20.20
Mass flow	$kg \cdot h^{-1}$	3,774.46
LHV biogas	kW	21,181.94
Hydrogen		
LHV hydrogen	$MJ \cdot kg^{-1}$	119.90
Mass flow	$kg \cdot h^{-1}$	574.75
LHV hydrogen	kW	19,142.34
Natural gas		
LHV natural gas	$MJ \cdot kg^{-1}$	48.85
Mass flow	$kg \cdot h^{-1}$	957.78
LHV natural gas	kW	12,995.41
Electricity		
Total electricity consumption	kW	9,653.66
PLANT OUTPUTS		
Electricity		
Total electricity production	kW	7,178.94
Steam		
Surplus steam production[a]	kW	5,072.00
FT-syncrude		
LHV FT-syncrude	$MJ \cdot kg^{-1}$	29.30
Mass flow	$kg \cdot h^{-1}$	586.20
LHV FT-syncrude	kW	5,251.39
FUEL MASS YIELD	%	15.5
FUEL ENERGY YIELD	%	24.8
OVERALL PLANT EFFICIENCY	%	15.9

[a]Saturated steam at 1.01 bar allowed to condense

5.3.6 PD-CHP2-OXY concept

The PD-CHP2-OXY process configuration is similar to PD-CHP2 but PD-CHP2-OXY employs oxygen for oxy-combustion of the upgraded bio-methane in the CHP unit instead of air. The PD-CHP2-OXY process concept implemented in Aspen Plus is shown in Fig. 5.6. Table 5.6 shows the results of the Aspen Plus simulation of the PD-CHP2-OXY concept. In the same way that with PD-CHP1-OXY, the electricity consumed by the cryogenic oxygen plant (Air Separation Unit, ASU) has been taken into account for the calculation of the overall plant energy efficiency.

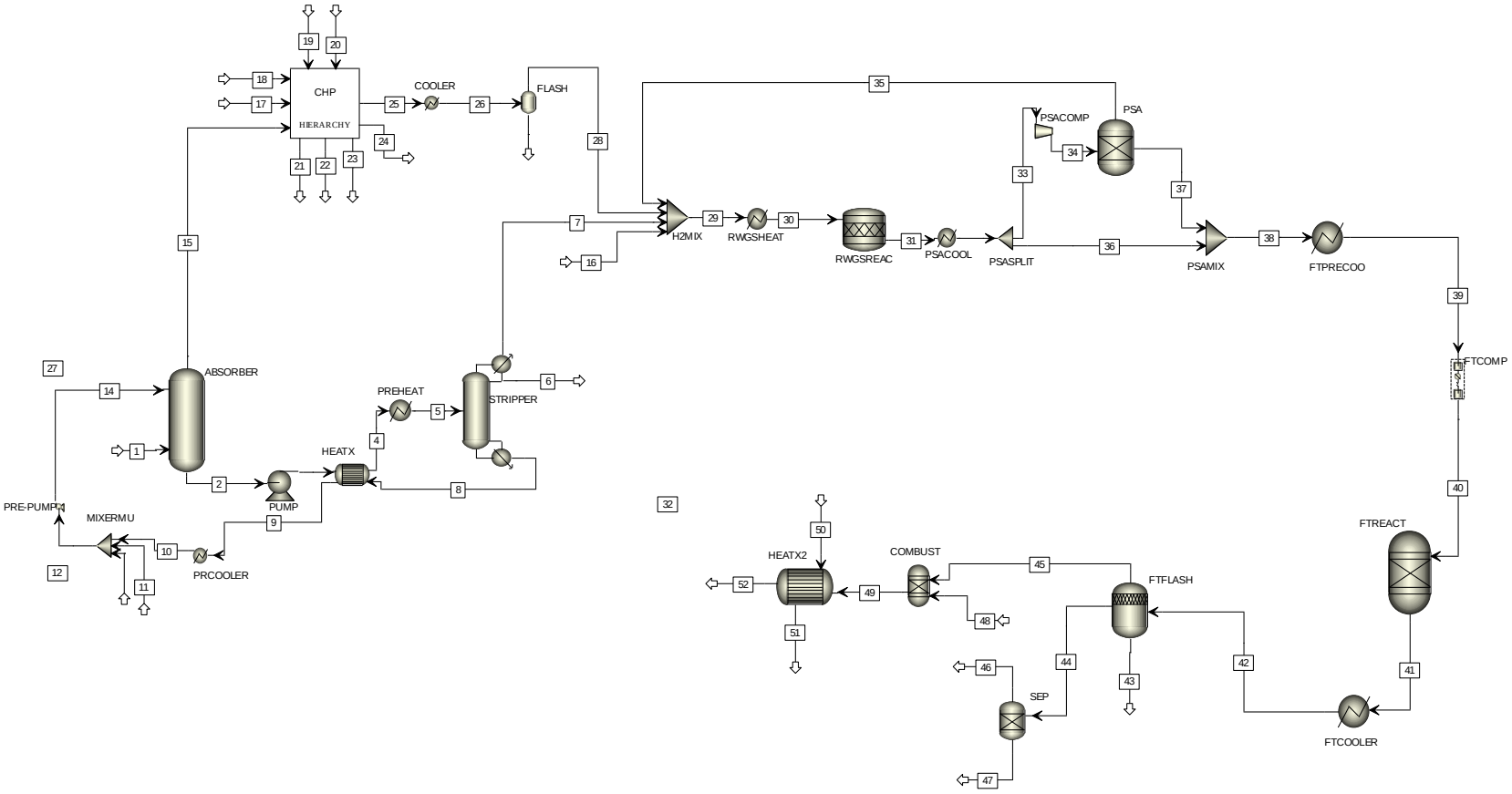

Fig. 5.6 Flow sheet of the PD-CHP2-OXY process concept (see section 4.1.3.2 for full details of “CHP”)

Table 5.6 Summary of inputs, outputs and results of the PD-CHP2-OXY concept

PLANT INPUTS		
Biogas		
LHV biogas	$MJ \cdot kg^{-1}$	20.20
Mass flow	$kg \cdot h^{-1}$	3,774.46
LHV biogas	kW	21,181.94
Hydrogen		
LHV hydrogen	$MJ \cdot kg^{-1}$	119.90
Mass flow	$kg \cdot h^{-1}$	573.17
LHV hydrogen	kW	19,089.81
Natural gas		
LHV natural gas	$MJ \cdot kg^{-1}$	48.85
Mass flow	$kg \cdot h^{-1}$	633.55
LHV natural gas	kW	8,596.08
Electricity		
Total electricity consumption	kW	5,724.45
PLANT OUTPUTS		
Electricity		
Total electricity production	kW	8,442.90
Steam		
Surplus steam production[a]	kW	2,738.00
FT-syncrude		
LHV FT-syncrude	$MJ \cdot kg^{-1}$	31.80
Mass flow	$kg \cdot h^{-1}$	705.45
LHV FT-syncrude	kW	6,319.67
FUEL MASS YIELD	%	18.7
FUEL ENERGY YIELD	%	29.8
OVERALL PLANT EFFICIENCY	%	23.2

[a]Saturated steam at 1.01 bar allowed to condense

5.3.7 PD-CHP1-POST concept

The PD-CHP1-POST is similar to PD-CHP1 but an MEA unit is incorporated after the CHP plant so that this process design is based on post-combustion CO_2 capture. In this case, the MEA unit also allows the removal of the excess air used in the CHP plant which acts as an inert diluent, decreasing the efficiency of the downstream processes and necessitating higher power consumption for the subsequent syngas compression. The PD-CHP1-POST process concept implemented in Aspen Plus is shown in Fig. 5.7. Table 5.7 shows the results of the Aspen Plus simulation of the PD-CHP1-POST concept.

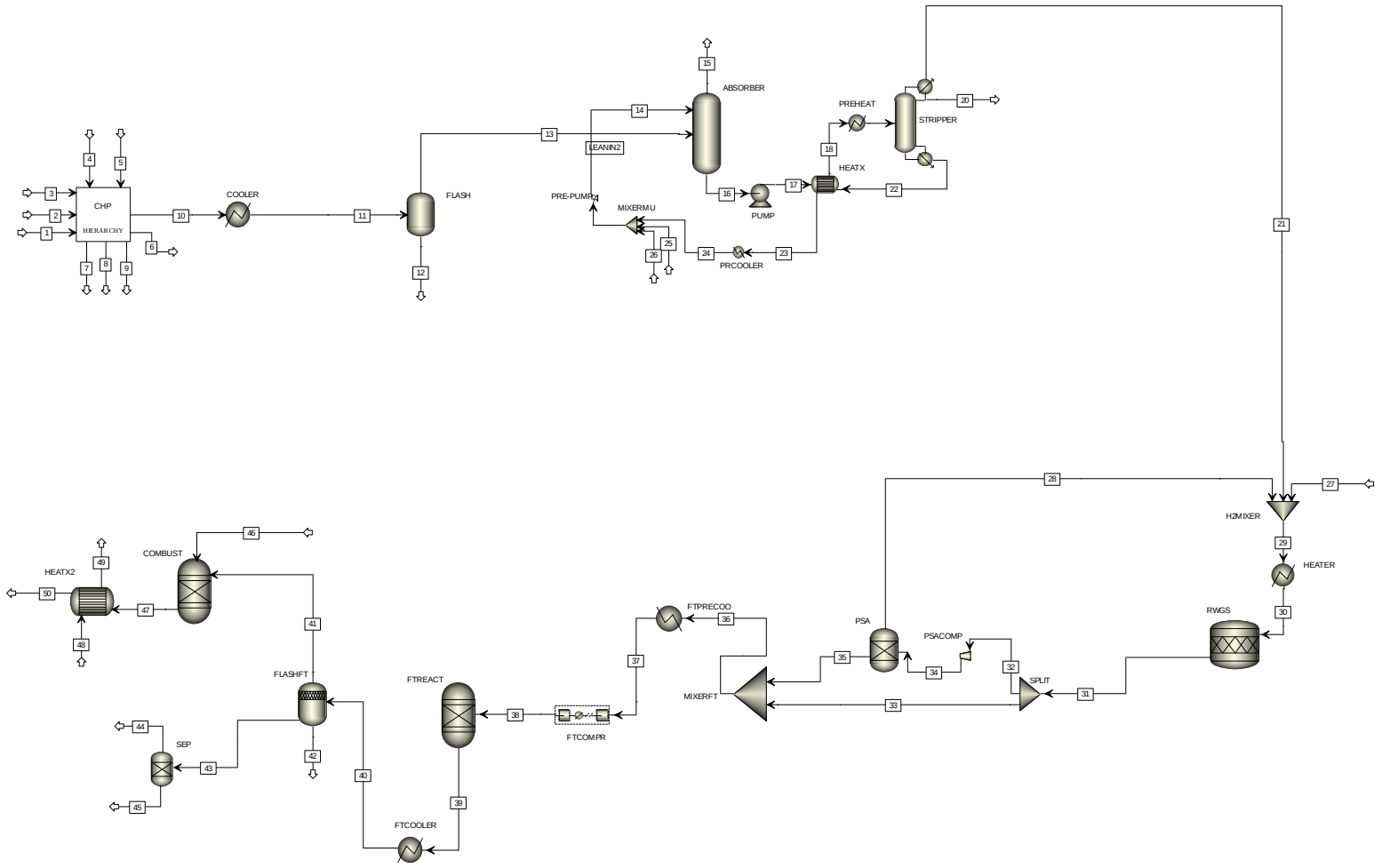

Fig. 5.7 Flow sheet of the PD-CHP1-POST process concept (see section 4.1.3.2 for full details of “CHP”)

Table 5.7 Summary of inputs, outputs and results of the PD-CHP1-POST concept

PLANT INPUTS		
Biogas		
LHV biogas	$MJ \cdot kg^{-1}$	20.20
Mass flow	$kg \cdot h^{-1}$	3,774.46
LHV biogas	kW	21,181.94
Hydrogen		
LHV hydrogen	$MJ \cdot kg^{-1}$	119.90
Mass flow	$kg \cdot h^{-1}$	517.92
LHV hydrogen	kW	17,249.62
Natural gas		
LHV natural gas	$MJ \cdot kg^{-1}$	48.85
Mass flow	$kg \cdot h^{-1}$	1,010.30
LHV natural gas	kW	13,708.01
Electricity		
Total electricity consumption	kW	3,079.06
PLANT OUTPUTS		
Electricity		
Total electricity production	kW	7,096.37
Steam		
Surplus steam production[a]	kW	3,702.00
FT-syncrude		
LHV FT-syncrude	$MJ \cdot kg^{-1}$	32.10
Mass flow	$kg \cdot h^{-1}$	648.03
LHV FT-syncrude	kW	5,805.24
FUEL MASS YIELD	%	17.2
FUEL ENERGY YIELD	%	27.4
OVERALL PLANT EFFICIENCY	%	22.3

[a]Saturated steam at 1.01 bar allowed to condense

5.3.8 Comparison between Base Case Models

Tables 5.1 to 5.7 show that the biogas is the major source of energy input (on a LHV basis) in all process concepts. Although this is true in all cases, hydrogen is a very important plant energy input (LHV basis). The high H_2 requirements are the result of the 3:1 H_2:CO_2 molar ratio required in the RWGS reactor to achieve 65% conversion of CO_2. In terms of FT-syncrude production rate, the PD-MEA1 process design, which incorporates a CO_2 capture plant and a steam methane reformer, results in the highest syncrude production rate with a value of 831.7 $kg \cdot h^{-1}$ (7,450.5 kW [LHV]). The fact that PD-MEA1 incorporates the steam methane reformer also significantly affects the hydrogen requirements of the process, since it requires much less extra hydrogen (imported to the fuel synthesis plant) than the other concepts. The higher FT-syncrude production of the PD-MEA1 design can be explained by the higher amount of syngas fed to the FT synthesis as a result of the upstream methane steam reforming unit which converts methane to syngas instead of simply burning it in a CHP plant. The syngas production rate is also the reason why PD-MEA2, which does not include a steam methane reformer (upgraded bio-methane is injected into the gas grid), results in the lowest FT-syncrude output. It can be then concluded that hydrogen imports to the plant should be minimised by generating hydrogen within the plant. One approach is using steam methane reforming, as it is case in PD-MEA1. Additionally, the RWGS reactor, which require a H_2:CO_2 molar ratio of 3 (see section 4.1.3.4) could be replaced by a process that generates H_2 *in situ*. One of the most advanced examples of such technology is the CO_2/H_2O co-electrolysis process that uses electricity and heat to co-reduce CO_2 and H_2O to syngas (CO + H_2) (Becker *et al.*, 2012; Fu *et al.*, 2010; O'Brien *et al.*, 2010). This would not only reduce drastically any H_2 imports to the plant but also would potentially increase the syngas production.

The design PD-CHP1, which involves direct biogas combustion in a CHP plant without biogas upgrading, results in a lower fuel production of 587.1 $kg \cdot h^{-1}$ (5,259.1 kW [LHV]). The PD-CHP2 concept, which involves upgraded bio-methane combustion in a CHP plant, produces almost the same FT-syncrude output as PD-CHP1 (586.2 $kg \cdot h^{-1}$ or 5,251.4 kW [LHV]). The process concepts employing oxy-combustion in the CHP plant (PD-CHP1-OXY and PD-CHP2-OXY are able to produce 705.9 $kg \cdot h^{-1}$ and 705.5 $kg \cdot h^{-1}$ of syncrude respectively (6,323.7 kW [LHV] and 6,319.7 kW [LHV] respectively). The reason for the higher FT-syncrude output of the oxy-combustion concepts than the air-combustion concepts is that in the designs employing air-combustion, the CHP exhaust stream that is processed downstream has a high content of N_2 (approx. 29 wt. %). This, results in a higher vapour pressure of the product stream coming from the FT reactor. When the FT product stream is fed into the FT Flash drum for vapour-liquid separation, some of the hydrocarbons are lost in the off-gas stream due to the higher vapour pressure of the FT product stream. PD-CHP1-OXY, PD-CHP2-OXY and PD-CHP1-POST are the only designs that are net producers of electricity, whereas the amount of electricity produced in the other designs is insufficient to cover their electricity requirements and thus electricity has to be imported from outside the plants. As for PD-CHP1 and PD-CHP2, this is due to the excessive N_2 that has to be processed downstream, which increases the electricity usage, in particular for compression. The process incorporating a post-combustion CO_2 capture plant, PD-CHP1-POST, produces 648.0 $kg \cdot h^{-1}$ of FT-syncrude (5,805.2 kW [LHV]). This FT-syncrude output is higher than the one from PD-CHP1 since the post combustion CO_2 capture is able to isolate most of the N_2 from the CHP exhaust stream, which prevents the loss of some hydrocarbons in the FT off-gas stream. On the contrary, PD-CHP1-POST results in a lower FT-syncrude production than PD-CHP1-OXY due to the fact that the capture plant only scrubs 90% of the CO_2 in the CHP exhaust stream, which results in less CO_2 being processed

downstream. Fig. 5.8 shows a comparison between the FT-syncrude productions from each process design.

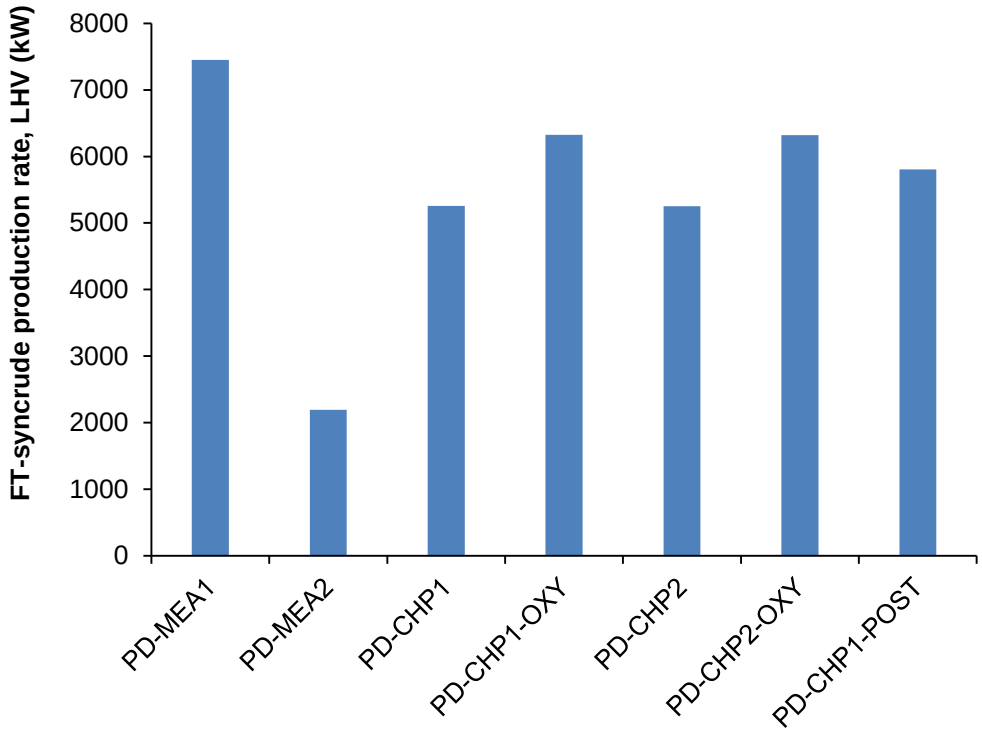

Fig. 5.8 Comparison of FT-syncrude production rates from each process design

As for the mass yields and fuel energy yield, increased hydrocarbon production leads to higher yields; therefore, the greatest mass yield and energy yield are achieved by PD-MEA1 (22.0% and 35.2% respectively). Fig. 5.9 shows a comparison of the mass yield and energy yield achieved by each process concept.

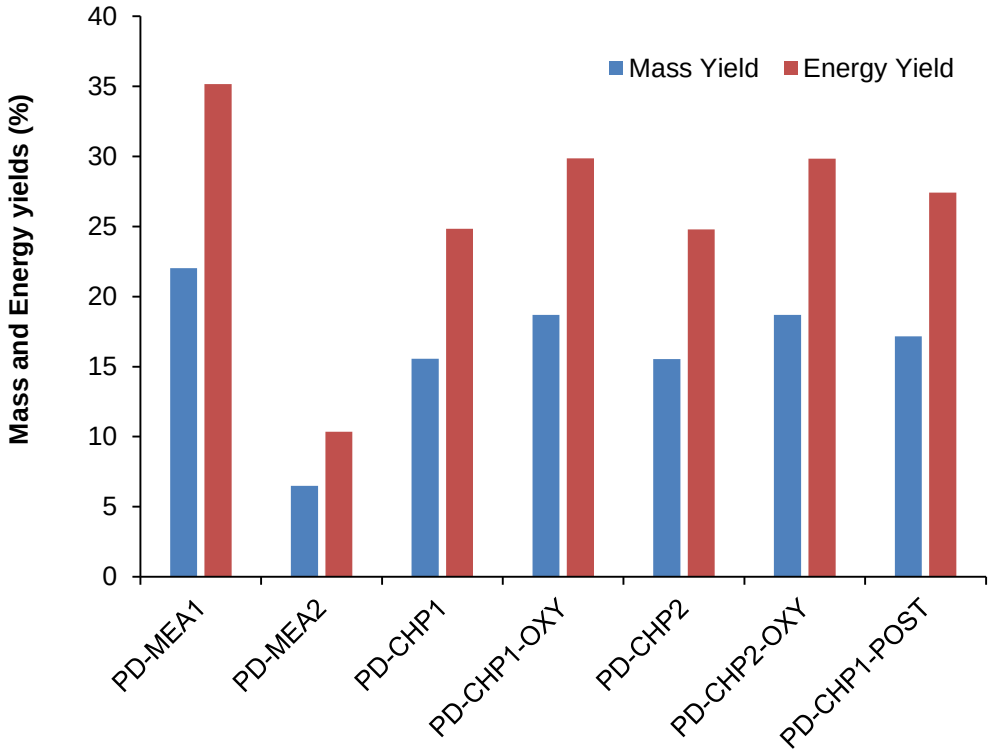

Fig. 5.9 Comparison of the mass yield and energy yield achieved by each process concept

Regarding the overall plant energy efficiency, which takes into account the total energy input (biogas, hydrogen, natural gas and electricity) and total energy output (FT syncrude and electricity), the highest efficiency is achieved by PD-CHP1 OXY (25.0%), followed by PD-CHP2-OXY (23.2%), PD-CHP1-POST (22.3%), PD-MEA1 (17.9%), PD-CHP1 (16.9%), PD-CHP2 (15.9%) and finally PD-MEA2 (6.0%). PD-CHP1-OXY results in the greatest efficiency since, although it produces slightly less FT-syncrude and consumes more H_2 than PD-MEA1 and, this is outweighed by the fact that PD-CHP1-OXY generates more electricity than it consumes and also the natural gas consumption (for heating purposes) is lower than that of PD-MEA1. PD-CHP2-OXY results in a similar efficiency as PD-CHP1-OXY, although slightly lower. This is due to the extra heat and electricity usage in the CO_2 capture plant, which is exacerbated in PD-CHP1-POST

(post-combustion capture) due to the larger volume of flue gas processed and lower CO_2 concentration in the CHP exhaust stream compared to the pre-combustion cases (biogas upgrading); 3,775 $kg \cdot h^{-1}$ biogas, 35 vol. % CO_2 versus 30,618 $kg \cdot^{h-1}$ fluegas, 15 vol. % CO_2. As for PD-CHP1, it achieves a lower efficiency due to the lower FT-syncrude production; this is the result of the N_2 present in the FT effluent, which causes some of the hydrocarbons to be lost in the FT off-gas. Another reason for the low efficiency of PD-CHP1 is the higher electricity and natural gas consumption than those of CHP1-OXY. This is the result of the higher volume processed in the air-combustion cases. PD-CHP1´s efficiency is also lower than that of PD-MEA1 due to the higher hydrogen requirements and lower FT-syncrude production rate. The efficiency of PD-CHP2 is slightly lower than that of PD-CHP1 due to the extra heat and electricity usage in the CO_2 capture plant, which suggest that combustion of upgraded bio-methane in a CHP plant does not benefit the overall process performance. Fig. 5.10 shows a comparison of the overall plant energy efficiencies achieved by each process design.

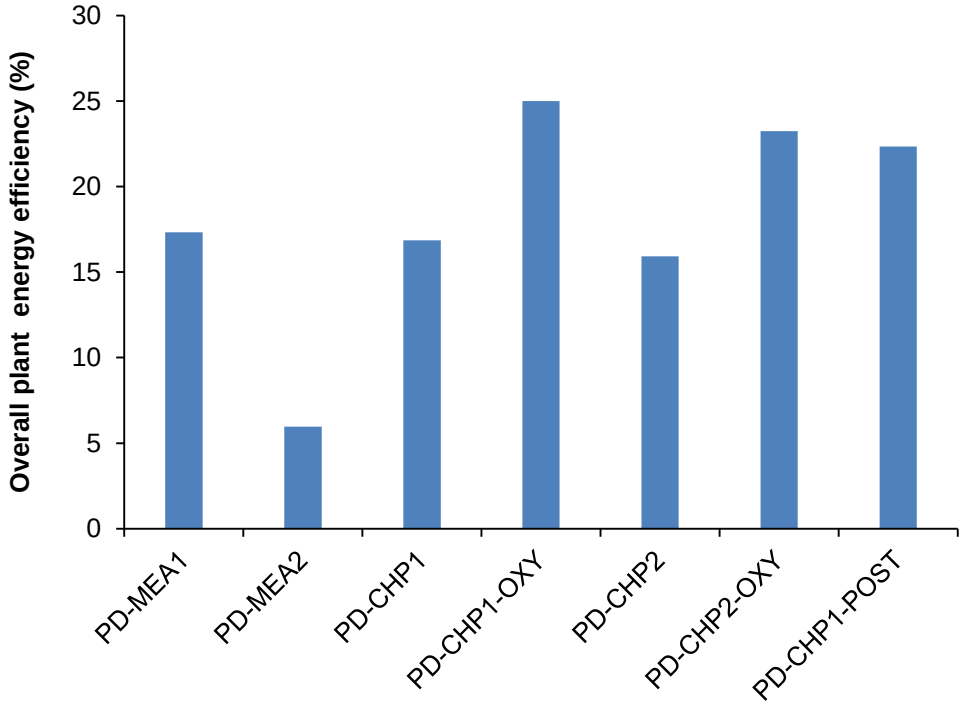

Fig. 5.10 Overall plant energy efficiencies achieved by each process design

5.4 Process employing CO_2 capture with ionic liquids

In this section, a developing technology such as CO_2 capture with ionic liquids is employed instead of CO_2 capture with monoethanolamine. The aim is to assess the effect that this developing technology could have on process performance. Aiming at presenting results in a clear way, the ionic-liquid based CO_2 capture plants will be compared with the MEA-base capture plant (Base Case Model) in terms of energy requirements, solvent capacity and cost.

As discussed in section 4.1.4.1, the target application is biogas upgrading (up to 95 mol. % CH_4) using, on one hand, ionic liquids which selectively absorb CO_2 physically and, on the other hand, an MEA solution (30 wt. % MEA).

The mass and energy flows as well as the mass yields, Y_M energy yields, Y_E and plant energy efficiencies, η_E for the four process concepts considered (three ionic liquids and MEA) are presented in Tables 5.8-5.11. In order to allow a fair comparison between the different concepts, the mass flow and energy content of the biogas are identical in all cases. Similarly, the CH_4 concentration in the bio-methane product stream is set to 95 mol. % in all cases.

The mass yield, Y_M which is a measure of the amount of raw biogas that ends up in the upgraded bio-methane, is defined as:

$$Y_M = \frac{M_{bio-methane}}{M_{biogas}} \quad \text{Eq. 5.4}$$

The energy yields and efficiencies of the evaluated processes are also presented in Tables 5.8-5.11 The energy yield, Y_E is a measure of the energy content of the biogas that ends up in the upgraded bio-methane on a LHV basis and is given by,

$$Y_E = \frac{M_{bio-methane} \cdot LHV_{bio-methane}}{M_{biogas} \cdot LHV_{biogas}} \quad \text{Eq. 5.5}$$

On the other hand, the energy efficiency, η_E takes into account the total energy input to the plant, *i.e.* biogas (LHV), electricity and heat, the later for the MEA process only. η_E also takes into account the total energy output from the plant, *i.e.* bio-methane and electricity, the later for the ionic liquid-based processes only. The energy efficiency is given by:

$$\eta_E = \frac{(M_{bio-methane} \cdot LHV_{bio-methane}) + electricity\ produced}{(M_{biogas} \cdot LHV_{biogas}) + Heat\ consumed + \frac{electricity\ consumed}{0.39}} \qquad \text{Eq. 5.6}$$

As in the base case models, the electricity consumed (grid electricity) is divided by the overall efficiency of the power cycle assumed to be 39% (Haro *et al.*, 2013).

As for energy flows, Tables 5.8-5.11 include both the lower heating value of the raw biogas and upgraded bio-methane coming in and out of the processes respectively, as well as the electricity inputs and outputs. In the processes using ionic liquids, biogas and electricity are the only plant inputs since no other energy inputs, *e.g.* heat, are fed into these plants. On the other hand, the plant based on the MEA solution has heat inputs (expressed in natural equivalents LHV) for the solvent regeneration. It should be noted that while the in ionic liquid-based plants the solvent is regenerated by pressure-swing, in the MEA-based plant the solvent is regenerated by temperature swing.

Table 5.8 Summary of inputs, outputs and results of the $[C_2MIm][Tf_2N]$concept

PLANT INPUTS		
Solvent: $[C_2MIm][Tf_2N]$	$kg \cdot h^{-1}$	56,997.63
Biogas		
LHV biogas	$MJ \cdot kg^{-1}$	20.20
Mass flow	$kg \cdot h^{-1}$	3,774.46
LHV biogas	kW	21,181.94
Electricity		
Total electricity consumption	kW	545.22
PLANT OUTPUTS		
Bio-methane		
LHV bio-methane	$MJ \cdot kg^{-1}$	43.70
Mass flow	$kg \cdot h^{-1}$	1,522.14
LHV bio-methane	kW	18,477.11
FUEL MASS YIELD	%	40.3
FUEL ENERGY YIELD	%	87.2
PLANT EFFICIENCY	%	82.2
IL capacity	**kg IL/kg BM**	**37.45**

Table 5.9 Summary of inputs, outputs and results of the $[C_6MIm][Tf_2N]$concept

PLANT INPUTS		
Solvent: $[C_6MIm][Tf_2N]$	$kg \cdot h^{-1}$	52,744.93
Biogas		
LHV biogas	$MJ \cdot kg^{-1}$	20.20
Mass flow	$kg \cdot h^{-1}$	3,774.46
LHV biogas	kW	21,181.94
Electricity		
Total electricity consumption	kW	575.23
PLANT OUTPUTS		
Bio-methane		
LHV bio-methane	$MJ \cdot kg^{-1}$	43.70
Mass flow	$kg \cdot h^{-1}$	1,454.91
LHV bio-methane	kW	17,660.95
FUEL MASS YIELD	%	38.5
FUEL ENERGY YIELD	%	83.4
PLANT EFFICIENCY	%	81.5
IL capacity	**kg IL/kg BM**	**36.25**

Table 5.10 Summary of inputs, outputs and results of the $[P_{66614}][Tf_2N]$ concept

PLANT INPUTS		
Solvent: $[P_{66614}][Tf_2N]$	$kg \cdot h^{-1}$	44,182.20
Biogas		
LHV biogas	$MJ \cdot kg^{-1}$	20.20
Mass flow	$kg \cdot h^{-1}$	3,774.46
LHV biogas	kW	21,181.94
Electricity		
Total electricity consumption	kW	595.24
PLANT OUTPUTS		
Bio-methane		
LHV bio-methane	$MJ \cdot kg^{-1}$	43.70
Mass flow	$kg \cdot h^{-1}$	1,263.60
LHV bio-methane	kW	15,338.70
FUEL MASS YIELD	%	33.5
FUEL ENERGY YIELD	%	72.4
PLANT EFFICIENCY	%	70.7
IL capacity	**kg IL/kg BM**	**34.97**

Table 5.11 Summary of inputs, outputs and results of the MEA concept

PLANT INPUTS		
Solvent: MEA[a]	$kg \cdot h^{-1}$	22,619.64
Biogas		
LHV biogas	$MJ \cdot kg^{-1}$	20.20
Mass flow	$kg \cdot h^{-1}$	3,774.46
LHV biogas	kW	21,181.94
Natural gas		
LHV natural gas	$MJ \cdot kg^{-1}$	48.85
Mass flow	$kg \cdot h^{-1}$	359.64
LHV natural gas	kW	4,880.12
Electricity		
Total electricity consumption	kW	6.00
PLANT OUTPUTS		
Bio-methane		
LHV bio-methane	$MJ \cdot kg^{-1}$	43.70
Mass flow	$kg \cdot h^{-1}$	1,645.30
LHV bio-methane	kW	19,959.73
FUEL MASS YIELD	%	43.6%
FUEL ENERGY YIELD	%	94.2%
PLANT EFFICIENCY	%	76.5%
MEA capacity[b]	**kg MEA/kg BM**	**13.76**

[a,b] Both the MEA requirements and absorption capacity are referred to pure MEA

The process using the MEA solution produces 1,644.3 $kg \cdot h^{-1}$ of bio-methane at 95 mol. %, followed by the process using $[C_2MIm][Tf_2N]$ ionic liquid, which produces 1522.14 $kg \cdot h^{-1}$, 1454.91 $kg \cdot h^{-1}$ produced by the second concept (based on $[C_6MIm][Tf_2N]$ ionic liquid) and 1263.60 $kg \cdot h^{-1}$ produced by the third concept (based on $[P_{66614}][Tf_2N]$ ionic liquid). The

difference in the bio-methane output produced by the MEA-based concept and the ionic liquid-based concepts relies on the CO_2 absorption selectivity. The MEA has a very low affinity for CH_4 compared to the affinity that it has for CO_2, while in the case of the ionic liquids the CH_4 affinity is higher. This causes a significant proportion of the CH_4 in the biogas to end up in the CO_2-rich ionic liquid solution. The difference in the bio-methane production rate from the ionic-liquids concepts can be explained by the fact that, although the $[C_6MIm][Tf_2N]$ and $[P_{66614}][Tf_2N]$ ionic liquids have a higher CO_2 absorption capacity, as shown in Tables 5.8-5.10, they also absorb more CH_4 than $[C_2MIm][Tf_2N]$. To produce these amounts of bio-methane, 56,997.63 $kg \cdot h^{-1}$ of the $[C_2MIm][Tf_2N]$ ionic liquid, 52,744.93 $kg \cdot h^{-1}$ of $[C_6MIm][Tf_2N]$ and 44,182.20 $kg \cdot h^{-1}$ of $[P_{66614}][Tf_2N]$ are needed, respectively. These results demonstrate that the $[P_{66614}][Tf_2N]$ has the highest CO_2 absorption capacity, followed by $[C_6MIm][Tf_2N]$ and $[C_2MIm][Tf_2N]$, which is in agreement with experimental data (Carvalho *et al.*, 2010; Zubeir *et al.*, 2015; Carvalho *et al.*, 2009). As for MEA, 22,619.64 $kg \cdot h^{-1}$ of pure MEA are needed to produce the reported bio-methane rate. These results are expectable since MEA reacts with the CO_2 while the ionic liquids only absorb CO_2 physically.

As for the electricity flows, it should be noted that the values presented in Tables 5.8-5.10 account for both the biogas compressor and the pump recirculation in the case of the ionic liquid-based plants. In all ionic liquid cases the biogas compressor consumed 500.20 kW. The pump in the first process concept needs 45.02 kW of electricity, while the pumps in the second and third concepts request up to 75.30 kW and 95.04 kW, respectively; therefore, the biogas compressor accounts for the vast majority of the plant electricity consumption. These results show that the viscosity of the ionic liquid has a predominant effect on the electricity used by the recirculation pump. As for the MEA, the recirculation pump only consumes 6 kW of electricity.

Taking into account Eq. 5.4-5.5, increasing bio-methane production will increase both the mass yield and the energy yield and thus the highest mass yield is achieved by MEA (44%), followed by $[C_2MIm][Tf_2N]$ (40%), $[C_6MIm][Tf_2N]$ (39%) and $[P_{66614}][Tf_2N]$ (34%). In this study, the theoretical maximum value of Y_M is 69%. This is the maximum achievable if the solvent did not absorb CH_4 at all for upgraded bio-methane production at 95 mol. %. As for the energy yields, the highest is achieved by MEA (94%), followed by $[C_2MIm][Tf_2N]$ (87%), $[C_6MIm][Tf_2N]$ (83%) and $[P_{66614}][Tf_2N]$ (72%).

The process using $[C_2MIm][Tf_2N]$ has the highest energy efficiency, achieving a value of 82%. The process using $[C_6MIm][Tf_2N]$ also achieves 82% plant energy efficiency, followed by MEA (77%) and $[P_{66614}][Tf_2N]$ (71%). The reason why $[C_2MIm][Tf_2N]$ and $[C_6MIm][Tf_2N]$ result in higher efficiencies than MEA relies on the energy savings that the pressure-swing processes (ionic liquids) offer in contrast with the temperature-swing process (MEA). This is true despite the lower absorption capacity (kg of ionic liquid needed per kg of bio-methane produced) of the processes using $[C_2MIm][Tf_2N]$ and $[C_6MIm][Tf_2N]$; therefore, it becomes clear that every energy inputs/outputs must be considered before making conclusions based solely on bio-methane production rates or solvent absorption capacity. Fig. 5.11 summarises the mass yields, energy yields and plant energy efficiencies of all process concepts considered.

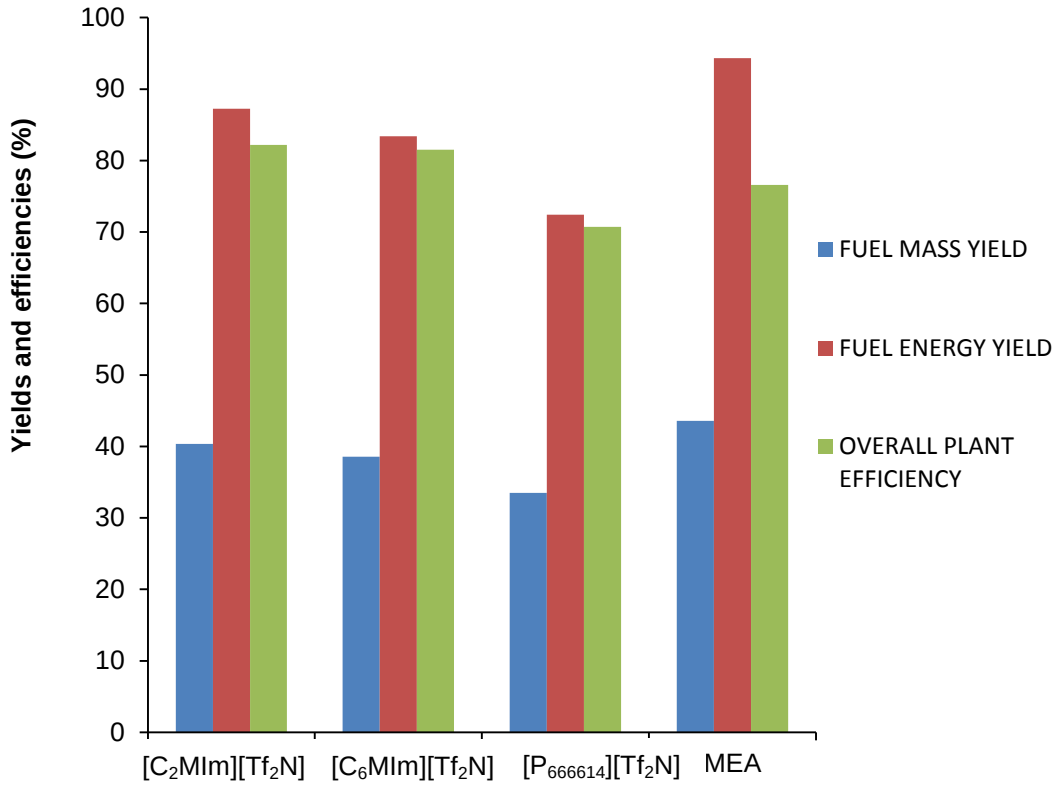

Fig. 5.11 Mass yields, energy yields and plant energy efficiency of the evaluated biogas upgrading processes

6. ECONOMIC ASSESSMENT

6.1 Introduction

This chapter discusses the methodology used to economically assess the selected process concepts which are compared in terms of capital, operating and production costs. The main aim is to identify the most cost-competitive CO_2 utilisation process concept. The software package Aspen Process Economic Analyzer (APEA), licensed by Aspen Tech (Aspen Technology, 2012b), with the UK set as the base country, was used to estimate the purchase cost of the equipment involved in every process concept. APEA is grounded in the *Icarus Systems* technology, which is based on the mathematical modelling technology developed by Icarus Corporation since 1969. Aspen Technology purchased Icarus Corporation in 2000. Stored in *Icarus Systems* are design and cost models for (Aspen Technology, 2012b):

- Over 250 kinds of liquid, gas and solids handling and processing equipment
- More than 60 kinds of plant bulk items
- Approximately 70 kinds of site preparation work
- Nearly a dozen types of buildings

Using the equipment costs, a cost model was developed in MS Excel, which allowed the estimation of the capital, operating and production costs of the evaluated process designs. Sensitivity analyses are carried out in order to evaluate the effect of different process parameters on fuel production costs.

6.2 General economic parameters

The assumptions for the economic evaluation of the different process designs are summarised in Table 6.1.

Table 6.1 General economic parameters assumed in the economic assessment

General economic parameters	
Base year	2013
Plant life, years	20
Plant annual operating hours	8,000
Loan interest rate	10%

The base year for the economic evaluation was chosen to be 2013 according to Aspen Process Economic Analyzer v8.4. The Bank of England inflation calculator (Bank of England, 2014) was used when prices needed to be inflated to 2013 values. Whenever US dollars ($US) needed to be converted to British pounds (£) a conversion factor of £1 <> 1.6 $US was used, according to the 2013 exchange rates (XEcurrency, 2015).

The life of the plant, *i.e.* the time that the plant is expected to be fully operational, was chosen to be 20 years which is a common value in techno-economic assessments of chemical processes at an early stage of development (Dimitriou, 2012; Swanson *et al.*, 2010a). The plant is designed to operate 8,000 hours per year, which means that a downtime of 760 hours per year is assumed (Dimitriou, 2012; Hamelinck *et al.*, 2004).

As for the loan interest rate, it represents the interest at which any loaned money will have to be repaid to the investors. The rate at which interest will be paid is usually fixed at the time the capital is borrowed. The interest rate depends on many factors but is often proportional to the financial risk associated with the investment. In light with this, a project that involves somewhat simple and proven technology will benefit from a lower interest rate than one that involves complex and unproven systems. Although some can argue that an interest rate of 10% is high compared to interest

rates usually offered to the chemical industry, it is justified by the high financial risk associated with a developing technology such as CO_2 utilisation. In fact, others can argue that an interest rate of 10% is too low given the complex nature of the assessed CDU process designs as well as the lack of experience in the operation of such plants. Furthermore, it could be argued that not all process concepts assessed in this thesis are at the same technology readiness level (TRL) and therefore they would be offered different interest rates. At this point, there is not enough information on equivalent real plants to make an accurate decision about the interest rate. It was decided that a 10% interest rate would be used in this study since it is in agreement to the interest rate assumed in other studies that also considered immature technology for fuel synthesis (Dimitriou, 2012; Tijmensen *et al.*, 2002). The interest rate will be included in the sensitivity analysis in order to assess the inherent uncertainty of this parameter.

6.3 Capital Expenditure (CAPEX)

In techno-economic assessments, it is required to determine the capital costs, which is the total investment needed to finance the project to the point at which the plant is ready to operate. In order for an industrial plant to become fully operational, a considerable investment must be supplied to acquire and install the necessary machinery and equipment (Peters *et al.*, 2004). In addition, land and service facilities must be obtained, and the plant must be constructed with all piping, controls, and services (Peters *et al.*, 2004). On top of that, the plant will incur in expenses associated with the plant operation.

The capital needed to supply the necessary manufacturing and plant facilities is called the *fixed-capital investment* (FCI). The investment necessary for a period of operation is termed the *working capital,* which include raw materials and supplies carried in stock, finished products in

stock and semi-finished products in the process of being manufactured, accounts receivable, cash kept on hand for monthly payment of operating expenses, such as salaries, wages, and raw-material purchases, accounts payable and taxes payable (Peters *et al.*, 2004). The sum of the fixed-capital investment (FCI) and the working capital is known as the total capital investment (TCI). The fixed-capital investment (FCI) may be further subdivided into *total direct cost* (TDC) and *total indirect cost* (TIC) (Peters *et al.*, 2004).

In this thesis, the total capital investment is calculated using an established method based on the percentage of *Delivered-Equipment Cost* (DEC), which is appropriate at the current (early) state of development of the processes considered in this study (Peters *et al.*, 2004). This method requires determination of the DEC while the rest of the items included in the TCI are estimated as percentages of the DEC, as shown in Table 6.2. The software Aspen Process Economic Analyzer (APEA), licensed by Aspen Tech (Aspen Technology, 2012b), was used to determine the Delivered-Equipment Cost (DEC) of each modelled process concept.

Table 6.2 Ratio factors for Total Capital Investment estimation

Total Capital Investment (TCI)	
Direct Cost	% of DEC
Purchased equipment	100
Equipment installation	47
Instrumentation and control	36
Piping	68
Electrical	11
Building and building services	18
Yard improvements	10
Service facilities	70
Total Direct Cost (TDC)	**360**
Indirect Cost	% of DEC
Engineering	33
Construction expenses	41
Legal costs	4
Contractor's fee	22
Contingency	44
Total Indirect Cost (TIC)	**144**
Fixed Capital Invest. (FCI) = TDC + TIC	**504**
Working capital[a]	15% of TCI
Total Capital Invest. (TCI) = TDC + TIC + Working capital	

The cost of purchasing the land is not included in the Fixed Capital Investment (FCI). This is because its value can be recovered at the end of the project and therefore it is not usually included in the estimation of the FCI (Peters *et al.*, 2004).

In the absence of measured factors for CO_2-to-fuels plants, the percentage factors presented in Table 6.2 are average values for typical chemical

plants. The expected accuracy is in the ±30% range. Comparability between the different process designs is guaranteed since the same method is used throughout all of them. In addition, the sensitivity analysis presented in section 6.7 will explore the consequences of potential fluctuations in the estimation of the TCI.

In the case of the CHP plant, investment cost data was taken from the literature instead of using the method described in Table 6.2. Since investment cost data are taken from real plants, it is expected that they are more accurate than if they were calculated using the factorial method described in Table 6.2. A total investment cost value of $\$925 \cdot kW^{-1}$ (2013) was considered in this study (Darrow *et al.*, 2015). This value refers to a gas engine generator in grid interconnected CHP applications. Although the CHP system considered in this thesis is in fact a combined cycle gas turbine (CCGT CHP), therefore not a gas engine (GE CHP), investment costs are comparable for both CHP systems at the scale considered in this work (Lako, 2010).

The capital investment needed to carry out a project is usually borrowed and then repaid annually over the lifetime of the plant at a given interest, which is the case of this study. The annuity method (Lauer, 2009) is used to calculate the payback of the investment by including the interest rate in the calculation of the annuity. The annuity is a fixed and constant annual payment usually over the lifetime of the investment, which comprises the capital payback and the interest. This method spreads the initial investment cost over the project lifetime using an assumed interest rate. It does not take into account any changes or diminution in the value of the incomes received or costs expended each year. Similarly, the method does not consider the inflation rate (and the rise of cost and of income over the lifetime). A 10% interest rate is assumed as discussed in section 6.2. The annual amount required to repay the loan on capital costs is given by:

$$A = TCI \cdot \frac{r \cdot (1+r)^N}{(1+r)^N - 1} \qquad \text{Eq. 6.1}$$

where *A* is the annuity of the capital investment, *TCI* the total capital investment, *r* the interest rate and *N* the lifetime of the project.

6.4 Operating and Maintenance costs (O&M)

The total annual costs consist of capital investment annuities (as calculated from Eq. 6.1) as well as O&M costs (also known as operating costs), *i.e.* fixed charges, direct production costs, general expenses and plant overhead. This section includes all expenses directly related to the manufacturing operation or the physical equipment of the different process designs (Peters *et al.*, 2004). The plant operating costs were estimated using the method summarised in Table 6.3, which was adapted from (Peters *et al.*, 2004). Once more, the percentage factors were taken as average values for typical chemical plants.

Table 6.3 General assumptions for operating cost estimation

Operating costs	
Fixed charge	
Local taxes	2% of FCI
Insurance	1% of FCI
Direct prod. cost[a]	
Raw materials	
Utilities	
Catalysts and PSA packing	
Maintenance (M)	7% of FCI
Operating labour (OL)[b,c]	£20·h^{-1}
Supervision (S)	15% of OL
Operating supplies	15% of M
Laboratory charges	15% of OL
Plant overhead	15% of (M + OL + S)
General expenses	
Administrative cost	15% of OL
Distribution and marketing	2% of O&M
R&D cost	2% of O&M

[a]Utility costs are also included in the direct production cost. [b]Hourly wages taken from APEA. [c]40 man-hours/day are assumed for the given plant capacity (Peters *et al.*, 2004).

The price of the utilities used in the modelled process designs are shown in Table 6.4.

Table 6.4 Utility prices used for the estimation of operating costs

Utility prices	
Steam, £·t^{-1}	17.91
Natural gas, £·kWh^{-1}	0.0270
Cooling water, £·m^{-3}	0.0317
Refrigerant, £·t^{-1}	0.1700
Electricity, £·kWh^{-1}	0.0775

The steam, cooling water, refrigerant and electricity prices are Aspen Process Economic Analyzer's default values for the UK and 2013. The natural gas price was retrieved from the Department of Energy and Climate Change (DECC, 2014a).

It must be noted that biogas, which is the feedstock for all evaluated process concepts, has no cost since it is assumed that the fuel synthesis plant is part of a large waste water treatment plant. The biogas produced from the anaerobic digestion of primary and secondary sludge would otherwise be flared or used to heat up the digester, which is not prevented by adding the fuel synthesis plant.

6.5 Production costs

Typically, the fuel production costs are calculated by dividing the total annual costs (which include both annual capital repayments and operating costs) by the amount of FT-syncrude produced in a year, on a LHV basis (Dimitriou *et al.*, 2015). The fuel productions costs are then defined by Eq. 6.2 as,

$$PROD_{COSTS} = \frac{Total\ annual\ costs}{FT{-}syncrude\ (LHV)} \quad (£ \cdot GJ^{-1}) \qquad \text{Eq. 6.2}$$

The annual basis is chosen in order to ease any seasonal fluctuations caused by occasional disturbances in plant operation, *e.g.* start-up period, programmed maintenance downtime, *etc*. (Peters *et al.*, 2004).

In this thesis, the effect of inflation on the total annual costs is not taken into consideration, *i.e.* constant prices are assumed throughout the life of the plant. This assumption can be made provided that it is kept consistently along all modelled process concepts, which is the case of this study (Sinnott, 2005).

In a typical industrial plant, operating costs are expected to be higher in the first years of operation mainly due to the reduced production output, which usually increase as the plant become more able to operate near the optimal point as years pass (Peters *et al.*, 2004). In this study, all process concepts are at the same early stage of development and therefore variations of total annual costs along the life of the plant due plant performance will be equivalent in all cases. Government subsidies or CO_2 credits are not considered in this study.

6.6 Results

In this section, the economic evaluation of all process designs considered in this thesis is presented. As explained above, the comparison between all process concepts is made based on their capital investment, operating costs and fuel production costs. An in-depth profitability analysis was not carried out due to the immaturity of the assessed processes; however, income streams originated from surplus heat, surplus electricity and upgraded bio-methane are included in this chapter. First, an economic assessment of the Base Case Models is presented in section 6.6.1. It should be noted that these process designs are based on well-established, best available technology. Subsequently, section 6.6.2 includes the economic evaluation of the process concepts that use ionic liquids for CO_2 capture. Detailed cost results for each design are presented in detail in Appendix D.

6.6.1 Base Case Models

The seven Base Case Models which are assessed in this section are summarised in Table 6.5.

Table 6.5 Summary of the technologies involved in the different process designs

Process sections	PD-MEA1	PD-MEA2	PD-CHP1	PD-CHP1-OXY	PD-CHP2	PD-CHP2-OXY	PD-CHP1-POST
CO_2 capture[a]	✔	✔			✔	✔	✔
CHP[b]							
Air-combustion			✔		✔		✔
Oxy-combustion				✔		✔	
H_2 recovery[c]	✔	✔	✔	✔	✔	✔	✔
Syngas production[d]	✔		✔	✔	✔	✔	✔
CO_2 conversion[e]	✔	✔	✔	✔	✔	✔	✔
Fuel synthesis[f]	✔	✔	✔	✔	✔	✔	✔

[a]MEA-based CO_2 capture. [b]Combined Heat and Power. [c]Pressure Swing Adsoprtion (PSA). [d]Steam reforming of methane. [e]Reverse Water-Gas-Shift (RWGS). [f]Fischer-Tropsch synthesis.

Income streams from surplus heat and surplus electricity are presented in Table 6.6. Surplus values are calculated using data from Tables 5.1-5.7 for a plant operating 8000 hours in a year. Unit prices for surplus steam and electricity were assumed at 4.82 p·kWh^{-1} and 7.81 p·kWh^{-1}, respectively (Aaron, 2012; OFGEM, 2016).

Table 6.6 Income streams originated from surplus heat, surplus electricity

	PD-MEA1	**PD-MEA2**	**PD-CHP1**	**PD-CHP1-OXY**	**PD-CHP2**	**PD-CHP2-OXY**	**PD-CHP1-POST**
Surplus Steam (kW)	0	0	5,411	3,061	5,072	2,738	3,702
Surplus steam annual income (M£)	0	0	2.09	1.18	1.96	1.06	1.43
Surplus electricity (kW)	0	0	0	2615.51	0	2718.45	4017.31
Surplus electricity annual income (M£)	0	0	0	1.63	0	1.70	2.51

6.6.1.1. Capital expenditure (CAPEX)

As discussed in section 6.3, the total capital investment (TCI) is calculated using a method based on the percentage of *Delivered-Equipment Costs* (DEC), which were estimated using Aspen Process Economic Analyzer (APEA). Fig. 6.1 shows the breakdown of the DEC for different areas of the CO_2-to-fuels plant and the resulting total DEC for the seven process designs.

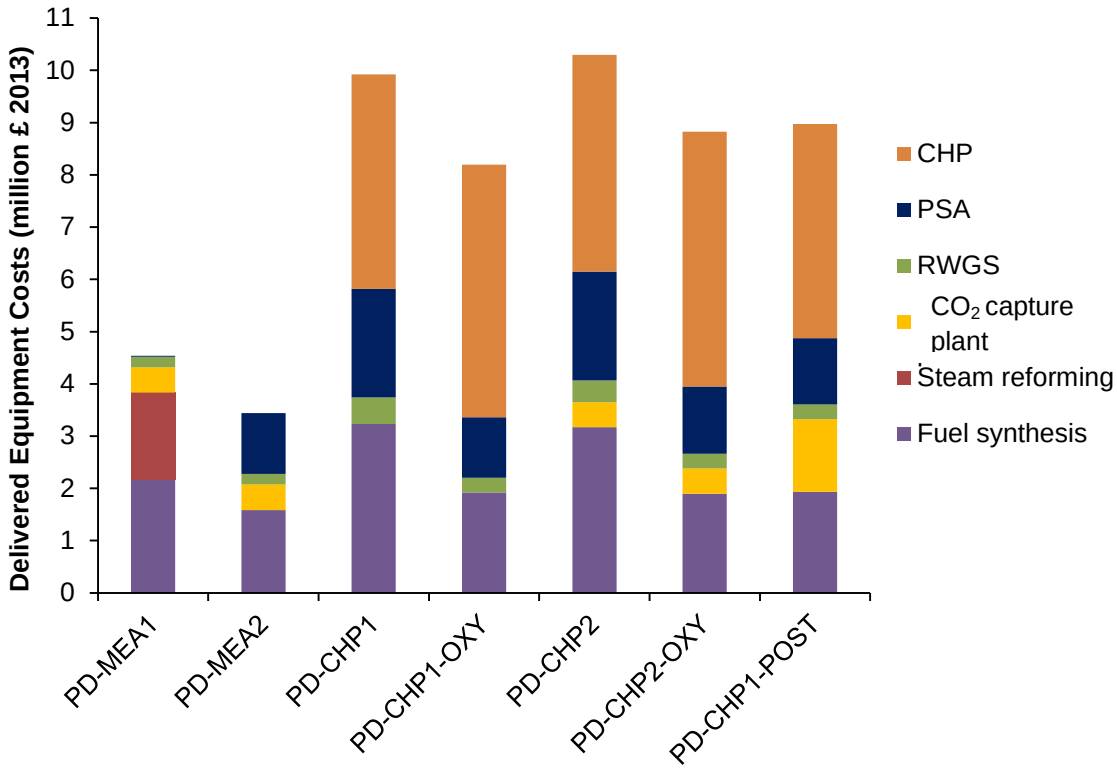

Fig. 6.1 Breakdown of the Delivered Equipment Costs of each Base Case Model

The DEC ranges from £3.44 million (PD-MEA2) to £10.30 million (PD-CHP2). The process designs that are based on a Combined Heat and Power (CHP) plant (PD-CHP1, PD-CHP1-OXY, PD-CHP2, PD-CHP2-OXY and PD-CHP1-POST) result in higher DEC than PD-MEA1 and PD-MEA2 as a result of including a CHP unit, which increases the equipment costs and thus the total DEC of the plant. The lower DEC of the PD-MEA2 is mainly a consequence of the steam methane reformer that the PD-MEA2 does not include. The CHP unit contributes 40–59% to the total DEC. The fuel synthesis area is also a major contributor to the total DEC ranging from 22%-48%. The main reason for the high contribution of the fuel synthesis area to the total DEC is the high purchase cost of the FT plant compressor. This is in line with other techno-economic studies that considered FT synthesis technology (Dimitriou, 2012; Swanson *et al.*, 2010). The steam reforming area, only present in PD-MEA1, represents

37% of the total DEC. The PSA plant represents a very small fraction of the DEC in PD-MEA1 (0.3%) but has a much higher contribution in all the rest of the concepts (14%-34%). The lower contribution of the PSA plant in PD-MEA1 is due to the fact that in this design the PSA plant does not necessitate a compressor since the stream to be treated in the PSA unit comes already pressurised from the steam methane reformer. The CO_2 capture plant represents 5%-16% of the total DEC while the RWGS area represents 3%-6%.

Fig. 6.1 also shows that PD-CHP1 and PD-CHP2 result in similar DEC (£9.9 million and £10.3 million respectively). This is explained by the very similar nature of both designs which only differ in the CO_2 capture plant that PD-CHP2 includes and PD-CHP1 does not. It can be also noticed that the fuel synthesis, the PSA and the RWGS contribution to the total DEC is higher in these two designs than in all the other as a consequence of the higher gas processing involved in both processes.

As for the CO_2 capture contribution, its contribution to the total DEC is the largest of all in PD-CHP1-POST due to larger gas flowrate that the capture plant has to process in this design. It should be noted that the CO_2 capture plant in PD-CHP1-POST processes the exhaust stream from the CHP plant rather than raw biogas, as in PD-MEA1, PD-MEA2, PD-CHP2 and PD-CHP2-OXY.

Fig. 6.2 shows the total capital investment (TIC) of the evaluated Base Case Models, ranging £21 million to £61 million. Since the TIC is proportional to the DEC (see Table 6.2), one can expect that those process design with higher DEC will result in higher TIC too.

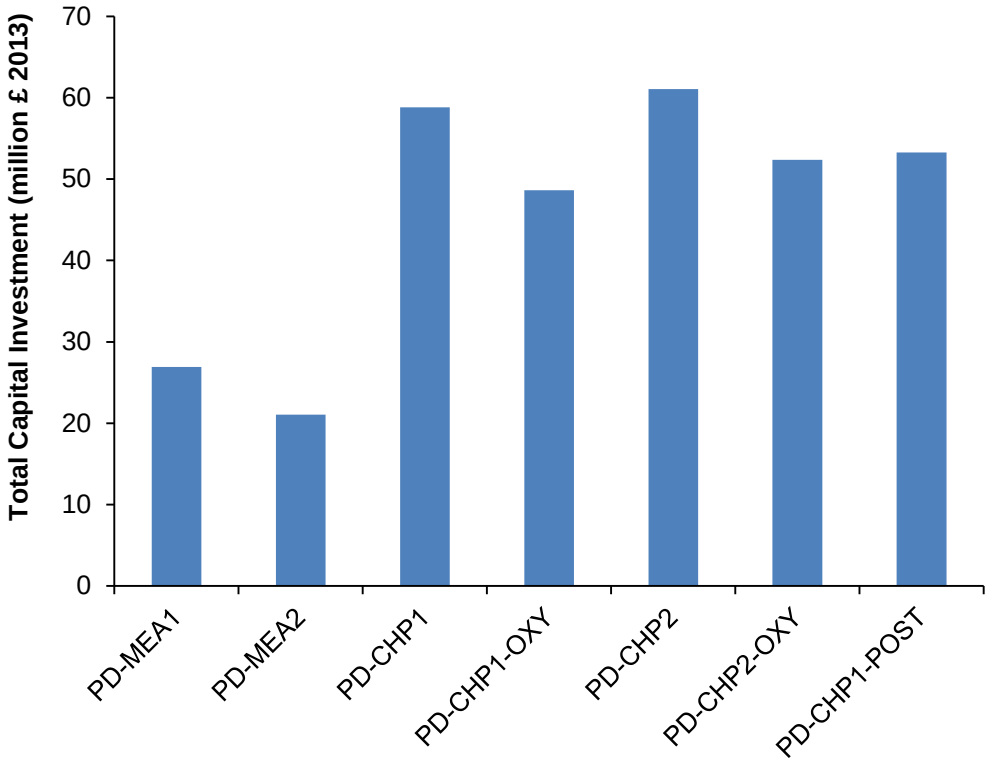

Fig. 6.2 Total Capital Investment of the evaluated process concepts

6.6.1.2. O&M costs

Fig. 6.3 shows the annual operating and maintenance costs as calculated using the method explained in section 6.4. The total O&M includes the expenditure in cooling, heating, electricity, hydrogen, oxygen (for the oxy-combustion CHP processes) and other charges (which represent all other charges). Under the “Other” category, the expenditure on maintenance, operating labour, supervision, operating supplies, laboratory charges, plant overhead, fixed charge and total general expenses are included. The “Other” category also includes the MEA make up cost which represents a very small fraction of the total O&M (0.01%-0.03%).

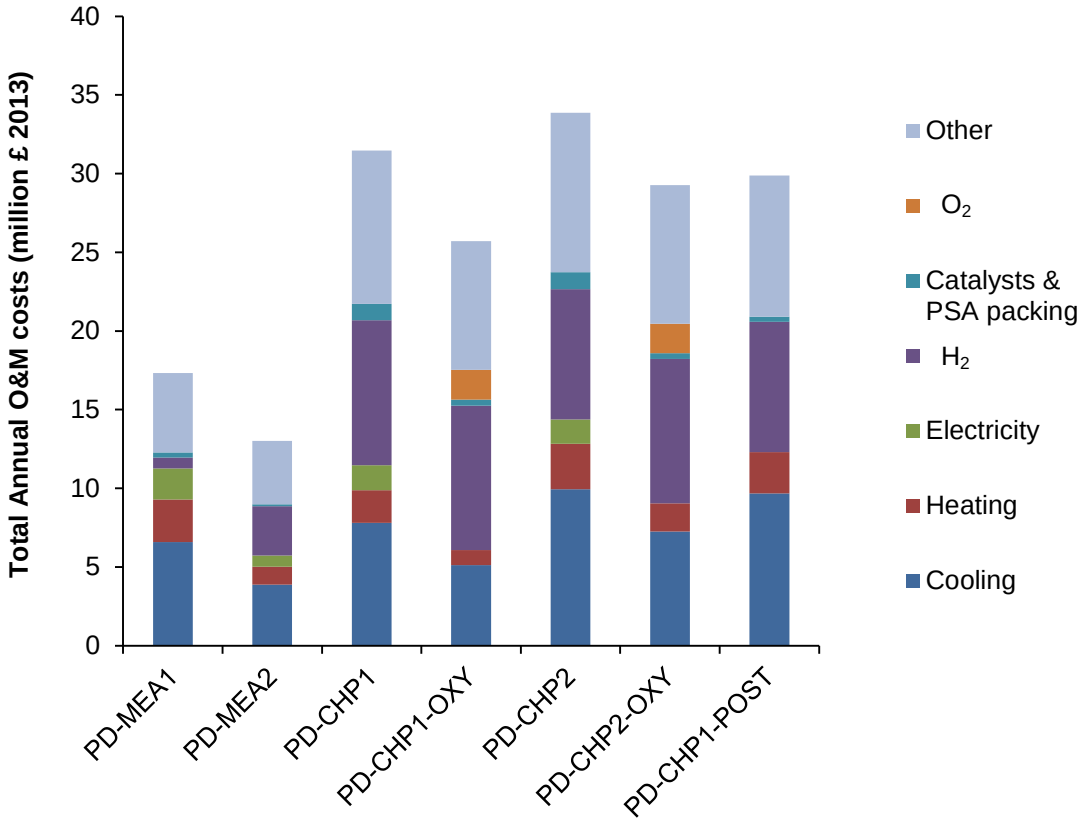

Fig. 6.3 Annual O&M costs of the evaluated process designs

The O&M costs range from £13–£34 million. Similarly to the DEC, the process designs that are based on a Combined Heat and Power (CHP) plant (PD-CHP1, PD-CHP1-OXY, PD-CHP2, PD-CHP2-OXY and PD-CHP1-POST) result in higher O&M than PD-MEA1 and PD-MEA2. This is mainly a result of the higher hydrogen requirements as the processes based on a CHP plant do not produce any hydrogen within the plants, as PD-MEA1 do, thanks to the steam methane reforming. PD-MEA2 results in lower O&M than PD-MEA1 first due to the savings in heating and electricity as a consequence of not employing a steam methane reformer. Additionally, the cooling costs of PD-MEA2 are lower because of the lower gas volume to be processed downstream (upgraded bio-methane injected into the grid, *i.e.* not processed downstream of the CO_2 capture plant). The contribution of the supply of hydrogen to the O&M costs ranges from 4%-

36%. The processes PD-CHP1 and PD-CHP2 result in higher heating, cooling and electricity than PD-CHP1-OXY and PD-CHP2-OXY due to the higher volume of gas that is processed in the designs employing air-combustion. The cost of the supplied oxygen for the oxy-combustion processes is £1.9 million in both PD-CHP1-OXY and PD-CHP2-OXY (6%-7% of total O&M costs). PD-CHP2 results in higher O&M than PD-CHP1 as a consequence of the extra cooling and heating required in the CO_2 capture plant. The O&M costs associated with PD-CHP1-POST are lower than those of PD-CHP1 and PD-CHP2 due to the net electricity production from PD-CHP1-POST and also due to the lower volume of gas to be processed downstream of the CO_2 capture plant. This decreases the cooling, heating and electricity consumption as well as catalyst and PSA packing requirements.

As for the catalyst and PSA packing, their cost is low compared to the other contributors to O&M as they only represent 2%-3% of the O&M. The details of how the catalyst and PSA packing costs were calculated for each process design can be found in Appendices B and C.

In all process designs, the cooling costs are higher than the heating costs and in all cases represent a significant contribution to the O&M (20%-38%). This is explained by the fact the cooling of a given stream is present in all areas of the different process designs except for the CHP plant. The main contributors to the cooling costs are, in this order, the stripping column condenser in the CO_2 capture plant, the FT compressor intercooling, the FT cooler and the FT reactor, representing 97%-98% of all cooling costs. One approach to tackle the high cooling costs could have been to perform heat integration throughout the plant. The process heat integration was attempted using the pinch analysis technique (Ebrahim & Kawari, 2000), using the Aspen Energy Analyzer software, licensed by Aspen Tech (Aspen Technology 2013a). After performing the pinch analysis in all process concepts, it was revealed that the scope for heat integration was negligible and thus any savings in cooling/heating was

outweighed by the extra equipment cost (mainly heat exchangers). As an example of this situation, Table 6.7 shows the heating and cooling costs of the base case and integrated designs for PD-MEA1. Figs. 6.4-6.6 depict such designs as a heat exchanger network (HEN).

Table 6.7 Results from Aspen Energy Analyzer for PD-MEA1

	NETWORK COST INDEXES		
PD-MEA1	Base Case	Integrated Design 1	Integrated Design 2
Heating (Cost·s^{-1})	$7.95 \cdot 10^{3}$	0	0
Cooling (Cost·s^{-1})	$5.02 \cdot 10^{-3}$	$-5.25 \cdot 10^{-4}$	$-1.49 \cdot 10^{-3}$
Operating (Cost·s^{-1})	$1.30 \cdot 10^{-2}$	$-5.25 \cdot 10^{-4}$	$-1.49 \cdot 10^{-3}$
Capital (Cost)	$7.01 \cdot 10^{5}$	$2.51 \cdot 10^{6}$	$2.35 \cdot 10^{6}$
TOTAL (Cost·s^{-1})	$2.01 \cdot 10^{-2}$	$2.51 \cdot 10^{-2}$	$2.25 \cdot 10^{-2}$

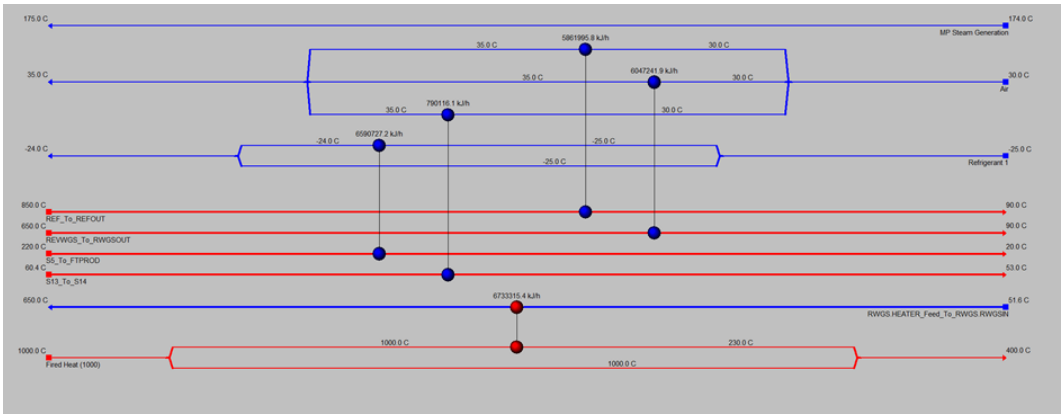

Fig. 6.4 Heat exchanger network of PD-MEA1 (base case)

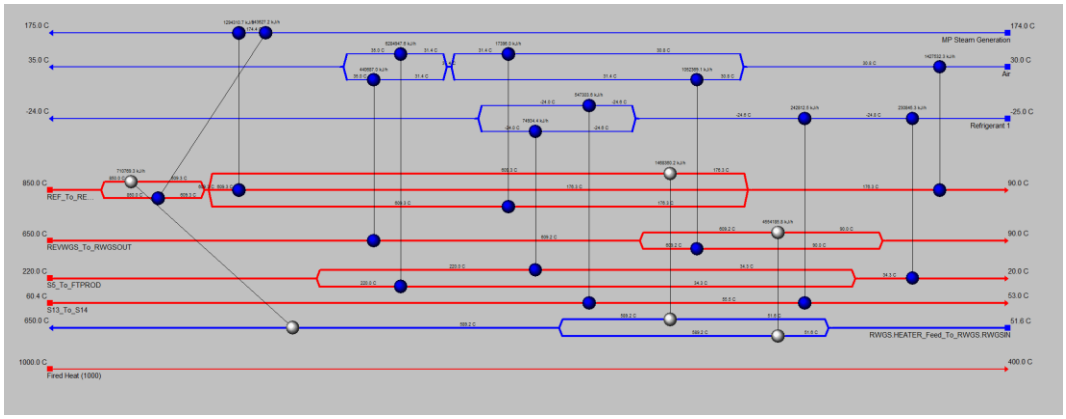

Fig. 6.5 Heat exchanger network of PD-MEA1 (integrated design 1)

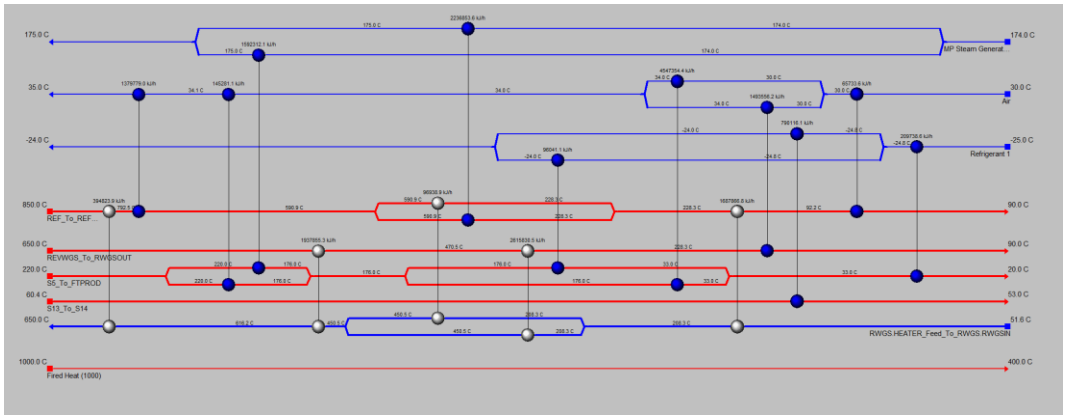

Fig. 6.6 Heat exchanger network of PD-MEA1 (integrated design 2)

It should be noted that the hydrogen needed in the RWGS reaction is considered to be produced within the same WWTP-CCU plant complex by water electrolysis, which is a well-developed low carbon technology (Bhandari *et al.*, 2014; Quadrelli *et al.*, 2011). However, the water electrolysis plant has not been modelled in this study due to the availability of hydrogen production cost data in the literature. In this study, a production costs value of £2 per kg of hydrogen produced by a Polymer Electrolyte Membrane (PEM) electrolyser (US Department of Energy,

2014), was assumed and added to the fuel production cost. The assumed hydrogen production cost includes both capital and operating expenditure.

Similarly, the oxygen needed by the CHP plants with oxy-combustion is also considered to be produced within the same WWTP-CCU plant complex by an Air Separation Unit (ASU). As highlighted in section 3.3.4.2, the ASU plant was not modelled in this study. Alternatively, since ASU is a well-established and mature technology, the production costs of O_2 at 99.9 mol. % and 8 bar were retrieved from the literature with a value of $\$35_{1994}$/tonne of oxygen, considering that the ASU is located next to the CO_2 utilisation plant and therefore no transport costs are involved (Rao & Muller, 2007). The oxygen production cost includes both capital and operating expenditure and was added to the fuel production cost.

6.6.1.3. Fuel production costs

The production costs per GJ of FT-syncrude (LHV) for each evaluated process design are presented in Fig. 6.7, along with the contribution of capital costs (as capital annuity) and O&M expenditure.

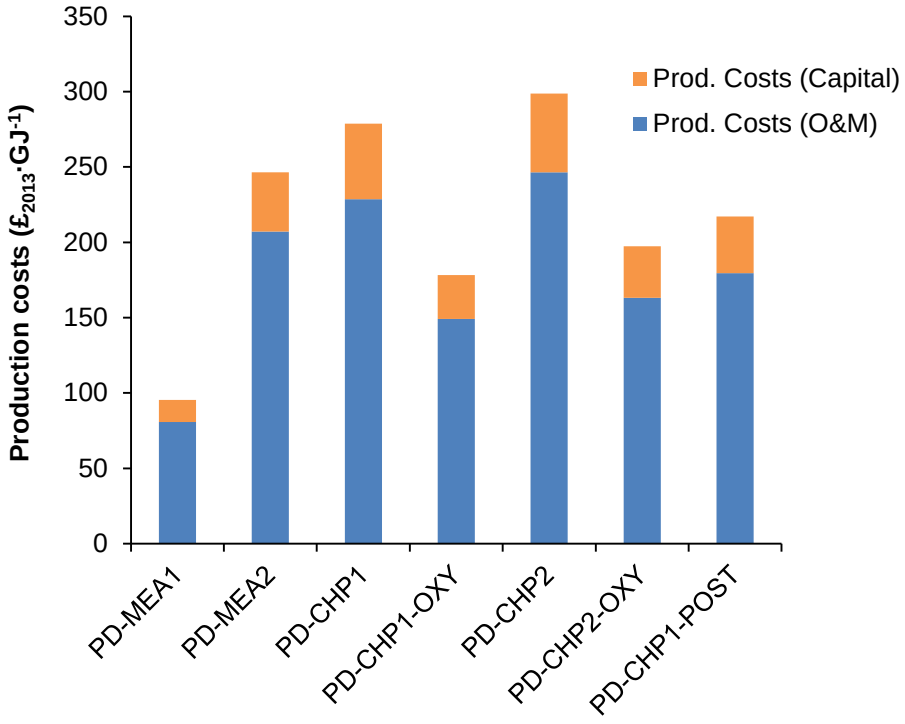

Fig. 6.7 Fuel production costs of the evaluated Base Case Models

The calculated production costs do not include tax, duties, producer and retailer profits, marketing expenditure and distribution costs. The fuel production costs range from £95.46·GJ^{-1} to £298.73·GJ^{-1}.

O&M costs are a more important contributor to the fuel production costs than the capital investment as they represent 83-85% of the total production costs. PD-MEA1 has the lowest production costs at £95.46·GJ^{-1} because of its lower capital and operating costs as well as higher fuel production compared to the other six cases. The next best option in terms of production costs is PD-CHP1-OXY (£178.32·GJ^{-1}), which has the lowest production costs among all CHP-based designs. PD-CHP2-OXY (£197.42·GJ^{-1}) results in slightly higher fuel production costs than PD-CHP1-OXY mainly due to the extra cost associated with the CO_2 capture plant. The next process design is PD-CHP1-POST, which produces fuels at £217.11·GJ^{-1}. This is followed by PD-MEA2 fuel production costs of £246.43·GJ^{-1}. In this case, the lower TCI and O&M of PD-MEA2 compared

to those of PD-MEA1 are outweighed by the much lower fuel production rate. It should be noted that the upgraded bio-methane stream produced by PD-MEA2 could generate an annual income of 11.98 M£ assuming a bio-methane selling price of 7.5·kWh^{-1} under the UK renewable heat initiative (DECC, 2014b).

Both process concepts that use an air-combustion CHP (PD-CHP1 and PD-CHP2) are associated with the highest fuel production costs at £278.81 and £298.73 per GJ, which is approximately 92% and 113% higher than for PD-MEA1, respectively. The main reason for this is that this concept produces a significantly lower amount of liquid fuels than PD-MEA1, as discussed in section 5.1.2.8. In addition, both TCI and O&M associated with PD-CHP1 and PD-CHP2 are considerably higher than those of PD-MEA1, as discussed in section 6.6.1.1 and 6.6.1.2. From these it is clear that the amount of fuel produced is a very important aspect of the production costs; thus, its effect is investigated in the sensitivity analysis later in this chapter (section 6.7).

6.6.1.4. Comparison with costs of conventional transport fuels

Several factors, such as fiscal regimes, debt/equity ratio, type of loans, and corporate return requirements as well as government subsidies and CO_2 credits may affect the selling prices of liquid fuels produced via the proposed CCU technologies. Another factor which significantly affects the fuel production costs of any industrial plant is the economies of scale in the sense that production costs are expected to decrease dramatically as production rates increase. This is the reason why the effect of the economies of scale is investigated in this section in order to assess the potential economic competiveness of CCU against conventional, fossil fuel technologies. The effect of economies of scale will be investigated only for PD-MEA1, since it is the process design that achieved the highest plant efficiency as well as the lowest production costs of all evaluated CCU process designs. Eighteen plant capacities are evaluated, ranging from 18.3 tonne·day^{-1} (base case) to 1670 tonnes of liquid fuels produced per

day. The latter capacity corresponds to the Shell Middle Distillate Synthesis (SMDS) Gas-to-Liquids (GTL) plant built in Bintulu (Malaysia), a large complex that produces naphta, kerosene and gas-oil from natural gas via an enhanced Fischer-Tropsch process (Eilers *et al.*, 1991). The TCI of the scaled-up plants were estimated using the six-tenths factor rule, defined by Eq. 6.3,

$$C_2 = C_1 \cdot \left(\frac{S_2}{S_1}\right)^{0.6} \quad \text{Eq. 6.3}$$

where C_1 and C_2 are the TCI of the PD-MEA1 base case and the 1670 tonne·day^{-1} plant, respectively, S_1 and S_2 are the capacities of the PD-MEA1 base case and the larger plant, respectively, and 0.6 is the scaling factor. The six-tenths factor equation is a rule of thumb developed over the years, which evolved in the public domain after large quantities of actual cost data were analysed retrospectively. The purpose of using such rule in this thesis is to explore the impact of the scale on the assessed processes; however, it should be noted that it is not intended to perform a rigorous analysis over the issues surrounding scale. The reader should be aware of the impracticality of building an AD reactor at the scale considered in the scaled-up case (C_2). As an alternative, the necessary flowrate of biogas could be transported from several waste water treatment plants to a centrally located CO_2-to-fuels plant.

The annual operating costs of PD-MEA1 are approximately 5.5 times the annualised cost of capital; therefore, the same percentage contribution was assumed in calculating the operating costs of the scaled-up plants. Using the six-tenths factor rule, the capital investment for the PD-MEA1 plant of the largest capacity considered here (1670 tonnes per day) is estimated at £405 million (£47.6 million annualised costs of capital). The annual O&M costs are estimated to be £260.5 million. The TCI of the scaled-up CCU plant is 51% lower than those of the Shell plant (£831 million), although the capital costs of the water electrolysis plant and the ASU of the CCU plant are not included in the TCI, as explained in section

6.6.1.2. On the other hand, the operating costs of the CCU plant are approximately 6 times higher than those of the Shell plant (£260.5 million). These results highlight the importance of the operating costs, which should be drastically reduced if successful implementation of the CCU technology is to be pursued (see section 6.6.1.5). It should also be noted that the Shell's GTL plant was built in 1990 in Malaysia and therefore one must be careful when making any comparisons between the GTL plant and the CCU plant, which is a much less developed technology that has been considered to be built and operated in the UK in this study.

Fig. 6.8 shows the effect of scale on the costs of CCU fuels. For the largest plant capacity, the fuel production costs are approximately 6 times lower than for the PD-MEA1 base case (£15.67·GJ^{-1} vs £95.46·GJ^{-1}).

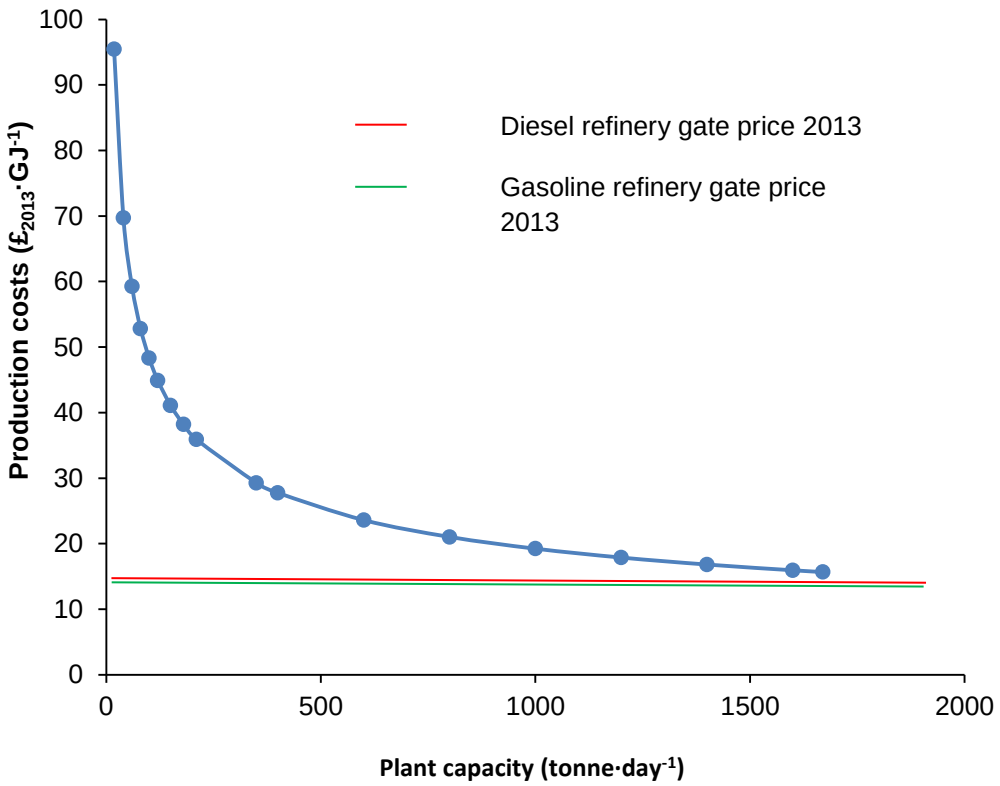

Fig. 6.8 Cost of liquid fuels in £ per GJ (LHV) at different plant capacities for PD-MEA1

As for the cost of producing conventional diesel and gasoline in 2013 and in the UK, their gate costs (composed of operating costs and capital amortisation) were £0.47 per litre for gasoline and £0.51 per litre for diesel

(UKPIA, 2015), excluding tax, duty, profits, marketing and distribution costs. On an LHV basis, the gate costs of gasoline and diesel were £14.3·GJ^{-1} and £14.6·GJ^{-1}, which are 7% and 9% lower than those of the CCU plant, respectively. Since the gate prices for gasoline and diesel are given in £ per litre, a volumetric energy density of 34 MJ per litre (LHV) and 32 MJ per litre (LHV) was assumed for diesel and gasoline, respectively (Edwards *et al.,* 2013). These results, although positive must be interpreted very carefully and any conclusions drawn from must take into account the assumptions made in the case of the CCU plant. First, the CCU plant does not produce gasoline nor diesel but a mixture of hydrocarbons (C_5-C_{30}); although a LHV basis was chosen for the comparison between the conventional and the CCU fuels, one should be aware of this fact since the FT upgrading island would incur in extra costs related to further processing (cracking, distillation, *etc.*). Second, the CCU plant is based on best available technology but it is a synthetic route to fuels at a very early stage of development; therefore, one should take into account the uncertainties associated with a process of this kind. Third, the gate prices of conventional fuels are, of course, highly dependent on crude oil prices. With crude oil prices falling continuously since 2012 (UKPIA, 2015), the CCU fuel synthesis processes proposed in this study will become less financially attractive; thus, it is anticipated that increases in fossil fuel prices, governmental subsidies or environmental legislation such as carbon taxes will be needed in order to make CCU fuels competitive in the market. All in all, the reported results encourage further research in the area, which should be focussed on areas highlighted in the following section 6.6.1.5.

In this section, it has been demonstrated that the fuel production costs decrease dramatically when the plant capacity increases; therefore, the results showed in Fig. 6.8 suggest that such technology will only achieve commercial success if large amounts of CO_2 can be converted into fuels. In light with this, alternative sources of carbon dioxide must also be assessed. One potential candidate could be CO_2 capture from power

plants and subsequent conversion to fuels since in this case large amounts of CO_2 are guaranteed. For instance, a 600 MWe coal-fired power plant would provide CO_2 in the region of 120 $kg \cdot s^{-1}$ (Abu-Zahra *et al.*, 2007). This represents an increase of more than two orders of magnitude compared to the amount of CO_2 in the biogas processed in the base case models. To put this in context, about 3,512 t·day-1 of FT syncrude could be produced, assuming a CO_2 to fuels mass yield of 37% (as in PD-MEA1). According to Fig. 6.8, these FT syncrude production rate could translate into a fuel production cost below conventional fuels (below £14·GJ^{-1}); however, a potential drawback of a power plant as the CO_2 source is the lack of endogenous production of the necessary H_2 as opposed to, for instance, PD-MEA1. This will require large imports of H_2, which would increase the OPEX substantially.

6.6.1.5. Identification of hotspots for CCU fuel production costs

The previous sections have set out the different contributors to the fuel production costs. At this stage, it is crucial to identify the hotspots for fuel production costs, which will be targeted for optimizing the process. Since PD-MEA1 is the process design that results in the lowest production costs, it will be targeted for hotspots identification.

As pointed in section 6.6.1.3, the TCI is one of the contributors to the fuel production costs and therefore the aim is to reduce them as much as possible. Fig 6.1 shows that the fuel synthesis area and the steam methane reformer are the main contributors to the DEC and therefore to the TCI with a share of 37% and 48%, respectively. As for the fuel synthesis area, which is based on Fischer-Tropsch synthesis, 66% of its DEC corresponds to the cost of the syngas compression equipment. This is in line with other studies that considered FT synthesis for fuel production (Swanson *et al.*, 2010a). The main target for optimization here would be to increase the water removal in the syngas (unreacted water in steam methane reformer), which would result in lower compression equipment complexity (due to reduced compression volume and potential

condensation). Additionally, R&D developments on FT synthesis that increases fuel yields and selectivity at lower operating pressures are required.

As for the steam methane reformer, which is a mature and well developed technology, it is expected that further improvements in the technology will be of much less scale than those on FT synthesis; however, as in the FT synthesis area, the compression equipment represents a large share of the steam methane reformer DEC (77%). It is then clear that, as in the FT area, R&D developments should focus on achieving high conversions of CH_4 at lower operating pressures.

Section 6.6.1.3 highlights that the bulk of the fuel production costs come from the O&M expenditure. Within the O&M expenditure, the largest contributors are, in this order, cooling, other charges and heating, accounting for 83% of all O&M costs. As discussed in section 6.6.1.2, 'other charges' includes maintenance, operating labour, supervision, operating supplies, laboratory charges, plant overhead, fixed charge and total general expenses. Most of these charges are estimated as a percentage of the TCI, as defined by Peters *et al.* (2004); therefore, in order to reduce their contribution to the O&M, the TCI must be reduced first.

Cooling is the main contributor to O&M (38%) in PD-MEA1 and therefore it is crucial to reduce this contribution. 52% of the cooling costs comes from the 'three-way' condenser used in the FT synthesis to separate the off-gas, the FT liquids and the water fractions. An additional 32% of the cooling costs are generated by the stripping column condenser, which condenses any water vapours produced during the regeneration of the MEA solution (70 wt. % water). The main target here would be to develop CO_2-absorbing solutions that allow either regeneration at temperatures below the water boiling point or solutions that can be used at 100% purity so that they do not have to be mixed with water to prevent corrosion-related problems, *e.g.* ionic liquids.

As for the heating, the steam methane reformer contributes to 56% of all heating costs, due to the high (endothermic) enthalpy of reaction. Since this technology has been used at an industrial scale for decades, major breakthroughs are not likely to happen; therefore the steam methane reforming is an area of the CCU plant that shows little scope for improvement. On the hand, the CO_2 capture plant, which represents 31% of all total heating costs, has been targeted by active research in the last years, as highlighted in section 2.5. The main focus here would be to develop capture media with high CO_2 affinity while at the same time requiring less energy to release the absorbed CO_2.

The final target for fuel production costs reduction would be to maximise the fuel production rate. This is mainly affected by the fuel yields in the Fischer-Tropsch reactor, which are at the same time dependant on the syngas production rates; therefore the process improvements should seek to maximise syngas production and FT fuel yields under moderate conditions (temperature and pressure).

6.6.2 CO_2 capture using ionic liquids

This section includes the economic evaluation of the CO_2 capture plants that use ionic liquids as a solvent for CO_2 capture. These results are compared with an MEA-based CO_2 capture plant, which is considered a well-developed technology. Ionic liquid-based processes and the MEA process are totally comparable to the biogas upgrading plants using ionic liquids in terms of flowrate and conditions of the biogas (composition, temperature and pressure), dimensions of the absorber, type of packing and composition of the upgraded bio-methane (95 vol. %). Detailed costs results for each design are presented in detail in Appendix D.

The total capital expenditure (TCI) was estimated using the same method as in the case of the base case models (Peters *et al.*, 2004). Table 6.8 shows the breakdown of the capital costs related to each process concept using the method described in Table 6.2.

Table 6.8 Summary of the total capital investment

	$[C_2MIm][Tf_2N]$ (£1000)	**$[C_6MIm][Tf_2N]$ (£1000)**	**$[P_{66614}][Tf_2N]$ (£1000)**	**MEA (£1000)**
Direct Cost				
Purchased equipment	1519.00	1550.80	1570.50	519.90
Equipment installation	713.93	728.88	738.14	244.35
Instrumentation and control	546.84	558.29	565.38	187.16
Piping	1032.92	1054.54	1067.94	353.53
Electrical	167.09	170.59	172.76	57.19
Building and building services	273.42	279.14	282.69	93.58
Yard improvements	151.90	155.08	157.05	51.99
Service facilities	1063.30	1085.56	1099.35	363.93
Indirect Cost				
Engineering	501.27	511.76	518.27	171.57
Construction expenses	622.79	635.83	643.91	213.16
Legal costs	60.76	62.03	62.82	20.80
Contractor's fee	334.18	341.18	345.51	114.38
Contingency	668.36	682.35	691.02	228.76
Other costs				
Working investment	1481.67	1502.685	1498.13	466.45
IL/MEA cost	740.97	685.68	574.37	22.62
TCI	**9878.40**	**10004.40**	**9987.82**	**3109.37**

The total capital investment costs for the three process concepts that use ionic liquids are £9.878 million for $[C_2MIm][Tf_2N]$, £10.004 million for $[C_6MIm][Tf_2N]$ and £9.988 million for $[P_{66614}][Tf_2N]$. In all cases, the purchased equipment, piping, service facilities and working investment are the items that contribute more significantly towards the total capital investment. $[C_2MIm][Tf_2N]$ concept results in lower capital costs due to the

fact that the cost of the regeneration pump and the flash evaporator are considerably cheaper than in the other two concepts. It should be noted that only the biogas upgrading section is being considered, not the whole system as in the base case models.

As for the MEA-based process, it can be seen that its TCI, as well as its DEC, is approximately 3 times lower than those of the ionic liquid-based processes. Fig. 6.9 shows a breakdown of the DEC of each CO_2 capture process.

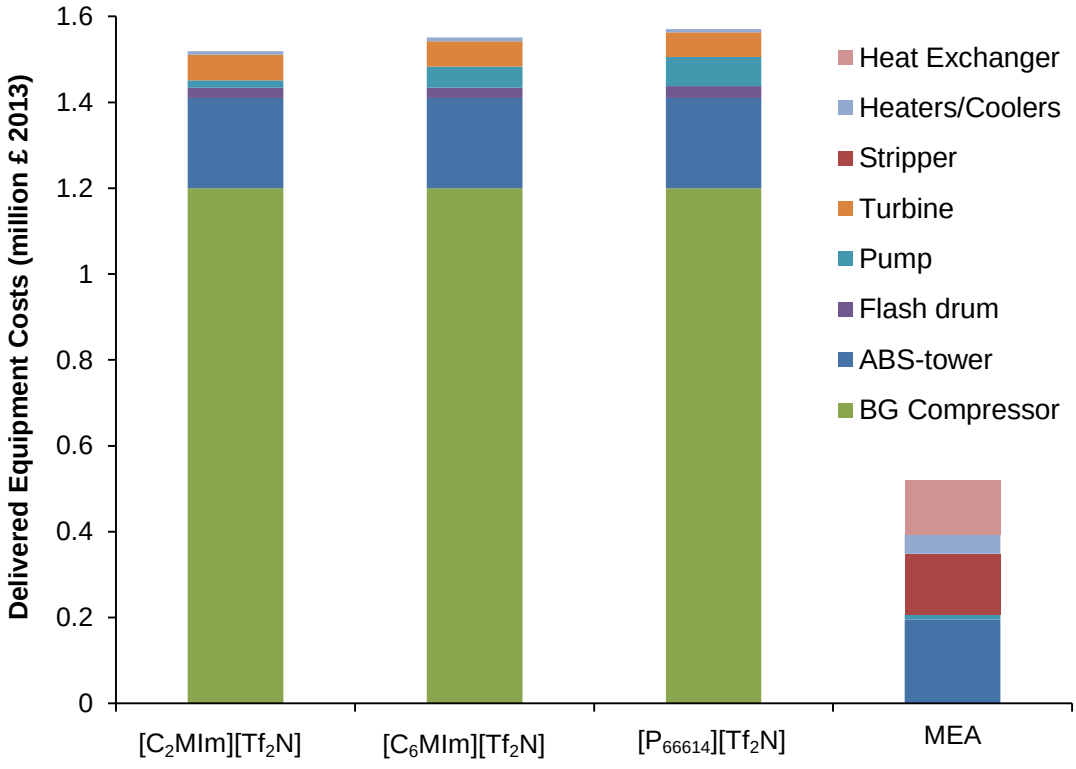

Fig. 6.9 Breakdown of the DEC of each biogas upgrading process

As one can see, the biogas compressor represents most of the DEC for the ionic liquid-based processes (76-79%). This is then the main reason of the high TCI associated with these processes compared with the MEA process. Following the biogas compressor, the second contributor to the DEC in the ionic liquid-based processes is the absorption column (13-14% of DEC). The contribution towards the DEC of the rest of the equipment is

as follows: high pressure turbine (4% in all cases), flash drum (2% in all cases), regeneration pump (1-4%), and absorber pre-cooler (0.5%).

As for the MEA process, the absorption column has a share of 38% of the DEC, followed by the stripper (including reboiler, condenser and related equipment) with a share of 27% of the DEC, the amine heat exchanger (24%), the pre-heater and pre-cooler (9%) and the recirculation pump with 2%.

The costs of the ionic liquid fluids are also included in Table 6.8 by using a selling price of £13·kg^{-1} for all the three ionic liquids considered, as already reported in the literature (Shiflett *et al.*, 2010). In fact, [C_2MIm][Tf_2N] results in the higher IL costs since it requires more fluid than [C_6MIm][Tf_2N] and [P_{66614}][Tf_2N] as this IL has a lower molar volume and CO_2 uptake than the two other investigated ILs. MEA requirements are approximately three times lower than those of the ionic liquids. As discussed in section 5.1.3 this is due to the fact that MEA chemically reacts with CO_2, as opposed to the ionic liquids which absorb the CO_2 physically.

The annual operating and maintenance costs of the four CO_2 capture processes considered are presented in Table 6.9. The operating costs range from £1.809 million to £2.256 million. As with the TCI, the process using MEA results in the lowest O&M costs.

Table 6.9 Summary of the O&M costs

	$[C_2MIm][Tf_2N]$ (£1000)	**$[C_6MIm][Tf_2N]$ (£1000)**	**$[P_{66614}][Tf_2N]$ (£1000)**	**MEA (£1000)**
Fixed charge				
Local taxes	153.12	156.32	158.31	52.41
Insurance	76.56	78.16	79.15	26.20
Direct prod. cost				
Heating	0.00	0.00	0.00	624.33
Cooling	53.34	58.58	57.80	65.45
Electricity	292.16	313.24	331.23	73.15
Solvent make-up	0.00	0.00	0.00	4.27
Maintenance	535.90	547.12	554.07	183.42
Operating labour	266.40	266.40	266.40	266.40
Supervision	39.96	39.96	39.96	39.96
Operating supplies	80.39	82.07	83.11	27.51
Laboratory charges	39.96	39.96	39.96	39.96
Plant overhead	505.36	512.09	516.26	293.87
General expenses				
Administrative cost	39.96	39.96	39.96	39.96
Distribution and marketing	43.87	44.71	44.74	36.17
R&D cost	42.18	43.09	45.02	36.35
TOTAL O&M	**2169.14**	**2221.66**	**2255.98**	**1809.42**

Fig. 6.10 summarises the O&M costs of each process as well as a breakdown of the O&M costs.

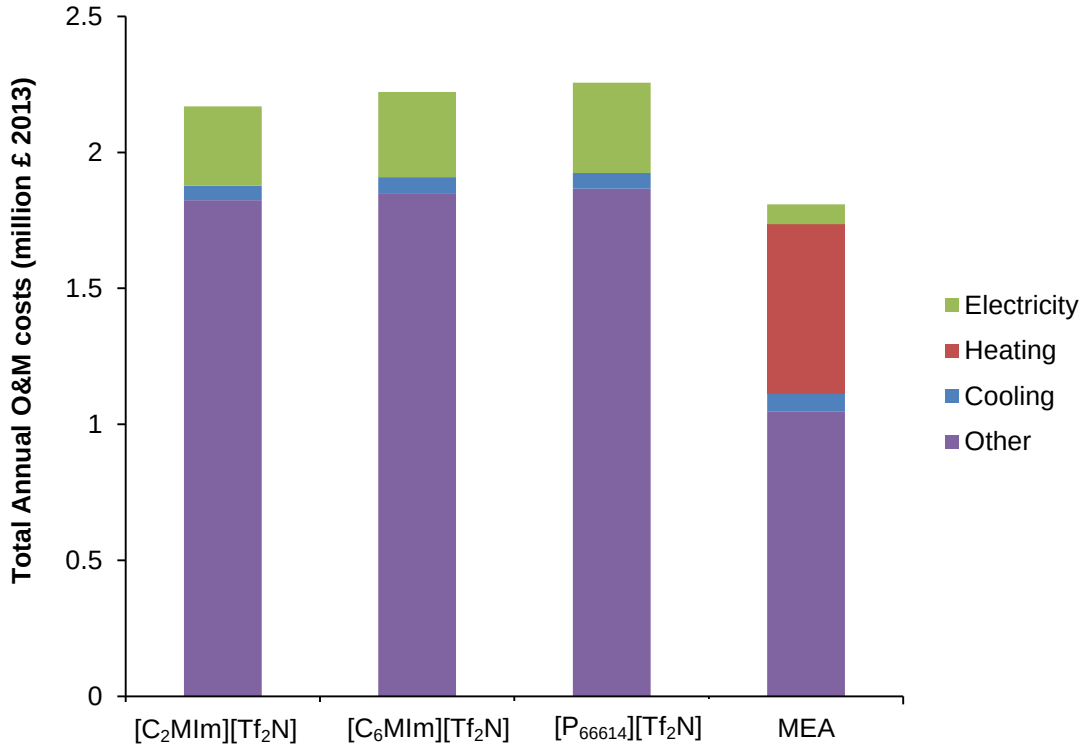

Fig. 6.10 Breakdown of the O&M of each biogas upgrading process

Among the processes using ionic liquids, the one employing $[C_2MIm][Tf_2N]$ results in the lowest operating costs as a result of its lower maintenance costs and plant overhead (both a function of TCI) as well as its lower electricity consumption. In fact, electricity consumption is one of the main contributors to the operating costs in the ionic liquid-based processes, representing 13%-15% of the total O&M. Other large contributors towards the O&M are the operating labour (around 12% in all cases), plant overhead (23%-24%) and maintenance (around 25% in all cases). The process using MEA results in the lowest O&M of the four. Heating for MEA regeneration is a major contributor towards O&M costs representing 35%.

The production costs per GJ [LHV] of bio-methane produced for all cases considered are shown in Table 6.10. The calculated production costs only

include the necessary investment to manufacture one GJ equivalent (LHV) of bio-methane, *i.e.* it does not include tax, duties, profits and marketing costs. As one can see from Table 6.10, the operating and maintenance costs play a significant role in the production costs, accounting for around 65% of the total production costs in all cases, while the capital annuity accounts for 35%. The lowest production cost is achieved by $[C_2MIm][Tf_2N]$, with a value of £6.26 per GJ (LHV), followed by $[C_6MIm][Tf_2N]$ and $[P_{66614}][Tf_2N]$ with values of £6.68 per GJ (LHV) and £7.76 per GJ (LHV), respectively. The reasons for this are that both the capital costs and O&M of $[C_2MIm][Tf_2N]$ are the lowest of the three concepts considered and also that the production rate of bio-methane is the highest of all cases.

Table 6.10 Bio-methane production costs for the selected process concepts

	$[C_2MIm][Tf_2N]$	**$[C_6MIm][Tf_2N]$**	**$[P_{66614}][Tf_2N]$**
TCI (£·GJ^{-1})	2.18	2.31	2.66
O&M (£·GJ^{-1})	4.08	4.37	5.11
Total (£·GJ^{-1})	6.26	6.68	7.76

Contrary to the initial belief, $[C_2MIm][Tf_2N]$ has the lowest production costs despite the fact that, among the ionic liquids evaluated in this study, it is the one with the lowest absorption capacity. This demonstrates the need of holistic evaluations of ionic liquids for CO_2 capture. These results reveal that parameters such as physical properties of the ionic liquid (heat capacity, viscosity, *etc*.) and the effect of other gaseous species in the gas stream should also be taken into account.

6.6.2.1 Production costs: ionic liquids and MEA comparison

To put the above results in context, comparison with existing biogas upgrading processes is essential. Current best practice of biogas upgrading include a wide range of technologies such as, pressure swing adsorption (PSA), high pressure physical absorption with water or the Selexol® solvent, chemical absorption with amines, membrane separation and cryogenic processes (Person, 2003). Given the scope of this study, a fair comparison can be only made with absorption processes which involve either physical or chemical absorption. It was decided to compare the performance of the ionic liquids studied in this work with an MEA-based CO_2 capture process. This decision was based on the lack of data regarding the proprietary Selexol® solvent when used in biogas upgrading applications and also the fact that high pressure absorption with water is limited to lower flowrates of biogas/flue-gas due to the low CO_2 absorption capacity of water (Person, 2003). This last statement is relevant since this work aims to develop a methodology that is not only suitable to CO_2 removal from biogas but is also applicable to larger applications like post-combustion CO_2 capture from industrial sources, *e.g.* power plants, refineries, *etc*.

Fig. 6.11 shows the production costs of all ionic liquid-based processes as well as the MEA process. The lowest bio-methane production costs are achieved by the MEA process with a value of £3.78·GJ^{-1} (LHV), which is 40%-51% lower than those of the processes using ionic liquids. These results encourage further research in the area specially taking into account that the ionic liquids evaluated in this work absorb the CO_2 physically as opposed to MEA, which absorbs the CO_2 mainly through chemical interactions. In addition, the current selling price of ionic liquids must be taken into consideration since as production and consumption of ionic liquids becomes more generalised their costs will be expected to decrease. In line with this, its effect is studied in the sensitivity analysis in section 6.7.2.

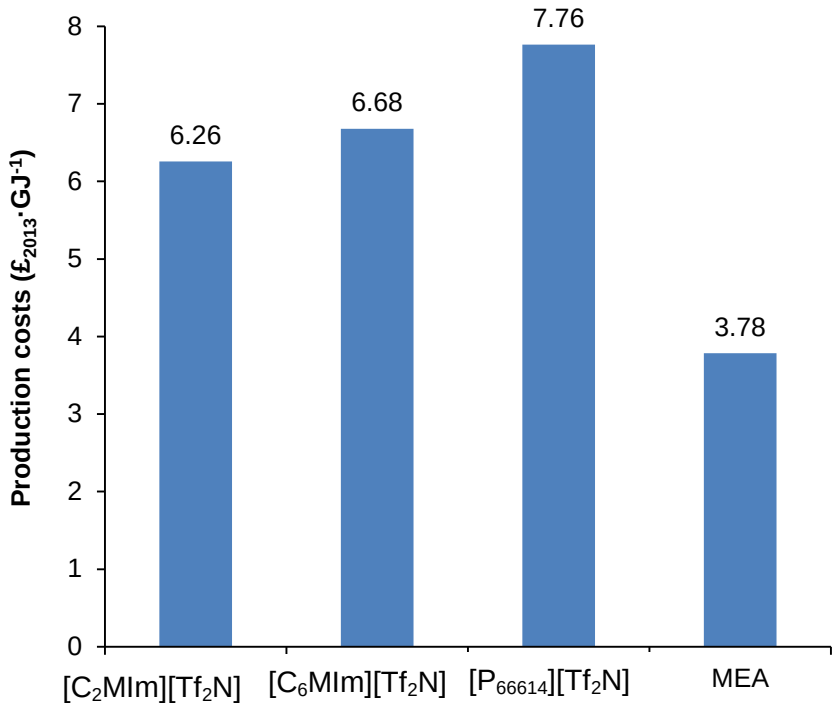

Fig. 6.11 Bio-methane production costs for the different process concepts

6.7 Sensitivity analysis

6.7.1 Base Case Models

In order to carry out the economic assessments included earlier in this chapter, assumptions for important technical and economic parameters (CO_2 conversion, electricity prices, *etc*.) had to be taken; therefore, the results of the economic evaluations are somewhat static, in the way that they only allow to draw conclusions for a given set of fixed parameters. This section discusses the sensitivity analysis study which investigates the effect of several important technical and economic parameters on the FT-syncrude production cost.

In section 6.6.1.5, some parameters were identified to play an important role on costs. In line with this, the parameters investigated in the sensitivity analysis are: CO_2 conversion, operating hours, capital investment, interest

rate, electricity price, plant life and H_2 production costs. The sensitivity analysis was carried out by varying each parameter at a time by ±30% of its base case value. In the case of the plant operating hours, the parameter was changed by ±9.5% from the base case value of 8,000 hours since it cannot exceed the number of hours in a year (8,760 hour in a year). The results from the six process concepts studied are shown in Fig. 6.12-6.18, where longer bars indicate a higher degree of deviation from the base case value.

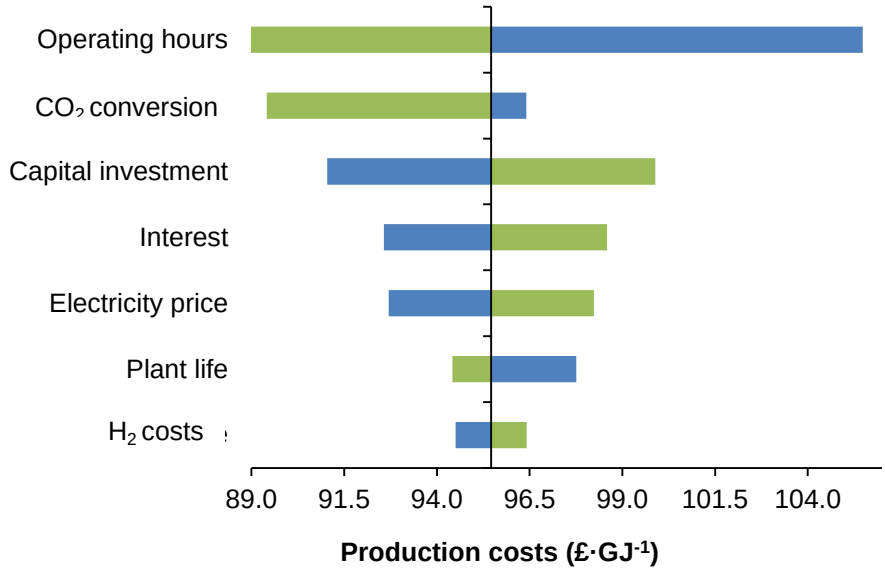

Fig. 6.12 Sensitivity of fuel production (PD-MEA1) costs to variations of selected technical and economic parameters (green bars represent an increase in the parameter)

In PD-MEA1, fuel production costs are most sensitive to plant operating hours since variations of just ±9.5% in this parameter results in higher variations of costs. Thus, this type of plants should be operated with the minimum periods of shutdown in order to achieve significantly lower bio-methane production costs. Production costs are also highly sensitive to increases in CO_2 fractional conversion to CO. It can be seen that increasing the CO_2 conversion by 30% results in the production costs to be reduced to £89.41 per GJ from a base case value of £95.46 per GJ (6% reduction). On the other hand, a reduction of 30% in the CO_2 conversion

results in a fuel production costs increase of 1%. This is because the reduction in the fuel production rate as a result of the reduction in the CO_2 conversion is offset by the lower H_2 requirements in the RWGS reactor. The latter is a consequence of the higher proportion of unreacted H_2 in the syngas that is recovered in the PSA unit and recycle back to the RWGS inlet. As for the capital investment, a variation of ±30% results in the production costs to vary by ±5%. This is an important result since errors of up to ±30% are common in capital investment estimates at this stage of development (Peters *et al.*, 2014).

The loan interest rate is the fourth more sensitive parameter and fluctuations of ±30% results in the production costs to vary by ±3%; interest rates affect the annuity of the capital investment and therefore, efforts should be made at the early stages of the project development to agree a fixed rate with lender throughout the lifespan of the project so that unexpected fluctuation can be avoided. Finally, the fuel production costs are less sensitive to fluctuation in the electricity price, the plant life of the project and the H_2 production cost. However, fluctuations in these parameters they should not be underestimated since they could affect the production costs significantly.

In the case of PD-MEA2, the sensitivity analysis results are similar to those of PD-MEA1, although with some differences as it can be seen from Fig. 6.13.

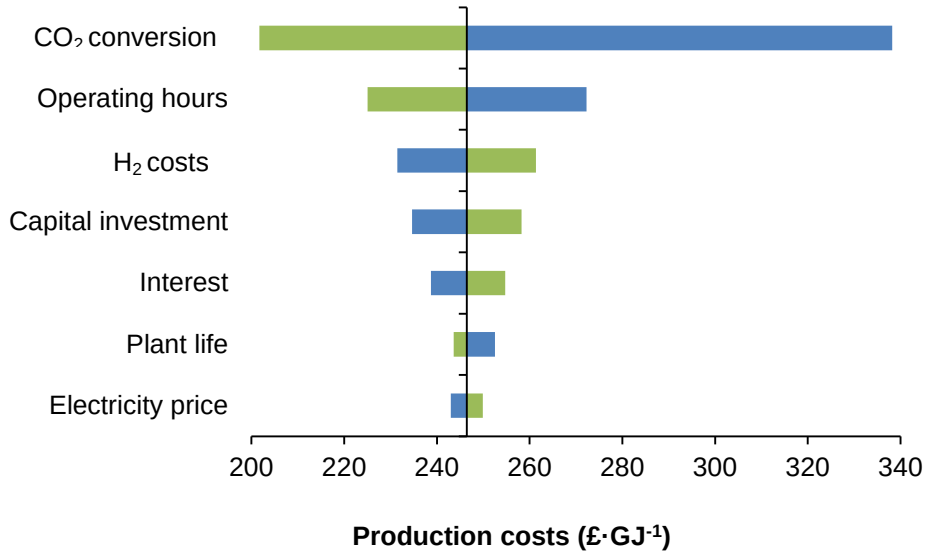

Fig. 6.13 Sensitivity of fuel production (PD-MEA2) costs to variations of selected technical and economic parameters (green bars represent an increase in the parameter)

In this case, as the plant does not include a steam methane reformer, all of the H_2 must be imported to the plant. This, results in that fluctuations in the H_2 production costs have a greater impact on fuel production costs in PD-MEA2 than in PD-MEA1

Figs. 6.14-6.18 show the sensitivity analysis results from the process concepts incorporating a CHP plant (PD-CHP1, PD-CHP1-OXY, PD-CHP2, PD-CHP2-OXY and PD-CHP-POST).

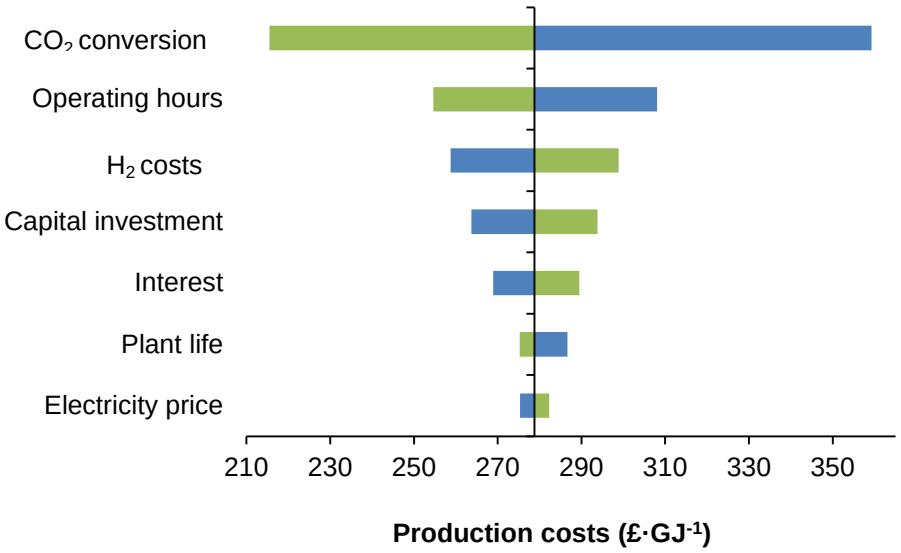

Fig. 6.14 Sensitivity of fuel production (PD-CHP1) costs to variations of selected technical and economic parameters (green bars represent an increase in the parameter)

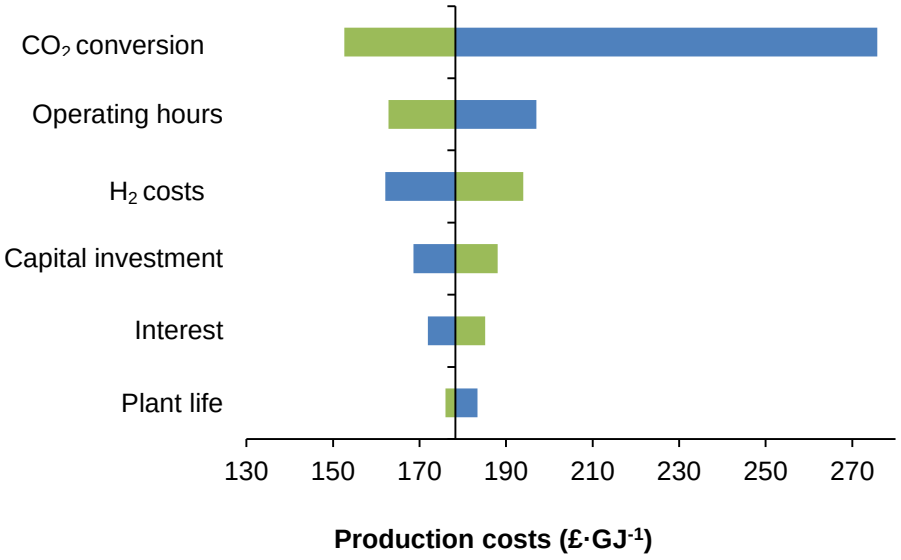

Fig. 6.15 Sensitivity of fuel production (PD-CHP1-OXY) costs to variations of selected technical and economic parameters (green bars represent an increase in the parameter)

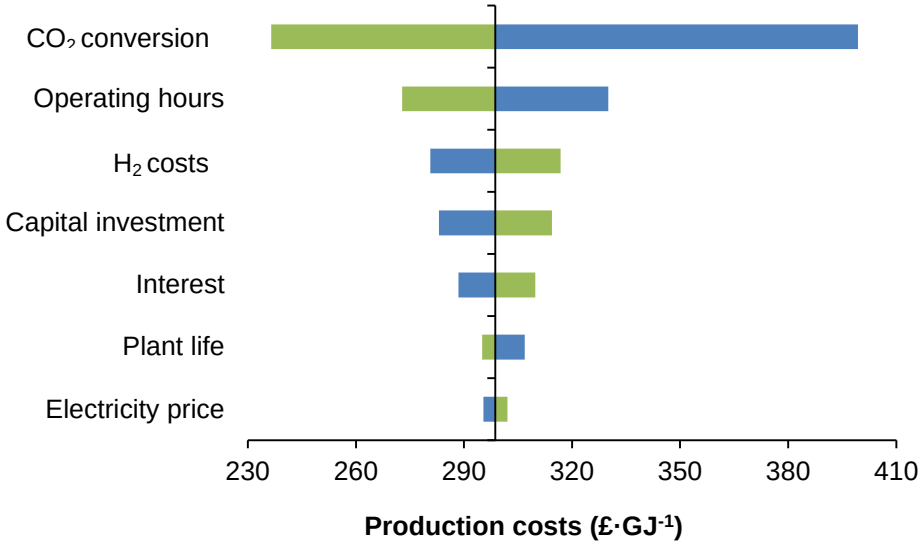

Fig. 6.16 Sensitivity of fuel production (PD-CHP2) costs to variations of selected technical and economic parameters (green bars represent an increase in the parameter)

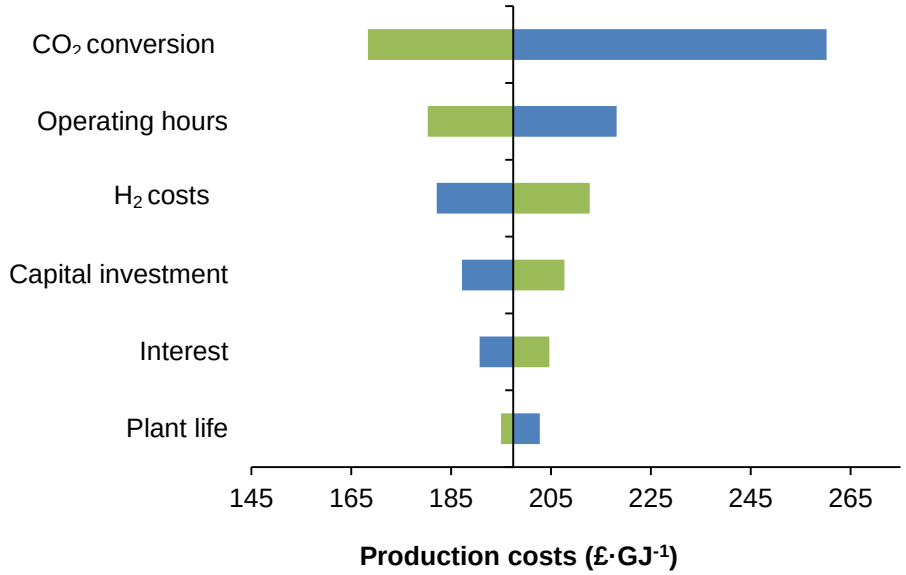

Fig. 6.17 Sensitivity of fuel production (PD-CHP2-OXY) costs to variations of selected technical and economic parameters (green bars represent an increase in the parameter)

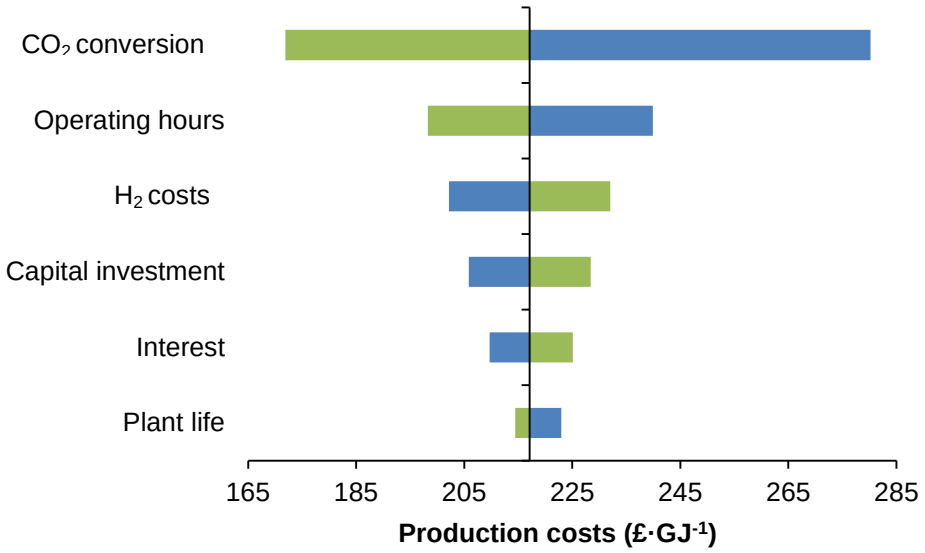

Fig. 6.18 Sensitivity of fuel production (PD-CHP1-POST) costs to variations of selected technical and economic parameters (green bars represent an increase in the parameter)

As one can see from Figs. 6.14-6.18, the results from the process incorporating a CHP plant are very similar. In all cases, the fuel production costs are most sensitive to CO_2 conversion and operating hours. In these cases, variations in the H_2 production costs has a more important effect on fuel production costs since all of the hydrogen consumed in these plants is imported (as opposed to PD-MEA1). As in PD-MEA1 and PD-MEA2, fuel production costs are somewhat less sensitive to variations in the capital investment, although this parameter is still important. The fuel production costs are less sensitive to interest rates, plant life and electricity prices. It should be noted that the sensitivity analysis of PD-CHP1-OXY, PD-CHP2-Oxy and PD-CHP1-POST do not include the electricity prices since these process designs are net exporters of electricity and thus electricity does not have to be purchased.

6.7.2 Ionic liquids

This section includes the sensitivity analysis of the CO_2 capture plants that use ionic liquids as a solvent for CO_2 capture. The effect of several important technical and economic parameters on the bio-methane production cost is considered. The parameters investigated are: absorber pressure, capital investment, plant operating hours, loan interest rate, plant lifespan, electricity price and ionic liquid cost. Fig. 6.19 shows how the absorber pressure affects the bio-methane production costs. When the absorber is operated at 20 bar, production costs decrease to £5.94·GJ^{-1}, £6.28·GJ^{-1} and £7.52·GJ^{-1} for $[P_{66614}][Tf_2N]$, $[C_6MIm][Tf_2N]$ and $[C_2MIm][Tf_2N]$, respectively; which represents a decrease between 3%-6%. If the operating pressure of the absorber is further reduced to 10 bar, productions costs of the bio-methane increase between 0.1%-10% with respect to the production costs at 20 bar. As a result, it can be concluded that, in all cases, a minimum production costs of the bio-methane is found when the absorber is operated at 20 bar. The reason for this minimum is that there is a trade-off between the higher absorption capacity of the ionic liquids at 30 bar, which reduces the amount of fluid needed, and the higher electricity consumption and equipment costs associated with operating the absorber at such high pressure. If the absorber pressure is further reduce to 10 bar the savings in electricity and equipment costs related to a high pressure operation are off-set by the dramatic increase in the ionic liquid fluid need to produce bio-methane at 95 mol. %.

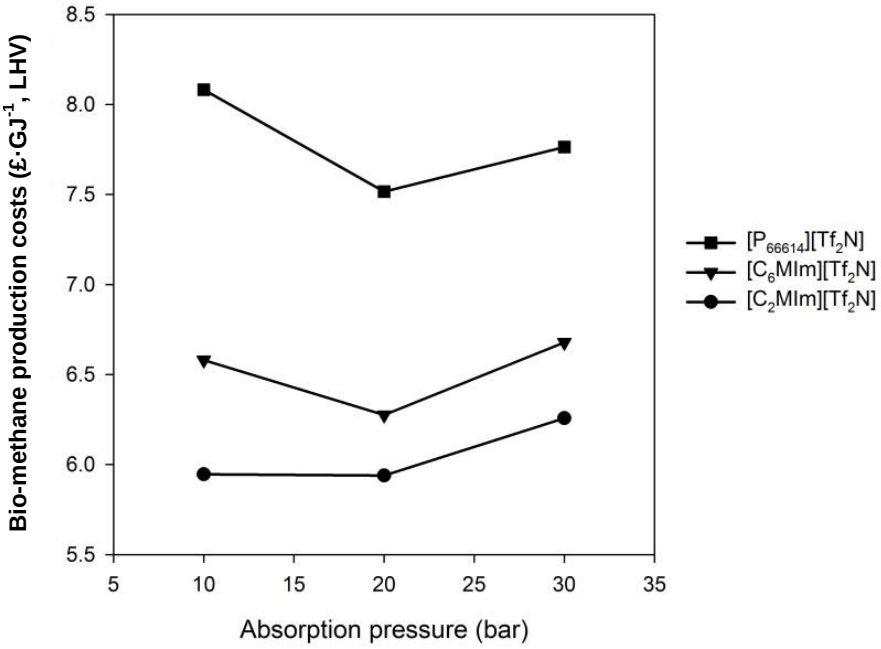

Fig. 6.19 Sensitivity of the bio-methane production costs to variations in the absorption pressure

For the other parameters, the sensitivity analysis was performed by changing each parameter at a time by ±30% of its base-case value. There is an exception with the plant operating hours which were varied by ±9.5% since the number of hours in a year (8,760 hours) cannot be exceeded. The results from the three process concepts studied are shown in Fig. 6.20, where longer bars indicate a higher degree of deviation from the base case value.

In all cases, bio-methane production costs are most sensitive to plant operating hours since variations of just ±9.5% in this parameter results in nearly identical effect than varying the capital costs by ±30%. Thus, this type of plants should be operated with the minimum periods of shutdown in order to achieve significantly lower bio-methane production costs.

Production costs are also highly sensitive to variations in the capital expenditure. A capital investment variation of ±30% results in the

production costs to vary by ±10% in all cases. This is an important result since errors of up to ±30% are common in capital investment estimates (Peters *et al.*, 2004)

The loan interest rate is the third most sensitive parameter and fluctuations of ±30% results in the production costs to vary by up to 7% in all cases; interest rates affect the annuity of the capital investment and therefore, efforts should be made at the early stages of the project development to agree a fixed rate with lender throughout the lifespan of the project so that unexpected fluctuation can be avoided. Finally, the bio-methane production costs are less sensitive to the plant life of the project, the electricity price and the ionic liquid costs. However, fluctuations in these parameters they should not be underestimated since they could affect the production costs significantly.

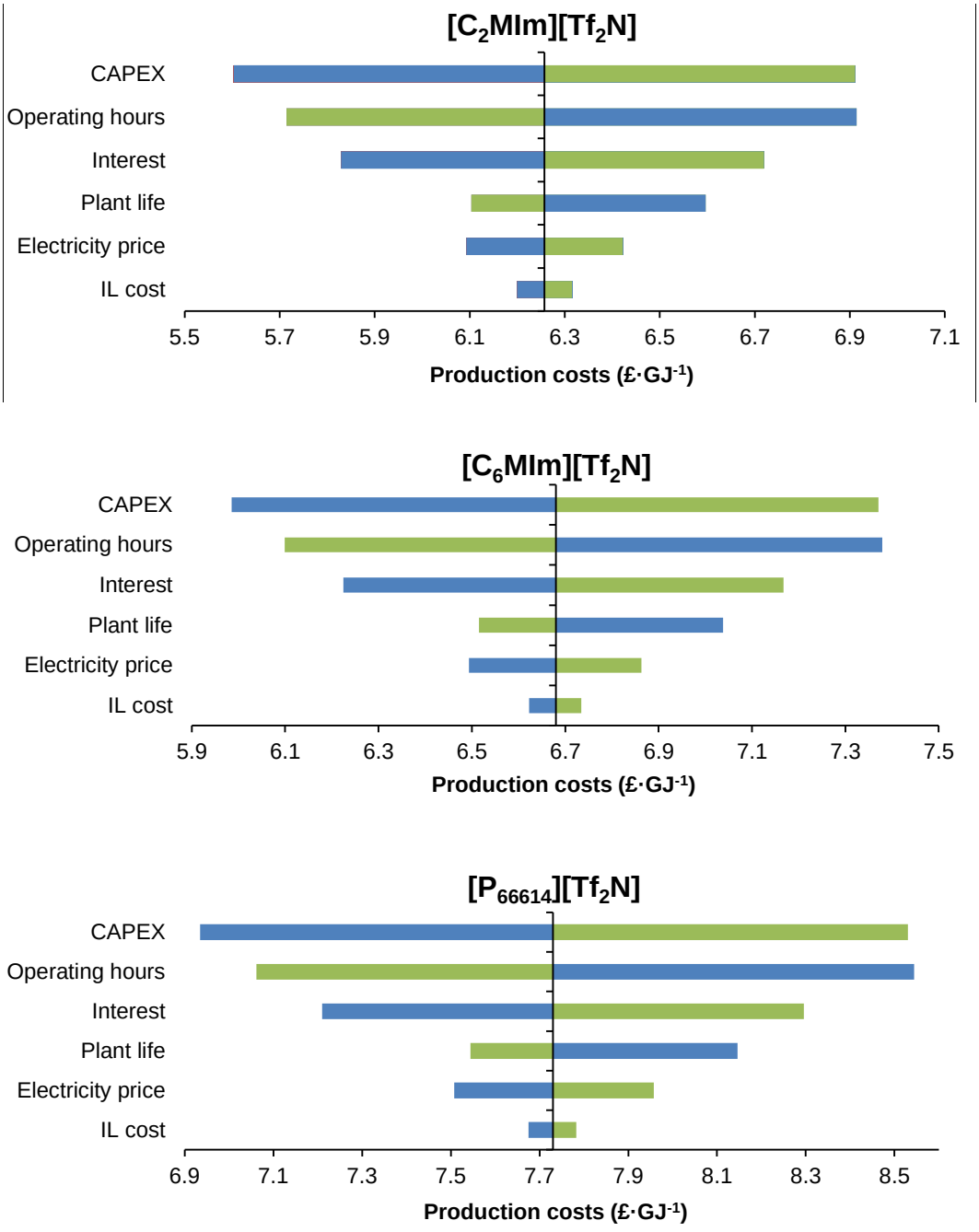

Fig. 6.20 Sensitivity of bio-methane production costs to variations of selected technical and economic parameters (all parameters are varied by ±30%, except for the plant operating hours which are varied by ±9.5%). The vertical line in the graphs represents the production cost of the base case for the different ionic liquids. Green bars represent an increase in the parameter

6.8 Closing review

In the previous chapters, several process concepts to produce a synthetic fuel from CO_2 were assessed. The process concepts evaluated in this work incorporate existing CCU technologies for the conversion of a carbon source, in this case biogas produced from the anaerobic digestion of sewage sludge. The first process configuration examined (PD-MEA1) comprises separation of CO_2 from biogas using MEA and steam reforming for conversion of methane to syngas. The second process concept (PD-MEA2) also incorporates a monoethanolamine (MEA) gas treatment unit; however PD-MEA2 does not include steam methane reforming since the upgraded bio-methane is assumed to be injected into the natural gas grid. The other five cases incorporate a CHP plant for co-generation of heat and power from biogas and the conversion of methane to CO_2. All cases include a RWGS reactor for reducing CO_2 to syngas and its subsequent conversion to fuels via Fischer-Tropsch synthesis. Aspen Plus was employed to determine the mass and energy balances that allowed the estimation of overall process efficiencies and costs. This was the first attempt to compare different routes of similar TRL to manufacture a liquid fuel from CO_2. Furthermore, the results from the mass and energy balances calculations were used by collaborators at The University of Manchester to perform cradle-to-grave sustainability assessments of the proposed CO_2-to-fuels synthetic routes.

The synthetic route based on CO_2 capture and steam methane reforming, PD-MEA1, was the most promising CO_2-to-fuels route since it was able to achieve the highest fuel production rate (831.68 kg·h-1; 7,450.47 kW [LHV]) as well as the highest overall plant energy efficiency (17.9%). This is because of the ability to produce a larger amount of syngas as a result of the steam reforming of methane. As for the processes based on a CHP plant, oxy-combustion of biogas (or upgraded bio-methane) results in considerably higher fuel production rates and plant efficiencies than their equivalent processes using air in the combustion of biogas (or upgraded

bio-methane) in the CHP plant (20% increase in fuel production rates and 46-48% increase in overall plant efficiency). Although the air separation unit (ASU) consumes large amounts of electricity to produce pure O_2 from air, this is outweighed by the reduction of gas processing needed downstream due to the absence of N_2 in the CHP flue gas, which eventually reduces the heating, cooling and compression duties.

The economic assessment of the different process designs revealed that the process concept based on CO_2 capture and steam methane reforming (PD-MEA1) results in the lowest fuel production costs of all process concepts evaluated (£95.46 per GJ [LHV]). This is the result of its lower TIC and O&M as well as its higher fuel production rate. The process designs based on a CHP result in higher TIC in all cases due to the equipment costs related to the CHP plant. O&M costs associated with PD-MEA1 are lower due to its endogenous production H_2 via steam reforming of methane as well as lower heating, cooling and compression costs since the processes based on a CHP plant have to process large amounts of inert gas. It can be concluded then that CO_2 capture coupled with steam methane reforming is the most promising option for commercial production of liquid fuels from CO_2.

The most important outcome from the economic assessment is that, at the current stage of development, synthetic fuel production from biogas via CO_2 utilisation is very far from commercial viability. At its base scale, the fuel production costs associated with the best performing route (PD-MEA1) are nearly one order of magnitude higher than those of conventional fossil fuels. Section 6.6.1.5 elaborates a discussion on the necessary improvements to advance this technology towards commercial viability. These can be summarised as follows:

- Decrease TCI by reducing the size of compressors in the steam reforming of methane and fuel synthesis area. This can be achieved by minimising the amount of inert gases as much as possible as well as reducing the compression pressure.

- Lower O&M costs by reducing the cooling, heating and compression duties.
- Reduce or eliminate the cooling requirements of the CO_2 capture plant by developing CO_2 capture solutions that allow either regeneration at temperatures below the water boiling point or solutions that can be used at 100% purity so that they do not have to be mixed with water to prevent corrosion-related problems, *e.g.* ionic liquids.
- Develop capture media with high CO_2 affinity while at the same time requiring less energy to release the absorbed CO_2.
- Increase the CO_2 conversion rate to maximize the production of syngas. The co-electrolysis of H_2O and CO_2 to produce syngas is a technology that could improve the syngas production considerably as well as increasing the plant efficiency by producing H_2 within the plant.
- Increase fuel yields and selectivity in the Fischer-Tropsch reactor
- Fig. 6.8 shows that economies of scale play a paramount role in the commercial viability of the assessed technology. In light with this, other sources of CO_2 should be considered so that much larger amounts of CO_2 can be converted into a synthetic fuel.

In this thesis, a developing technology such as CO_2 capture using ionic liquids was used in order to investigate its effect on plant efficiencies and costs. The simulation methodology developed in this study based on the COSMO-SAC property method in Aspen Plus was able to predict the ionic liquids' physical properties (heat capacity, density and viscosity) as well as the interaction between the gases (CO_2 and CH_4) with the liquids accurately, without having to reply on experimental data. This allowed for the first time simulation of biogas upgrading plants using ionic liquids as physical absorbents. The results prove that the methodology can be used for any combination of cation and anion as well as any gas species.

The results revealed that the processes using [C_2MIm][Tf_2N] and [C_6MIm][Tf_2N] were able to achieve the highest plant efficiency (82%), whereas the process based on MEA achieved 77% efficiency. These results highlight that ionic liquids can be more energetically efficient than MEA when used in biogas upgrading plants. This is due to the large energy penalty of the MEA regeneration process. The fact that [C_2MIm][Tf_2N] and [C_6MIm][Tf_2N] can be more efficient than MEA is true despite the lower absorption capacity (kg of ionic liquid needed per kg of bio-methane produced) of the processes using [C_2MIm][Tf_2N] and [C_6MIm][Tf_2N]; therefore, it becomes clear that these kind of processes must be evaluated using a "whole system" approach (simulation of actual biogas upgrading plant) rather making conclusions based solely on, for instance, solvent absorption capacity at equilibrium.

On the other hand, the bio-methane production costs associated with the process using ionic liquids are higher than those of the process using MEA. The upgrading process using [C_2MIm][Tf_2N] results in the lowest bio-methane production costs (£6.26 per GJ [LHV]), whereas the bio-methane production costs of the process using MEA were (£3.78 per GJ [LHV]), which are 40% lower. The higher bio-methane production costs of the ionic liquid-based process are due to the high unit cost of the biogas compressor as well as the large amount of electricity required to compress the biogas to 30 bar. These results encourage further research in the area specially taking into account that the ionic liquids evaluated in this work absorb the CO_2 physically as opposed to MEA, which absorbs the CO_2 mainly through chemical interactions.

7. CONCLUSIONS, RECOMMENDATIONS AND FUTURE WORK

7.1 Conclusions

In line with the main objectives highlighted in section 1.2.1, this research has measured the technical and economic performance of seven Carbon Capture and Utilisation (CCU) process designs (Base Case Models) based on best available technology. The work was carried out in order to provide the necessary data to identify the most promising routes for the conversion of Carbon Dioxide into a synthetic fuel. In addition, this thesis also examined the techno-economic feasibility of selective CO_2 capture processes from biogas streams using ionic liquids as physical absorbents. This developing technology was considered in order to assess the potential improvements that it could have on process performance, compared to MEA-based CO_2 capture.

Since this thesis considered all the process designs to be based in the UK, the conclusions and future recommendations may not be relevant to other countries. It should be also noted that, in order to model the different CO_2-to-fuels synthetic routes, extensive use of publicly available data was made. This could affect the results which are highly dependent on the accuracy of available data.

As for the Base Case Models, the main results from the process simulation are summarised below:

- The synthetic route based on CO_2 capture and steam methane reforming, PD-MEA1, was the most promising CO_2-to-fuels since it was able to achieve the highest fuel production rate (831.68 $kg \cdot h^{-1}$; 7,450.47 kW [LHV]) as well as the highest overall plant energy efficiency (17.9%).
- The synthetic route based on CO_2 capture and direct bio-methane grid injection resulted in the lowest fuel production rate (244.76 $kg \cdot h^{-1}$; 2,192.67 kW [LHV]) and the lowest overall plant energy

efficiency (6.0%). This highlights the importance of an energy-rich stream such as the bio-methane stream in the CCU plants.

- The process design based on upgraded bio-methane combustion in a CHP plant, PD-CHP2, results in the lowest fuel production rate (586.20 $kg \cdot h^{-1}$; 5,251.39 kW [LHV]) and overall plant energy efficiency of all evaluated CHP-based concepts. The process design based on direct biogas combustion in a CHP plant, PD-CHP1, results in similar results to those from PD-CHP2. It can be concluded that the extra investment in the CO_2 capture plant is not justified from an efficiency point of view.
- PD-CHP1-OXY and PD-CHP2-OXY, which employ oxygen, result in considerably higher fuel production rates and plant efficiencies than their equivalent processes using air in the combustion of biogas (or upgraded bio-methane) in the CHP plant (20% increase in fuel production rates and 46-48% increase in overall plant efficiency).
- The process incorporating a post-combustion CO_2 capture plant, PD-CHP1-POST results in higher fuel production rate and overall plant efficiency than the equivalent concept based on pre-combustion CO_2 capture (10% increase in fuel production rate and 32% increase in overall plant efficiency).

The results from the economic assessment of the Base Case Models showed the following:

- The process concept that results in the lowest Total Capital Investment (TIC) is PD-MEA2 (£21.05 million). The process concept that involves the highest TIC is PD-CHP2 (£61.07 million). In all cases, the designs employing a CHP plant resulted in higher TIC than the ones that did not employ CHP.
- The CHP plant is a major contributor towards the Delivered Equipment Cost (DEC) ranging 40-59%. The fuel synthesis area is also a major contributor to the TIC with a share 22-48%. In the

process considering steam methane reforming (PD-MEA1), the steam methane reformer represents 37% of the TIC.

- Similarly to the TIC, the designs employing a CHP plant results in higher Operating and Maintenance (O&M) costs mainly due to the hydrogen imports as these processes do not produce hydrogen within the plant, as PD-MEA1 does.
- The process concept that results in the lowest Operating and Maintenance (O&M) costs is PD-MEA2 (£13.02 million). The process concept that involves the highest O&M is PD-CHP2 (£33.87 million).
- The cost of H_2 is a major contributor to the O&M costs since it represents 4-36% of all O&M costs. Cooling costs also contribute significantly to the O&M with share of 20-38% of all O&M costs.
- The process concept based on CO_2 capture and steam methane reforming (PD-MEA1) results in the lowest fuel production costs of all process concepts evaluated (£95.46 per GJ [LHV]). This is the result of its lower TIC and O&M as well as its higher fuel production rate. The rest of the process concepts result in higher production costs by 87-192%. It can be concluded then that CO_2 capture coupled with steam methane reforming is the most promising option for commercial production of liquid fuels from CO_2.
- A scaling up study of PD-MEA1 was carried out so that eighteen plant capacities were evaluated, ranging from 18.3 tonne·day^{-1} (base case) to 1,670 tonnes of liquid fuels produced per day. The latter capacity corresponds to the Shell Middle Distillate Synthesis (SMDS) Gas-to-Liquids (GTL) plant built in Bintulu (Malaysia). It was found that The TCI of the scaled-up CCU plant is 51% lower than those of the Shell plant (£831 million), although the capital costs of the water electrolysis plant and the ASU of the CCU plant are not included in the TCI. The O&M costs of the CCU plant are approximately 6 times higher than those of the Shell plant.

- The scaling up study also revealed that for the largest plant capacity (1,670 $t \cdot day^{-1}$), the fuel production costs are approximately 6 times lower than for the PD-MEA1 base case (£15.67·GJ^{-1} vs £95.46·GJ^{-1}). At the base case, even the best performing process concept (PD-MEA1) is very far from being economically competitive. This highlights the importance of economies of scale in process such as the ones evaluated in this study.
- In a LHV basis, the gate costs of gasoline and diesel were £14.3·GJ^{-1} and £14.6·GJ^{-1}, which are 7% and 9% lower than those of the scaled up CCU plant, respectively. However, the impracticality of building such a large AD plant is a crucial drawback towards commercial implementation of this technology using biogas produced from the anaerobic digestion of sewage sludge.
- The sensitivity analysis revealed that, in all cases, the fuel production costs are most sensitive to CO_2 conversion and operating hours; therefore efforts should be made towards increasing CO_2 conversion rates and operating the plants with a downtime as lowest as possible.

With crude oil prices falling continuously, the CCU fuel synthesis processes proposed in this study will become less financially attractive; thus, it is anticipated that increases in fossil fuel prices, governmental subsidies or environmental legislation such as carbon taxes will be needed in order to make CCU fuels competitive in the market.

In addition to the Base Case Models, a simulation methodology was developed in order to model three ionic liquid-based CO_2 capture processes. It consists of a novel modelling approach, which produces data hitherto not calculable without experimental data, *e.g.* plant efficiencies, capital costs, operating and maintenance costs, *etc*. The methodology was based on the COSMO-SAC property method in Aspen Plus, which

provides relevant information on gas-liquid interaction without having to rely on experimental data.

As for the ionic liquid-based CO_2 capture processes, the main results from the process simulation are summarised below:

- The capture process using $[C_2MIm][Tf_2N]$ ionic liquid resulted in the highest bio-methane production rate (1522.14 $kg \cdot h^{-1}$), followed by 1454.91 $kg \cdot h^{-1}$ produced by the second concept (based on $[C_6MIm][Tf_2N]$ ionic liquid) and 1263.60 $kg \cdot h^{-1}$ produced by the third concept (based on $[P_{66614}][Tf_2N]$ ionic liquid). The process based on MEA produced 1,645.3 $kg \cdot h^{-1}$.
- As for the plant energy efficiency, the processes using $[C_2MIm][Tf_2N]$ and $[C_6MIm][Tf_2N]$ respectively, were able to achieve the highest value (82%). The process using $[P_{66614}][Tf_2N]$ resulted in 71% plant energy efficiency. The process based on MEA achieved 77% efficiency.
- The process based on $[C_2MIm][Tf_2N]$ resulted in the lowest TIC (£9.878 million), followed by $[C_6MIm][Tf_2N]$ (£10.004 million) and $[P_{66614}][Tf_2N]$ (£9.988 million).
- As for the O&M costs, the process using $[C_2MIm][Tf_2N]$ resulted in £2.169 million, followed by $[C_6MIm][Tf_2N]$ (£2.222 million) and $[P_{66614}][Tf_2N]$ (£2.256 million).
- The process using $[C_2MIm][Tf_2N]$ results in the lowest bio-methane production costs (£6.26 per GJ [LHV]) as a result of its lowest TCI and O&M as well as its higher bio-methane production. The bio-methane production costs of the process using MEA were (£3.78 per GJ [LHV]), which are 40% lower than those of $[C_2MIm][Tf_2N]$.
- The sensitivity analysis revealed that the ionic liquid-based CO_2 capture plants are best operated at an intermediate pressure of 20 bar, since this results in the lowest bio-methane production costs. The sensitivity analysis also demonstrated that production costs are

most sensitive to the operating hours, capital expenditure and interest rate.

The presented results show that the simulation methodology developed in this study is a robust tool for predicting plant efficiencies and production costs of large scale CO_2 capture processes using ionic liquids without relying on gas solubility experimental data.

7.2 Recommendations for future work

The areas that are recommended for further work on this topic are as follows:

- Only biogas from the anaerobic digestion of sewage sludge has been considered in this thesis as the feedstock for synthetic fuel production. Other CO_2-rich streams with industrial importance could be investigated, *e.g.* flue gas from power plants, refineries, cement plants, *etc.* These stationary sources of CO_2 guarantee a much larger scale in terms of CO_2 converted to synthetic fuels, which is, as stated before in this thesis, of paramount importance if serious efforts are to be made towards commercial implementation of the technologies assessed in this study.
- The main product of the CCU plants evaluated in this research was FT-syncrude, which was assessed in terms of its LHV. An upgrading plant could be modelled in future work so that gasoline and diesel are the main products of the plants.
- In addition to the FT-syncrude, future work in the field could consider alternative CCU fuels such as methanol or formic acid.
- Sensitivity analyses were carried out in order to assess how variations in certain process and economic parameters affect production costs. This is important at the current early stage of

development of CO_2-to-fuels systems, where accurate assumptions are difficult to make. One step further could consist of performing Monte Carlo simulations so that probability distributions of the synthetic fuel production costs are generated.

- Fischer-Tropsch synthesis was the only fuel synthesis technology evaluated in this thesis, as it is a well-developed and mature technology. Other fuel synthesis technologies such as the Methanol to Gasoline (MTG) synthesis or the Topsoe Integrated Gasoline (TIGAS) synthesis could be assessed in the CCU plants.
- Since the feedstock for the CCU plant was biogas in all cases, Dry Methane reforming (DMR) is a technology that could be evaluated and modelled. However, It should be noted that the biogas production from the anaerobic digestion of sewage sludge is an industry of small scale, which could be a hindrance towards economic viability. DMR was not included in the Base Case Models since it is not a mature and proven technology.
- Ionic liquids that absorb CO_2 physically were considered in this study. Due to time and resources constraints, ionic liquids that absorb CO_2 mainly by chemical interactions could not be modelled. Ongoing collaboration between The University of Sheffield and QUB will aim to model CO_2 capture process using chemically absorbing ionic liquids. The modelling methodology will not require experimental data and these will only be required for model validation.

This thesis has evaluated different process designs, which convert biogas into a synthetic liquid fuel. The results showed that the CCU fuel synthesis processes are unlike to compete commercially with conventional fuels, mainly primarily due to the: low CO_2 conversion and high hydrogen consumption in the RWGS process, low selectivity of the Fischer–Tropsch synthesis and high MEA regeneration costs in the capture plant. This highlights the need for new CCU technologies, such as superbasic ionic

liquids for CO_2 capture, co-electrolysis of CO_2 and water to produce syngas or advanced FT processes. These technologies are currently being researched under the 4CU Project. The recommendation for future work is that they are considered in the process designs of this thesis to test the potential improvement that they could have on process performance and costs.

REFRENCES

4CU Project. (2012). A Coordinated, Comprehensive approach to Carbon Capture and Utilisation. Retrieved on 12th February 2014 from: http://4cu.org.uk/

Aaron, G. (2012). District Heating - Heat Metering Cost Benefit Analysis. Retrieved on 21st July 2016 from: https://www.gov.uk/government/uploads/system/uploads/attachment_data/file/48389/5462-district-heating--heat-metering-cost-benefit-anal.pdf

Abu-zahra, M.R.M., Feron, P.H.M. and Versteeg, G.F. (2007). CO_2 capture from power plants Part I. A parametric study of the technical performance based on monoethanolamine. *International Journal of Greenhouse Gas Control*, 1, 37–46.

ADE. (2015). What is Combined Heat and Power? Retrieved on 19th October 2015 from http://www.theade.co.uk/what-is-combined-heat-and-power_15.html

Ahlrichs, R., Bär, M., Häser, M., Horn, H. and Kölmel, C. (1989). Electronic structure calculations on workstation computers: The program system turbomole. *Chemical Physics Letters*, 162 (3), 165–169.

Allum, K.G. and Williams, A.R. (1988). Operation of the World's First Gas-to-Gasoline Plant. *Studies in Surface Science and Catalysis*, 36, 691-711.

AMEC. (2007). Techno-Economic Evaluation of Emerging Biodiesel Production Technologies. NNFCC Project NFC 07/009, London, UK.

Aneke, M. and Wang, M. (2015). Potential for improving the energy efficiency of cryogenic air separation unit (ASU) using binary heat recovery cycles. *Applied Thermal Engineering*, 81, 223–231.

Anthony, J.L., Anderson, J.L., Maginn, E.J. and Brennecke, J.F. (2005). Anion effects on gas solubility in ionic liquids. *The journal of physical chemistry. B*, 109 (13), 6366–74.

Appels, L., Lauwers, J., Degrève, J., Helsen, L., Lievens, B., Willems, K., Van Impe, J. and Dewil, R. (2011). Anaerobic digestion in global bio-energy production: Potential and research challenges. *Renewable and Sustainable Energy Reviews*, 15 (9), 4295–4301.

Armstrong, K. (2015). Emerging Industrial Applications. In: Styring, P., Quadrelli, E.A. and Armstrong, K. (eds). *Carbon Dioxide Utilisation: closing the carbon*

cycle. Oxford, UK: Elsevier B.V., 237–251.

Aspen Technology. (2000). Aspen Plus User Guide. Burlington, USA.

Aspen Technology. (2012a). Aspen Plus Cogeneration Model. Burlington, USA.

Aspen Technology. (2012b). Aspen Process Economic Analyzer - User Guide. Burlington, USA.

Aspen Technology. (2012c). Rate-based model of the CO_2 Capture Process by MEA using AspenPlus. Burlington, USA.

Aspen Technology. (2013a). Aspen Energy Analyzer - User Guide. Burlington, USA.

Aspen Technology. (2013b). Aspen Physical Property System - Physical Property Models. Burlington, USA.

Aspen Technology. (2013c). Aspen Plus Process Simulator - AspenTech. Retrieved on 2nd February 2013 from: http://www.aspentech.com/products/aspen-plus.aspx

Aspen Technology. (2013d). Aspen Plus Version 8.4. Burlington, USA

Aydin, G., Karakurt, I. and Aydiner, K. (2010). Evaluation of geologic storage options of CO_2: Applicability, cost, storage capacity and safety. *Energy Policy*, 38 (9), 5072–5080.

Bank of England. (2014). Bank of England inflation calculator. Retrieved on 1st December 2015 from: http://www.bankofengland.co.uk/education/Pages/resources/inflationtools/calculator/flash/default.aspx

Basha, O.M., Heintz, Y.J., Keller, M.J., Luebke, D.R., Resnik, K.P. and Morsi, B.I. (2014). Development of a Conceptual Process for Selective Capture of CO_2 from Fuel Gas Streams Using Two TEGO Ionic Liquids as Physical Solvents. *Industrial & Engineering Chemistry Research*, 53 (8), 3184–3195.

Basha, O.M., Keller, M.J., Luebke, D.R., Resnik, K.P., Morsi, B.I. (2013). Development of a Conceptual Process for Selective CO_2 Capture from Fuel Gas Streams Using [hmim][Tf_2N] Ionic Liquid as a Physical Solvent. *Energy&Fuels*, 27 (7), 3905–3917.

Bayer MaterialScience. (2012). Use of carbon dioxide for the production of plastics. Retrieved on 6th January 2016 from: http://www.ikem.se/MediaBinaryLoader.axd?MediaArchive_FileID=2294fc8b-2f21-4833-b07e-18fbc088efb7&FileName=CO2-Projekte_kurz_EN.pdf

Bechtel. (1998). Aspen process flowsheet simulation model of a battelle biomass-based gasification, Fischer-Tropsch liquefaction and combined-cycle power plant, Contract No.: DE-AC22-93PC91029. Pittsburgh, PA.

Becker, W.L., Braun, R.J., Penev, M. and Melaina, M. (2012). Production of Fischer-Tropsch liquid fuels from high temperature solid oxide co-electrolysis units. *Energy*, 47 (1), 99–115.

Bergman, P.C.A., Boersma, A.R., Kiel, J.H.A., Prins, M.J., Ptasinski, K.J., and Janssen, F.J.J.G. (2005). Torrefaction for entrained-flow gasification of biomass. Report ECN-C--05-067, Energy Research Centre of the Netherlands.

Bhandari, R., Trudewind, C.A. and Zapp, P. (2014). Life cycle assessment of hydrogen production via electrolysis – a review. *Journal of Cleaner Production*, 85,151–163.

Billet, R. and Schultes, M. (1993). Predicting mass transfer in packed columns. *Chemical Engineering & Technology*, 16 (1),1–9.

Blokhin, A. V., Paulechka, Y.U. and Kabo, G.J. (2006). Thermodynamic Properties of $[C_6mim][NTf_2]$ in the Condensed State. *Journal of Chemical & Engineering Data*, 51 (4), 1377–1388.

Brennecke, J.F. and Gurkan, B.E. (2010). Ionic Liquids for CO_2 Capture and Emission Reduction. *The Journal of Physical Chemistry Letters*, 1 (24), 3459–3464.

British Petroleum. (2014). BP 2035 Energy Outlook. Retrieved on 10th February 2014 from: http://www.bp.com/content/dam/bp/pdf/Energy-economics/Energy-Outlook/Energy_Outlook_2035_booklet.pdf

Britt, H. and Luecke, R. (1973). The Estimation of Parameters in a Non-linear, Implicit Model. *Technometrics*, 15 (2), 233–247.

Cadena, C., Anthony, J.L., Shah, J.K., Morrow, T.I., Brennecke, J.F, Maginn, E.J. (2004). Why Is CO_2 so soluble in imidazolium-based ionic liquids? *Journal of the American Chemical Society*, 126 (16), 5300–8.

Carvalho, P.J., Álvarez, V.H., Marrucho, I.M., Aznar, M., Coutinho, J.A.P. (2010). High carbon dioxide solubilities in trihexyltetradecylphosphonium-based ionic liquids. *The Journal of Supercritical Fluids*, 52 (3), 258–265.

Carvalho, P.J., Álvarez, V.H., Machado, J.J.B., Pauly, J., Daridon, J.-L., Marrucho, I.M., Aznar, M., Coutinho, J.A.P. (2009). High pressure phase behavior of carbon dioxide in 1-alkyl-3-methylimidazolium bis(trifluoromethylsulfonyl)imide ionic liquids. *The Journal of Supercritical Fluids*, 48 (2), 99–107.

Centi, G. and Perathoner, S. (2009). Opportunities and prospects in the chemical recycling of carbon dioxide to fuels. *Catalysis Today*, 148, 191–205.

Chemical Engineering. (2015). POLYMER PRODUCED FROM CO_2 WASTE GAS MAKES COMMERCIAL DEBUT. Retrieved on 11th February 2015 from: http://www.chemengonline.com/polymer-produced-co2-waste-gas-makes-commercial-debut/

COSMOlogic. (2015). COSMOtherm: Predicting Solutions since 1999. Retrieved on 2nd July 2015 from: http://www.cosmologic.de/products/cosmotherm.html

Coulson, J.M, Richardson, J.F., Backhurst, J.R and Harker,J.H. (1995). *Coulson and Richardson's Chemical Engineering: Fluid Flow, Heat Transfer and Mass Transfer v. 1* 5th ed., Oxford, UK: Butterworth-Heinemann Ltd.

CRI. (2012). Carbon Recycling International. Retrieved on 11th February 2014 from: http://www.carbonrecycling.is/index.php?option=com_content&view=article&id=6&Itemid=19&lang=en

Cuéllar-Franca, R., Dimitriou, I., García-Gutiérrez, P., Elder, R.H., Allen, R.W.K., Azapagic, A. (2015). Carbon Capture and Utilisation: Application of Life Cycle Thinking to Process Design. In *12th International Symposium on Process Systems Engineering and 25th European Symposium on Computer Aided Process Engineering*, Elsevier, 1457–1462.

Darrow, K., Tidball, R., Wang, J. and Hampson, A. (2015). EPA Combined heat and Power Partnership - Catalog of CHP technologies. Retrieved on 28th June 2016 from: https://www.epa.gov/sites/production/files/2015-07/documents/catalog_of_chp_technologies.pdf

DECC. (2014a). Non-Domestic Energy prices. Retrieved on 1st December 2015 from: https://www.gov.uk/government/statistical-data-sets/gas-and-electricity-prices-in-the-non-domestic-sector

DECC. (2014b). RHI Biomethane Injection to Grid Tariff Review. Retrieved on 9th June 2015 from: https://www.gov.uk/government/uploads/system/uploads/attachment_data/file/315608/Biomethane_Review_Final_-_FOR_PUBLICATION.pdf

De Klerk, A., Li, Y.W. and Zennaro, R. (2013). *Greener Fischer–Tropsch Processes for Fuels and Feedstocks.* 1st ed. Maitlis, P.M. and De Klerk, A. (eds.) John Wiley & Sons, Inc.

Dimitriou, I. (2012). Techno-economic assessment and uncertainty analysis of thermochemical processes for second generation transport biofuels. PhD thesis, Aston University.

Dimitriou, I. and Bridgwater, A.V. (2010). Syngas Production for Biomass-to-Liquids (BTL) Applications. Process Analysis and Optimisation. In *Proceedings of the BioTen Conference on Biomass, Bioenergy, Biofuels and Biorefineries*. Birmingham, UK, 244–252.

Dimitriou, I., García-Gutiérrez, P., Elder, R.H., Cuéllar-Franca, R.M., Azapagic, A., Allen, R.W.K. (2015). Carbon dioxide utilisation for production of transport fuels: process and economic analysis. *Energy Environ. Sci.*, 8 (6), 1775–1789.

Dry, M.E. (2002). High quality diesel via the Fischer-Tropsch process - a review. *Journal of Chemical Technology & Biotechnology*, 77 (1), 43–50.

Ebbesen, S.D., Høgh, J., Nielsen, K.A., Nielsen, J.U., Mogensen, M. (2011). Durable SOC stacks for production of hydrogen and synthesis gas by high temperature electrolysis. *International Journal of Hydrogen Energy*, 36 (13), 7363–7373.

Ebbesen, S.D., Knibbe, R. and Mogensen, M. (2012). Co-Electrolysis of Steam and Carbon Dioxide in Solid Oxide Cells. *Journal of the Electrochemical Society*, 159 (8), F482–F489.

Ebrahim, M. and Kawari, A. (2000). Pinch technology: an efficient tool for chemical-plant energy and capital-cost saving. *Applied Energy*, 65 (1-4), 45–49.

Edwards, R., Larivé, J.F., Rickeard, D. and Weindorf, W. (2013). Well-to-wheels

analysis of future automotive fuels and powertrains in the European context; Report Version 4.0, JRC Technical Reports, Italy.

Eilers, J., Posthuma, S.A. and Sie, S.T. (1991). The shell middle distillate synthesis process (SMDS). *Catalysis Letters*, 7 (1-4), 253–269.

Eisinger, R.S. and Keller, G.E. (2014). Process for CO_2 Capture Using Ionic Liquid That Exhibits Phase Change. *Energy & Fuels*, 28 (11), 7070–7078.

Elder, R., Cumming, D. and Mogensen, M.B. (2015). High Temperature Electrolysis. In: Styring, P., Quadrelli, E.A. and Armstrong, K. (eds). *Carbon Dioxide Utilisation: closing the carbon cycle*. Oxford, UK: Elsevier B.V. 183–209.

EPA. (2011). *Opportunities for Combined Heat and Power at Wastewater Treatment Facilities: Market Analysis and Lessons from the Field*. Retrieved on 28th August 2015 from: http://www.epa.gov/sites/production/files/2015-07/documents/opportunities_for_combined_heat_and_power_at_wastewater_treatment_facilities_market_analysis_and_lessons_from_the_field.pdf

EPSRC. (2012). A Coordinated, Comprehensive approach to Carbon Capture and Utilisation - Programme Grant. Retrieved on 21st June 2013 from: http://gow.epsrc.ac.uk/NGBOViewGrant.aspx?GrantRef=EP/K001329/1

European Academies Science Advisory Council. (2013). Carbon capture and storage in Europe. ISBN: 978-3-8047-3180-6

Ferreira, A.G.M., Simões, P.N., Ferreira, A.F., Fonseca, M.A., Oliveira, M.S.A. and Trino, A.S.M. (2013). Transport and thermal properties of quaternary phosphonium ionic liquids and IoNanofluids. *The Journal of Chemical Thermodynamics*, 64, 80–92.

Figueroa, J.D., Fout, T., Plasynski, S., McIlvried, H.and Srivastava, R. D. (2008). Advances in CO_2 capture technology: The U.S. Department of Energy's Carbon Sequestration Program. *International Journal of Greenhouse Gas Control*, 2 (1), 9–20.

Fleisch, T.H., Sills, R.A. and Briscoe, M.D. (2002). Emergence of the gas-to-liquids industry: a review of global GTL developments. *Journal of Natural Gas Chemistry*, 11, 1–14.

Forster, P., Ramaswamy, V., Artaxo, P., Berntsen, T., Betts, R., Fahey, D.W.,

Haywood, J., Lean, J., Lowe, D.C., Myhre, G., Nganga, J., Raga, R.P.G., Schulz, M. and Van Dorland, R. (2007). Changes in Atmospheric Constituents and in Radiative Forcing. In: Solomon, S., Qin, D., Manning, M., Chen, Z., Marquis, M., Averyt, K.B., Tignor, M. and Miller, H.L. (eds) *Climate Change 2007: The Physical Science Basis. Contribution of Working Group I to the Fourth Assessment Report of the Intergovernmental Panel on Climate Change*. Cambridge University Press, Cambridge, United Kingdom and New York, NY, USA. 129-234

France, L.F. Edwards, P.P., Kuznetsov, V.L., Almegren, H. (2015). The Indirect and Direct Conversion of CO_2 into Higher Carbon Fuels. In: Styring, P., Quadrelli, E.A. and Armstrong, K. (eds) *Carbon Dioxide Utilisation: closing the carbon cycle*. Oxford, UK: Elsevier B.V.161–182.

Fu, Q., Mabilat, C., Zahid, M., Brisse, A. and Gautier, L. (2010). Syngas production via high-temperature steam/CO_2 co-electrolysis: an economic assessment. *Energy & Environmental Science*, 3 (10), 1382-1397.

Gadikota, G. and Park, A.A. (2015). Accelerated Carbonation of Ca- and Mg-Bearing Minerals and Industrial Wastes Using CO_2. In Styring, P., Quadrelli, E.A. and Armstrong, K. (eds) *Carbon Dioxide Utilisation: closing the carbon cycle*. Oxford, UK: Elsevier B.V. 115–137.

Gale, J., Herzog, H., Braitsch, J., Blomen, E., Hendriks, C., and Neele, F. (2009). Capture technologies: Improvements and promising developments. *Energy Procedia*, *1*(1), 1505–1512.

Graves, C., Ebbesen, S.D. and Mogensen, M. (2011). Co-electrolysis of CO_2 and H_2O in solid oxide cells: Performance and durability. *Solid State Ionics*, 192 (1), 398–403

Gray, D.M.D., Suto, P. and Peck, C. (2008). Anaerobic Digestion of Food Waste, Funding Opportunity No. EPA-R9-WST-06-004, Final Report.

Ha, K.-S., Bae, J.W., Woo, K.-J., Jun and K.-W. (2010). Efficient utilization of greenhouse gas in a gas-to-liquids process combined with carbon dioxide reforming of methane. *Environmental science & technology*, 44 (4), 1412–7.

Hagen, M., Polman, E., Myken, A., Jensen, J., Jönsson, O. and Dahl, A. (2001). Adding gas from biomass to the gas grid, Contract No: XVII/4.1030/Z/99-412, Final Report. Malmö, Sweden.

Halmann, M. and Steinfeld, A. (2006). Thermoneutral tri-reforming of flue gases from coal- and gas-fired power stations. *Catalysis Today*, 115 (1-4), 170–178

Hamelinck, C., Faaij, A., Denuil, H. and Boerrigter, H. (2004). Production of FT transportation fuels from biomass; technical options, process analysis and optimisation, and development potential. *Energy*, 29 (11), 1743–1771.

Hanlon, P.C. (2001). *Compressor Handbook*, New York: McGraw-Hill.

Haro, P., Ollero, P., Villanueva Perales, A.L. and Gómez-Barea, A. (2013). Thermochemical biorefinery based on dimethyl ether as intermediate: Technoeconomic assessment. *Applied Energy*, 102, 950–961.

Herzog, H., Braitsch, J., Blomen, E., Hendriks, C. and Neele, F. (2009). Capture technologies: Improvements and promising developments. *Energy Procedia*, 1 (1), 1505–1512.

Hu, B., Guild, C. and Suib, S.L. (2013). Thermal, electrochemical, and photochemical conversion of CO_2 to fuels and value-added products. *Journal of CO_2 Utilization*, 1, 18–27.

Hunt, A.J., Sin, E.H.K., Marriott, R. and Clark, J.H. (2010). Generation, Capture and Utilization of Industrial Carbon Dioxide. *ChemSusChem*, 3, 306–322.

International Energy Agency. (2008). Energy Technology Perspectives 2008: Scenarios and strategies to 2050, Paris, France: OECD/IEA.

IPHE, 2011. Renewable Hydrogen Report. Retrieved on 28th September 2015 from: http://www.iphe.net/docs/Renewable_H2_Rpt_040411.pdf

IUPAC, 2014. Standard conditions for gases. Retrieved on 20th May 2015 from: http://goldbook.iupac.org/S05910.html.

Jacquemin, J., Husson, P., Majer, V. and Costa Gomes, M.F. (2007). Influence of the Cation on the Solubility of CO_2 and H_2 in Ionic Liquids Based on the Bis(trifluoromethylsulfonyl)imide Anion. *Journal of Solution Chemistry*, 36 (8), 967–979.

Jager, B. and Espinoza, R. (1995). Advances in low temperature Fischer-Tropsch synthesis. *Catalysis Today*, 23 (1), 17–28.

Jaramillo, P., Griffin, W.M. and McCoy, S.T. (2009). Life cycle inventory of CO_2 in an enhanced oil recovery system. *Environmental science & technology*, 43 (21),

8027–32.

Jiang, Z., Xiao, T., Kuznetsov, V. L. and Edwards, P. P. (2010). Turning carbon dioxide into fuel. *Philosophical Transactions of the Royal Society A*, 368, 3343–3364.

Kaneko, T., Derbyshire, F., Makino, E., Gray, D., Tamura, M., Li, K. (2000). *Ullmann's Encyclopedia of Industrial Chemistry*, Wiley-VCH Verlag GmbH & Co. KGaA.

Kanniche, M., Gros-Bonnivard, R., Jaud, P., Valle-Marcos, J., Amann, J.-M. and Bouallou, C. (2010). Pre-combustion, post-combustion and oxy-combustion in thermal power plant for CO_2 capture. *Applied Thermal Engineering*, 30 (1), 53–62.

Kittel, J., Idem, R., Gelowitz, D., Tontiwachwuthikul, P., Parrain, G. and Bonneau, A. (2009). Corrosion in MEA units for CO_2 capture: Pilot plant studies. *Energy Procedia*, 1(1), 791–797.

Kumełan, J., Pérez-Salado Kamps, Á., Tuma, D. and Maurer, G. (2007). Solubility of the Single Gases Methane and Xenon in the Ionic Liquid [hmim][Tf_2N]. *Industrial & Engineering Chemistry Research*, 46(24), 8236–8240.

Laguna-Bercero, M.A. (2012). Recent advances in high temperature electrolysis using solid oxide fuel cells: A review. *Journal of Power Sources*, 203, 4–16.

Lako, P. (2010). IEA Energy technology Network - Combined Heat and Power. retrieved on 28th June 2016 from: http://www.iea-etsap.org/web/e-techds/pdf/e04-chp-gs-gct_adfinal.pdf

Lau, F.S., Zabransky, R., Bowen, D.A., Kinoshita, C.M., Turn, S.Q., Hughes, E.E. (2002). Techno-Economic Analysis of Hydrogen Production by Gasification of Biomass. In *U.S. DoE Hydrogen Program Review*. NREL/CP-610-32405. Golden, CO.

Lauer, M. (2009). Economics and methodology of guideline for techno-economic assessment (TEA). In: Bridgwater, A.V., Hofbauer, H., van Loo, S., (eds.)*Thermal Biomass Conversion*. CPL Press, 355-371.

LeBlanc, J.R., Schneider, R.V. and Strait, R.B. (1994). Production of Methanol. In Cheng, W.H. and Kung, H.H. (eds.) *Methanol production and use*. New York: Marcel Dekker.

Lee, B. and Lin, S. (2015). Screening of ionic liquids for CO_2 capture using the COSMO-SAC model. *Chemical Engineering Science*, 121, 157–168.

Lei, Z., Dai, C. and Chen, B. (2014). Gas solubility in ionic liquids. *Chemical Reviews*, 114, 1289–1326.

Linde. (2014). Hydrogen Recovery by Pressure Swing Adsorption. Retrieved on 22nd March 2015 from: http://www.linde-engineering.com/internet.global.lindeengineering.global/en/images/HA_H_1_1_e_12_150dpi19_6130.pdf

Liu, X., Afzal, W. and Prausnitz, J.M. (2013). Solubilities of small hydrocarbons in tetrabutylphosphonium bis(2,4,4-trimethylpentyl) phosphinate and in 1-ethyl-3-methylimidazolium bis(trifluoromethylsulfonyl)imide. *Industrial and Engineering Chemistry Research*, 52, 14975–14978.

Maiden, C.J. (1988). The New Zealand Gas-to-Gasoline Project. *Studies in Surface Science and Catalysis*, 36, 1-16.

Manan, N.A., Hardacre, C., Jacquemin, J., Rooney, D.W. and Youngs, T.G.A. (2009). Evaluation of Gas Solubility Prediction in Ionic Liquids using COSMOthermX. *Journal of Chemical & Engineering Data*, 54 (7), 2005–2022.

Mantra Energy. (2014). Process overview. Retrieved on 4th April 2015 from: http://mantraenergy.com/mantra-energy/technology/overview/

Methanex Corporation. (2013). Methanex and carbon recycling international sign landmark investment agreement for advanced renewable fuel production. Retrieved on 5th May 2015 from: https://www.methanex.com/news/methanex-and-carbon-recycling-international-sign-landmark-investment-agreement-advanced

Mikkelsen, M., Jørgensen, M. and Krebs, F.C. (2010). The teraton challenge. A review of fixation and transformation of carbon dioxide. *Energy & Environmental Science*, 3, 43–81.

Muradov, N.Z. (2009). Production of Hydrogen from Hydrocarbons. In: Gupta, R.M. (ed) *HYDROGEN FUEL - Production, transport and storage*, Boca Raton, FL: Taylor & Francis Group. 33-101.

NETL. (2012). COMMERCIAL TECHNOLOGIES FOR OXYGEN PRODUCTION. Retrieved on 22nd december 2015 from:

http://www.netl.doe.gov/research/coal/energy-systems/gasification/gasifipedia/commercial-oxygen

Neves, C.M.S.S., Carvalho, P.J., Freire, M.G., Coutinho, J.A.P. (2011). Thermophysical properties of pure and water-saturated tetradecyltrihexylphosphonium-based ionic liquids. *The Journal of Chemical Thermodynamics*, 43(6), 948–957.

NIST, 2013. Ionic Liquids Database - ILThermo (v2.0). Retrieved on 2nd October 2015 from: http://ilthermo.boulder.nist.gov/

North, M. (2015). What is CO_2? Thermodynamics, basic reactions and physical chemistry. In: Styring, P., Quadrelli, E.A. and Armstrong, K. (eds.) *Carbon Dioxide Utilisation: closing the carbon cycle*. Oxford, UK: Elsevier B.V. 3–17.

Notz, R., Prasad, H. and Hasse, H. (2012). Post combustion CO_2 capture by reactive absorption: Pilot plant description and results of systematic studies with MEA. *International Journal of Greenhouse Gas Control*, 6, 84–112.

Notz, R.J., Tönnies, I., McCann, N., Scheffknecht, G. and Hasse, H. (2011). CO_2 Capture for Fossil Fuel-Fired Power Plants. *Chemical Engineering & Technology*, 34(2), 163–172.

O'Brien, J.E., McKellar, M.G., Harvego, E.A. and Stoots, C.M. (2010). High-temperature electrolysis for large-scale hydrogen and syngas production from nuclear energy – summary of system simulation and economic analyses. *International Journal of Hydrogen Energy*, 35 (10), 4808–4819.

O'Brien, J.E., McKellar, M.G., Stoots, C.M., Herring, J.S. and Hawkes, G.L. (2009). Parametric study of large-scale production of syngas via high-temperature co-electrolysis. *International Journal of Hydrogen Energy*, 34 (9), 4216–4226.

OFGEM. (2016). Feed-in Tariff (FIT) Generation & Export Payment Rate Table. Retrieved on 21st July 2016 from: https://www.ofgem.gov.uk/system/files/docs/2016/04/01_april_2016_tariff_table.pdf

Oh-Shim, J., Kwang-Deog, J., & Yonsoo, J. (2003). CAMERE Process for Methanol synthesis from CO2 hydrogenation. In G. Centi (Ed.), *CARBON DIOXIDE UTILIZATION FOR GLOBAL SUSTAINABILITY* (pp. 67–72). ELSEVIER SCIENCE BV.

Owens, J.M. and Chynoweth, D.P. (1993). Biochemical Methane Potential of Municipal Solid Waste (MSW) Components. *Water Science & Technology*, 27 (2), 1–14.

Palomar, J., Gonzalez-Miquel, M., Polo, A. and Rodriguez, F. (2011). Understanding the physical absorption of CO_2 in ionic liquids using the COSMO-RS method. *Industrial and Engineering Chemistry Research*, 50, 3452–3463.

Park, S.-E., Chang, J.-S., Lee, K.-W., Joo, O.-S., Jung, K.-D. and Jung, Y. (2004). Camere Process for methanol synthesis from CO_2 hydrogenation. *Studies in Surface Science and Catalysis*, 153, 67–72.

Paulechka, Y.U., Blokhin, A.V., Kabo, G.J. and Strechan, A.A. (2007). Thermodynamic properties and polymorphism of 1-alkyl-3-methylimidazolium bis(triflamides). *The Journal of Chemical Thermodynamics*, 39 (6), 866–877.

Pekdemir, T. (2015). Integrated Capture and Conversion. In: Styring, P., Quadrelli, E.A. and Armstrong, K. (eds) *Carbon Dioxide Utilisation: closing the carbon cycle*. Oxford, UK: Elsevier B.V. 253–272.

Person, M. (2003). Evaluation of upgrading techniques for biogas. Swedish Gas Center, Report SGC 142. Lund, Sweden.

Peters, M.S., Klaus D. Timmerhaus and West, R.E. (2004). *Plant design and economics for chemical engineers* 5th Edition., New Tork: McGraw-Hill.

Quadrelli, E.A., Centi, G., Duplan, J.-L. and Perathoner, S. (2011). Carbon dioxide recycling: emerging large-scale technologies with industrial potential. *ChemSusChem*, 4 (9), 1194–215.

Rajendran, K., Kankanala, H.R., Martinsson, R. and Taherzadeh, M.J. (2014). Uncertainty over techno-economic potentials of biogas from municipal solid waste (MSW): A case study on an industrial process. *Applied Energy*, 125, 84–92.

Rao, P. and Muller, M. (2007). Industrial Oxygen: Its Generation and Use. Retrieved on 10th October 2015 from: http://aceee.org/files/proceedings/2007/data/papers/78_6_080.pdf

REA. (2013). Minworth Sewage Treatment Works - A case study for Biomethane to Grid. Retrieved on 21st November 2015 from: http://www.r-e-a.net/images/upload/events1335-SimonFarris-SevernTrentMinworthUKBiomethaneDay2013.pdf

Reddy, R.G. (2009). Novel applications of ionic liquids in materials processing. *Journal of Physics: Conference Series*, 165 (1), 012076.

Rubin, E.S., Mantripragada, H., Marks, A., Versteeg, P. and Kitchin, J. (2012). The outlook for improved carbon capture technology. *Progress in Energy and Combustion Science*, 38 (5), 630–671.

Schreiner, C., Zugmann, S., Hartl, R. and Gores, H.J. 2012. Fractional Walden Rule for Ionic Liquids: Examples from Recent Measurements and a Critique of the So-Called Ideal KCl Line for the Walden Plot. *Journal of Chemical & Engineering Data*, 55 (5), 1784–1788.

Severn Trent Water, 2015. Minworth Sewage Treatment Works - A case study for Biomethane to Grid. Retrieved on 2nd March 2015 from: http://www.r-e-a.net/images/upload/events_133_5_-Simon_Farris_-_Severn_Trent_Minworth_-_UK_Biomethane_Day_2013.pdf

Shiflett, M.B., Drew, D.W., Cantini, R.A. and Yokozeki, A. (2010). Carbon Dioxide Capture Using Ionic Liquid 1-Butyl-3-methylimidazolium Acetate. *Energy & Fuels*, 24 (10), 5781–5789.

SIGMA-ALDRICH. (2015). Sigma-Aldrich catalogue. Retrieved on 3rd April 2015 from: http://www.sigmaaldrich.com/united-kingdom.html

Sinnott, R.K. (2005). *Coulson and Richardson's Chemical Engineering Volume 6 - Chemical Engineering Design* 4th edition. Oxford, UK: Butterworth-Heinemann Ltd.

Sizhen, P. (2011). Carbon Capture, Utilization and Storage (CCUS) Technology Development Technology Development in China. Retrieved on 1st November 2015 from: http://www.cslforum.org/publications/documents/Edmonton2011/Sizhen-TG-CCUSTechnologyDevelopmentChina-Edmonton0511.pdf

Skeptical Science. (2014). Is there a scientific consensus on global warming? Retrieved on 13th January 2014 from: http://www.skepticalscience.com/global-warming-scientific-consensus-advanced.htm

Smet, E., Van Langenhove, H. and De Bo, I. (1999). The emission of volatile compounds during the aerobic and the combined anaerobic/aerobic composting of biowaste. *Atmospheric Environment*, 33 (8), 1295–1303.

Sonderby, T.L., Carlsen, K.B., Fosbol, P.L., Kiorboe, L.G. and von Solms, N. (2013). A new pilot absorber for CO_2 capture from flue gases: Measuring and modelling capture with MEA solution. *International Journal of Greenhouse Gas Control*, 12, 181–192.

Song, C. and Pan, W. (2004). Tri-reforming of methane: a novel concept for catalytic production of industrially useful synthesis gas with desired H_2/CO ratios. *Catalysis Today*, 98 (4), 463–484.

Spath, P.L. and Dayton, D.C. (2003). Preliminary Screening - Technical and Economic Assessment of Synthesis Gas to Fuels and Chemicals with Emphasis on the Potential for Biomass-Derived Syngas, Report NREL/TP-510-34929, National Renewable Energy Laboratory.

Spigarelli, B.P. and Kawatra, S.K. (2013). Opportunities and challenges in carbon dioxide capture. *Journal of CO_2 Utilization*, 1, 69–87.

Stocker, T.F., Qin, D., Plattner, G.-K., Tignor, M., Allen, S.K., Boschung, J., Nauels, A., Xia, Y., Bex, V. and Midgley, P.M. (2013). *IPCC, 2013: Climate Change 2013: The Physical Science Basis. Contribution of Working Group I to the Fifth Assessment Report of the Intergovernmental Panel on Climate Change*. Cambridge, United Kingdom and New York, NY, USA: Cambridge University Press.

Stoots, C.M., O'Brien, J.E., Condie, K.G. and Hartvigsen, J.J. (2010). High-temperature electrolysis for large-scale hydrogen production from nuclear energy – Experimental investigations. *International Journal of Hydrogen Energy*, 35 (10), 4861–4870.

Strazisar, B.R., Anderson, R.R. and White, C.M., 2003. Degradation Pathways for Monoethanolamine in a CO_2 Capture Facility. *Energy & Fuels*, 17 (4), 1034–1039.

Styring, P., Jansen, D., de Coninck, H., Reith, H. and Amstrong, K. (2011). Carbon Capture and Utilisation in the Green Economy. ISBN: 978-0-9572588-1-5.

Styring, P. (2015). Carbon Dioxide Capture Agents and Processes. In: Styring, P., Quadrelli, E.A. and Armstrong, K. (eds) *Carbon Dioxide Utilisation: closing the carbon cycle*. Oxford, UK: Elsevier B.V. 19–32.

Sumon, K.Z. and Henni, A. (2011). Ionic liquids for CO_2 capture using COSMO-RS: Effect of structure, properties and molecular interactions on solubility and selectivity. *Fluid Phase Equilibria*, 310 (1-2), 39–55.

Swanson, R.M. (2009). Techno-economic analysis of biomass-to-liquids production based on gasification. Master thesis, Iowa State University.

Swanson, R.M., Platon, A., Satrio, J.A., Brown, R.C. (2010b). Techno-economic analysis of biomass-to-liquids production based on gasification. *Fuel*, 89, S11-S19.

Swanson, R.M., Satrio, J.A., Brown, R.C., Platon, A., and Hsu, D.D. (2010a). Techno-Economic Analysis of Biofuels Production Based on Gasification. Report NREL/TP-6A20-46587, National Renewable Energy Laboratory.

Talaty, E.R., Raja, S., Storhaug, V.J., Dölle, A.and Carper, W.R. (2004). Raman and Infrared Spectra and ab Initio Calculations of C2-4 MIm Imidazolium Hexafluorophosphate Ionic Liquids. *The Journal of Physical Chemistry B*, 108 (35), 13177–13184.

Tijmensen, M.J.A., Faaij, A.P.C., Hamelinck, C.N., van Hardeveld and M.R.M. (2002). Exploration of the possibilities for production of Fischer Tropsch liquids and power via biomass gasification. *Biomass and Bioenergy*, 23 (2), 129–152.

Tippayawong, N., Thanompongchart, P. and Olabi, A.G. (2010). Biogas quality upgrade by simultaneous removal of CO_2 and H_2S in a packed column reactor. *Energy*, 35 (12), 4531–4535.

UKPIA. (2015). Statistical Review 2015. Retrieved on 3rd March 2015 from: http://www.ukpia.com/docs/default-source/default-document-library/ukpia-2015-statistical-review4e465c889f1367d7a07bff0000a71495.pdf?sfvrsn=0

US Department of Energy. (2014). Hydrogen Production Cost From PEM Electrolysis. Retrivied on 25th July 2015 from: http://www.hydrogen.energy.gov/pdfs/14004_h2_production_cost_pem_electrolysis.pdf

Valderrama, J.O. and Rojas, R.E. (2009). Critical Properties of Ionic Liquids. Revisited. *Industrial & Engineering Chemistry Research*, 48, 6890–6900.

Van der Drift, A. and Boerrigter, H. (2006). Synthesis gas from biomass for fuels and chemicals, Report ECN-C--06-001, Energy Research Centre of the

Netherlands.

Wang, S., Lu, G.Q.M. and Millar, G.J. (1996). Carbon Dioxide Reforming of Methane To Produce Synthesis Gas over Metal-Supported Catalysts : State of the Art. *Energy and Fuels*, 10, 896–904.

Weigend, F. & Häser, M., 1997. RI-MP2: first derivatives and global consistency. *Theoretical Chemistry Accounts: Theory, Computation, and Modeling (Theoretica Chimica Acta)*, 97 (1-4), 331–340.

Widegren, J.A. and Magee, J.W. (2007). Density, Viscosity, Speed of Sound, and Electrolytic Conductivity for the Ionic Liquid 1-Hexyl-3-methylimidazolium Bis(trifluoromethylsulfonyl)imide and Its Mixtures with Water. *Journal of Chemical & Engineering Data*, 52 (6), 2331–2338.

Working Group III of the Intergovernmental Panel on Climate Change (2005), CARBON DIOXIDE CAPTURE AND STORAGE, Cambridge University Press, New York. ISBN: 9780521863360

XEcurrency. (2015). XE Currency Converter. Retrieved on 29th May 2015 from: http://www.xe.com/en/

Xie, H.-B., Zhou, Y., Zhang, Y., Johnson, J.K. (2010). Reaction mechanism of monoethanolamine with CO_2 in aqueous solution from molecular modeling. *The journal of physical chemistry. A*, 114 (43), 11844–52.

Yan, Y., Gu, J., Zeitler, E.L. and Bocarsly, A.B. (2015). Photoelectrocatalytic Reduction of Carbon Dioxide. In: Styring, P., Quadrelli, E.A. and Armstrong, K. (eds.) Carbon Dioxide Utilisation: closing the carbon cycle. Oxford, UK: Elsevier B.V. 211–233.

Zapp, P., Schreiber, A., Marx, J., Haines, M., Hake, J.-F. and Gale, J. (2012). Overall environmental impacts of CCS technologies—A life cycle approach. *International Journal of Greenhouse Gas Control*, 8, 12–21.

Zhan, Z., Kobsiriphat, W., Wilson, J.R., Pillai, M., Kim, I. and Barnett, S.A. (2009). Syngas Production By Coelectrolysis of CO_2 /H_2O: The Basis for a Renewable Energy Cycle. *Energy & Fuels*, 23 (6), 3089–3096.

Zhang, X., Liu, Z. & Wang, W. (2008). Screening of ionic liquids to capture CO_2 by COSMO-RS and experiments. *AIChE Journal*, 54 (10), 2717–2728.

Zhang, X., Zhang, X., Dong, H., Zhao, Z., Zhang, S. and Huang, Y. (2012). Carbon capture with ionic liquids: overview and progress. *Energy & Environmental Science*, 5, 6668.

Zhu, L., Schade, G.W. and Nielsen, C.J. (2013). Real-Time Monitoring of Emissions from Monoethanolamine-Based Industrial Scale Carbon Capture Facilities. *Environmental science & technology*, 47 (24), 14306–14314.

Zoannou, K.-S., Sapsford, D.J. and Griffiths, A.J. (2013). Thermal degradation of monoethanolamine and its effect on CO_2 capture capacity. *International Journal of Greenhouse Gas Control*, 17, 423–430.

Zubeir, L.F., Romanos, G.E., Weggemans, W.M.A., Iliev, B., Schubert, T.J.S. and Kroon, M.C. (2015). Solubility and Diffusivity of CO_2 in the Ionic Liquid 1-Butyl-3-methylimidazolium Tricyanomethanide within a Large Pressure Range (0.01 MPa to 10 MPa). *Journal of Chemical & Engineering Data*, 60 (6), 1544–1562.

Appendix A. Summary of streams

Table A.1 Input stream summary of PD-MEA1

PD-MEA1	INPUTS						
Mass Flow kg·h^{-1}	**BIOGAS (1)**	**WATER MU (12)**	**MEA MU (13)**	**STEAM (17)**	**H2 INPUT (16)**	**AIR (41)**	**WATER (45)**
MEA	0.00	0.00	0.05	0.00	0.00	0.00	0.00
H2O	0.00	1370.82	0.00	2048.48	0.00	0.00	17734.01
CO2	2250.75	0.00	0.00	0.00	0.00	7.26	0.00
H2S	0.00	0.00	0.00	0.00	0.00	0.00	0.00
H3O+	0.00	0.00	0.00	0.00	0.00	0.00	0.00
OH-	0.00	0.00	0.00	0.00	0.00	0.00	0.00
HCO3-	0.00	0.00	0.00	0.00	0.00	0.00	0.00
CO3-2	0.00	0.00	0.00	0.00	0.00	0.00	0.00
HS-	0.00	0.00	0.00	0.00	0.00	0.00	0.00
S-2	0.00	0.00	0.00	0.00	0.00	0.00	0.00
MEAH+	0.00	0.00	0.00	0.00	0.00	0.00	0.00
MEACOO-	0.00	0.00	0.00	0.00	0.00	0.00	0.00
N2	0.00	0.00	0.00	0.00	0.00	11483.96	0.00
O2	0.00	0.00	0.00	0.00	0.00	3519.47	0.00
CO	0.00	0.00	0.00	0.00	0.00	0.00	0.00
H2	0.00	0.00	0.00	0.00	42.85	0.00	0.00
CH4	1523.71	0.00	0.00	0.00	0.00	0.00	0.00
ARGON	0.00	0.00	0.00	0.00	0.00	195.89	0.00
ETHANE	0.00	0.00	0.00	0.00	0.00	0.00	0.00
PROPANE	0.00	0.00	0.00	0.00	0.00	0.00	0.00
BUTANE	0.00	0.00	0.00	0.00	0.00	0.00	0.00
PENTANE	0.00	0.00	0.00	0.00	0.00	0.00	0.00
HEXANE	0.00	0.00	0.00	0.00	0.00	0.00	0.00
HEPTANE	0.00	0.00	0.00	0.00	0.00	0.00	0.00
OCTANE	0.00	0.00	0.00	0.00	0.00	0.00	0.00
NONANE	0.00	0.00	0.00	0.00	0.00	0.00	0.00
DECANE	0.00	0.00	0.00	0.00	0.00	0.00	0.00
UNDECANE	0.00	0.00	0.00	0.00	0.00	0.00	0.00
N-DOD-01	0.00	0.00	0.00	0.00	0.00	0.00	0.00
N-TRI-01	0.00	0.00	0.00	0.00	0.00	0.00	0.00
N-TET-01	0.00	0.00	0.00	0.00	0.00	0.00	0.00
N-PEN-01	0.00	0.00	0.00	0.00	0.00	0.00	0.00
N-HEX-01	0.00	0.00	0.00	0.00	0.00	0.00	0.00
N-HEP-01	0.00	0.00	0.00	0.00	0.00	0.00	0.00
N-OCT-01	0.00	0.00	0.00	0.00	0.00	0.00	0.00
N-NON-01	0.00	0.00	0.00	0.00	0.00	0.00	0.00
N-EIC-01	0.00	0.00	0.00	0.00	0.00	0.00	0.00
N-HEN-01	0.00	0.00	0.00	0.00	0.00	0.00	0.00
N-DOC-01	0.00	0.00	0.00	0.00	0.00	0.00	0.00
N-TRI-02	0.00	0.00	0.00	0.00	0.00	0.00	0.00
N-TET-02	0.00	0.00	0.00	0.00	0.00	0.00	0.00
N-PEN-02	0.00	0.00	0.00	0.00	0.00	0.00	0.00
N-HEX-02	0.00	0.00	0.00	0.00	0.00	0.00	0.00
N-HEP-02	0.00	0.00	0.00	0.00	0.00	0.00	0.00
N-OCT-02	0.00	0.00	0.00	0.00	0.00	0.00	0.00
N-NON-02	0.00	0.00	0.00	0.00	0.00	0.00	0.00
N-TRI-03	0.00	0.00	0.00	0.00	0.00	0.00	0.00
Mass Flow kg·h^{-1}	**3774.46**	**1370.82**	**0.05**	**2048.48**	**42.85**	**15206.57**	**17734.01**

Table A.2 Output stream summary of PD-MEA1

PD-MEA1	OUTPUTS						
Mass Flow kg·h^{-1}	**CONDENSATE (8)**	**FLASH COND (33)**	**FT COND (38)**	**FT SYNCR (43)**	**REST (42)**	**FLUEGAS (47)**	**STEAM (46)**
MEA	0.00	0.00	0.03	0.00	0.01	0.01	0.00
H2O	1288.19	486.87	2385.01	0.00	0.99	1916.39	17734.01
CO2	2.45	0.00	0.01	0.00	0.94	3846.67	0.00
H2S	0.00	0.00	0.00	0.00	0.00	0.00	0.00
H3O+	0.00	0.00	0.00	0.00	0.00	0.00	0.00
OH-	0.00	0.00	0.00	0.00	0.00	0.00	0.00
HCO3-	3.95	0.00	0.00	0.00	0.00	0.00	0.00
CO3-2	0.00	0.00	0.00	0.00	0.00	0.00	0.00
HS-	0.00	0.00	0.00	0.00	0.00	0.00	0.00
S-2	0.00	0.00	0.00	0.00	0.00	0.00	0.00
MEAH+	4.02	0.00	0.00	0.00	0.00	0.00	0.00
MEACOO-	0.00	0.00	0.00	0.00	0.00	0.00	0.00
N2	0.00	0.00	0.00	0.00	0.00	11483.96	0.00
O2	0.00	0.00	0.00	0.00	0.00	4.08	0.00
CO	0.00	0.00	0.00	0.00	0.06	0.00	0.00
H2	0.00	0.00	0.00	0.00	0.00	0.00	0.00
CH4	0.00	0.00	0.00	0.00	0.09	0.00	0.00
ARGON	0.00	0.00	0.00	0.00	0.00	195.89	0.00
ETHANE	0.00	0.00	0.00	0.00	0.09	0.00	0.00
PROPANE	0.00	0.00	0.00	0.00	0.40	0.00	0.00
BUTANE	0.00	0.00	0.00	0.00	1.58	0.00	0.00
PENTANE	0.00	0.00	0.00	5.52	0.00	0.00	0.00
HEXANE	0.00	0.00	0.00	16.23	0.00	0.00	0.00
HEPTANE	0.00	0.00	0.00	35.20	0.00	0.00	0.00
OCTANE	0.00	0.00	0.00	53.72	0.00	0.00	0.00
NONANE	0.00	0.00	0.00	61.94	0.00	0.00	0.00
DECANE	0.00	0.00	0.00	62.56	0.00	0.00	0.00
UNDECANE	0.00	0.00	0.00	59.69	0.00	0.00	0.00
N-DOD-01	0.00	0.00	0.00	55.69	0.00	0.00	0.00
N-TRI-01	0.00	0.00	0.00	51.35	0.00	0.00	0.00
N-TET-01	0.00	0.00	0.00	47.01	0.00	0.00	0.00
N-PEN-01	0.00	0.00	0.00	42.79	0.00	0.00	0.00
N-HEX-01	0.00	0.00	0.00	38.78	0.00	0.00	0.00
N-HEP-01	0.00	0.00	0.00	35.01	0.00	0.00	0.00
N-OCT-01	0.00	0.00	0.00	31.49	0.00	0.00	0.00
N-NON-01	0.00	0.00	0.00	28.24	0.00	0.00	0.00
N-EIC-01	0.00	0.00	0.00	25.26	0.00	0.00	0.00
N-HEN-01	0.00	0.00	0.00	22.54	0.00	0.00	0.00
N-DOC-01	0.00	0.00	0.00	20.06	0.00	0.00	0.00
N-TRI-02	0.00	0.00	0.00	17.82	0.00	0.00	0.00
N-TET-02	0.00	0.00	0.00	15.80	0.00	0.00	0.00
N-PEN-02	0.00	0.00	0.00	13.99	0.00	0.00	0.00
N-HEX-02	0.00	0.00	0.00	12.36	0.00	0.00	0.00
N-HEP-02	0.00	0.00	0.00	10.91	0.00	0.00	0.00
N-OCT-02	0.00	0.00	0.00	9.62	0.00	0.00	0.00
N-NON-02	0.00	0.00	0.00	8.47	0.00	0.00	0.00
N-TRI-03	0.00	0.00	0.00	49.61	0.00	0.00	0.00
Mass Flow kg·h^{-1}	**1298.61**	**486.87**	**2385.05**	**831.68**	**4.17**	**17446.98**	**17734.01**

Table A.3 Input stream summary of PD-MEA2

PD-MEA2	INPUTS					
Mass Flow kg·h^{-1}	**BIOGAS (1)**	**WATER MU (12)**	**MEA MU (13)**	**H2 INPUT (16)**	**AIR (38)**	**WATER (40)**
MEA	0.00	0.00	0.00	0.00	0.00	0.00
H2O	0.00	1305.56	0.00	0.00	0.00	3706.36
CO2	2250.75	0.00	0.00	0.00	1.48	0.00
H2S	0.00	0.00	0.00	0.00	0.00	0.00
H3O+	0.00	0.00	0.00	0.00	0.00	0.00
OH-	0.00	0.00	0.00	0.00	0.00	0.00
HCO3-	0.00	0.00	0.00	0.00	0.00	0.00
CO3-2	0.00	0.00	0.00	0.00	0.00	0.00
HS-	0.00	0.00	0.00	0.00	0.00	0.00
S-2	0.00	0.00	0.00	0.00	0.00	0.00
MEAH+	0.00	0.00	0.00	0.00	0.00	0.00
MEACOO-	0.00	0.00	0.00	0.00	0.00	0.00
N2	0.00	0.00	0.00	0.00	2340.54	0.00
O2	0.00	0.00	0.00	0.00	717.30	0.00
CO	0.00	0.00	0.00	0.00	0.00	0.00
H2	0.00	0.00	0.00	195.67	0.00	0.00
CH4	1523.71	0.00	0.00	0.00	0.00	0.00
ARGON	0.00	0.00	0.00	0.00	39.92	0.00
ETHANE	0.00	0.00	0.00	0.00	0.00	0.00
PROPANE	0.00	0.00	0.00	0.00	0.00	0.00
BUTANE	0.00	0.00	0.00	0.00	0.00	0.00
PENTANE	0.00	0.00	0.00	0.00	0.00	0.00
HEXANE	0.00	0.00	0.00	0.00	0.00	0.00
HEPTANE	0.00	0.00	0.00	0.00	0.00	0.00
OCTANE	0.00	0.00	0.00	0.00	0.00	0.00
NONANE	0.00	0.00	0.00	0.00	0.00	0.00
DECANE	0.00	0.00	0.00	0.00	0.00	0.00
UNDECANE	0.00	0.00	0.00	0.00	0.00	0.00
N-DOD-01	0.00	0.00	0.00	0.00	0.00	0.00
N-TRI-01	0.00	0.00	0.00	0.00	0.00	0.00
N-TET-01	0.00	0.00	0.00	0.00	0.00	0.00
N-PEN-01	0.00	0.00	0.00	0.00	0.00	0.00
N-HEX-01	0.00	0.00	0.00	0.00	0.00	0.00
N-HEP-01	0.00	0.00	0.00	0.00	0.00	0.00
N-OCT-01	0.00	0.00	0.00	0.00	0.00	0.00
N-NON-01	0.00	0.00	0.00	0.00	0.00	0.00
N-EIC-01	0.00	0.00	0.00	0.00	0.00	0.00
N-HEN-01	0.00	0.00	0.00	0.00	0.00	0.00
N-DOC-01	0.00	0.00	0.00	0.00	0.00	0.00
N-TRI-02	0.00	0.00	0.00	0.00	0.00	0.00
N-TET-02	0.00	0.00	0.00	0.00	0.00	0.00
N-PEN-02	0.00	0.00	0.00	0.00	0.00	0.00
N-HEX-02	0.00	0.00	0.00	0.00	0.00	0.00
N-HEP-02	0.00	0.00	0.00	0.00	0.00	0.00
N-OCT-02	0.00	0.00	0.00	0.00	0.00	0.00
N-NON-02	0.00	0.00	0.00	0.00	0.00	0.00
N-TRI-03	0.00	0.00	0.00	0.00	0.00	0.00
Mass Flow kg·h^{-1}	**3774.46**	**1305.56**	**0.00**	**195.67**	**3099.24**	**3706.36**

Table A.4 Output stream summary of PD-MEA1

PD-MEA2	OUTPUTS						
Mass Flow kg·h^{-1}	**CONDENSATE (8)**	**CH4 OUT (3)**	**FT COND (31)**	**FT SYNCR (34)**	**REST (35)**	**FLUEGAS (39)**	**STEAM (38)**
MEA	0.00	0.05	0.00	0.00	0.00	0.00	0.00
H2O	1288.19	65.26	1053.68	0.00	0.29	383.05	3706.36
CO2	2.45	59.82	0.01	0.00	0.70	1439.24	0.00
H2S	0.00	0.00	0.00	0.00	0.00	0.00	0.00
H3O+	0.00	0.00	0.00	0.00	0.00	0.00	0.00
OH-	0.00	0.00	0.00	0.00	0.00	0.00	0.00
HCO3-	3.95	0.00	0.00	0.00	0.00	0.00	0.00
CO3-2	0.00	0.00	0.00	0.00	0.00	0.00	0.00
HS-	0.00	0.00	0.00	0.00	0.00	0.00	0.00
S-2	0.00	0.00	0.00	0.00	0.00	0.00	0.00
MEAH+	4.02	0.00	0.00	0.00	0.00	0.00	0.00
MEACOO-	0.00	0.00	0.00	0.00	0.00	0.00	0.00
N2	0.00	0.00	0.00	0.00	0.00	2340.54	0.00
O2	0.00	0.00	0.00	0.00	0.00	3.74	0.00
CO	0.00	0.00	0.00	0.00	0.02	0.00	0.00
H2	0.00	0.00	0.00	0.00	0.00	0.00	0.00
CH4	0.00	1520.16	0.00	0.00	0.00	0.00	0.00
ARGON	0.00	0.00	0.00	0.00	0.00	39.92	0.00
ETHANE	0.00	0.00	0.00	0.00	0.02	0.00	0.00
PROPANE	0.00	0.00	0.00	0.00	0.09	0.00	0.00
BUTANE	0.00	0.00	0.00	0.00	0.38	0.00	0.00
PENTANE	0.00	0.00	0.00	1.34	0.00	0.00	0.00
HEXANE	0.00	0.00	0.00	4.05	0.00	0.00	0.00
HEPTANE	0.00	0.00	0.00	9.29	0.00	0.00	0.00
OCTANE	0.00	0.00	0.00	15.10	0.00	0.00	0.00
NONANE	0.00	0.00	0.00	18.08	0.00	0.00	0.00
DECANE	0.00	0.00	0.00	18.56	0.00	0.00	0.00
UNDECANE	0.00	0.00	0.00	17.80	0.00	0.00	0.00
N-DOD-01	0.00	0.00	0.00	16.64	0.00	0.00	0.00
N-TRI-01	0.00	0.00	0.00	15.35	0.00	0.00	0.00
N-TET-01	0.00	0.00	0.00	14.06	0.00	0.00	0.00
N-PEN-01	0.00	0.00	0.00	12.80	0.00	0.00	0.00
N-HEX-01	0.00	0.00	0.00	11.60	0.00	0.00	0.00
N-HEP-01	0.00	0.00	0.00	10.47	0.00	0.00	0.00
N-OCT-01	0.00	0.00	0.00	9.42	0.00	0.00	0.00
N-NON-01	0.00	0.00	0.00	8.45	0.00	0.00	0.00
N-EIC-01	0.00	0.00	0.00	7.56	0.00	0.00	0.00
N-HEN-01	0.00	0.00	0.00	6.74	0.00	0.00	0.00
N-DOC-01	0.00	0.00	0.00	6.00	0.00	0.00	0.00
N-TRI-02	0.00	0.00	0.00	5.33	0.00	0.00	0.00
N-TET-02	0.00	0.00	0.00	4.73	0.00	0.00	0.00
N-PEN-02	0.00	0.00	0.00	4.18	0.00	0.00	0.00
N-HEX-02	0.00	0.00	0.00	3.70	0.00	0.00	0.00
N-HEP-02	0.00	0.00	0.00	3.26	0.00	0.00	0.00
N-OCT-02	0.00	0.00	0.00	2.88	0.00	0.00	0.00
N-NON-02	0.00	0.00	0.00	2.53	0.00	0.00	0.00
N-TRI-03	0.00	0.00	0.00	14.84	0.00	0.00	0.00
Mass Flow kg·h^{-1}	**1298.61**	**1645.30**	**1053.70**	**244.76**	**1.51**	**4206.50**	**3706.36**

Table A.5 Input stream summary of PD-CHP1

PD-CHP1	INPUTS							
Mass Flow kg·h^{-1}	**BIOGAS (1)**	**AIR (2)**	**NOX STEAM (3)**	**WATER1 CHP (4)**	**WATER 2 CHP (5)**	**H2 INPUT (10)**	**AIR OFFGAS (26)**	**WATER STEAM (30)**
H2O	0.00	0.00	45521.15	10590.12	3054.84	0.00	0.00	12285.40
N2	0.00	22754.33	0.00	0.00	0.00	0.00	5337.31	0.00
O2	0.00	6973.48	0.00	0.00	0.00	0.00	1635.72	0.00
CO	0.00	0.00	0.00	0.00	0.00	0.00	0.00	0.00
CO2	2250.75	14.38	0.00	0.00	0.00	0.00	3.37	0.00
ARGON	0.00	388.13	0.00	0.00	0.00	0.00	91.04	0.00
CH4	1523.71	0.00	0.00	0.00	0.00	0.00	0.00	0.00
ETHANE	0.00	0.00	0.00	0.00	0.00	0.00	0.00	0.00
PROPANE	0.00	0.00	0.00	0.00	0.00	0.00	0.00	0.00
H2	0.00	0.00	0.00	0.00	0.00	575.63	0.00	0.00
BUTANE	0.00	0.00	0.00	0.00	0.00	0.00	0.00	0.00
PENTANE	0.00	0.00	0.00	0.00	0.00	0.00	0.00	0.00
HEXANE	0.00	0.00	0.00	0.00	0.00	0.00	0.00	0.00
HEPTANE	0.00	0.00	0.00	0.00	0.00	0.00	0.00	0.00
OCTANE	0.00	0.00	0.00	0.00	0.00	0.00	0.00	0.00
NONANE	0.00	0.00	0.00	0.00	0.00	0.00	0.00	0.00
DECANE	0.00	0.00	0.00	0.00	0.00	0.00	0.00	0.00
UNDECANE	0.00	0.00	0.00	0.00	0.00	0.00	0.00	0.00
N-DOD-01	0.00	0.00	0.00	0.00	0.00	0.00	0.00	0.00
N-TRI-01	0.00	0.00	0.00	0.00	0.00	0.00	0.00	0.00
N-TET-01	0.00	0.00	0.00	0.00	0.00	0.00	0.00	0.00
N-PEN-01	0.00	0.00	0.00	0.00	0.00	0.00	0.00	0.00
N-HEX-01	0.00	0.00	0.00	0.00	0.00	0.00	0.00	0.00
N-HEP-01	0.00	0.00	0.00	0.00	0.00	0.00	0.00	0.00
N-OCT-01	0.00	0.00	0.00	0.00	0.00	0.00	0.00	0.00
N-NON-01	0.00	0.00	0.00	0.00	0.00	0.00	0.00	0.00
N-EIC-01	0.00	0.00	0.00	0.00	0.00	0.00	0.00	0.00
N-HEN-01	0.00	0.00	0.00	0.00	0.00	0.00	0.00	0.00
N-DOC-01	0.00	0.00	0.00	0.00	0.00	0.00	0.00	0.00
N-TRI-02	0.00	0.00	0.00	0.00	0.00	0.00	0.00	0.00
N-TET-02	0.00	0.00	0.00	0.00	0.00	0.00	0.00	0.00
N-PEN-02	0.00	0.00	0.00	0.00	0.00	0.00	0.00	0.00
N-HEX-02	0.00	0.00	0.00	0.00	0.00	0.00	0.00	0.00
N-HEP-02	0.00	0.00	0.00	0.00	0.00	0.00	0.00	0.00
N-OCT-02	0.00	0.00	0.00	0.00	0.00	0.00	0.00	0.00
N-NON-02	0.00	0.00	0.00	0.00	0.00	0.00	0.00	0.00
N-TRI-03	0.00	0.00	0.00	0.00	0.00	0.00	0.00	0.00
Mass Flow kg·h^{-1}	**3774.46**	**30130.31**	**45521.15**	**10590.12**	**3054.84**	**575.63**	**7067.44**	**12285.40**

Table A.6 Output stream summary of PD-CHP1

PD-CHP1	OUTPUTS									
Mass Flow kg·h^{-1}	**STEAM-A (6)**	**STEAM-B (7)**	**STEAM-C (8)**	**COND CHP (9)**	**FLASH COND (12)**	**FT COND (31)**	**FT SYNCR (36)**	**REST (35)**	**FLUEGAS (38)**	**STEAM (37)**
H2O	1588.52	458.23	11345.79	252.43	48807.66	2877.68	0.00	0.56	1601.10	12285.40
N2	0.00	0.00	0.00	0.00	0.01	0.00	0.00	0.14	28091.50	0.00
O2	0.00	0.00	0.00	0.00	0.01	0.00	0.00	0.01	2.73	0.00
CO	0.00	0.00	0.00	0.00	0.00	0.00	0.00	0.00	0.00	0.00
CO2	0.00	0.00	0.00	0.00	0.55	0.00	0.00	0.16	4620.51	0.00
ARGON	0.00	0.00	0.00	0.00	0.00	0.00	0.00	0.00	479.16	0.00
CH4	0.00	0.00	0.00	0.00	0.00	0.00	0.00	0.00	0.00	0.00
ETHANE	0.00	0.00	0.00	0.00	0.00	0.00	0.00	0.00	0.00	0.00
PROPANE	0.00	0.00	0.00	0.00	0.00	0.00	0.00	0.02	0.00	0.00
H2	0.00	0.00	0.00	0.00	0.00	0.00	0.00	0.00	0.00	0.00
BUTANE	0.00	0.00	0.00	0.00	0.00	0.00	0.00	0.09	0.00	0.00
PENTANE	0.00	0.00	0.00	0.00	0.00	0.00	0.32	0.00	0.00	0.00
HEXANE	0.00	0.00	0.00	0.00	0.00	0.00	1.08	0.00	0.00	0.00
HEPTANE	0.00	0.00	0.00	0.00	0.00	0.00	3.39	0.00	0.00	0.00
OCTANE	0.00	0.00	0.00	0.00	0.00	0.00	9.58	0.00	0.00	0.00
NONANE	0.00	0.00	0.00	0.00	0.00	0.00	21.93	0.00	0.00	0.00
DECANE	0.00	0.00	0.00	0.00	0.00	0.00	37.00	0.00	0.00	0.00
UNDECANE	0.00	0.00	0.00	0.00	0.00	0.00	45.09	0.00	0.00	0.00
N-DOD-01	0.00	0.00	0.00	0.00	0.00	0.00	46.53	0.00	0.00	0.00
N-TRI-01	0.00	0.00	0.00	0.00	0.00	0.00	44.39	0.00	0.00	0.00
N-TET-01	0.00	0.00	0.00	0.00	0.00	0.00	41.09	0.00	0.00	0.00
N-PEN-01	0.00	0.00	0.00	0.00	0.00	0.00	37.57	0.00	0.00	0.00
N-HEX-01	0.00	0.00	0.00	0.00	0.00	0.00	34.09	0.00	0.00	0.00
N-HEP-01	0.00	0.00	0.00	0.00	0.00	0.00	30.79	0.00	0.00	0.00
N-OCT-01	0.00	0.00	0.00	0.00	0.00	0.00	27.71	0.00	0.00	0.00
N-NON-01	0.00	0.00	0.00	0.00	0.00	0.00	24.85	0.00	0.00	0.00
N-EIC-01	0.00	0.00	0.00	0.00	0.00	0.00	22.23	0.00	0.00	0.00
N-HEN-01	0.00	0.00	0.00	0.00	0.00	0.00	19.83	0.00	0.00	0.00
N-DOC-01	0.00	0.00	0.00	0.00	0.00	0.00	17.65	0.00	0.00	0.00
N-TRI-02	0.00	0.00	0.00	0.00	0.00	0.00	15.68	0.00	0.00	0.00
N-TET-02	0.00	0.00	0.00	0.00	0.00	0.00	13.91	0.00	0.00	0.00
N-PEN-02	0.00	0.00	0.00	0.00	0.00	0.00	12.31	0.00	0.00	0.00
N-HEX-02	0.00	0.00	0.00	0.00	0.00	0.00	10.88	0.00	0.00	0.00
N-HEP-02	0.00	0.00	0.00	0.00	0.00	0.00	9.60	0.00	0.00	0.00
N-OCT-02	0.00	0.00	0.00	0.00	0.00	0.00	8.46	0.00	0.00	0.00
N-NON-02	0.00	0.00	0.00	0.00	0.00	0.00	7.45	0.00	0.00	0.00
N-TRI-03	0.00	0.00	0.00	0.00	0.00	0.00	43.65	0.00	0.00	0.00
Mass Flow kg·h^{-1}	**1588.52**	**458.23**	**11345.79**	**252.43**	**48808.24**	**2877.68**	**587.07**	**0.99**	**34795.00**	**12285.40**

Table A.7 Input stream summary of PD-CHP1-OXY

PD-CHP1-OXY	INPUTS							
Mass Flow kg·h^{-1}	**BIOGAS (1)**	**OXYGEN (2)**	**NOX STEAM (3)**	**WATER1 CHP (4)**	**WATER 2 CHP (5)**	**H2 INPUT (10)**	**AIR OFFGAS (26)**	**WATER STEAM (30)**
H2O	0.00	0.00	55329.03	8792.83	2536.39	0.00	0.00	10964.59
N2	0.00	0.00	0.00	0.00	0.00	0.00	4374.84	0.00
O2	0.00	6842.75	0.00	0.00	0.00	0.00	1340.75	0.00
CO	0.00	0.00	0.00	0.00	0.00	0.00	0.00	0.00
CO2	2250.75	0.00	0.00	0.00	0.00	0.00	2.76	0.00
ARGON	0.00	0.00	0.00	0.00	0.00	0.00	74.62	0.00
CH4	1523.71	0.00	0.00	0.00	0.00	0.00	0.00	0.00
ETHANE	0.00	0.00	0.00	0.00	0.00	0.00	0.00	0.00
PROPANE	0.00	0.00	0.00	0.00	0.00	0.00	0.00	0.00
H2	0.00	0.00	0.00	0.00	0.00	574.05	0.00	0.00
BUTANE	0.00	0.00	0.00	0.00	0.00	0.00	0.00	0.00
PENTANE	0.00	0.00	0.00	0.00	0.00	0.00	0.00	0.00
HEXANE	0.00	0.00	0.00	0.00	0.00	0.00	0.00	0.00
HEPTANE	0.00	0.00	0.00	0.00	0.00	0.00	0.00	0.00
OCTANE	0.00	0.00	0.00	0.00	0.00	0.00	0.00	0.00
NONANE	0.00	0.00	0.00	0.00	0.00	0.00	0.00	0.00
DECANE	0.00	0.00	0.00	0.00	0.00	0.00	0.00	0.00
UNDECANE	0.00	0.00	0.00	0.00	0.00	0.00	0.00	0.00
N-DOD-01	0.00	0.00	0.00	0.00	0.00	0.00	0.00	0.00
N-TRI-01	0.00	0.00	0.00	0.00	0.00	0.00	0.00	0.00
N-TET-01	0.00	0.00	0.00	0.00	0.00	0.00	0.00	0.00
N-PEN-01	0.00	0.00	0.00	0.00	0.00	0.00	0.00	0.00
N-HEX-01	0.00	0.00	0.00	0.00	0.00	0.00	0.00	0.00
N-HEP-01	0.00	0.00	0.00	0.00	0.00	0.00	0.00	0.00
N-OCT-01	0.00	0.00	0.00	0.00	0.00	0.00	0.00	0.00
N-NON-01	0.00	0.00	0.00	0.00	0.00	0.00	0.00	0.00
N-EIC-01	0.00	0.00	0.00	0.00	0.00	0.00	0.00	0.00
N-HEN-01	0.00	0.00	0.00	0.00	0.00	0.00	0.00	0.00
N-DOC-01	0.00	0.00	0.00	0.00	0.00	0.00	0.00	0.00
N-TRI-02	0.00	0.00	0.00	0.00	0.00	0.00	0.00	0.00
N-TET-02	0.00	0.00	0.00	0.00	0.00	0.00	0.00	0.00
N-PEN-02	0.00	0.00	0.00	0.00	0.00	0.00	0.00	0.00
N-HEX-02	0.00	0.00	0.00	0.00	0.00	0.00	0.00	0.00
N-HEP-02	0.00	0.00	0.00	0.00	0.00	0.00	0.00	0.00
N-OCT-02	0.00	0.00	0.00	0.00	0.00	0.00	0.00	0.00
N-NON-02	0.00	0.00	0.00	0.00	0.00	0.00	0.00	0.00
N-TRI-03	0.00	0.00	0.00	0.00	0.00	0.00	0.00	0.00
Mass Flow kg·h^{-1}	**3774.46**	**6842.75**	**55329.03**	**8792.83**	**2536.39**	**574.05**	**5792.98**	**10964.59**

Table A.8 Output stream summary of PD-CHP1-OXY

PD-CHP1-OXY	OUTPUTS									
Mass Flow kg·h^{-1}	**STEAM-A (6)**	**STEAM-B (7)**	**STEAM-C (8)**	**COND CHP (9)**	**FLASH COND (12)**	**FT COND (31)**	**FT SYNCR (36)**	**REST (35)**	**FLUEGAS (38)**	**STEAM (37)**
H2O	1318.93	380.46	9420.25	209.59	58727.83	3055.19	0.00	0.81	1126.84	10964.59
N2	0.00	0.00	0.00	0.00	0.00	0.00	0.00	0.00	4374.84	0.00
O2	0.00	0.00	0.00	0.00	0.07	0.00	0.00	0.08	9.17	0.00
CO	0.00	0.00	0.00	0.00	0.00	0.00	0.00	0.04	0.00	0.00
CO2	0.00	0.00	0.00	0.00	3.87	0.04	0.00	1.64	4231.16	0.00
ARGON	0.00	0.00	0.00	0.00	0.00	0.00	0.00	0.00	74.62	0.00
CH4	0.00	0.00	0.00	0.00	0.00	0.00	0.00	0.00	0.00	0.00
ETHANE	0.00	0.00	0.00	0.00	0.00	0.00	0.00	0.05	0.00	0.00
PROPANE	0.00	0.00	0.00	0.00	0.00	0.00	0.00	0.22	0.00	0.00
H2	0.00	0.00	0.00	0.00	0.00	0.00	0.00	0.00	0.00	0.00
BUTANE	0.00	0.00	0.00	0.00	0.00	0.00	0.00	0.88	0.00	0.00
PENTANE	0.00	0.00	0.00	0.00	0.00	0.00	3.15	0.00	0.00	0.00
HEXANE	0.00	0.00	0.00	0.00	0.00	0.00	9.76	0.00	0.00	0.00
HEPTANE	0.00	0.00	0.00	0.00	0.00	0.00	23.62	0.00	0.00	0.00
OCTANE	0.00	0.00	0.00	0.00	0.00	0.00	41.08	0.00	0.00	0.00
NONANE	0.00	0.00	0.00	0.00	0.00	0.00	51.46	0.00	0.00	0.00
DECANE	0.00	0.00	0.00	0.00	0.00	0.00	53.89	0.00	0.00	0.00
UNDECANE	0.00	0.00	0.00	0.00	0.00	0.00	52.05	0.00	0.00	0.00
N-DOD-01	0.00	0.00	0.00	0.00	0.00	0.00	48.77	0.00	0.00	0.00
N-TRI-01	0.00	0.00	0.00	0.00	0.00	0.00	45.03	0.00	0.00	0.00
N-TET-01	0.00	0.00	0.00	0.00	0.00	0.00	41.24	0.00	0.00	0.00
N-PEN-01	0.00	0.00	0.00	0.00	0.00	0.00	37.55	0.00	0.00	0.00
N-HEX-01	0.00	0.00	0.00	0.00	0.00	0.00	34.03	0.00	0.00	0.00
N-HEP-01	0.00	0.00	0.00	0.00	0.00	0.00	30.72	0.00	0.00	0.00
N-OCT-01	0.00	0.00	0.00	0.00	0.00	0.00	27.63	0.00	0.00	0.00
N-NON-01	0.00	0.00	0.00	0.00	0.00	0.00	24.78	0.00	0.00	0.00
N-EIC-01	0.00	0.00	0.00	0.00	0.00	0.00	22.16	0.00	0.00	0.00
N-HEN-01	0.00	0.00	0.00	0.00	0.00	0.00	19.78	0.00	0.00	0.00
N-DOC-01	0.00	0.00	0.00	0.00	0.00	0.00	17.60	0.00	0.00	0.00
N-TRI-02	0.00	0.00	0.00	0.00	0.00	0.00	15.64	0.00	0.00	0.00
N-TET-02	0.00	0.00	0.00	0.00	0.00	0.00	13.87	0.00	0.00	0.00
N-PEN-02	0.00	0.00	0.00	0.00	0.00	0.00	12.28	0.00	0.00	0.00
N-HEX-02	0.00	0.00	0.00	0.00	0.00	0.00	10.85	0.00	0.00	0.00
N-HEP-02	0.00	0.00	0.00	0.00	0.00	0.00	9.57	0.00	0.00	0.00
N-OCT-02	0.00	0.00	0.00	0.00	0.00	0.00	8.44	0.00	0.00	0.00
N-NON-02	0.00	0.00	0.00	0.00	0.00	0.00	7.43	0.00	0.00	0.00
N-TRI-03	0.00	0.00	0.00	0.00	0.00	0.00	43.53	0.00	0.00	0.00
Mass Flow kg·h^{-1}	**1318.93**	**380.46**	**9420.25**	**209.59**	**58731.77**	**3055.22**	**705.91**	**3.73**	**9816.64**	**10964.59**

Table A.9 Input stream summary of PD-CHP2

PD-CHP2	INPUTS									
Mass Flow kg·h^{-1}	**BIOGAS (1)**	**WATER MU (11)**	**MEA MU (12)**	**H2 INPUT (16)**	**AIR CHP (17)**	**NOX STEAM (18)**	**WATER1 CHP (19)**	**WATER 2 CHP (20)**	**AIR (48)**	**WATER (50)**
MEA	0.00	0.00	0.05	0.00	0.00	0.00	0.00	0.00	0.00	0.00
H2O	0.00	1370.82	0.00	0.00	0.00	46365.03	10409.39	3002.71	0.00	12332.90
CO2	2250.75	0.00	0.00	0.00	14.34	0.00	0.00	0.00	3.40	0.00
H2S	0.00	0.00	0.00	0.00	0.00	0.00	0.00	0.00	0.00	0.00
H3O+	0.00	0.00	0.00	0.00	0.00	0.00	0.00	0.00	0.00	0.00
OH-	0.00	0.00	0.00	0.00	0.00	0.00	0.00	0.00	0.00	0.00
HCO3-	0.00	0.00	0.00	0.00	0.00	0.00	0.00	0.00	0.00	0.00
CO3-2	0.00	0.00	0.00	0.00	0.00	0.00	0.00	0.00	0.00	0.00
HS-	0.00	0.00	0.00	0.00	0.00	0.00	0.00	0.00	0.00	0.00
S-2	0.00	0.00	0.00	0.00	0.00	0.00	0.00	0.00	0.00	0.00
MEAH+	0.00	0.00	0.00	0.00	0.00	0.00	0.00	0.00	0.00	0.00
MEACOO-	0.00	0.00	0.00	0.00	0.00	0.00	0.00	0.00	0.00	0.00
N2	0.00	0.00	0.00	0.00	22701.33	0.00	0.00	0.00	5381.06	0.00
O2	0.00	0.00	0.00	0.00	6957.23	0.00	0.00	0.00	1649.12	0.00
CO	0.00	0.00	0.00	0.00	0.00	0.00	0.00	0.00	0.00	0.00
H2	0.00	0.00	0.00	574.75	0.00	0.00	0.00	0.00	0.00	0.00
CH4	1523.71	0.00	0.00	0.00	0.00	0.00	0.00	0.00	0.00	0.00
ARGON	0.00	0.00	0.00	0.00	387.22	0.00	0.00	0.00	91.79	0.00
ETHANE	0.00	0.00	0.00	0.00	0.00	0.00	0.00	0.00	0.00	0.00
PROPANE	0.00	0.00	0.00	0.00	0.00	0.00	0.00	0.00	0.00	0.00
BUTANE	0.00	0.00	0.00	0.00	0.00	0.00	0.00	0.00	0.00	0.00
PENTANE	0.00	0.00	0.00	0.00	0.00	0.00	0.00	0.00	0.00	0.00
HEXANE	0.00	0.00	0.00	0.00	0.00	0.00	0.00	0.00	0.00	0.00
HEPTANE	0.00	0.00	0.00	0.00	0.00	0.00	0.00	0.00	0.00	0.00
OCTANE	0.00	0.00	0.00	0.00	0.00	0.00	0.00	0.00	0.00	0.00
NONANE	0.00	0.00	0.00	0.00	0.00	0.00	0.00	0.00	0.00	0.00
DECANE	0.00	0.00	0.00	0.00	0.00	0.00	0.00	0.00	0.00	0.00
UNDECANE	0.00	0.00	0.00	0.00	0.00	0.00	0.00	0.00	0.00	0.00
N-DOD-01	0.00	0.00	0.00	0.00	0.00	0.00	0.00	0.00	0.00	0.00

Table A.9 (cont.) Input stream summary of PD-CHP2

PD-CHP2	INPUTS									
Mass Flow	**BIOGAS (1)**	**WATER MU (11)**	**MEA MU (12)**	**H2 INPUT (16)**	**AIR CHP (17)**	**NOX STEAM (18)**	**WATER1 CHP (19)**	**WATER 2 CHP (20)**	**AIR (48)**	**WATER (50)**
N-TRI-01	0.00	0.00	0.00	0.00	0.00	0.00	0.00	0.00	0.00	0.00
N-TET-01	0.00	0.00	0.00	0.00	0.00	0.00	0.00	0.00	0.00	0.00
N-PEN-01	0.00	0.00	0.00	0.00	0.00	0.00	0.00	0.00	0.00	0.00
N-HEX-01	0.00	0.00	0.00	0.00	0.00	0.00	0.00	0.00	0.00	0.00
N-HEP-01	0.00	0.00	0.00	0.00	0.00	0.00	0.00	0.00	0.00	0.00
N-OCT-01	0.00	0.00	0.00	0.00	0.00	0.00	0.00	0.00	0.00	0.00
N-NON-01	0.00	0.00	0.00	0.00	0.00	0.00	0.00	0.00	0.00	0.00
N-EIC-01	0.00	0.00	0.00	0.00	0.00	0.00	0.00	0.00	0.00	0.00
N-HEN-01	0.00	0.00	0.00	0.00	0.00	0.00	0.00	0.00	0.00	0.00
N-DOC-01	0.00	0.00	0.00	0.00	0.00	0.00	0.00	0.00	0.00	0.00
N-TRI-02	0.00	0.00	0.00	0.00	0.00	0.00	0.00	0.00	0.00	0.00
N-TET-02	0.00	0.00	0.00	0.00	0.00	0.00	0.00	0.00	0.00	0.00
N-PEN-02	0.00	0.00	0.00	0.00	0.00	0.00	0.00	0.00	0.00	0.00
N-HEX-02	0.00	0.00	0.00	0.00	0.00	0.00	0.00	0.00	0.00	0.00
N-HEP-02	0.00	0.00	0.00	0.00	0.00	0.00	0.00	0.00	0.00	0.00
N-OCT-02	0.00	0.00	0.00	0.00	0.00	0.00	0.00	0.00	0.00	0.00
N-NON-02	0.00	0.00	0.00	0.00	0.00	0.00	0.00	0.00	0.00	0.00
N-TRI-03	0.00	0.00	0.00	0.00	0.00	0.00	0.00	0.00	0.00	0.00
Mass Flow kg·h^{-1}	**3774.46**	**1370.82**	**0.05**	**574.75**	**30060.13**	**46365.03**	**10409.39**	**3002.71**	**7125.36**	**12332.90**

Table A.10 Output stream summary of PD-CHP2

PD-CHP2	OUTPUTS										
Mass Flow kg·h^{-1}	**CONDENSATE (6)**	**STEAM-A (21)**	**STEAM-B (22)**	**STEAM-C (23)**	**COND CHP (24)**	**FLASH COND (27)**	**FT COND (43)**	**FT SYNCR (47)**	**REST (46)**	**FLUEGAS (52)**	**STEAM (51)**
MEA	0.00	0.00	0.00	0.00	0.00	0.00	0.00	0.00	0.00	0.00	0.00
H2O	1288.19	1561.41	450.41	11152.17	248.12	49716.04	2883.90	0.00	0.56	1606.41	12332.90
CO2	2.45	0.00	0.00	0.00	0.00	0.39	0.00	0.00	0.16	4623.12	0.00
H2S	0.00	0.00	0.00	0.00	0.00	0.00	0.00	0.00	0.00	0.00	0.00
H3O+	0.00	0.00	0.00	0.00	0.00	0.00	0.00	0.00	0.00	0.00	0.00
OH-	0.00	0.00	0.00	0.00	0.00	0.00	0.00	0.00	0.00	0.00	0.00
HCO3-	3.95	0.00	0.00	0.00	0.00	0.00	0.00	0.00	0.00	0.00	0.00
CO3-2	0.00	0.00	0.00	0.00	0.00	0.00	0.00	0.00	0.00	0.00	0.00
HS-	0.00	0.00	0.00	0.00	0.00	0.00	0.00	0.00	0.00	0.00	0.00
S-2	0.00	0.00	0.00	0.00	0.00	0.00	0.00	0.00	0.00	0.00	0.00
MEAH+	4.02	0.00	0.00	0.00	0.00	0.00	0.00	0.00	0.00	0.00	0.00
MEACOO-	0.00	0.00	0.00	0.00	0.00	0.00	0.00	0.00	0.00	0.00	0.00
N2	0.00	0.00	0.00	0.00	0.00	0.01	0.00	0.00	0.14	28082.25	0.00
O2	0.00	0.00	0.00	0.00	0.00	0.01	0.00	0.00	0.01	3.78	0.00
CO	0.00	0.00	0.00	0.00	0.00	0.00	0.00	0.00	0.00	0.00	0.00
H2	0.00	0.00	0.00	0.00	0.00	0.00	0.00	0.00	0.00	0.00	0.00
CH4	0.00	0.00	0.00	0.00	0.00	0.00	0.00	0.00	0.00	0.00	0.00
ARGON	0.00	0.00	0.00	0.00	0.00	0.00	0.00	0.00	0.00	479.00	0.00
ETHANE	0.00	0.00	0.00	0.00	0.00	0.00	0.00	0.00	0.00	0.00	0.00
PROPANE	0.00	0.00	0.00	0.00	0.00	0.00	0.00	0.00	0.02	0.00	0.00
BUTANE	0.00	0.00	0.00	0.00	0.00	0.00	0.00	0.00	0.09	0.00	0.00
PENTANE	0.00	0.00	0.00	0.00	0.00	0.00	0.00	0.32	0.00	0.00	0.00
HEXANE	0.00	0.00	0.00	0.00	0.00	0.00	0.00	1.08	0.00	0.00	0.00
HEPTANE	0.00	0.00	0.00	0.00	0.00	0.00	0.00	3.39	0.00	0.00	0.00
OCTANE	0.00	0.00	0.00	0.00	0.00	0.00	0.00	9.57	0.00	0.00	0.00
NONANE	0.00	0.00	0.00	0.00	0.00	0.00	0.00	21.90	0.00	0.00	0.00
DECANE	0.00	0.00	0.00	0.00	0.00	0.00	0.00	36.95	0.00	0.00	0.00
UNDECANE	0.00	0.00	0.00	0.00	0.00	0.00	0.00	45.02	0.00	0.00	0.00
N-DOD-01	0.00	0.00	0.00	0.00	0.00	0.00	0.00	46.46	0.00	0.00	0.00

Table A.10 (cont.) Output stream summary of PD-CHP2

PD-CHP2	OUTPUTS										
Mass Flow kg·h^{-1}	**CONDENSATE (6)**	**STEAM-A (21)**	**STEAM-B (22)**	**STEAM-C (23)**	**COND CHP (24)**	**FLASH COND (27)**	**FT COND (43)**	**FT SYNCR (47)**	**REST (46)**	**FLUEGAS (52)**	**STEAM (51)**
N-TRI-01	0.00	0.00	0.00	0.00	0.00	0.00	0.00	44.33	0.00	0.00	0.00
N-TET-01	0.00	0.00	0.00	0.00	0.00	0.00	0.00	41.03	0.00	0.00	0.00
N-PEN-01	0.00	0.00	0.00	0.00	0.00	0.00	0.00	37.51	0.00	0.00	0.00
N-HEX-01	0.00	0.00	0.00	0.00	0.00	0.00	0.00	34.04	0.00	0.00	0.00
N-HEP-01	0.00	0.00	0.00	0.00	0.00	0.00	0.00	30.75	0.00	0.00	0.00
N-OCT-01	0.00	0.00	0.00	0.00	0.00	0.00	0.00	27.66	0.00	0.00	0.00
N-NON-01	0.00	0.00	0.00	0.00	0.00	0.00	0.00	24.81	0.00	0.00	0.00
N-EIC-01	0.00	0.00	0.00	0.00	0.00	0.00	0.00	22.19	0.00	0.00	0.00
N-HEN-01	0.00	0.00	0.00	0.00	0.00	0.00	0.00	19.80	0.00	0.00	0.00
N-DOC-01	0.00	0.00	0.00	0.00	0.00	0.00	0.00	17.63	0.00	0.00	0.00
N-TRI-02	0.00	0.00	0.00	0.00	0.00	0.00	0.00	15.66	0.00	0.00	0.00
N-TET-02	0.00	0.00	0.00	0.00	0.00	0.00	0.00	13.88	0.00	0.00	0.00
N-PEN-02	0.00	0.00	0.00	0.00	0.00	0.00	0.00	12.29	0.00	0.00	0.00
N-HEX-02	0.00	0.00	0.00	0.00	0.00	0.00	0.00	10.86	0.00	0.00	0.00
N-HEP-02	0.00	0.00	0.00	0.00	0.00	0.00	0.00	9.59	0.00	0.00	0.00
N-OCT-02	0.00	0.00	0.00	0.00	0.00	0.00	0.00	8.45	0.00	0.00	0.00
N-NON-02	0.00	0.00	0.00	0.00	0.00	0.00	0.00	7.44	0.00	0.00	0.00
N-TRI-03	0.00	0.00	0.00	0.00	0.00	0.00	0.00	43.59	0.00	0.00	0.00
Mass Flow kg·h^{-1}	**1298.61**	**1561.41**	**450.41**	**11152.17**	**248.12**	**49716.46**	**2883.90**	**586.20**	**0.99**	**34794.56**	**12332.90**

Table A.11 Input stream summary of PD-CHP2-OXY

PD-CHP2-OXY	INPUTS									
Mass Flow kg·h^{-1}	**BIOGAS (1)**	**WATER MU (11)**	**MEA MU (12)**	**H2 INPUT (16)**	**OXYGEN (17)**	**NOX STEAM (18)**	**WATER1 CHP (19)**	**WATER 2 CHP (20)**	**AIR (48)**	**WATER (50)**
MEA	0.00	0.00	0.05	0.00	0.00	0.00	0.00	0.00	0.00	0.00
H2O	0.00	1370.82	0.00	0.00	0.00	56175.54	2484.60	8613.26	0.00	10999.30
CO2	2250.75	0.00	0.00	0.00	0.00	0.00	0.00	0.00	2.87	0.00
H2S	0.00	0.00	0.00	0.00	0.00	0.00	0.00	0.00	0.00	0.00
H3O+	0.00	0.00	0.00	0.00	0.00	0.00	0.00	0.00	0.00	0.00
OH-	0.00	0.00	0.00	0.00	0.00	0.00	0.00	0.00	0.00	0.00
HCO3-	0.00	0.00	0.00	0.00	0.00	0.00	0.00	0.00	0.00	0.00
CO3-2	0.00	0.00	0.00	0.00	0.00	0.00	0.00	0.00	0.00	0.00
HS-	0.00	0.00	0.00	0.00	0.00	0.00	0.00	0.00	0.00	0.00
S-2	0.00	0.00	0.00	0.00	0.00	0.00	0.00	0.00	0.00	0.00
MEAH+	0.00	0.00	0.00	0.00	0.00	0.00	0.00	0.00	0.00	0.00
MEACOO-	0.00	0.00	0.00	0.00	0.00	0.00	0.00	0.00	0.00	0.00
N2	0.00	0.00	0.00	0.00	0.00	0.00	0.00	0.00	4549.84	0.00
O2	0.00	0.00	0.00	0.00	6778.63	0.00	0.00	0.00	1394.38	0.00
CO	0.00	0.00	0.00	0.00	0.00	0.00	0.00	0.00	0.00	0.00
H2	0.00	0.00	0.00	573.17	0.00	0.00	0.00	0.00	0.00	0.00
CH4	1523.71	0.00	0.00	0.00	0.00	0.00	0.00	0.00	0.00	0.00
ARGON	0.00	0.00	0.00	0.00	0.00	0.00	0.00	0.00	77.61	0.00
ETHANE	0.00	0.00	0.00	0.00	0.00	0.00	0.00	0.00	0.00	0.00
PROPANE	0.00	0.00	0.00	0.00	0.00	0.00	0.00	0.00	0.00	0.00
BUTANE	0.00	0.00	0.00	0.00	0.00	0.00	0.00	0.00	0.00	0.00
PENTANE	0.00	0.00	0.00	0.00	0.00	0.00	0.00	0.00	0.00	0.00
HEXANE	0.00	0.00	0.00	0.00	0.00	0.00	0.00	0.00	0.00	0.00
HEPTANE	0.00	0.00	0.00	0.00	0.00	0.00	0.00	0.00	0.00	0.00
OCTANE	0.00	0.00	0.00	0.00	0.00	0.00	0.00	0.00	0.00	0.00
NONANE	0.00	0.00	0.00	0.00	0.00	0.00	0.00	0.00	0.00	0.00
DECANE	0.00	0.00	0.00	0.00	0.00	0.00	0.00	0.00	0.00	0.00
UNDECANE	0.00	0.00	0.00	0.00	0.00	0.00	0.00	0.00	0.00	0.00
N-DOD-01	0.00	0.00	0.00	0.00	0.00	0.00	0.00	0.00	0.00	0.00
N-TRI-01	0.00	0.00	0.00	0.00	0.00	0.00	0.00	0.00	0.00	0.00
N-TET-01	0.00	0.00	0.00	0.00	0.00	0.00	0.00	0.00	0.00	0.00
N-PEN-01	0.00	0.00	0.00	0.00	0.00	0.00	0.00	0.00	0.00	0.00
N-HEX-01	0.00	0.00	0.00	0.00	0.00	0.00	0.00	0.00	0.00	0.00
N-HEP-01	0.00	0.00	0.00	0.00	0.00	0.00	0.00	0.00	0.00	0.00
N-OCT-01	0.00	0.00	0.00	0.00	0.00	0.00	0.00	0.00	0.00	0.00

Table A.11 (cont.) Input stream summary of PD-CHP2-OXY

PD-CHP2-OXY	INPUTS									
Mass Flow kg·h^{-1}	**BIOGAS (1)**	**WATER MU (11)**	**MEA MU (12)**	**H2 INPUT (16)**	**OXYGEN (17)**	**NOX STEAM (18)**	**WATER1 CHP (19)**	**WATER 2 CHP (20)**	**AIR (48)**	**WATER (50)**
N-NON-01	0.00	0.00	0.00	0.00	0.00	0.00	0.00	0.00	0.00	0.00
N-EIC-01	0.00	0.00	0.00	0.00	0.00	0.00	0.00	0.00	0.00	0.00
N-HEN-01	0.00	0.00	0.00	0.00	0.00	0.00	0.00	0.00	0.00	0.00
N-DOC-01	0.00	0.00	0.00	0.00	0.00	0.00	0.00	0.00	0.00	0.00
N-TRI-02	0.00	0.00	0.00	0.00	0.00	0.00	0.00	0.00	0.00	0.00
N-TET-02	0.00	0.00	0.00	0.00	0.00	0.00	0.00	0.00	0.00	0.00
N-PEN-02	0.00	0.00	0.00	0.00	0.00	0.00	0.00	0.00	0.00	0.00
N-HEX-02	0.00	0.00	0.00	0.00	0.00	0.00	0.00	0.00	0.00	0.00
N-HEP-02	0.00	0.00	0.00	0.00	0.00	0.00	0.00	0.00	0.00	0.00
N-OCT-02	0.00	0.00	0.00	0.00	0.00	0.00	0.00	0.00	0.00	0.00
N-NON-02	0.00	0.00	0.00	0.00	0.00	0.00	0.00	0.00	0.00	0.00
N-TRI-03	0.00	0.00	0.00	0.00	0.00	0.00	0.00	0.00	0.00	0.00
Mass Flow kg·h^{-1}	**3774.46**	**1370.82**	**0.05**	**573.17**	**6778.63**	**56175.54**	**2484.60**	**8613.26**	**6024.70**	**10999.30**

Table A.12 Output stream summary of PD-CHP2-OXY

PD-CHP2-OXY	OUTPUTS										
Mass Flow kg·h^{-1}	**CONDENSATE (6)**	**STEAM-A (21)**	**STEAM-B (22)**	**STEAM-C (23)**	**COND CHP (24)**	**FLASH COND (27)**	**FT COND (43)**	**FT SYNCR (47)**	**REST (46)**	**FLUEGAS (52)**	**STEAM (51)**
MEA	0.00	0.00	0.00	0.00	0.00	0.00	0.00	0.00	0.00	0.00	0.00
H2O	1288.19	1291.99	372.69	9227.87	205.31	59638.77	3061.34	0.00	0.81	1131.69	10999.30
CO2	2.45	0.00	0.00	0.00	0.00	3.71	0.04	0.00	1.65	4232.57	0.00
H2S	0.00	0.00	0.00	0.00	0.00	0.00	0.00	0.00	0.00	0.00	0.00
H3O+	0.00	0.00	0.00	0.00	0.00	0.00	0.00	0.00	0.00	0.00	0.00
OH-	0.00	0.00	0.00	0.00	0.00	0.00	0.00	0.00	0.00	0.00	0.00
HCO3-	3.95	0.00	0.00	0.00	0.00	0.00	0.00	0.00	0.00	0.00	0.00
CO3-2	0.00	0.00	0.00	0.00	0.00	0.00	0.00	0.00	0.00	0.00	0.00
HS-	0.00	0.00	0.00	0.00	0.00	0.00	0.00	0.00	0.00	0.00	0.00
S-2	0.00	0.00	0.00	0.00	0.00	0.00	0.00	0.00	0.00	0.00	0.00
MEAH+	4.02	0.00	0.00	0.00	0.00	0.00	0.00	0.00	0.00	0.00	0.00
MEACOO-	0.00	0.00	0.00	0.00	0.00	0.00	0.00	0.00	0.00	0.00	0.00
N2	0.00	0.00	0.00	0.00	0.00	0.00	0.00	0.00	0.00	4549.85	0.00
O2	0.00	0.00	0.00	0.00	0.00	0.09	0.00	0.00	0.07	4.02	0.00
CO	0.00	0.00	0.00	0.00	0.00	0.00	0.00	0.00	0.04	0.00	0.00
H2	0.00	0.00	0.00	0.00	0.00	0.00	0.00	0.00	0.00	0.00	0.00
CH4	0.00	0.00	0.00	0.00	0.00	0.00	0.00	0.00	0.01	0.00	0.00
ARGON	0.00	0.00	0.00	0.00	0.00	0.00	0.00	0.00	0.00	77.61	0.00
ETHANE	0.00	0.00	0.00	0.00	0.00	0.00	0.00	0.00	0.05	0.00	0.00
PROPANE	0.00	0.00	0.00	0.00	0.00	0.00	0.00	0.00	0.22	0.00	0.00
BUTANE	0.00	0.00	0.00	0.00	0.00	0.00	0.00	0.00	0.89	0.00	0.00
PENTANE	0.00	0.00	0.00	0.00	0.00	0.00	0.00	3.18	0.00	0.00	0.00
HEXANE	0.00	0.00	0.00	0.00	0.00	0.00	0.00	9.85	0.00	0.00	0.00
HEPTANE	0.00	0.00	0.00	0.00	0.00	0.00	0.00	23.77	0.00	0.00	0.00
OCTANE	0.00	0.00	0.00	0.00	0.00	0.00	0.00	41.19	0.00	0.00	0.00
NONANE	0.00	0.00	0.00	0.00	0.00	0.00	0.00	51.47	0.00	0.00	0.00
DECANE	0.00	0.00	0.00	0.00	0.00	0.00	0.00	53.84	0.00	0.00	0.00
UNDECANE	0.00	0.00	0.00	0.00	0.00	0.00	0.00	51.98	0.00	0.00	0.00
N-DOD-01	0.00	0.00	0.00	0.00	0.00	0.00	0.00	48.70	0.00	0.00	0.00
N-TRI-01	0.00	0.00	0.00	0.00	0.00	0.00	0.00	44.96	0.00	0.00	0.00
N-TET-01	0.00	0.00	0.00	0.00	0.00	0.00	0.00	41.17	0.00	0.00	0.00
N-PEN-01	0.00	0.00	0.00	0.00	0.00	0.00	0.00	37.49	0.00	0.00	0.00
N-HEX-01	0.00	0.00	0.00	0.00	0.00	0.00	0.00	33.97	0.00	0.00	0.00
N-HEP-01	0.00	0.00	0.00	0.00	0.00	0.00	0.00	30.67	0.00	0.00	0.00
N-OCT-01	0.00	0.00	0.00	0.00	0.00	0.00	0.00	27.59	0.00	0.00	0.00

Table A.12 (cont.) Output stream summary of PD-CHP2-OXY

PD-CHP2-OXY	OUTPUTS										
Mass Flow kg·h^{-1}	**CONDENSATE (6)**	**STEAM-A (21)**	**STEAM-B (22)**	**STEAM-C (23)**	**COND CHP (24)**	**FLASH COND (27)**	**FT COND (43)**	**FT SYNCR (47)**	**REST (46)**	**FLUEGAS (52)**	**STEAM (51)**
N-NON-01	0.00	0.00	0.00	0.00	0.00	0.00	0.00	24.74	0.00	0.00	0.00
N-EIC-01	0.00	0.00	0.00	0.00	0.00	0.00	0.00	22.13	0.00	0.00	0.00
N-HEN-01	0.00	0.00	0.00	0.00	0.00	0.00	0.00	19.75	0.00	0.00	0.00
N-DOC-01	0.00	0.00	0.00	0.00	0.00	0.00	0.00	17.58	0.00	0.00	0.00
N-TRI-02	0.00	0.00	0.00	0.00	0.00	0.00	0.00	15.62	0.00	0.00	0.00
N-TET-02	0.00	0.00	0.00	0.00	0.00	0.00	0.00	13.85	0.00	0.00	0.00
N-PEN-02	0.00	0.00	0.00	0.00	0.00	0.00	0.00	12.26	0.00	0.00	0.00
N-HEX-02	0.00	0.00	0.00	0.00	0.00	0.00	0.00	10.83	0.00	0.00	0.00
N-HEP-02	0.00	0.00	0.00	0.00	0.00	0.00	0.00	9.56	0.00	0.00	0.00
N-OCT-02	0.00	0.00	0.00	0.00	0.00	0.00	0.00	8.43	0.00	0.00	0.00
N-NON-02	0.00	0.00	0.00	0.00	0.00	0.00	0.00	7.42	0.00	0.00	0.00
N-TRI-03	0.00	0.00	0.00	0.00	0.00	0.00	0.00	43.47	0.00	0.00	0.00
Mass Flow kg·h^{-1}	**1298.61**	**1291.99**	**372.69**	**9227.87**	**205.31**	**59642.57**	**3061.38**	**705.45**	**3.75**	**9995.73**	**10999.30**

Table A.13 Input stream summary of PD-CHP1-POST

PD-CHP1-POST	INPUTS									
Mass Flow kg·h^{-1}	**BIOGAS (1)**	**AIR CHP (2)**	**NOX STEAM (3)**	**WATER1 CHP (4)**	**WATER 2 CHP (5)**	**WATER MU (25)**	**MEA MU (26)**	**H2 INPUT (27)**	**AIR (46)**	**WATER (48)**
H2O	0.00	0.00	45521.15	10590.12	3054.84	2644.09	0.00	0.00	0.00	9633.35
N2	0.00	22754.33	0.00	0.00	0.00	0.00	0.00	0.00	6037.28	0.00
O2	0.00	6973.48	0.00	0.00	0.00	0.00	0.00	0.00	1850.24	0.00
CO	0.00	0.00	0.00	0.00	0.00	0.00	0.00	0.00	0.00	0.00
CO2	2250.75	14.38	0.00	0.00	0.00	0.00	0.00	0.00	3.81	0.00
ARGON	0.00	388.13	0.00	0.00	0.00	0.00	0.00	0.00	102.98	0.00
CH4	1523.71	0.00	0.00	0.00	0.00	0.00	0.00	0.00	0.00	0.00
ETHANE	0.00	0.00	0.00	0.00	0.00	0.00	0.00	0.00	0.00	0.00
PROPANE	0.00	0.00	0.00	0.00	0.00	0.00	0.00	0.00	0.00	0.00
H2	0.00	0.00	0.00	0.00	0.00	0.00	0.00	517.92	0.00	0.00
BUTANE	0.00	0.00	0.00	0.00	0.00	0.00	0.00	0.00	0.00	0.00
PENTANE	0.00	0.00	0.00	0.00	0.00	0.00	0.00	0.00	0.00	0.00
HEXANE	0.00	0.00	0.00	0.00	0.00	0.00	0.00	0.00	0.00	0.00
HEPTANE	0.00	0.00	0.00	0.00	0.00	0.00	0.00	0.00	0.00	0.00
OCTANE	0.00	0.00	0.00	0.00	0.00	0.00	0.00	0.00	0.00	0.00
NONANE	0.00	0.00	0.00	0.00	0.00	0.00	0.00	0.00	0.00	0.00
DECANE	0.00	0.00	0.00	0.00	0.00	0.00	0.00	0.00	0.00	0.00
UNDECANE	0.00	0.00	0.00	0.00	0.00	0.00	0.00	0.00	0.00	0.00
N-DOD-01	0.00	0.00	0.00	0.00	0.00	0.00	0.00	0.00	0.00	0.00
N-TRI-01	0.00	0.00	0.00	0.00	0.00	0.00	0.00	0.00	0.00	0.00
N-TET-01	0.00	0.00	0.00	0.00	0.00	0.00	0.00	0.00	0.00	0.00
N-PEN-01	0.00	0.00	0.00	0.00	0.00	0.00	0.00	0.00	0.00	0.00
N-HEX-01	0.00	0.00	0.00	0.00	0.00	0.00	0.00	0.00	0.00	0.00
N-HEP-01	0.00	0.00	0.00	0.00	0.00	0.00	0.00	0.00	0.00	0.00
N-OCT-01	0.00	0.00	0.00	0.00	0.00	0.00	0.00	0.00	0.00	0.00
N-NON-01	0.00	0.00	0.00	0.00	0.00	0.00	0.00	0.00	0.00	0.00
N-EIC-01	0.00	0.00	0.00	0.00	0.00	0.00	0.00	0.00	0.00	0.00
N-HEN-01	0.00	0.00	0.00	0.00	0.00	0.00	0.00	0.00	0.00	0.00
N-DOC-01	0.00	0.00	0.00	0.00	0.00	0.00	0.00	0.00	0.00	0.00
N-TRI-02	0.00	0.00	0.00	0.00	0.00	0.00	0.00	0.00	0.00	0.00
N-TET-02	0.00	0.00	0.00	0.00	0.00	0.00	0.00	0.00	0.00	0.00
N-PEN-02	0.00	0.00	0.00	0.00	0.00	0.00	0.00	0.00	0.00	0.00
N-HEX-02	0.00	0.00	0.00	0.00	0.00	0.00	0.00	0.00	0.00	0.00
N-HEP-02	0.00	0.00	0.00	0.00	0.00	0.00	0.00	0.00	0.00	0.00
N-OCT-02	0.00	0.00	0.00	0.00	0.00	0.00	0.00	0.00	0.00	0.00
N-NON-02	0.00	0.00	0.00	0.00	0.00	0.00	0.00	0.00	0.00	0.00
N-TRI-03	0.00	0.00	0.00	0.00	0.00	0.00	0.00	0.00	0.00	0.00
N-HEN-02	0.00	0.00	0.00	0.00	0.00	0.00	0.00	0.00	0.00	0.00
H2S	0.00	0.00	0.00	0.00	0.00	0.00	0.00	0.00	0.00	0.00
MEA	0.00	0.00	0.00	0.00	0.00	0.00	0.60	0.00	0.00	0.00
H3O+	0.00	0.00	0.00	0.00	0.00	0.00	0.00	0.00	0.00	0.00
OH-	0.00	0.00	0.00	0.00	0.00	0.00	0.00	0.00	0.00	0.00
HCO3-	0.00	0.00	0.00	0.00	0.00	0.00	0.00	0.00	0.00	0.00
CO3-2	0.00	0.00	0.00	0.00	0.00	0.00	0.00	0.00	0.00	0.00
HS-	0.00	0.00	0.00	0.00	0.00	0.00	0.00	0.00	0.00	0.00
S-2	0.00	0.00	0.00	0.00	0.00	0.00	0.00	0.00	0.00	0.00
MEAH+	0.00	0.00	0.00	0.00	0.00	0.00	0.00	0.00	0.00	0.00
MEACOO-	0.00	0.00	0.00	0.00	0.00	0.00	0.00	0.00	0.00	0.00
Mass Flow kg·h^{-1}	**3774.46**	**30130.31**	**45521.15**	**10590.12**	**3054.84**	**2644.09**	**0.60**	**517.92**	**7994.31**	**9633.35**

Table A.14 Output stream summary of PD-CHP1-POST

PD-CHP1-POST	OUTPUTS											
Mass Flow kg·h^{-1}	**STEAM-A (7)**	**STEAM-B (8)**	**STEAM-C (9)**	**COND CHP (6)**	**CHP FG (15)**	**COND. (20)**	**FLASH (12)**	**FT COND (42)**	**FT SYNCR (45)**	**REST (44)**	**FG (50)**	**STEAM (49)**
H2O	1588.52	458.23	11345.79	252.43	743.90	1989.88	48807.66	2789.04	0.00	0.76	992.53	9633.35
N2	0.00	0.00	0.00	0.00	22746.12	0.00	0.01	0.00	0.00	0.00	6045.48	0.00
O2	0.00	0.00	0.00	0.00	894.50	0.00	0.01	0.00	0.00	0.00	0.06	0.00
CO	0.00	0.00	0.00	0.00	0.00	0.00	0.00	0.00	0.00	0.04	0.00	0.00
CO2	0.00	0.00	0.00	0.00	644.13	3.79	0.55	0.04	0.00	1.87	3783.25	0.00
ARGON	0.00	0.00	0.00	0.00	387.84	0.00	0.00	0.00	0.00	0.00	103.26	0.00
CH4	0.00	0.00	0.00	0.00	0.00	0.00	0.00	0.00	0.00	0.01	0.00	0.00
ETHANE	0.00	0.00	0.00	0.00	0.00	0.00	0.00	0.00	0.00	0.05	0.00	0.00
PROPANE	0.00	0.00	0.00	0.00	0.00	0.00	0.00	0.00	0.00	0.25	0.00	0.00
H2	0.00	0.00	0.00	0.00	0.00	0.00	0.00	0.00	0.00	0.00	0.00	0.00
BUTANE	0.00	0.00	0.00	0.00	0.00	0.00	0.00	0.00	0.00	1.01	0.00	0.00
PENTANE	0.00	0.00	0.00	0.00	0.00	0.00	0.00	0.00	3.56	0.00	0.00	0.00
HEXANE	0.00	0.00	0.00	0.00	0.00	0.00	0.00	0.00	10.75	0.00	0.00	0.00
HEPTANE	0.00	0.00	0.00	0.00	0.00	0.00	0.00	0.00	24.64	0.00	0.00	0.00
OCTANE	0.00	0.00	0.00	0.00	0.00	0.00	0.00	0.00	40.01	0.00	0.00	0.00
NONANE	0.00	0.00	0.00	0.00	0.00	0.00	0.00	0.00	47.89	0.00	0.00	0.00
DECANE	0.00	0.00	0.00	0.00	0.00	0.00	0.00	0.00	49.14	0.00	0.00	0.00
UNDECANE	0.00	0.00	0.00	0.00	0.00	0.00	0.00	0.00	47.12	0.00	0.00	0.00
N-DOD-01	0.00	0.00	0.00	0.00	0.00	0.00	0.00	0.00	44.05	0.00	0.00	0.00
N-TRI-01	0.00	0.00	0.00	0.00	0.00	0.00	0.00	0.00	40.64	0.00	0.00	0.00
N-TET-01	0.00	0.00	0.00	0.00	0.00	0.00	0.00	0.00	37.21	0.00	0.00	0.00
N-PEN-01	0.00	0.00	0.00	0.00	0.00	0.00	0.00	0.00	33.88	0.00	0.00	0.00
N-HEX-01	0.00	0.00	0.00	0.00	0.00	0.00	0.00	0.00	30.70	0.00	0.00	0.00
N-HEP-01	0.00	0.00	0.00	0.00	0.00	0.00	0.00	0.00	27.71	0.00	0.00	0.00
N-OCT-01	0.00	0.00	0.00	0.00	0.00	0.00	0.00	0.00	24.93	0.00	0.00	0.00
N-NON-01	0.00	0.00	0.00	0.00	0.00	0.00	0.00	0.00	22.36	0.00	0.00	0.00
N-EIC-01	0.00	0.00	0.00	0.00	0.00	0.00	0.00	0.00	20.00	0.00	0.00	0.00
N-HEN-01	0.00	0.00	0.00	0.00	0.00	0.00	0.00	0.00	17.84	0.00	0.00	0.00
N-DOC-01	0.00	0.00	0.00	0.00	0.00	0.00	0.00	0.00	15.88	0.00	0.00	0.00

Table A.14 (cont.) Output stream summary of PD-CHP1-POST

PD-CHP1-POST	OUTPUTS											
Mass Flow	**STEAM-A (7)**	**STEAM-B (8)**	**STEAM-C (9)**	**COND CHP (6)**	**CHP FG (15)**	**COND. (20)**	**FLASH (12)**	**FT COND (42)**	**FT SYNCR (45)**	**REST (44)**	**FG (50)**	**STEAM (49)**
N-TRI-02	0.00	0.00	0.00	0.00	0.00	0.00	0.00	0.00	14.11	0.00	0.00	0.00
N-TET-02	0.00	0.00	0.00	0.00	0.00	0.00	0.00	0.00	12.51	0.00	0.00	0.00
N-PEN-02	0.00	0.00	0.00	0.00	0.00	0.00	0.00	0.00	11.08	0.00	0.00	0.00
N-HEX-02	0.00	0.00	0.00	0.00	0.00	0.00	0.00	0.00	9.79	0.00	0.00	0.00
N-HEP-02	0.00	0.00	0.00	0.00	0.00	0.00	0.00	0.00	8.64	0.00	0.00	0.00
N-OCT-02	0.00	0.00	0.00	0.00	0.00	0.00	0.00	0.00	7.61	0.00	0.00	0.00
N-NON-02	0.00	0.00	0.00	0.00	0.00	0.00	0.00	0.00	6.70	0.00	0.00	0.00
N-TRI-03	0.00	0.00	0.00	0.00	0.00	0.00	0.00	0.00	39.28	0.00	0.00	0.00
N-HEN-02	0.00	0.00	0.00	0.00	0.00	0.00	0.00	0.00	0.00	0.00	0.00	0.00
H2S	0.00	0.00	0.00	0.00	0.00	0.00	0.00	0.00	0.00	0.00	0.00	0.00
MEA	0.00	0.00	0.00	0.00	0.59	0.00	0.00	0.00	0.00	0.00	0.00	0.00
H3O+	0.00	0.00	0.00	0.00	0.00	0.00	0.00	0.00	0.00	0.00	0.00	0.00
OH-	0.00	0.00	0.00	0.00	0.00	0.00	0.00	0.00	0.00	0.00	0.00	0.00
HCO3-	0.00	0.00	0.00	0.00	0.00	4.56	0.00	0.00	0.00	0.00	0.00	0.00
CO3-2	0.00	0.00	0.00	0.00	0.00	0.00	0.00	0.00	0.00	0.00	0.00	0.00
HS-	0.00	0.00	0.00	0.00	0.00	0.00	0.00	0.00	0.00	0.00	0.00	0.00
S-2	0.00	0.00	0.00	0.00	0.00	0.00	0.00	0.00	0.00	0.00	0.00	0.00
MEAH+	0.00	0.00	0.00	0.00	0.00	4.64	0.00	0.00	0.00	0.00	0.00	0.00
MEACOO-	0.00	0.00	0.00	0.00	0.00	0.00	0.00	0.00	0.00	0.00	0.00	0.00
Mass Flow kg·h^{-1}	**1588.52**	**458.23**	**11345.79**	**252.43**	**25417.09**	**2002.86**	**48808.24**	**2789.08**	**648.03**	**3.99**	**10924.57**	**9633.35**

Table A.15 Stream summary of upgrading process using $[C_2MIm][Tf_2N]$

$[C_2MIm][Tf_2N]$	INPUTS	OUTPUT	
Mass Flow kg·h^{-1}	**BIOGAS (1)***	**BIO-METHANE (5)**	**CO2 OUT (6)**
CH4	1523.71	1330.10	193.59
CO2	2250.75	192.04	2056.89
C2MIMNTF	0.00	0.00	0.00
TOTAL (kg·h^{-1})	**3774.46**	**1522.14**	**2250.48**

Table A.16 Stream summary of upgrading process using $[C_6MIm][Tf_2N]$

$[C_6MIm][Tf_2N]$	INPUTS	OUTPUT	
Mass Flow kg·h^{-1}	**BIOGAS (1)**	**BIO-METHANE (5)**	**CO2 OUT (6)**
CH4	1523.709	1271.346	252.336
CO2	2250.749	183.561	2065.454
C6MIMNTF	0.00	0.00	0.00
TOTAL (kg·h^{-1})	**3774.46**	**1454.91**	**2317.79**

Table A.17 Stream summary of upgrading process using $[P_{66614}][Tf_2N]$

$[P_{66614}][Tf_2N]$	INPUTS	OUTPUT	
Mass Flow kg·h^{-1}	**BIOGAS (1)**	**BIO-METHANE (5)**	**CO2 OUT (6)**
CH4	1523.709	1104.176	419.468
CO2	2250.749	159.425	2089.77
C6MIMNTF	0.00	0.00	0.00
TOTAL (kg·h^{-1})	**3774.46**	**1263.60**	**2509.24**

***Stream numbers refer to flowsheet shown in Fig. 3.9

Appendix B. Catalyst cost

The calculations described below refer to the PD-MEA1 process concept for illustrative purposes. The catalyst costs for the rest of the process concepts are calculated using the same methodology.

a) FT reactor

The volume of the catalyst bed, V is calculated using hourly space velocity, $GHSV$ and actual volumetric flow rate, ν_0; (Swanson, 2009).

$$GHSV = \frac{\nu_0}{V}$$

$$GHSV_{FT}\,(STP) = 1{,}000\ h^{-1} \qquad \text{(Assumed)}$$

$$STP = Standard\ Temperature\ and\ Pressure\ (IUPAC), i.e.\ 0\ °C\ and\ 1\ bar$$

$$\nu_{0\_FT} = 562.44\ m^3 \cdot h^{-1}\ @\ 220\ °C\ and\ 30\ bar \qquad \text{(From Aspen)}$$

Using,

(1) Charles' Law: $\frac{V_1}{T_2} = \frac{V_2}{T_2}$

(2) Boyle's Law: $P_1V_1 = P_2V_2$

to convert ν_{0_FT} to STP:

$$V_{FT} = \frac{\nu_{0\_FT}\,(STP)}{GHSV_{FT}\,(STP)}$$

$$V_{FT} = 9.35\ m^3$$

<u>Catalyst costs</u>

$Cost_{CAT\_FT} = 22\ £ \cdot kg^{-1}$ (Swanson, 2010b) $\rho_{CAT\_FT} = 1025\ kg \cdot m^{-3}$ (Swanson, 2009)

$$\boldsymbol{COST_{CAT\ BED\_FT}} = 9.35\ m^3 \cdot 22\ £ \cdot kg^{-1} \cdot 1025\ kg \cdot m^{-3} = \mathbf{210,747.36}\ £$$

b) RWGS reactor

$$GHSV = \frac{\nu_0}{V}$$

$$GHSV_{RGWS}\,(STP) = 3{,}000\ h^{-1} \qquad \text{(Park } \textit{et al.}\text{, 2004)}$$

$$STP = Standard\ Temperature\ and\ Pressure\ (IUPAC), i.e.\ 0\ °C\ and\ 1\ bar$$

$$\nu_{0\_RGWS} = 13{,}975.41\ m^3 \cdot h^{-1}\ @\ 650\ °C\ and\ 1\ atm \qquad \text{(From Aspen)}$$

Using,

(3) Charles' Law: $\frac{V_1}{T_2} = \frac{V_2}{T_2}$

(4) Boyle's Law: $P_1V_1 = P_2V_2$

to convert ν_{0_RGWS} to STP:

$$V_{RWGS} = \frac{\nu_{0\_RGWS}\,(STP)}{GHSV_{RGWS}\,(STP)}$$

$$V_{RWGS} = 1.40\ m^3$$

Catalyst costs

$Cost_{CAT\_RWGS} = 22\ £ \cdot kg^{-1}$ (Swanson, 2010b) $\rho_{CAT\_RWGS} = 1025\ kg \cdot m^{-3}$ (Swanson, 2009)

$$\boldsymbol{COST_{CAT\ BED\_RWGS}} = 1.40\ m^3 \cdot 22\ £ \cdot kg^{-1} \cdot 1025\ kg \cdot m^{-3} = \mathbf{31,494.55}\ £$$

c) SMR reactor

$$GHSV = \frac{\nu_0}{V}$$

$$GHSV_{SMR}\,(STP) = 2{,}600\ h^{-1} \qquad \text{(Swanson, 2009)}$$

$$STP = Standard\ Temperature\ and\ Pressure\ (IUPAC), i.e.\ 0\ °C\ and\ 1\ bar$$

$$\nu_{0\_SMR} = 797.29\ m^3 \cdot h^{-1}\ @\ 850\ °C\ and\ 25\ bar \qquad \text{(From Aspen)}$$

Using,

(5) Charles' Law: $\frac{V_1}{T_2} = \frac{V_2}{T_2}$

(6) Boyle's Law: $P_1V_1 = P_2V_2$

to convert ν_{0_SMR} to STP:

$$V_{SMR} = \frac{\nu_{0\_SMR}\,(STP)}{GHSV_{SMR}\,(STP)}$$

$$V_{SMR} = 1.86\ m^3$$

Catalyst costs

$Cost_{CAT\_SMR} = 22\ £ \cdot kg^{-1}$ (Swanson, 2010b) $\rho_{CAT\_SMR} = 1025\ kg \cdot m^{-3}$ (Swanson, 2009)

$$\boldsymbol{COST_{CAT\ BED\_SMR}} = 1.86\ m^3 \cdot 22\ £ \cdot kg^{-1} \cdot 1025\ kg \cdot m^{-3} = \mathbf{42{,}042.94}\ £$$

Appendix C. PSA bed cost

The calculations described below refer to the PD-MEA1 process concept for illustrative purposes. The PSA bed costs for the rest of the process concepts are calculated using the same methodology.

The PSA bed is assumed to be made of the molecular sieve (1/3) and activated carbon (2/3), according to the work by Swanson (2009). The adsorption capacity of the bed is estimated from Fig. C.1 as a function of the adsorbed gases' partial pressure (Swanson, 2009).

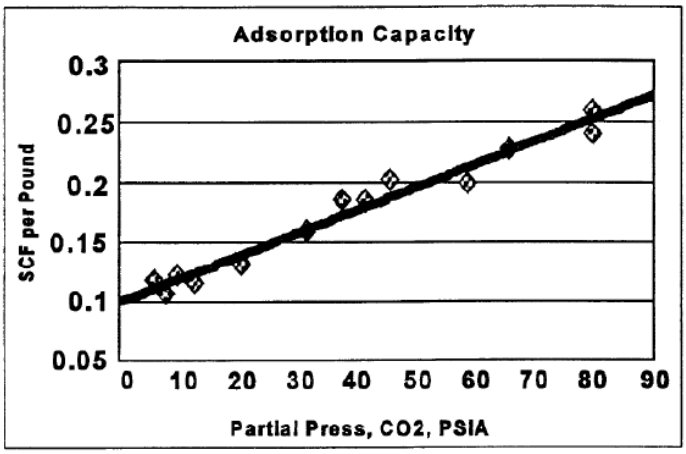

Fig. C.1 Molecular sieve adsorption capacity as a function of partial pressure

The adsorption capacity estimated from Fig. C.1 is in Standard Cubic Feet per pound (SCF/lb); therefore P and T are corrected to the actual adsorption conditions (10 bar and 483 °C) using Charles' Law and Boyle's Law.

Volumetric flowrate of syngas (from Aspen): $v_{0_{SYNGAS}}(10\ bar\ and\ 483\ °C) = 709.40\ m^3 \cdot h^{-1}$

Molar fraction of adsorbed gases (from Aspen): $x_{ads} = 0.39$

Volumetric flowrate of adsorbed gases: $v_{0_{ads}} = 709.40\ m^3 \cdot h^{-1} \cdot 0.39 = 276.67\ m^3 \cdot h^{-1}$

Assuming a adsorption/desorption cycle time of 5 minutes (Swanson, 2009), the mass of molecular sieve required is given by,

$$Mass_{MolSieve} = \frac{\nu_{0_{ads}} \cdot Cycle\ time}{Ads_{Cap}} = \frac{276.67\ m^3 \cdot h^{-1} \cdot \left({}^{5min}/_{60min}\right)}{0.0017\ m^3 \cdot kg^{-1}}$$
$$= 13{,}562.25\ kg$$

Since the bed is bed is 1/3 molsieve and 2/3 activated carbon,

$$Mass_{Bed} = 3 \cdot 13{,}562.25\ kg = 40{,}686.77\ kg$$

Assuming a packing bed cost of 3 £·kg^{-1}; Swanson (2009),

$$\boldsymbol{COST_{Bed}} = 40{,}686.77\ kg \cdot 3\ £ \cdot kg^{-1} = \mathbf{122{,}060.31}\ £$$

Appendix D. Cost results

Appendix D.1 Total Capital Investment (TCI) of the evaluated CCU process designs

PD-MEA1

Table D.1 TCI costs results of the PD-MEA1 design

TCI		
Direct Cost		COST (£)
	Purchased equipment	4534725
	Equipment installation	2131321
	Instrumentation and control	1632501
	Piping	3083613
	Electrical	498820
	Building and building services	816251
	Yard improvements	453473
	Service facilities	3174308
	Total Direct Cost	16325010
Indirect Cost		
	Engineering	1496460
	Construction expenses	1859238
	Legal costs	181389
	Contractor's fee	997640
	Contingency	1995279
	Total Indirect Cost	6530004
	FCI	**22855014**
Working investment		4059143
MEA cost		22620
MEA requirements	22619.6	kg
MEA cost (£·kg^{-1})	1	
	TCI	**£26,936,777**

PD-MEA2

Table D.2 TCI costs results of the PD-MEA2 design

TCI		
Direct Cost		COST (£)
	Purchased equipment	3444025
	Equipment installation	1618692
	Instrumentation and control	1239849
	Piping	2341937
	Electrical	378843
	Building and building services	619925
	Yard improvements	344403
	Service facilities	2410818
	Total Direct Cost	12398490
Indirect Cost		
	Engineering	1136529
	Construction expenses	1412050
	Legal costs	137761
	Contractor's fee	757686
	Contingency	1515371
	Total Indirect Cost	4959396
	FCI	**17357886**
Working investment		3673253
MEA cost		22620
MEA requirements	22619.6	kg
MEA cost (£·kg^{-1})	1	
	TCI	**£21,053,758**

PD-CHP1

Table D.3 TCI costs results of the PD-CHP1 design

TCI		
Direct Cost		COST (£)
	Purchased equipment	9919763
	Equipment installation	4662289
	Instrumentation and control	3571115
	Piping	6745439
	Electrical	1091174
	Building and building services	1785557
	Yard improvements	991976
	Service facilities	6943834
	Total Direct Cost	35711146
Indirect Cost		
	Engineering	3273522
	Construction expenses	4067103
	Legal costs	396791
	Contractor's fee	2182348
	Contingency	4364696
	Total Indirect Cost	14284458
	FCI	**49995604**
Working investment		8811317
MEA cost		0
MEA requirements	0	kg
MEA cost (£·kg^{-1})	1	
	TCI	**£58,806,922**

PD-CHP1-OXY

Table D.4 TCI costs results of the PD-CHP1-OXY design

TCI		
Direct Cost		COST (£)
	Purchased equipment	8194361
	Equipment installation	3851350
	Instrumentation and control	2949970
	Piping	5572166
	Electrical	901380
	Building and building services	1474985
	Yard improvements	819436
	Service facilities	5736053
	Total Direct Cost	29499701
Indirect Cost		
	Engineering	2704139
	Construction expenses	3359688
	Legal costs	327775
	Contractor's fee	1802760
	Contingency	3605519
	Total Indirect Cost	11799881
	FCI	**41299582**
Working investment		7310670
MEA cost		0
MEA requirements	0	kg
MEA cost (£·kg^{-1})	1	
	TCI	**£48,610,252**

PD-CHP2

Table D.5 TCI costs results of the PD-CHP2 design

TCI		
Direct Cost		COST (£)
	Purchased equipment	10296349
	Equipment installation	4839284
	Instrumentation and control	3706684
	Piping	7001517
	Electrical	1132598
	Building and building services	1853343
	Yard improvements	1029635
	Service facilities	7207444
	Total Direct Cost	37066856
Indirect Cost		
	Engineering	3397795
	Construction expenses	4221503
	Legal costs	411854
	Contractor's fee	2265197
	Contingency	4530394
	Total Indirect Cost	14826742
	FCI	**51893598**
Working investment		9156443
MEA cost		22620
MEA requirements	22619.6	kg
MEA cost (£·kg^{-1})	1	
	TCI	**£61,072,661**

PD-CHP2-OXY

Table D.6 TCI costs results of the PD-CHP2-OXY design

TCI		
Direct Cost		COST (£)
	Purchased equipment	8828527
	Equipment installation	4149408
	Instrumentation and control	3178270
	Piping	6003398
	Electrical	971138
	Building and building services	1589135
	Yard improvements	882853
	Service facilities	6179969
	Total Direct Cost	31782697
Indirect Cost		
	Engineering	2913414
	Construction expenses	3619696
	Legal costs	353141
	Contractor's fee	1942276
	Contingency	3884552
	Total Indirect Cost	12713079
	FCI	**44495776**
Working investment		7849425
MEA cost		22620
MEA requirements	22619.6	kg
MEA cost (£·kg^{-1})	1	
	TCI	**£52,367,820**

PD-CHP1-POST

Table D.7 TCI costs results of the PD-CHP1-POST design

TCI		
Direct Cost		COST (£)
	Purchased equipment	8975263
	Equipment installation	4218374
	Instrumentation and control	3231095
	Piping	6103179
	Electrical	987279
	Building and building services	1615547
	Yard improvements	897526
	Service facilities	6282684
	Total Direct Cost	32310946
Indirect Cost		
	Engineering	2961837
	Construction expenses	3679858
	Legal costs	359011
	Contractor's fee	1974558
	Contingency	3949116
	Total Indirect Cost	12924378
	FCI	**45235324**
Working investment		7989651
MEA cost		49661
MEA requirements	49660.4	kg
MEA cost (£·kg^{-1})	1	
	TCI	**£53,274,635**

Appendix D.2 Total Capital Investment (TCI) of the evaluated ionic liquid and MEA-based CO_2 capture processes

$[C_2MIm][Tf_2N]$

Table D.8 TCI costs results of the $[C_2MIm][Tf_2N]$ CO_2 capture design

TIC		
Direct Cost		COST (£)
	Purchased equipment	1519000
	Equipment installation	713930
	Instrumentation and control	546840
	Piping	1032920
	Electrical	167090
	Building and building services	273420
	Yard improvements	151900
	Service facilities	1063300
	Total Direct Cost	5468400
Indirect Cost		
	Engineering	501270
	Construction expenses	622790
	Legal costs	60760
	Contractor's fee	334180
	Contingency	668360
	Total Indirect Cost	2187360
	FCI	**7655760**
Working investment		1481674
IL cost		740970
IL requirements	56997.6	kg
IL Cost (£·kg^{-1})	13	
	TIC	**£9,878,403**

$[C_6MIm][Tf_2N]$

Table D.9 TCI costs results of the $[C_6MIm][Tf_2N]$ CO_2 capture design

TIC		
Direct Cost		COST (£)
	Purchased equipment	1550800
	Equipment installation	728876
	Instrumentation and control	558288
	Piping	1054544
	Electrical	170588
	Building and building services	279144
	Yard improvements	155080
	Service facilities	1085560
	Total Direct Cost	5582880
Indirect Cost		
	Engineering	511764
	Construction expenses	635828
	Legal costs	62032
	Contractor's fee	341176
	Contingency	682352
	Total Indirect Cost	2233152
	FCI	**7816032**
Working investment		1502682
IL cost		685684
IL requirements	52744.9	kg
IL Cost (£·kg^{-1})	13	
	TIC	**£10,004,398**

$[P_{66614}][Tf_2N]$

Table D.10 TCI costs results of the $[P_{66614}][Tf_2N]$ CO_2 capture design

TIC		
Direct Cost		COST (£)
	Purchased equipment	1570500
	Equipment installation	738135
	Instrumentation and control	565380
	Piping	1067940
	Electrical	172755
	Building and building services	282690
	Yard improvements	157050
	Service facilities	1099350
	Total Direct Cost	5653800
Indirect Cost		
	Engineering	518265
	Construction expenses	643905
	Legal costs	62820
	Contractor's fee	345510
	Contingency	691020
	Total Indirect Cost	2261520
	FCI	**7915320**
Working investment		1498131
IL cost		574366
IL requirements	44182	kg
IL Cost (£/kg)	13	
	TIC	**£9,987,817**

MEA

Table D.11 TCI costs results of the MEA CO_2 capture design

TCI		
Direct Cost		COST (£)
	Purchased equipment	519900
	Equipment installation	244353
	Instrumentation and control	187164
	Piping	353532
	Electrical	57189
	Building and building services	93582
	Yard improvements	51990
	Service facilities	363930
	Total Direct Cost	1871640
Indirect Cost		
	Engineering	171567
	Construction expenses	213159
	Legal costs	20796
	Contractor's fee	114378
	Contingency	228756
	Total Indirect Cost	748656
	FCI	**2620296**
Working investment		466453
MEA cost		22620
MEA requirements	22619.6	kg
MEA cost (£·kg^{-1})	1	
	TCI	**£3,109,369**

Appendix D.3 Annual Operating and Maintenance (O&M) costs of the evaluated CCU process designs

PD-MEA1

Table D.12 Annual O&M costs results of the PD-MEA1 design

O&M		
Fixed charge		COST (£·year^{-1})
	Local taxes	457100
	Insurance	228550
	Total Fixed charge	685650
Direct prod. cost		
	Cooling	6587475
	Heating	2704151
	Electricity (value from Aspen)	1979040
	MEA make up	4256
	H_2 and Steam Reformer	685644
	Catalysts & PSA packing	319488
	Maintenance	1599851
	Operating labour	399600
	Supervision	59940
	Operating supplies	239978
	Laboratory charges	59940
	Total direct prod. Cost	14639363
Plant overhead		1235635
	Production cost	16560648
General expenses		
	Administrative cost	59940
	Distribution and marketing	349276
	R&D cost	349904
	Total General expenses	759120

ANNUAL O&M	**£17,319,768**

PD-MEA2

Table D.13 Annual O&M costs results of the PD-MEA2 design

O&M		
Fixed charge		COST (£·year^{-1})
	Local taxes	347158
	Insurance	173579
	Total Fixed charge	520737
Direct prod. cost		
	Cooling	3870663
	Heating	1144945
	Electricity (value from Aspen)	721680
	MEA make up	4256
	H_2	3130678
	Catalysts & PSA packing	12374
	Maintenance	1215052
	Operating labour	399600
	Supervision	59940
	Operating supplies	182258
	Laboratory charges	59940
	Total direct prod. Cost	10912762
Plant overhead		1004755
	Production cost	12438253
General expenses		
	Administrative cost	59940
	Distribution and marketing	259573
	R&D cost	258388
	Total General expenses	577900

ANNUAL O&M	**£13,016,154**

PD-CHP1

Table D.14 Annual O&M costs results of the PD-CHP1 design

O&M		
Fixed charge		COST (£·year^{-1})
	Local taxes	999912
	Insurance	499956
	Total Fixed charge	1499868
Direct prod. cost		
	Cooling	7802093
	Heating	2073400
	Electricity	1592160
	MEA make up	0
	H_2	9210040
	Catalysts & PSA packing	1040992
	Maintenance	3499692
	Operating labour	399600
	Supervision	59940
	Operating supplies	524954
	Laboratory charges	59940
	Total direct prod. Cost	26262811
Plant overhead		2375539
	Production cost	30138218
General expenses		
	Administrative cost	59940
	Distribution and marketing	631795
	R&D cost	628944
	Total General expenses	1320679

ANNUAL O&M	**£31,458,897**

PD-CHP1-OXY

Table D.15 Annual O&M costs results of the PD-CHP1-OXY design

O&M		
Fixed charge		COST (£·year^{-1})
	Local taxes	825992
	Insurance	412996
	Total Fixed charge	1238988
Direct prod. cost		
	Cooling	5124934
	Heating	950382
	Electricity	0
	MEA make up	0
	H_2 and O_2	11066515
	Catalysts & PSA	382259
	Maintenance	2890971
	Operating labour	399600
	Supervision	59940
	Operating supplies	433646
	Laboratory charges	59940
	Total direct prod. Cost	21368186
Plant overhead		2010306
	Production cost	24617480
General expenses		
	Administrative cost	59940
	Distribution and marketing	517359
	R&D cost	513457
	Total General expenses	1090757

ANNUAL O&M	**£25,708,236**

PD-CHP2

Table D.16 Annual O&M costs results of the PD-CHP2 design

O&M		
Fixed charge		COST (£·year^{-1})
	Local taxes	1037872
	Insurance	518936
	Total Fixed charge	1556808
Direct prod. cost		
	Cooling	9935834
	Heating	2902271
	Electricity	1534500
	MEA make up	4256
	H_2	8286720
	Catalysts & PSA	1083628
	Maintenance	3632552
	Operating labour	399600
	Supervision	59940
	Operating supplies	544883
	Laboratory charges	59940
	Total direct prod. Cost	28444124
Plant overhead		2455255
	Production cost	32456187
General expenses		
	Administrative cost	59940
	Distribution and marketing	680537
	R&D cost	677357
	Total General expenses	1417834

ANNUAL O&M	**£33,874,021**

PD-CHP2-OXY

Table D.17 Annual O&M costs results of the PD-CHP2-OXY design

O&M		
Fixed charge		COST (£·year^{-1})
	Local taxes	889916
	Insurance	444958
	Total Fixed charge	1334873
Direct prod. cost		
	Cooling	7263747
	Heating	1779549
	Electricity	0
	MEA make up	4256
	H_2 and O_2	11034874
	Catalysts & PSA	382456
	Maintenance	3114704
	Operating labour	399600
	Supervision	59940
	Operating supplies	467206
	Laboratory charges	59940
	Total direct prod. Cost	24566273
Plant overhead		2144547
	Production cost	28045693
General expenses		
	Administrative cost	59940
	Distribution and marketing	588465
	R&D cost	585030
	Total General expenses	1233435

ANNUAL O&M	**£29,279,128**

PD-CHP1-POST

Table D.18 Annual O&M costs results of the PD-CHP1-POST design

O&M		
Fixed charge		COST (£·year^{-1})
	Local taxes	904706
	Insurance	452353
	Total Fixed charge	1357060
Direct prod. cost		
	Cooling	9684692
	Heating	2610665
	Electricity	0
	MEA make up	11266
	H_2	8286720
	Catalysts & PSA/O_2 plant packing	327396
	Maintenance	3166473
	Operating labour	399600
	Supervision	59940
	Operating supplies	474971
	Laboratory charges	59940
	Total direct prod. Cost	25081663
Plant overhead		2175608
	Production cost	28614330
General expenses		
	Administrative cost	59940
	Distribution and marketing	600656
	R&D cost	596970
	Total General expenses	1257565

ANNUAL O&M	**£29,871,895**

Appendix D.4 Annual Operating and Maintenance (O&M) costs of the evaluated ionic liquid and MEA-based CO_2 capture processes

$[C_2MIm][Tf_2N]$

Table D.19 Annual O&M costs results of the $[C_2MIm][Tf_2N]$ CO_2 capture design

O&M		
Fixed charge		COST (£·year^{-1})
	Local taxes	153115
	Insurance	76558
	Total Fixed charge	229673
Direct prod. cost		
	Cooling	53340
	Heating	0
	Electricity	292156
	IL make-up	0
	Maintenance	535903
	Operating labour	266400
	Supervision	39960
	Operating supplies	80385
	Laboratory charges	39960
	Total direct prod. Cost	1308105
Plant overhead		505358
	Production cost	2043136
General expenses		
	Administrative cost	39960
	Distribution and marketing	43869
	R&D cost	42179
	Total General expenses	126008

ANNUAL O&M	**£2,169,144**

$[C_6MIm][Tf_2N]$

Table D.20 Annual O&M costs results of the $[C_2MIm][Tf_2N]$ CO_2 capture design

O&M		
Fixed charge		COST (£·year^{-1})
	Local taxes	156321
	Insurance	78160
	Total Fixed charge	234481
Direct prod. cost		
	Cooling	58577
	Heating	0
	Electricity	313243
	IL & Water make-up	0
	Maintenance	547122
	Operating labour	266400
	Supervision	39960
	Operating supplies	82068
	Laboratory charges	39960
	Total direct prod. Cost	1347330
Plant overhead		512089
	Production cost	2093901
General expenses		
	Administrative cost	39960
	Distribution and marketing	44713
	R&D cost	43089
	Total General expenses	127762

ANNUAL O&M	**£2,221,662**

$[P_{66614}][Tf_2N]$

Table D.21 Annual O&M costs results of the $[P_{66614}][Tf_2N]$ CO_2 capture design

O&M		
Fixed charge		COST (£·year^{-1})
	Local taxes	158306
	Insurance	79153
	Total Fixed charge	237460
Direct prod. cost		
	Cooling	57796
	Heating	0
	Electricity	331229
	IL & Water make-up	0
	Maintenance	554072
	Operating labour	266400
	Supervision	39960
	Operating supplies	83111
	Laboratory charges	39960
	Total direct prod. Cost	1372528
Plant overhead		516259
	Production cost	2126247
General expenses		
	Administrative cost	39960
	Distribution and marketing	44737
	R&D cost	45023
	Total General expenses	129720

ANNUAL O&M	**£2,255,967**

MEA

Table D.22 Annual O&M costs results of the MEA CO_2 capture design

O&M		
Fixed charge		COST (£·year^{-1})
	Local taxes	52406
	Insurance	26203
	Total Fixed charge	78609
Direct prod. cost		
	Cooling	65450
	Heating	624332
	Electricity	73154
	MEA & Water make-up	4272
	Maintenance	183421
	Operating labour	266400
	Supervision	39960
	Operating supplies	27513
	Laboratory charges	39960
	Total direct prod. Cost	1324462
Plant overhead		293868
	Production cost	1696939
General expenses		
	Administrative cost	39960
	Distribution and marketing	36167
	R&D cost	36353
	Total General expenses	112480

ANNUAL O&M	**£1,809,419**

Appendix D.5 Sensitivity analysis results of the evaluated CCU process designs

Note that in all process concepts, the operating hours were varied by ±9.5%.

PD-MEA1

Table D.23 Sensitivity analysis results of the PD-MEA1 concept as a result of parameters' variations

Production costs (£·GJ^{-1})	-30%	Base Case	+30%
Capital investment	91.04	95.46	99.89
Interest	92.57	95.46	98.59
Plant life	97.76	95.46	94.42
Operating hours	105.48	95.46	87.18
Electricity price	92.70	95.46	98.23
H_2 price	94.50	95.46	96.42
CO_2 conversion	96.41	95.46	89.41

PD-MEA2

Table D.24 Sensitivity analysis results of the PD-MEA2 concept as a result of parameters' variations

Production costs (£·GJ^{-1})	-30%	Base Case	+30%
Capital investment	234.62	246.43	258.23
Interest	238.70	246.43	254.76
Plant life	252.55	246.43	243.65
Operating hours	272.29	246.43	225.05
Electricity price	242.98	246.43	249.87
H_2 price	231.48	246.43	261.37
CO_2 conversion	338.20	246.43	201.70

PD-CHP1

Table D.25 Sensitivity analysis results of the PD-CHP1 concept as a result of parameters' variations

Production costs (£·GJ^{-1})	-30%	Base Case	+30%
Capital investment	263.75	278.81	293.87
Interest	268.95	278.81	289.45
Plant life	286.62	278.81	275.26
Operating hours	308.08	278.81	254.62
Electricity price	275.34	278.81	282.28
H_2 price	258.73	278.81	298.89
CO_2 conversion	359.30	278.81	215.50

PD-CHP1-OXY

Table D.26 Sensitivity analysis results of the PD-CHP1-OXY concept as a result of parameters' variations

Production costs (£·GJ^{-1})	-30%	Base Case	+30%
Capital investment	168.59	178.32	188.04
Interest	171.95	178.32	185.18
Plant life	183.36	178.32	176.03
Operating hours	197.03	178.32	162.84
H_2 price	162.08	178.32	193.95
CO_2 conversion	275.79	178.32	152.59

PD-CHP2

Table D.27 Sensitivity analysis results of the PD-CHP2 concept as a result of parameters' variations

Production costs (£·GJ^{-1})	-30%	Base Case	+30%
Capital investment	283.07	298.73	314.40
Interest	288.48	298.73	309.80
Plant life	306.86	298.73	295.04
Operating hours	330.09	298.73	272.82
Electricity price	295.38	298.73	302.08
H_2 price	280.64	298.73	316.83
CO_2 conversion	399.34	298.73	236.52

PD-CHP2-OXY

Table D.28 Sensitivity analysis results of the PD-CHP2-OXY concept as a result of parameters' variations

Production costs (£·GJ^{-1})	-30%	Base Case	+30%
Capital investment	187.14	197.42	207.70
Interest	190.69	197.42	204.68
Plant life	202.76	197.42	195.00
Operating hours	218.14	197.42	180.29
H_2 price	182.09	197.42	212.75
CO_2 conversion	260.19	197.42	168.31

PD-CHP1-POST

Table D.29 Sensitivity analysis results of the PD-CHP1-POST concept as a result of parameters' variations

Production costs (£·GJ^{-1})	-30%	Base Case	+30%
Capital investment	205.83	217.11	228.39
Interest	209.72	217.11	225.08
Plant life	222.96	217.11	214.45
Operating hours	239.90	217.11	198.27
H_2 price	202.17	217.11	232.05
CO_2 conversion	280.21	217.11	171.88

Appendix D.6 Sensitivity analysis results of the evaluated ionic liquid and MEA-based CO_2 capture processes

$[C_2MIm][Tf_2N]$

Table D.30 Sensitivity analysis results of the $[C_2MIm][Tf_2N]$ CO_2 capture design as a result of parameters' variations

Production costs (£·GJ^{-1})	-30%	Base Case	+30%
IL cost	6.20	6.26	6.32
Electricity price	6.09	6.26	6.42
Plant life	6.60	6.26	6.10
Interest	5.83	6.26	6.72
Operating hours	6.91	6.26	5.71
Capital investment	5.60	6.26	6.91

$[C_6MIm][Tf_2N]$

Table D.31 Sensitivity analysis results of the $[C_6MIm][Tf_2N]$ CO_2 capture design as a result of parameters' variations

Production costs (£·GJ^{-1})	-30%	Base Case	+30%
IL cost	6.62	6.68	6.73
Electricity price	6.49	6.68	6.86
Plant life	7.04	6.68	6.52
Interest	6.22	6.68	7.17
Operating hours	7.38	6.68	6.10
Capital investment	5.99	6.68	7.37

$[P_{66614}][Tf_2N]$

Table D.32 Sensitivity analysis results of the $[P_{66614}][Tf_2N]$ CO_2 capture design as a result of parameters' variations

Production costs (£/GJ)	-30%	Base Case	+30%
IL cost	7.67	7.76	7.78
Electricity price	7.51	7.76	7.96
Plant life	8.15	7.76	7.54
Interest	7.21	7.76	8.30
Operating hours	8.54	7.76	7.06
Capital investment	6.93	7.76	8.53

Appendix E. Aspen Plus parameters of ionic liquid models

Pure-component parameters implemented in AspenPlus for the ionic liquids

Table E.1 Model parameters and corresponding physical properties

Parameter	Property model	Physical property
CPIG	Aspen Ideal gas heat capacity Polynomial	Ideal gas heat capacity
DNLDIP	DIPPR equation	Liquid molar volume (liquid density)
MULAND	Andrade equation	Liquid viscosity

Equations:

- **Aspen Ideal Gas Heat Capacity Polynomial**

$$C_p^{*ig} = C_1 + C_2 T + C_3 T^2 + \cdots + C_n T^{n-1}$$

- **DIPPR equation**

$$\rho_L = \frac{C_1}{C_2^{\left[1+\left(1-(T/C_3)\right)^{C_4}\right]}}$$

- **Andrade equation**

$$ln(\mu_l) = A + \frac{B}{T} + C\ ln(T)$$

CPIG parameter (ideal gas heat capacity)

Table E.2 Ideal gas heat capacity polynomial coefficients for $[C_2MIm][Tf_2N]$

Component	**$[C_2MIm][Tf_2N]$**
Parameter	CPIG
Physical property	Ideal gas heat capacity
Temperature units	K
Property units	J/kmol-K
1	351324.888
2	491.204363
3	-0.059570441
4	5.48E-05
5	0
6	0
7	0
8	1000
9	0
10	0
11	0

Table E.3 Ideal gas heat capacity polynomial coefficients for $[C_6MIm][Tf_2N]$

Component	**$[C_6MIm][Tf_2N]$**
Parameter	CPIG
Physical property	Ideal gas heat capacity
Temperature units	K
Property units	J/kmol-K
1	529611.939
2	-104.194741
3	1.61685781
4	-0.0009216
5	0
6	0
7	0
8	1000
9	0
10	0
11	0

Table E.4 Ideal gas heat capacity polynomial coefficients for $[P_{66614}][Tf_2N]$

Component	**$[P_{66614}][Tf_2N]$**
Parameter	CPIG
Physical property	Ideal gas heat capacity
Temperature units	°C
Property units	J/kmol-K
1	1227085.26
2	2300.82035
3	-3.59688255
4	0.00274
5	0
6	0
7	-273.15
8	726.85
9	0
10	0
11	0

.

DNLDIP parameter (liquid molar volume)

Table E.5 DIPPR equation coefficients for $[C_2MIm][Tf_2N]$

Components	**$[C_2MIm][Tf_2N]$**
Parameter	DNLDIP
Physical property	Liquid molar volume
Temperature units	°C
Property units	kmol/cum
1	0.353418419
2	0.275785506
3	1100.38374
4	0.477783803
5	0
6	-273.15
7	726.85

Table E.6 DIPPR equation coefficients for $[C_6MIm][Tf_2N]$

Components	**$[C_6MIm][Tf_2N]$**
Parameter	DNLDIP
Physical property	Liquid molar volume
Temperature units	K
Property units	kmol/cum
1	0.141575074
2	0.196354965
3	1283.70363
4	0.44450507
5	0
6	0
7	1000

Table E.7 DIPPR equation coefficients for $[P_{66614}][Tf_2N]$

Components	**$[P_{66614}][Tf_2N]$**
Parameter	DNLDIP
Physical property	Liquid molar volume
Temperature units	°C
Property units	kmol/cum
1	0.014059989
2	0.091041506
3	1908.04139
4	0.5
5	0
6	-273.15
7	726.85

MULAND parameter (liquid viscosity)

Table E.8 Andrade equation coefficients for $[C_2MIm][Tf_2N]$

Components	**$[C_2MIm][Tf_2N]$**
Parameter	MULAND
Physical property	Liquid viscosity
Temperature units	°C
Property units	cP
1	-166.591
2	10367.08
3	23.745

Table E.9 Andrade equation coefficients for $[C_6MIm][Tf_2N]$

Components	**$[C_6MIm][Tf_2N]$**
Parameter	MULAND
Physical property	Liquid viscosity
Temperature units	K
Property units	cP
1	-139.37
2	9863.8
3	19.4

Table E.10 Andrade equation coefficients for $[P_{66614}][Tf_2N]$

Components	**$[P_{66614}][Tf_2N]$**
Parameter	MULAND
Physical property	Liquid viscosity
Temperature units	°C
Property units	cP
1	-166.04383
2	12027.5942
3	23.0845053
4	-273.15
5	226.85

Table E.11 Coefficients of the SGPRF1 molecular component s-profile parameter

	SGPRF1				
	$[C_2MIm][Tf_2N]$	$[C_6MIm][Tf_2N]$	$[P_{66614}][Tf_2N]$	CO_2	CH_4
Parameter					
1	0.0000	0.0000	0.0000	0.0000	0.0000
2	0.0000	0.0000	0.0000	0.0000	0.0000
3	0.0000	0.0000	0.0000	0.0000	0.0000
4	0.0000	0.0000	0.0000	0.0000	0.0000
5	0.0000	0.0000	0.0000	0.0000	0.0000
6	0.0000	0.0000	0.0000	0.0000	0.0000
7	0.0000	0.0000	0.0000	0.0000	0.0000
8	0.0293	0.0663	0.0000	0.0000	0.0000
9	0.5117	0.5745	0.0000	0.0000	0.0000
10	1.5850	1.5230	0.0000	0.0000	0.0000
11	2.7077	2.5953	0.0000	0.0000	0.0000
12	3.8183	3.8998	0.0000	0.0000	0.0000

Table E.12 Coefficients of the SGPRF2 molecular component s-profile parameter

	SGPRF2				
	$[C_2MIm][Tf_2N]$	$[C_6MIm][Tf_2N]$	$[P_{66614}][Tf_2N]$	CO_2	CH_4
Parameter					
1	5.1627	5.4098	0.4020	0.0000	0.0000
2	6.2802	6.4383	3.4570	0.0000	0.0000
3	8.9108	8.7745	8.8712	0.1050	0.0000
4	13.8980	13.0858	12.0615	2.8640	0.0000
5	16.5543	14.4793	13.2078	6.6930	0.0000
6	16.8038	14.1375	15.9835	6.3210	0.0000
7	18.0195	15.9373	19.3168	3.5510	0.0000
8	19.0132	19.5700	27.5197	2.4270	0.0000
9	16.8320	23.6263	50.1048	2.5120	0.0000
10	12.2243	25.5933	81.1903	1.2930	2.7082
11	10.1955	26.1660	102.4308	1.0620	5.4569
12	13.4023	26.5018	101.7848	2.3450	8.9848

Table E.13 Coefficients of the SGPRF3 molecular component s-profile parameter

	SGPRF3				
	$[C_2MIm][Tf_2N]$	$[C_6MIm][Tf_2N]$	$[P_{66614}][Tf_2N]$	CO_2	CH_4
Parameter					
1	21.3303	29.8080	89.5632	1.6370	5.8897
2	31.8400	38.9005	85.1365	1.0130	6.0301
3	33.5305	41.4693	81.3280	3.2090	7.2904
4	20.3542	27.7665	61.9112	4.4650	15.8236
5	7.6435	11.4365	32.6507	2.8160	3.8237
6	3.3810	4.0245	10.1092	6.2550	0.0000
7	2.6405	2.6405	2.6333	10.7980	0.0000
8	4.1775	4.1775	4.3037	6.1000	0.0000
9	6.6040	6.6040	7.0310	0.7000	0.0000
10	9.3445	9.3445	9.7947	0.0000	0.0000
11	14.4585	14.4585	15.0143	0.0000	0.0000
12	18.4210	18.4210	18.8207	0.0000	0.0000

Table E.14 Coefficients of the SGPRF4 molecular component s-profile parameter

	SGPRF4				
	$[C_2MIm][Tf_2N]$	$[C_6MIm][Tf_2N]$	$[P_{66614}][Tf_2N]$	CO_2	CH_4
Parameter					
1	15.3105	15.3105	14.9800	0.0000	0.0000
2	7.7535	7.7535	7.0797	0.0000	0.0000
3	2.1670	2.1670	1.7777	0.0000	0.0000
4	0.2845	0.2845	0.1770	0.0000	0.0000
5	0.0295	0.0295	0.0177	0.0000	0.0000
6	0.0000	0.0000	0.0000	0.0000	0.0000
7	0.0000	0.0000	0.0000	0.0000	0.0000
8	0.0000	0.0000	0.0000	0.0000	0.0000
9	0.0000	0.0000	0.0000	0.0000	0.0000
10	0.0000	0.0000	0.0000	0.0000	0.0000
11	0.0000	0.0000	0.0000	0.0000	0.0000
12	0.0000	0.0000	0.0000	0.0000	0.0000

Table E.15 Coefficients of the SGPRF5 molecular component s-profile parameter

	SGPRF5				
	$[C_2MIm][Tf_2N]$	$[C_6MIm][Tf_2N]$	$[P_{66614}][Tf_2N]$	CO_2	CH_4
Parameter					
1	0	0	0	0	0
2	0	0	0	0	0
3	0	0	0	0	0
4	0	0	0	0	0
5	0	0	0	0	0
6	0	0	0	0	0
7	0	0	0	0	0
8	0	0	0	0	0
9	0	0	0	0	0
10	0	0	0	0	0
11	0	0	0	0	0
12	0	0	0	0	0

Appendix F. Publications

Dimitriou, I., García-Gutiérrez, P., Elder, R.H., Cuéllar-Franca, R.M., Azapagic, A., Allen, R.W.K. (2015). Carbon dioxide utilisation for production of transport fuels: process and economic analysis. *Energy Environ. Sci.*, 8 (6), 1775–1789.

Carbon dioxide utilisation for production of transport fuels: process and economic analysis

Abstract

Utilising CO_2 as a feedstock for chemicals and fuels could help mitigate climate change and reduce dependence on fossil fuels. For this reason, there is an increasing world-wide interest in carbon capture and utilisation (CCU). As part of a broader project to identify key technical advances required for sustainable CCU, this work considers different process designs, each at a high level of technology readiness and suitable for large-scale conversion of CO_2 into liquid hydrocarbon fuels, using biogas from sewage sludge as a source of CO_2. The main objective of the paper is to estimate fuel production yields and costs of different CCU process configurations in order to establish whether the production of hydrocarbon fuels from commercially proven technologies is economically viable. Four process concepts are examined, developed and modelled using the process simulation software Aspen Plus to determine raw materials, energy and utility requirements. Three design cases are based on typical biogas applications: (1) biogas upgrading using a monoethanolamine (MEA) unit to remove CO_2, (2) combustion of raw biogas in a combined heat and power (CHP) plant and (3) combustion of upgraded biogas in a CHP plant which represents a combination of the first two options. The fourth case examines a post-combustion CO_2 capture and utilisation system where the CO_2 removal unit is placed right after the CHP plant to remove the excess air with the aim of improving the energy efficiency of the plant. All four concepts include conversion of CO_2 to CO via a reverse water-gas-shift reaction process and subsequent conversion to diesel and gasoline via Fischer–Tropsch synthesis. The studied CCU options are compared in terms of liquid fuel yields, energy requirements, energy efficiencies, capital investment and production costs. The overall plant energy efficiency and production costs range from 12–17% and £15.8–29.6 per litre of liquid fuels, respectively. A sensitivity analysis is also carried out to examine the effect of different economic

and technical parameters on the production costs of liquid fuels. The results indicate that the production of liquid hydrocarbon fuels using the existing CCU technology is not economically feasible mainly because of the low CO_2 separation and conversion efficiencies as well as the high energy requirements. Therefore, future research in this area should aim at developing novel CCU technologies which should primarily focus on optimising the CO_2 conversion rate and minimising the energy consumption of the plant.

Cuéllar-Franca, R., Dimitriou, I., García-Gutiérrez, P., Elder, R.H., Allen, R.W.K., Azapagic, A. (2015). Carbon Capture and Utilisation: Application of Life Cycle Thinking to Process Design. *Computer Aided Chemical Engineering*, 37, 1457–1462.

Carbon Capture and Utilisation: Application of Life Cycle Thinking to Process Design

Abstract

Global emissions of CO_2 from fossil fuels are increasing steadily and are currently 60% above the 1990 levels, despite the need to reduce them by at least 50% to limit the rise of the global average temperature to 2°C by 2050 (IPCC, 2013). A range of options that could help towards this target are being considered, including carbon capture and utilisation (CCU) which converts waste CO_2 to valuable products such as fuels (Styring *et al.*, 2011). However, conversion of CO_2 to fuels is very energy intensive because of its thermodynamic stability, as well as requiring the use of different chemicals, so that it is not clear if this option is environmentally more sustainable than conventional fossil or biofuels. As CCU technologies are currently being developed, this presents an ideal opportunity to evaluate and optimise their potential for mitigating climate change, the main driver for their development. This is best carried out at an early design stage, taking a life cycle approach to avoid shifting of environmental burdens from one life cycle stage to another (Azapagic *et al.,* 2006). Therefore, this paper sets out to demonstrate how this can be achieved by considering a CCU system for the production of synthetic diesel from waste CO_2.

Techno-Economic Feasibility of Selective CO_2 Capture Processes from Biogas Streams Using Ionic Liquids as Physical Absorbents

Pelayo Garcia-Gutierrez, Johan Jacquemin, Corina McCrellis, Ioanna Dimitriou, S. F. Rebecca Taylor, Christopher Hardacre and Ray W. K. Allen. (2016). Techno-Economic Feasibility of Selective CO_2 Capture Processes from Biogas Streams Using Ionic Liquids as Physical Absorbents. *Energy Fuels*, 30 (6), 5052–5064.

Abstract

Biogas from anaerobic digestion of sewage sludge is a renewable resource with high energy content, which is composed mainly of CH_4 (40–75 vol %) and CO_2 (15–60 vol %). Other components, such as water (H_2O, 5–10 vol %) and trace amounts of hydrogen sulfide and siloxanes, can also be present. A CH_4-rich stream can be produced by removing the CO_2 and other impurities so that the upgraded bio-methane can be injected into the natural gas grid or used as a vehicle fuel. The main objective of this paper is to assess the technical and economic performance of biogas upgrading processes using ionic liquids that physically absorb CO_2. The simulation methodology is based on the COSMO-SAC model as implemented in Aspen Plus. Three different ionic liquids, namely, 1-ethyl-3-methylimidazolium bis[(trifluoromethyl)sulfonyl]imide, 1-hexyl-3-methylimidazoliumbis[(trifluoromethyl)sulfonyl]imide, and trihexyl(tetradecyl)phosphonium bis[(trifluoromethyl)sulfonyl]imide, are considered for CO_2 capture in a pressure-swing regenerative absorption process. The simulation software Aspen Plus and Aspen Process Economic Analyzer is used to account for mass and energy balances as well as equipment cost. In all cases, the biogas upgrading plant consists of a multistage compressor for biogas compression, a packed absorption column for CO_2 absorption, a flash evaporator for solvent regeneration, a centrifugal pump for solvent recirculation, a pre-absorber solvent cooler, and a gas turbine for electricity recovery. The evaluated processes are compared in terms of energy efficiency, capital investment, and bio-methane production costs. The overall plant efficiency ranges from 71 to 86%, and the bio-methane production cost ranges from $9.18–11.32 per GJ (LHV). A sensitivity analysis is also performed to determine how several technical and economic parameters affect the bio-methane production costs. The results of this study show that the simulation methodology developed can predict plant efficiencies and production costs of large scale CO_2 capture processes using ionic liquids without having to rely on gas solubility experimental data.